

Dissertation
submitted to the
Combined Faculties for Natural Sciences and for Mathematics
of the Ruperto-Carola University of Heidelberg, Germany
for the degree of
Doctor of Natural Sciences

presented by
Sevim Özgür M.Sc. in Molecular and Cellular Biology
born in V.Preslav, Shumen, Bulgaria
Oral examination on December 15th, 2011

**Characterization of human Pat1b,
an essential P-body protein that links
deadenylation to decapping in 5' to 3' mRNA decay**

Referees: Prof. Dr. Christine Clayton
Dr. Georg Stoecklin

I hereby declare that I have written the submitted dissertation myself and in this process have used no other sources or materials than those expressly indicated.
The work was carried out in the German Cancer Research Center (DKFZ) Heidelberg in the group "*Posttranscriptional Control Of Gene Expression*" of Dr. Georg Stoecklin.

Heidelberg, November 2011

Sevim Özgür

Abstract

In eukaryotic cells, degradation of many mRNAs is initiated by removal of the polyA tail followed by decapping and 5' to 3' exonucleolytic decay. Although the order of these events is well established, we are still lacking a mechanistic understanding of how deadenylation and decapping are linked. During my PhD studies, I characterized the human Pat1b protein and showed that Pat1b links the deadenylation complex to the decapping complex both physically and functionally. Pat1b is tightly associated with the Ccr4-NOT deadenylation complex as well as with the Dcp1-Dcp2 decapping complex. In addition, Pat1b overexpression increases the association of the deadenylation complex with the decapping complex. When tethered to a reporter mRNA, Pat1b induces its rapid degradation. Pat1b-mediated mRNA decay depends on the deadenylase Caf1a and the decapping enzyme Dcp2, indicating that these interactions are functionally important. Moreover, Pat1b interacts with the decapping enhancers Rck, the Lsm1-7 complex, Hedls and Edc3. Pat1b interacts with the deadenylation complex, the decapping complex and the decapping enhancers via at least three different domains, suggesting that Pat1b serves as a scaffolding protein. Together, the data provide evidence that human Pat1b is a central component of the mRNA decay machinery that connects deadenylation with decapping.

Most enzymes of the 5' to 3' mRNA decay pathway, including the Ccr4-NOT deadenylation complex, are localized in cytoplasmic foci called processing (P) bodies. I could show that Pat1b is required for P-body formation, and that it strongly induces P-body numbers when overexpressed. My data indicate that an amino-terminal region within Pat1b serves as an aggregation-prone domain that nucleates P-bodies, whereas an acidic domain controls the size of P-bodies. Although Rck specifically interacts with the acidic domain of Pat1b, point mutations in Pat1b that abolish the Rck interaction did not alter P-body size. On the other hand, I also identified point mutations in Rck that abolish Pat1b binding, and found that Rck needs to associate with Pat1b in order to promote P-body formation. Furthermore, I purified Pat1b and identified additional binding partners via mass spectrometry. Further characterization of these interactions may help to understand how Pat1b controls P-body numbers and size, and what additional functions Pat1b may have.

Zusammenfassung

In eukaryontischen Zellen wird der Abbau vieler mRNAs mit der Entfernung des Poly(A)-Schwanzes initiiert, wonach das Cap am 5' Ende entfernt und anschließend der Rest der mRNA exonukleolytisch vom 5' zum 3' Ende abgebaut wird. Obwohl die Reihenfolge dieser Vorgänge sehr gut beschrieben ist, ist bis heute wenig bekannt über den genauen Mechanismus, der Deadenylierung und Decapping verbindet. In meiner Doktorarbeit habe ich das humane Protein Pat1b charakterisiert und konnte zeigen, dass Pat1b den Deadenylierungs-Komplex sowohl physisch als auch funktionell mit dem Decapping-Komplex verbindet. Pat1b ist zum einen stark mit dem Ccr4-NOT Deadenylierungs-Komplex, zum anderen aber auch mit dem Dcp1-Dcp2 Decapping-Komplex assoziiert. Zudem verstärkt die Überexpression von Pat1b die Kopplung von Deadenylierung und Decapping. Wenn Pat1b experimentell an eine Reporter-mRNA gebunden wird, induziert Pat1b den schnellen Abbau dieser mRNA. Pat1b-vermittelter mRNA-Abbau hängt von der Deadenylase Caf1a und dem Decapping-Enzym Dcp2 ab, was darauf hindeutet, dass die Interaktion mit Pat1b wichtig ist für deren Funktion. Darüber hinaus interagiert Pat1b mit den Proteinen Rck, Hedls, Edc3 und dem Lsm1-7 Komplex, die den Decapping-Prozess fördern. Pat1b assoziiert mit dem Deadenylierungs-Komplex, dem Decapping-Komplex und weiteren Decapping-Proteinen über mindestens drei verschiedene Domänen, was darauf schließen lässt, dass Pat1b eine Plattform-Funktion einnimmt. Zusammenfassend liefern diese Daten Hinweise darauf, dass das humane Pat1b eine zentrale Komponente der mRNA-Abbaumaschinerie ist, die Deadenylierung mit Decapping verbindet.

Die meisten Enzyme, die beim mRNA Abbau vom 3' zum 5' Ende beteiligt sind, einschließlich dem Ccr4-NOT-Komplex, lokalisieren in zytoplasmatischen Foci, sogenannten Processing Bodies (PBs). Ich konnte zeigen, dass Pat1b notwendig ist für die Bildung von PBs, und dass die Überexpression von Pat1b die Anzahl an PBs erhöht. Meine Daten weisen darauf hin, dass ein Bereich am aminoterminalen Ende von Pat1b als aggregationsfördernde Domäne dient, die zur PB-Bildung führt, während ein anderer Bereich, der mehrere saure Aminosäuren enthält, die Größe der PBs kontrolliert. Obwohl Rck spezifisch mit eben dieser sauren Domäne in Pat1b interagiert, zeigten Punktmutationen in Pat1b, die die Interaktion mit Rck verhindern, keinen Einfluss auf die PB-Größe. Andererseits konnte ich durch Punktmutationen in Rck, die die Assoziation mit Pat1b verhindern, zeigen, dass die Interaktion von Rck und Pat1b für die Bildung von PBs benötigt wird. Außerdem konnte ich Pat1b aufreinigen und mittels Massenspektrometrie weitere Proteine identifizieren, die mit Pat1b interagieren. Die genauere Charakterisierung dieser Interaktionen könnte helfen zu verstehen, wie Pat1b die Anzahl und Größe von PBs kontrolliert, und welche zusätzlichen Funktionen Pat1b noch haben könnte.

Contents

List of Figures	1
List of Tables	3
1 Introduction	5
1.1 mRNA-Specific Decay Pathways	6
1.1.1 ARE-Mediated mRNA Decay (AMD)	6
1.1.2 RNAi-Mediated mRNA Decay	7
1.2 Deadylation	8
1.2.1 The PARN Deadenylase	8
1.2.2 The PAN2-PAN3 Deadylation Complex	8
1.2.3 The Ccr4-NOT Deadenylation Complex	9
1.3 Decapping and 5' to 3' mRNA Decay	13
1.3.1 The Dcp1/Dcp2 Decapping Complex	13
1.3.2 Decapping Enhancers	18
1.3.3 Nudt16, an Alternative to Mammalian Dcp2?	23
1.4 Processing Bodies	23
1.5 Pat1	25
1.6 Aim of the Study	27
2 Results	28
2.1 Previous Work on Pat1b	28
2.2 Pat1b, but not Pat1a, Is a P-body Protein	29
2.2.1 Cloning of Pat1a	29
2.2.2 Comparison of Pat1a and Pat1b Localization	29
2.2.3 Comparison of Pat1a and Pat1b Interactions	30
2.3 Role of Pat1b in P-body Assembly	31
2.3.1 Pat1b Is Essential for P-body Formation	31
2.3.2 Localization of Pat1b Deletion Constructs	32
2.3.3 Pat1b Induced P-bodies Are Resistant to Cycloheximide	34
2.4 Interactions of Pat1b	35
2.4.1 Interactions of Pat1b with Decapping Enhancers	35
2.4.2 Pat1b Interacts with the Decapping Complex	38
2.4.3 Pat1b Interacts with the Ccr4-NOT Deadenylation Complex	39
2.4.4 Pat1b Enhances the Interaction between Dcp2 and Caf1a	40
2.4.5 Other Interactions of Pat1b	41
2.4.6 Summary of Pat1b Interactions	44
2.5 Function of Pat1b	45
2.5.1 Pat1b as a Suppressor of Translation?	45
2.5.2 Pat1b as an Essential Protein in mRNA Degradation?	46

2.5.3	Pat1b Tethering Assay	47
2.5.4	Pat1b-Mediated mRNA Decay Utilizes Dcp2 and Caf1a	49
2.5.5	Pat1-N Is Necessary and Sufficient for Pat1b Function	51
2.5.6	Is Pat1b Required for Caf1a Activity or Coupling of Deadenylation and Decapping?	52
2.6	Endogenous mRNA Targets of Pat1b	53
2.6.1	Strategy and Quality Control of Samples	53
2.6.2	Data Analysis	55
2.6.3	Data Verification	56
2.7	A Closer Look at the Pat1b-Rck Interaction	57
2.7.1	Pat1b and Rck Interaction Mutants	58
2.7.2	Rck Binding Is not Required for Pat1b-Mediated mRNA Degradation	59
2.7.3	Rck Requires Pat1b Binding for P-body Localization and Formation	59
3	Discussion	62
3.1	Role of Pat1b in P-body Formation	62
3.2	Role of Pat1b in mRNA Degradation	65
3.3	Summary	69
3.4	Possible Future Directions	70
4	Materials and Methods	71
4.1	Materials	71
4.1.1	DNA and RNA Oligos	71
4.1.2	List of Antibodies	74
4.1.3	Technical Equipment	75
4.1.4	Chemicals and Enzymes	76
4.1.5	Disposable Materials and Kits	79
4.2	Methods	80
4.2.1	Plasmids and Cloning	80
4.2.2	Cell Culture and Transfection	82
4.2.3	Immunofluorescence Microscopy	84
4.2.4	Co-IP and Western Blot Analysis	84
4.2.5	Northern Blot Analysis	84
4.2.6	Quantitative Real Time PCR	85
4.2.7	³⁵ S-Methionine/Cysteine Metabolic Labeling and Autoradiography	85
4.2.8	Luciferase Assay	86
	Acronyms	87
	Acknowledgement	89
	Bibliography	91
5	Appendix	103
5.1	Results of HPLC-MS/MS Analysis	103
5.2	Results of Microarray Analysis	107
5.3	Publication by Özgür et al.: Human Pat1b Connects Deadenylation with mRNA Decapping and Controls the Assembly of Processing Bodies	111

List of Figures

1.1	Deadenylation-dependent mRNA degradation and the enzymes and protein complexes involved.	6
1.2	Model explaining the regulation of Dcp1p/Dcp2p decapping activity by open and closed conformations.	16
2.1	Schematic representation of Pat1b domains, and amino acid sequence conservation between Pat1b and Pat1a.	29
2.2	Localization of YFP, YFP-Pat1a and YFP-Pat1b in COS7 cells.	30
2.3	Interactions of Pat1a.	31
2.4	Pat1b is an essential P-body protein.	32
2.5	Localization of Pat1b deletion constructs.	33
2.6	Localization of Pat1b in presence of CHX.	35
2.7	Salt resistance of Pat1b interactions.	36
2.8	Separate interaction domains within Pat1b.	37
2.9	Pat1b interacts with Dcp2 and Dcp1a.	38
2.10	Pat1b interacts with the Ccr4-NOT complex.	39
2.11	Pat1b enhances the interaction between Dcp2 and Caf1a.	40
2.12	Pat1b interacts with TTP and BRF1.	41
2.13	Pat1b interacts with effector proteins of RNAi.	42
2.14	Pat1b interacts with itself.	43
2.15	Confirmation of novel Pat1b interacting proteins.	44
2.16	Summary of Pat1b interactions.	45
2.17	Pat1b does not affect general translation.	46
2.18	Pat1b knockdown does not affect degradation of reporter mRNAs.	47
2.19	Pat1b tethering reduces mRNA levels.	48
2.20	Pat1b tethering induces mRNA decay.	50
2.21	mRNA decay induced by Pat1b tethering utilizes Caf1a and Dcp2.	51
2.22	Tethering of Pat1b fragments.	52
2.23	Effect of Pat1b knockdown on Caf1a activity.	53
2.24	Quality control of Rck and Pat1b knockdown levels and integrity of RNA samples for microarray analysis.	54
2.25	qPCR analysis of two putative Pat1b targets identified by microarray.	57
2.26	Pat1b and Rck interaction mutants.	58
2.27	Rck is dispensable for the activity of Pat1b in a tethering assay.	59
2.28	Localization of YFP-Pat1b-4A and YFP-Rck-m4.	60
3.1	Summary of Pat1 interactions and functional domains.	66

List of Tables

1.1	Comparison of yeast and human Ccr4-NOT complex components.	10
4.1	DNA oligos used in this study.	71
4.2	List of siRNAs used in this study.	73
4.3	Antibodies used in this study.	74
4.4	Technical Equipment	75
4.5	Chemicals and Enzymes	76
4.6	Disposable Material and Kits	79
4.7	Cell lines used in this study.	83
4.8	Light Cycler Program.	85
5.1	List of proteins identified to interact with YFP-Pat1b and/or YFP-Pat1b-A by HPCL-MS/MS.	103
5.2	List of potential mRNA targets of Pat1b, Rck or both, identified by microarray analysis.	107

1 Introduction

All of the cells in an organism have the same sequence of DNA, yet not all cells express every gene encoded in the genome. Moreover, expression of most genes needs to be tightly regulated according to internal and external stimuli. During evolution, several mechanisms have emerged to control gene expression and to thereby achieve such tight regulation. One efficient way to enable rapid responses to internal and environmental stimuli is to control the levels of messenger RNAs (mRNAs) in the cell and the availability of mRNAs to the translation machinery. Keeping the amount of mRNA stable but blocking its translation gives the cell capacity to generate high amounts of the corresponding protein in a short time once the translation inhibition is removed. Moreover, restricting the levels of the mRNA by degradation ensures the suppression of protein levels which can be deleterious to the cell unless tightly controlled. To achieve this, the 5' and 3' untranslated regions (UTRs) of certain mRNAs contain regulatory sequences that control the translation or degradation rate of that particular mRNA without affecting other transcripts in the cell. These sequences mostly function as binding sites for regulatory proteins or small regulatory RNAs such as microRNAs (miRNAs) and small interfering RNAs (siRNAs).

Despite different regulatory elements which give the initial trigger to degrade mRNAs, there are common steps in different mRNA decay pathways (see Figure 1.1). The first and rate limiting step in cytoplasmic mRNA degradation is the removal of the poly adenosine (polyA) tail [1, 2]. Exceptions to this rule are histone mRNAs, which do not have polyA tails, and mRNA decay initiated by endonucleolytic cleavage. After removal of the polyA tail, degradation of the mRNA body can follow two routes. First, it can be degraded from its 3' end by a large ribonuclease complex termed the exosome. At the end of this decay pathway 5' cap will be metabolized by the scavenger decapping enzyme DcpS. Alternatively, following deadenylation, mRNA can be decapped by the Dcp1/Dcp2 decapping complex and degraded in the 5' to 3' direction by the exoribonuclease Xrn1 [1, 3, 4, 5].

Deadenylation is reversible and highly utilized to control translation during vertebrate oocyte maturation and early embryogenesis. On the other hand, decapping and exoribonucleolytic degradation either by the exosome or Xrn1 are irreversible steps that lead to degradation of mRNA body. The 5' to 3' decay pathway was suggested to be the primary mode of degradation both for stable and labile mRNAs in *Saccharomyces cerevisiae* [1, 4, 2]. Nevertheless, the 3' to 5' decay and decapping followed by the 5' to 3' decay appear to be redundant pathways in mRNA decay. Knocking out components of either pathway in *S. cerevisiae* has only minimal effects on the transcriptome [5].

Since my PhD project aimed to characterize human Pat1, whose yeast homolog was suggested to be a decapping enhancer, in the following I will focus on deadenylation and the 5' to 3' mRNA decay pathway.

1 Introduction

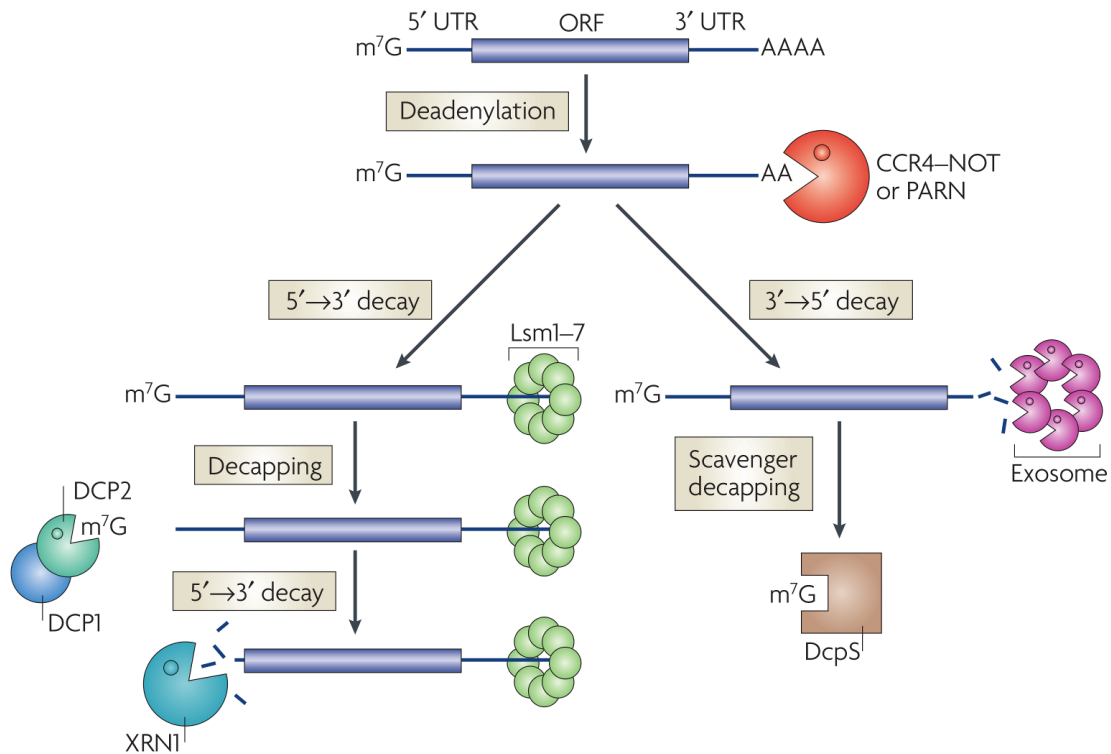


Figure 1.1. Deadenylation-dependent mRNA degradation and the enzymes and protein complexes involved. Figure was reproduced from Garneau et al. [5].

1.1 mRNA-Specific Decay Pathways

Before going into details of deadenylation and decapping I will briefly introduce two mRNA-specific degradation pathways.

1.1.1 ARE-Mediated mRNA Decay (AMD)

AU-rich elements (AREs) are 3' UTR sequence elements characteristic for many short-lived mRNAs. ARE-containing mRNAs usually code for the proteins with functions in cell growth (e.g. c-fos, c-myc), inflammatory response (e.g. cytokines IL2, TNF α , GM-CSF) and response to other environmental stimuli (e.g. iNOS, VEGF, cyclin b1). Precise temporal regulation required for the translation of these mRNAs is achieved by the help of AREs [6, 7, 8].

AREs are 50-150 nt long, uridine-rich sequences with frequently overlapping AUUUA pentamers. Presence of this pentamer alone is not enough to trigger rapid mRNA degradation, but 2-4 copies of the UUAUUUA(U/A)(U/A) nanomer are required for efficient enhancement of mRNA turnover. The stability of these ARE-containing mRNAs is regulated by ARE-binding proteins (ARE-BPs). Most of the ARE-BPs that have been identified so far activate mRNA decay (e.g. tristetraprolin (TTP), BRF1/2, KSRP), some stabilize the bound mRNA (e.g. HuR, HuD), and some regulate translation (e.g. TIA-1). The functions of these proteins were reported to be cell type-specific [6, 9, 10, 8]. This implies the interplay of other regulatory

factors in ARE-mediated mRNA decay (AMD) and/or dependency of the mRNA half life on the relative abundance of the stabilizing and destabilizing proteins. AMD was shown to be deadenylation-dependent [9, 8]. Moreover, TTP and KSRP are known to stimulate the deadenylases polyA-specific ribonuclease (PARN) and Caf1. TTP interacts with the mammalian Ccr4-NOT deadenylase complex, the decapping enzyme Dcp2, and the decapping enhancer Edc3 [7, 9, 11]. Both 3' to 5' degradation by the exosome and 5' to 3' degradation by Xrn1 participate in AMD [12]. In support of both pathways, KSRP, BRF1 and TTP interact with the exosome, and the latter two also with the decapping complex [6]. Several ARE-BPs including TTP and TIA-1 are associated with stress granules and Processing bodies (P-bodies), where 5' to 3' degradation enzymes are concentrated. Nevertheless, depletion of Xrn1 and Lsm1 (an activator of decapping) blocks AMD to a larger extent than depletion of exosome components [12]. Furthermore, tethering of TTP or BRF1 to an mRNA that does not contain an ARE is sufficient to target the mRNA to P-bodies and to induce decay [13, 9]. These observations suggest that the 5' to 3' degradation pathway is predominant in AMD.

1.1.2 RNAi-Mediated mRNA Decay

siRNAs and miRNAs are 20-25 nucleotide (nt) long RNA species that originate from extracellular sources or from the genomic transcripts. After being processed in the nucleus by the protein factors Drosha and Pasha, miRNA precursors are exported to the cytoplasm where they share the same pathway with siRNAs for maturation. The evolutionary conserved, cytoplasmic protein Dicer (DCR) cleaves the siRNA and miRNA precursors into 20-25 nt long double stranded RNA (dsRNA) species. While being loaded onto the RNA-induced silencing complex (RISC), which contains Angonauite (Ago) and GW182 proteins, the dsRNAs are unwound. One strand serves to target mRNAs in RISC whereas the other strand is usually degraded [14, 15, 16]. Recently, miRNAs that do not follow these canonical maturation steps have also been identified [17]. In the RISC, the function of the miRNA or the siRNA is determined partially by the identity of the interacting Ago proteins. Ago proteins are a large family of conserved proteins. The N-terminal PAZ domain mediates sequence-independent single stranded RNA (ssRNA)-binding. The C-terminal PIWI domain has a ribonuclease (RNase)-H like fold which mediates endonucleolytic cleavage of the siRNA and its target mRNA. In fact, the PIWI domain is not catalytically active in all Ago proteins; only Ago2 associated RISC having cleavage activity in humans [18, 5].

After intensive research on the mechanism of RNAi-mediated gene silencing, it is now clear that miRNAs or siRNAs target the RISC to mRNAs via sequence-specific interactions, and GW182 mediates silencing [19, 20, 21, 22]. RNA interference (RNAi)-mediated gene silencing can result in translational suppression and/or degradation of the target mRNA [23, 24, 5]. What determines this decision remains to be resolved. A possible answer to this question can include interacting proteins. Ago proteins are, indeed, known to interact with several proteins that have roles in translational regulation or mRNA decay, either directly or in an RNA-dependent manner. In *Drosophila*, miRNA-mediated mRNA decay was reported to require the decapping complex Dcp1/Dcp2, the decapping enhancer Edc3, the deadenylase Ccr4-NOT complex [16, 23].

1.2 Deadeylation

In the cytoplasm, the polyA tail together with the polyA-binding protein (PABP) supports translation and protects the 3' end of the mRNA from exoribonucleases. Therefore, removal of the polyA tail is a prerequisite for degradation, and the rate of deadenylation is the major determinant of mRNA half life [1]. There are three main eukaryotic deadenylases: (1) the polyA-specific ribonuclease, PARN, (2) the PAN2-PAN3 deadenylase and (3) the Ccr4-NOT deadenylation complex. While PARN has important roles in control of polyA tail length in embryogenesis, the PAN2-PAN3 and Ccr4-NOT complexes are the main cytoplasmic deadenylases [5, 25]. Deadenylation was shown to be biphasic in mammalian cells: First, PAN2-PAN3, stimulated by PABP, shortens the polyA tail down to 100-110 nt. This deadenylation step is slow and synchronous. In the second phase, the Ccr4-NOT complex takes over and deadenylates the mRNA rapidly. This phase of deadenylation is asynchronous, and decapping and degradation of the mRNA body already start to take place [25, 26]. Zheng et al. [27] showed that the PAN2-PAN3 and Ccr4-NOT complexes interact with each other, and that overexpression of a Caf1 dominant negative mutant impairs not only the second phase of deadenylation but also the first one. These data indicate that the two complexes communicate with each other to coordinate deadenylation.

1.2.1 The PARN Deadenylase

PolyA-specific ribonuclease, PARN, also known as deadenylating nuclease, DAN, is a single polypeptide, which functions as homooligomer. PARN is a magnesium (Mg^{2+})-dependent enzyme and belongs to the DEDD family of nucleases. It has a distributive deadenylation activity that requires a free 3'-hydroxyl group and releases solely 5'-AMP [28]. In contrast to the PAN2-PAN3 and Ccr4-NOT deadenylases, PARN interacts with the 7-methylated guanosine cap (m^7G). Its *in vitro* activity is stimulated by the presence of the cap but inhibited by the cap-binding protein 80 (CBP80) and the eukaryotic translation initiation factor 4E (eIF4E), which also binds to the cap [29, 30]. At the 3' end of the mRNA, PABP was shown to inhibit the activity of PARN [28, 31, 32].

PARN is a nucleo-cytoplasmic shuttling protein, mainly localized to the nucleus [25]. It is essential for embryogenesis in plants, catalyzes the deadenylation of maternal mRNAs in *Xenopus laevis* oocytes during maturation [5], and represents the main deadenylase in HeLa S100 extracts [30]. Despite these early data, Yamashita et al. [25] demonstrated that PARN does not play a major role in mammalian mRNA degradation. Lack of homologs of PARN in *S. cerevisiae* or in *Drosophila melanogaster* also indicates that PARN is not required in all eukaryotes [25, 5].

1.2.2 The PAN2-PAN3 Deadeylation Complex

PolyA nuclease (PAN), is a heterodimeric complex, largely localized to the cytoplasm. PAN2 is the catalytic and PAN3 the regulatory subunit of the complex [33, 34]. Like PARN, PAN2-PAN3 is a distributive exonuclease dependent on Mg^{2+} . It also requires a free 3'-OH group and releases 5'-AMP as a product. PAN shortens the mammalian polyA tails down to 110 nt from their normal length of 200-250 nt, and the yeast polyA tails to 50 nt from 70-90 nt [35]. This implies the need for a second complex to take over the PAN activity after the first step of deadenylation is catalyzed by PAN [25]. On the other hand, deletion of *PAN2* in *S. cerevisiae*

or siRNA knockdown in mammalian cells has only subtle effects on mRNA degradation. This suggests that PAN2-PAN3 is not the main deadenylase in the cell [25, 34, 36]

In contrast to the PARN and Ccr4-NOT deadenylases, which are both inhibited by PABP, PAN activity is stimulated by PABP [35, 33, 34]. PAN3 interacts with the C-terminus of PABP [37]. This interaction is needed for the stimulatory effect of PABP on the enzymatic activity of PAN as overexpression of PABP can suppress the deadenylation defect of a *pan* mutant yeast strain. Moreover, interaction of PAN with PABP together with the observation that PAN does not degrade the polyA tail completely suggests that PAN has the ability to sense the number of PABP proteins on the polyA tail. This would eventually lead PAN to lose its affinity for the polyA tail as the number of PABP decreases in the course of deadenylation, explaining why PAN mediates only the first step of deadenylation [36, 25]. Besides its stimulatory role, PABP interaction also increases the substrate specificity of the human PAN2-PAN3 complex [38]. On the other hand, Lowell et al. [35] provided evidence that the activity of PAN can also be regulated by *cis*-acting sequences within an mRNA, like AREs in the 3' UTR.

In addition to its role in cytoplasmic deadenylation and mRNA degradation, PAN is also implicated in the final step of mRNA biogenesis in the nucleus. It is responsible for the trimming of the newly synthesized polyA tail to its mature length, in an mRNA-specific manner [36]. Retention of mRNAs at the site of transcription is observed in yeast cells lacking PAN [39]. This finding points towards the idea of coupling of polyA tail maturation to mRNA export [8].

1.2.3 The Ccr4-NOT Deadenylation Complex

The Ccr4-NOT complex is a global regulator of gene expression, involved not only in mRNA deadenylation but also transcription. As the focus of my thesis is cytoplasmic mRNA decay, I will only mention functions of the Ccr4-NOT complex that are related to mRNA deadenylation. I will first summarize what is known about the composition of the complex, and then focus on the deadenylase subunits Ccr4 and Caf1.

The Ccr4-NOT complex is an evolutionary conserved, multi-subunit complex (see Table 1.1 for comparison of the yeast and human complexes). In gel filtration experiments, Ccr4-NOT is found in two major complexes, ~ 1.0 MDa and ~ 1.9 MDa in size [40]. The ~ 1.0 MDa complex is the core complex while the ~ 1.9 MDa complex includes associated proteins. Thus, the Ccr4-NOT core complex is thought to be a platform that recruits different interactors via its individual subunits to mediate its diverse functions in the cell [41, 42].

Together with PAN2-PAN3, the Ccr4-NOT complex represents the major deadenylases in the cell. While deletion of *CCR4* or *CAF1* slows down deadenylation, double deletion of *CCR4* and *PAN2* completely blocks deadenylation [43]. In contrast to PAN2-PAN3, Ccr4-NOT activity is inhibited by PABP [25]. In addition to the role of Ccr4-NOT in bulk mRNA degradation, the complex can also be recruited to mRNAs via adaptor proteins that recognize sequence motifs in 3' UTRs. For example, Sandler et al. [11] showed that human TTP recruits the Ccr4-NOT complex via its interaction with CNOT1 to ARE-containing mRNAs. Moreover, Behm-Ansmant et al. [20] and Fabian et al. [22] provided evidence that miRNAs interact with the Ccr4-NOT complex, and that this interaction is necessary for mRNA degradation.

In *S. cerevisiae*, the ~ 1.0 MDa complex was shown to contain Not1p-5p, Ccr4p, Caf1p, Caf40p and Caf130p [40]. The largest subunit Not1p is the only essential protein for yeast viability while mutations in Not2p, Not4p and Not5p lead to growth defects. These *in vivo* observations can be explained by the finding that Not2p, Not3p and Not5p contribute to the

1 Introduction

Yeast core subunit	Aliases for yeast subunits	Human core subunit (HGNC)	Aliases for human subunits
Not1	CDC39 ROS1 SMD6	CNOT1	hNOT1
Not2	CDC36 DNA19	CNOT2	hNOT2
Not3		CNOT3S	hNOT3
Not5		CNOT3L	
Not4	MOT2 SIG1	CNOT4N CNOT4S CNOT4L	hNOT4
Ccr4	FUN27 NUT21	CNOT6	hCCR4, Ccr4a
Caf1	POP2	CNOT6L CNOT7 CNOT8	Ccr4b hCAF1, Caf1a hPOP2, CALIF, Caf1b
Caf40		CNOT9	hRcd1, Rqcd1, hCAF40
Caf130		CNOT10 TAB182 C2ORF29	

Table 1.1. Comparison of yeast and human Ccr4-NOT complex components. Table reproduced from Collart and Timmers [42].

stability of Ccr4-NOT complex. Not1p is suggested to be the scaffold of the complex, and the C-terminal 800 amino acids (aas) of the protein appear to be sufficient for this function. The other Not proteins interact with this C-terminal part of Not1p, while the Ccr4p and Caf1p bind with a more N-terminal region in the middle of the protein. Ccr4p is associated with the complex via Caf1p, and is the major deadenylase in the yeast complex. In cells lacking any of the Not proteins, both Ccr4p and Caf1p become essential. This points towards a role of Ccr4p and Caf1p in integrity of the Ccr4-NOT complex, or alternatively, their deadenylation activity becoming more important when other functions of the complex are impaired. Interestingly, Caf130p, interacts with both the N- and C-terminal parts of Not1p. Caf40p behaves like Caf130p, though its interaction site on Not1p has not been determined. These two proteins appear to interact with Not1p on site(s) separate from other Ccr4-NOT proteins, since they do not depend on any other component for Not1p interaction and their deletion does not impair association of other components with Not1p [40, 42].

Recently, Temme et al. [44] published a detailed analysis of the Ccr4-NOT complex in *Drosophila melanogaster*. First of all, the authors found that in the *Drosophila* genome there is one ortholog for yeast Not3p and Not5p, called NOT3. They further showed that the Ccr4-NOT complex has a stable core formed of NOT1, NOT2, NOT3, CAF40, CCR4 and CAF1, while NOT4 is excluded from the core. Surprisingly, RNAi-mediated depletion of individual subunits results in co-depletion of other subunits. This indicates that the subcomplex formation is required for the stability of the Ccr4-NOT complex itself. CCR4 and CAF1 are expressed

throughout the lifetime of the fly, from oogenesis to the adult with a punctuate staining in the cytoplasm [45]. CAF1, NOT1, NOT2 and NOT3 are required for the deadenylation activity of the *Drosophila* Ccr4-NOT complex. In contrast to yeast, CCR4 is dispensable for deadenylation and CAF1 appears to be the main deadenylase [44].

In humans, the Ccr4-NOT complex is conserved with some differences to the yeast complex. Like *Drosophila*, humans have only one ortholog of Not3p and Not5p. The human protein, CNOT3, is expressed as a short and a long isoform: CNOT3S and CNOT3L. In yeast, Not2p and Not5p interact with each other via their Not-Box motifs. CNOT3S lacking the Not-Box motif, does not interact with the human Ccr4-NOT complex. CNOT3L associates with the complex via the Not-Box-mediated interaction with CNOT2 [42, 46]. On the other hand, similar to the situation in *Drosophila*, CNOT4, which can complement yeast Not4p [47], is not an integral subunit of the human Ccr4-NOT complex. Indeed, CNOT4 was detected in a separate 200 kDa complex and its association with the Ccr4-NOT complex may be regulated [46]. Not4 is the only Not protein that has catalytic activity. Both yeast and human Not4 proteins have a RING finger domain at their N-terminus and were shown to have E3 ubiquitin ligase activity [48, 49]. Dimitrova et al. [50] showed that Not4p, in conjunction with the Ubc4p/Ubc5p E2 enzyme, ubiquitinates and leads to proteasomal degradation of translationally arrested nascent polypeptides containing polylysine or polyarginine. Nevertheless, degradation of protein products of mRNAs lacking a stop codon (non-stop mRNAs) was not dependent on Not4p. Deletion of other Not proteins did not affect degradation of the polylysine-containing peptides raising the question if it is Ccr4-NOT associated or free Not4p that mediates this activity.

Lau et al. [46] identified two additional proteins, TAB182 and C2ORF29, being involved in the human Ccr4-NOT complex. In addition, there are two orthologs of both yeast Caf1p and Ccr4p in humans: Caf1a (CNOT7) and Caf1b (CNOT8), and Ccr4a (CNOT6) and Ccr4b (CNOT6L), respectively. The human Ccr4-NOT complex exists in 4 different forms specified by the associated Caf1 and Ccr4 proteins [46]. Moreover, Ccr4a and Ccr4b interact more tightly with Caf1a than with Caf1b. Gene Ontology analysis of the interactors of these complexes indicates that the Caf1a-containing complexes may be involved in mRNA splicing, transport and localization, while the Caf1b-containing complexes may be associated only with splicing [46].

Ccr4 Ccr4, like PARN and PAN2, is a Mg^{2+} -dependent 3' to 5' exoribonuclease. Chen et al. [51] showed that yeast Ccr4p can use both ssDNA and RNA as substrate *in vitro*, with preference for RNA with a 3' polyA tail. Ccr4p processivity depends on the length of the substrate RNA. With substrates longer than 45 nt, it is processive while with shorter substrates it shows distributive activity. Unlike PARN, Ccr4 activity is not enhanced by the 5' cap [52]. In contrast to PAN2-PAN3, Ccr4 is inhibited by PABP [53]. Ccr4 has three main domains: N-terminal activation domain, a central leucine-rich repeat (LRR) with five tandem repeats, and a C-terminal exonuclease III-like domain. The LRR domain binds to Caf1. The activity of the exonuclease domain was confirmed via mutational analysis [51, 52].

Ccr4 is connected to the Ccr4-NOT complex via Caf1, which is also an exoribonuclease. Presence of two deadenylases in the same complex resulted in questioning the contribution of the individual enzymes to deadenylation. In *S. cerevisiae*, deletion of either *CCR4* or *CAF1* leads to slower deadenylation and mRNA degradation rates [43]. Tucker et al. [53] showed that Caf1p is dispensable for Ccr4p catalytic activity *in vitro*, and overexpression of Ccr4p

1 Introduction

in *CAF1* deletion strains could rescue the deadenylation defect. These data suggest that Ccr4p is the major deadenylase in yeast, and that Caf1p may contribute to the affinity of the Ccr4p/Caf1p complex to the substrate mRNA.

Despite its proven role in deadenylation in yeast, the importance of Ccr4 in higher eukaryotes has been challenged by several findings. In *Trypanosoma brucei* no homolog of Ccr4 was found, while orthologs of Caf1, Not1, Not2, Not5 and Caf130 form the Ccr4-NOT complex [54]. Temme et al. [45] showed that in *Drosophila* S2 cells, knockdown of CCR4 does not have a detectable effect on either steady-state polyA tail length or the rate of Hsp70 mRNA deadenylation. In mouse, which has two homologs of Ccr4, Ccr4a and Ccr4b, overexpression of wild type (wt) Ccr4 accelerates decay of stable β -globin mRNA. Moreover, knockdown of both Ccr4 homologs in mouse NIH3T3 cells impairs the second phase of mRNA degradation [25]. Nevertheless, further studies in the same cell line showed that overexpression of Caf1 does also increase the decay rate of β -globin mRNA, and Caf1 knockdown stabilizes the reporter mRNA to a greater extent than the Ccr4 knockdown [27]. Thus, in mouse, Ccr4 is not the major deadenylase but has complementary roles to Caf1 activity. As in mouse, there are two homologs of Ccr4 in humans: Ccr4a (CNOT6) and Ccr4b (CNOT6L). Morita et al. [55] found that both homologs associate with the Ccr4-NOT complex. The authors also provided evidence that the deadenylase activity of Ccr4b, but not Ccr4a, is necessary for proper cell cycle control. Schwede et al. [54] compared the importance of human Ccr4 and Caf1. The results did not show a statistically significant effect of Ccr4a and Ccr4b knockdown on average polyA lengths.

Caf1 Caf1 is a member of the DEDDh family of exonucleases. Some *in vitro* deadenylase activity was detected for yeast Caf1p. Nevertheless, it lacks residues that are thought to be critical for enzymatic activity in the RNase domain [53]. Speaking against the deadenylase activity of yeast Caf1p, Caf1p purified from strains lacking Ccr4p does not possess nuclease activity [43]. Interestingly, employing Caf1p mutants Ohn et al. [56] showed that Caf1p can affect deadenylation independently of its interaction with Ccr4p. This idea is supported by the synthetic lethality of *CAF1* deletion, but not of *CCR4* deletion, with defects in PABP or DHH1, whose protein products are involved in translation. These data indicate that yeast Caf1p contributes to deadenylation both via its interaction with Ccr4p and by an undetermined mechanism independently of Ccr4p.

In contrast to yeast, Caf1 homologs in higher eukaryotes have functional exoribonuclease domains and appear to be the major deadenylase. In *Trypanosomes*, which lack detectable Ccr4 orthologs, Caf1 is an active deadenylase. It is essential for cell survival and reducing its levels increases the average polyA tail length [54]. In *Drosophila* cells, overexpression of a catalytically dead CAF1 mutant inhibits mRNA decay in a dominant-negative manner, whereas, overexpression of inactive CCR4 does not have any effect [44]. This suggests that CAF1 is the major deadenylase also in *Drosophila*. Viswanathan et al. [57] showed that mouse Caf1 is a 3' to 5' exoribonuclease whose processivity is positively affected by the longer substrates. PolyA substrates are preferred by mouse Caf1 and its activity is not influenced by the 5' cap or PABP on mRNA. In human cells, simultaneous depletion of both Caf1 homologs, Caf1a and Caf1b, inhibits deadenylation of bulk mRNA leading to longer polyA tails in average. In addition, knockdown of both Caf1a and Caf1b stabilized a labile reporter mRNA containing an ARE in its 3' UTR [54].

1.3 Decapping and 5' to 3' mRNA Decay

Even though deadenylation is the first and rate limiting step in mRNA degradation, it is not the ultimate death sentence for the mRNA. Deadenylated mRNAs can be stored as translationally silenced species in P-bodies (see Section 1.4). These mRNAs can become readenylated and regain translational ability [58, 59]. On the other hand, removal of the 5' m⁷G structure leaves the mRNA body accessible to degradation, which is an irreversible decision in the life of an mRNA. Once decapped, the mRNA body becomes a substrate for the 5' to 3' exoribonuclease Xrn1 and is quickly degraded [4]. Decapping is catalyzed by the evolutionary conserved Dcp1/Dcp2 decapping complex and several decapping enhancer proteins that stimulate its activity have been identified [60, 61, 62, 63, 64, 13].

The first indications for the presence of decapping and 5' to 3' decay were published by Decker and Parker [1] in 1993. The authors were able to visualize decay intermediates of mRNAs by inserting a poly guanosine (polyG) sequence in the mRNA 3' UTR sequence. polyG forms a strong secondary structure that hinders the yeast exoribonucleases. mRNA fragments lacking the 5' portion were detected from reporters both with short and long half lives, suggesting that degradation of mRNA from its 5' is a general pathway. In parallel, Xrn1 was identified as a processive exoribonuclease, whose deletion led to accumulation of full length but deadenylated mRNAs, that also lacked the cap structure. Furthermore, polyadenylated and capped mRNAs were resistant to hydrolysis by Xrn1 [3, 4]. A detailed analysis of both stable PGK1 mRNA [2] and labile MFA2 mRNA [4] indicated that decapping followed by 5' to 3' decay is the major mode of mRNA degradation in yeast. These studies also put decapping as a potentially regulated step in addition to deadenylation, because 5' to 3' exoribonucleolytic degradation was estimated to be much faster than either of the two previous steps.

1.3.1 The Dcp1/Dcp2 Decapping Complex

The Dcp1/Dcp2 complex responsible for decapping was identified in *S. cerevisiae* and termed mRNA decapping enzyme (Dcp). Initially, Dcp1p was thought to be the active enzyme of the decapping complex [60]. But later on, Dcp2p was shown to be the catalytically active protein, and Dcp1p enhances Dcp2 decapping activity [65]. The reason for this confusion appears to be the selection of the divalent cation in the reaction [66]. Dcp2 has a low level, rather unspecific activity in the presence of Mg²⁺. Both the substrate specificity and the processivity of Dcp2 is enhanced significantly by manganese (Mn²⁺).

Deletion of either *DCP1* or *DCP2* causes accumulation of deadenylated but capped *MFA2* mRNA in addition to several transcripts with slowed turnover rates. Furthermore, both in *DCP1* and in *DCP2* deletion strains there was no detectable decapping activity, as judged by pull-down of reporter mRNA with anti-cap antisera [60, 67]. Moreover, neither Dcp1p purified from a *dcp2*Δ strain nor Dcp2p purified from a *dcp1*Δ strain showed decapping activity. These data strongly indicated that Dcp1p and Dcp2p function as a complex. Supporting this idea, Dcp2p and Dcp1p interact with each other both *in vitro* and *in vivo* [67].

Dcp2p contains a Nucleotide diphosphate linked to an X moiety (Nudix) pyrophosphatase motif. The N-terminal region of Dcp2 containing this motif is necessary and sufficient for decapping of both yeast and human mRNAs [67, 68]. Characterization of the decapping complex showed that 7-methyl group on the cap and 5' of the mRNA body are important for substrate recognition, and longer substrates (>25 nt) are preferred [69]. The cap is cleaved at the 5'-triphosphate linkage, and the decapping reaction releases 7-methylated guanosine

1 Introduction

diphosphate (m^7GDP) and 5'-monophosphate mRNA [60]. Importantly, cap structure alone or cap analogs are not utilized by the decapping enzyme [69].

Via *in silico* searches two homologs of yeast Dcp1p, termed Dcp1a and Dcp1b, and one homolog of Dcp2p were identified in humans by several groups [61, 70, 68]. The N termini of the human Dcp1 proteins show homology to both the N- (which is important for decapping) and the C-termini of the yeast protein. Both of the human Dcp1 proteins include ~ 450 aa long C-terminal extensions compared to the yeast Dcp1p. Likewise, Dcp2 proteins share high homology at their N-termini, where the NudIX motif responsible for decapping activity is located, however human Dcp2 lacks the central region of the yeast protein. Human Dcp1 and Dcp2 interact independently of RNA, implying complex formation as shown for the yeast proteins. Nevertheless, human Dcp1 and Dcp2 depend on Hedls, a metazoan-specific decapping enhancer, for their interaction [13]. Recombinant hDcp2 purified from *E. coli* exhibits *in vitro* decapping activity while no activity is detectable with recombinant hDcp1. Recombinant hDcp1 also failed to stimulate the activity of recombinant hDcp2, probably due to the requirement for additional protein(s) to mediate the hDcp1-hDcp2 interaction. Mutations in the NudIX motif of hDcp2 (either glutamic acid 147 (E147) alone or together with E148) abolishes its activity, supporting the notion that hDcp2 is the decapping enzyme in humans [61, 70]. The functional properties of human Dcp2 are similar to the yeast decapping complex. hDcp2 recognizes the methylated cap in context of the mRNA body, with increasing processivity on longer mRNAs. Substrate hydrolysis releases m^7GDP [68, 71]. It was shown that the activity of human Dcp2 is minimal unless Mn^{2+} is present in the reaction [66].

Dcp2 binds RNA Dcp2 substrate recognition and activity depend on the mRNA body, raising the question whether Dcp2 binds to RNA. This was proved to be the case by Piccirillo et al. [66] and Deshmukh et al. [72]. Cap recognition by Dcp2 requires RNA binding, which is independent of cap itself. The N-terminal NudIX fold and conserved sequences flanking it were shown to be important for RNA binding [66]. In addition to these data, the structure of the NudIX domain of Dcp2p (aa 100-245) proved that Dcp2p is an RNA-binding protein [72]. RNA binding is predicted to occur at a basic channel that runs along the dorsal surface of the NudIX domain. Deshmukh et al. [72] also provided evidence that cap recognition by the Nudix domain is weak, but specific, and requires the cap to be bound to a longer RNA. Moreover, the authors showed that RNA binding by Dcp2p is sequence-independent and stronger than binding to the cap. RNA binding was, therefore, suggested to increase the local cap concentration, thereby accelerating the slow, rate limiting step of cap hydrolysis.

Substrate specificity of the Dcp1/Dcp2 decapping complex The ability of Dcp2 to bind RNA then raised another question: Is Dcp2 a canonical enzyme, or does it have preference for a subset of mRNAs? Li et al. [73] addressed this question by analyzing mRNAs associated with human Dcp2 protein. In addition to several hundreds of mRNAs identified to interact with Dcp2, the mRNA encoding Rrp41 was enriched >6 -fold compared to control. Rrp41 is a component of the core exosome, the machinery that degrades mRNAs from the 3' end [74]. Rrp41 mRNA being a high affinity substrate for Dcp2 indicates a potential interplay between the 5' to 3' and 3' to 5' mRNA degradation complexes. A 60 nt GC rich sequence at the 5' end of the Rrp41 mRNA is able to trigger faster degradation of a chimeric reporter mRNA in a position-dependent manner. Hence, the GC rich sequence is important for higher association with Dcp2 and the enhanced rate of decapping. Li et al. [75] analyzed this 60 nt

sequence further and showed that the first 33 nt form a stem-loop structure. The stem-loop structure and not the primary sequence is important for Dcp2 binding. Using bioinformatics, the authors were able to identify 239 potential transcripts with similar stem-loops in their 5' UTR. 3 examples chosen from this set of mRNAs were confirmed to have higher decapping rates [75]. Moreover, phosphorylation of yeast Dcp2p upon stress was shown to interfere with only a small subset of mRNAs. The group of mRNAs up-regulated more than 2-fold in the phosphomimetic Dcp2p strain included several mRNAs coding for ribosomal proteins [76]. Therefore, although Dcp2 is believed to catalyze decapping of all cellular mRNAs, it does have a preference for certain mRNAs and exhibits different rates of decapping on its substrates.

Recent data indicates that Dcp1a also contributes to the selective targeting of some substrates by Dcp2 [77]. It was shown that phosphorylation of Dcp1 by the c-Jun N-terminal kinase (JNK) pathway (see paragraph *Regulation of decapping via phosphorylation*) can lead to stabilization of some mRNAs while increasing the turnover rate of others. Nevertheless, the observation that small amounts of Dcp1a localize in the nucleus raises the possibility of transcriptional regulation by Dcp1a. This puts into question the differential decapping hypothesis, at least the contribution by Dcp1. Importantly, phosphorylation of Dcp1a did not affect the decapping activity of Dcp2 on a given substrate [77].

Role of Dcp1 in Dcp2 activation Dcp1 and Dcp2 work as a complex with Dcp2 being the catalytic subunit. Dcp1p is required for activation of Dcp2p as its deletion leads to complete loss of decapping in yeast [60, 67]. Nevertheless, it remained elusive how Dcp1p enhances Dcp2p activity. The decapping complex was shown to possess low basal catalytic activity, and several proteins were identified to interact with the complex and to stimulate the decapping activity (see Subsection 1.3.2). Therefore, it is proposed that Dcp1p is the critical factor that mediates interactions of the complex with these decapping enhancers [62].

The crystal structure of Dcp1p revealed its resemblance to the Enabled/VASP homology 1 (EVH1) family of proteins, which share proline-rich sequence (PRS)-binding sites [78]. There are two apparent conserved sequence patches on the surface of Dcp1p and an additional conserved hydrophobic patch. All three patches are located at the N-terminal half of the protein. The first patch corresponds to the EVH1 PRS-binding site and was proposed to be the interaction site for the decapping enhancers. Mutations in this patch do not affect the decapping activity of recombinant Dcp2p *in vitro*. The second patch is important for the activity of Dcp1p/Dcp2p, but not for the interaction of Dcp1p with Dcp2p. Dcp1p mutated in the second patch inhibits decapping both *in vivo* and *in vitro*. Similar to patch 2, the hydrophobic patch is also required for decapping activity, but dispensable for Dcp1p-Dcp2p interaction. The hydrophobic patch is located C-terminal to patch 2. Their close proximity suggests that they can regulate Dcp2 activity together, possibly via ligand binding [78]. Deshmukh et al. [72] determined the structure of yeast Dcp1p together with the NudiX domain of Dcp2p by nuclear magnetic resonance (NMR). The data showed that Dcp1p promotes the catalytic step of decapping by roughly 1000-fold, but does not affect RNA binding. In conclusion, Dcp1p enhances the rate limiting catalytic step of decapping by Dcp2p, but not substrate recognition.

The structure of *Schizosaccharomyces pombe* Dcp1p in complex with Dcp2p by She et al. [79] revealed that Dcp2p exists in an open and a closed conformation (see Figure 1.2). Residues N-terminal to Dcp2p NudiX domain (NTD), which interact with Dcp1p, form a separate globular lobe together with Dcp1p. In the open conformation, this lobe does not contact the

1 Introduction

NudiX domain. The closed conformation is defined by the presence of the Dcp2p NTD and Dcp1p in close proximity of the NudiX domain, thereby putting the two lobes of the complex together. The closed conformation is catalytically active, and the protein cycles between open and closed states. Introducing prolines in the interdomain linker that connects the two lobes disables the closed state and inhibits decapping [80]. Both the NTD and the catalytic domain of *S. pombe* Dcp2p specifically interact with the cap with almost identical affinities. These data imply that the active site of Dcp2p is formed by contribution of both domains and needs closure to occur. Therefore, the closed conformation is stimulated by substrate binding and is stabilized by binding of Dcp1p and decapping enhancers. Alternatively, Dcp1p can also exert its enhancing effect by increasing the rate of closure [80, 79]. The PRS-binding site of Dcp1p does not overlap with its Dcp2p interaction site, allowing Dcp1p to interact with Dcp2p and decapping enhancers simultaneously. This gives Dcp1p the ability to enhance Dcp2p activity even further [79, 81].

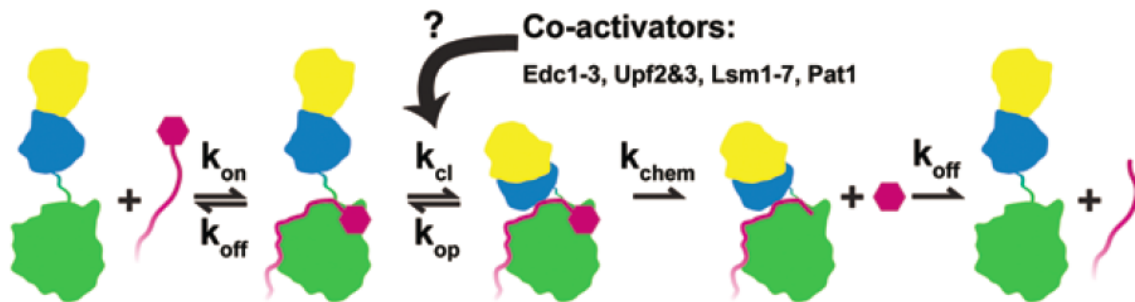


Figure 1.2. Model explaining the regulation of Dcp1p/Dcp2p decapping activity by open and closed conformations. Cartoon represents yeast Dcp1p (yellow) in complex with Nudix domain (aa 100-245) of Dcp2p (blue: N-terminal part preceding Nudix domain (NTD), green: Dcp2p NudiX domain, purple: mRNA with cap depicted as a hexagon). Please refer to text for details. (NMD factors Upf2 and Upf3 are also known to interact with, and stimulate decapping activity of the Dcp1/Dcp2 complex. As NMD is out of scope of this thesis I did not mention them in the text.) Figure was taken from Floor et al. [82].

The structure of Dcp1 from human and *Drosophila* revealed that the protein forms a trimeric complex [83]. Dcp1 proteins from metazoa, except for *Caenorhabditis elegans*, and plants share a conserved C-terminal proline rich extension that is missing in yeast proteins. This domain adopts a kinked α -helix and mediates trimerization of the protein in an asymmetrical antiparallel assembly. The two human Dcp1 homologs, Dcp1a and Dcp1b, can also form heteromers via trimerization. Indeed, trimerization is a requirement for formation of an active decapping complex and decapping activity *in vivo*. Trimerization is also important for the interaction of human Dcp1a with Dcp2 and human enhancer of decapping large subunit (Hedls), but not with other decapping activators. In line with its requirement for active decapping complex formation, trimerization is also needed for Dcp1a to localize to P-bodies [83].

Role of PABP and eIF4E in decapping Decapping is preceded by deadenylation. This implies an inhibitory effect of the polyA tail or PABP on the decapping complex. In *S. cerevisiae*, deletion of the *PAB1* gene, which encodes for yeast PABPp, abolishes the need for deadenylation, i.e. in this strain mRNA decapping takes place prior to deadenylation [84].

In addition, decapping of a polyadenylated reporter mRNA can be enhanced by introducing a polyA RNA as a competitor in an *in vitro* assay [85]. Therefore, PABP appears to be a factor that blocks Dcp1p/Dcp2p activity. Negative regulation of decapping by the polyA tail and PABP is also conserved in humans [70]. Looking for the mechanism behind the PABP-mediated inhibition of decapping Khanna and Kiledjian [71] showed that this inhibition cannot be competed out by a cap analog. This implies an eIF4E-independent mechanism. Indeed, the authors provided evidence that PABP itself, via its second RNA-recognition motif (RRM), binds the m⁷G cap, with simultaneous polyA binding. The PABP-cap interaction is proposed to protect the cap from the Dcp1/Dcp2 complex. This function of PABP seems to be specific to the mammalian cytoplasmic PABP, as neither yeast PABP nor human nuclear PABP, PABPN1, can protect the cap from Dcp1/Dcp2.

The decapping complex is also inhibited by the cap-binding protein eIF4E. In yeast, eIF4Ep competes with Dcp1p/Dcp2p for cap binding [86]. Addition of recombinant eIF4Ep to an *in vitro* decapping reaction inhibits decapping activity. On the other hand, addition of cap analog to cell extracts increases decapping [85]. Moreover, a temperature sensitive *eIF4E* mutant rescues both the decapping defect and the slow mRNA decay in a *dcp1* mutant strain. In contrast to yeast, Wang et al. [70] failed to detect enhancement of decapping activity by cap analog in mammalian cell extracts.

3' uridine tracts (U-tracts) stimulate decapping in mammalian cell extracts In addition to the 5' cap and 3' polyA tail, Song and Kiledjian [87] demonstrated that a 3' U-tract also influences the decapping rate. Addition of up to 15 uridines at the 3' end of the reporter mRNA stimulated decapping by Dcp2 and prevented degradation from the 3' end, in a position-dependent manner. Nevertheless, recombinant Dcp2 fails to recognize U-tract-containing mRNA. This points towards the requirement of additional factors to signal the 3' U-tract to Dcp2. In fact, several proteins known to enhance decapping (see Subsection 1.3.2) were found to bind U-tract-containing mRNAs [63, 88].

Regulation of decapping via phosphorylation Dcp1p is known to be a phosphoprotein since 1998 [69] but the role of this phosphorylation on decapping remained unaddressed. Recently, Rzczkowski et al. [77] identified serine 15 (S315) in human Dcp1a to be phosphorylated by JNK. JNK co-immunoprecipitates with Dcp1a and co-localizes with Dcp1a in P-bodies. Explanation of the role of this phosphorylation is not straightforward. Continuous activation of JNK leads to delocalization of Dcp1a from P-bodies while IL-1 induced transient activation of JNK increases Dcp1a positive P-body numbers. Nonetheless, S315 is not included in the regions that are important for stimulating decapping or binding of Dcp1a interaction partners. Although differential stabilization of some transcripts has been reported, the exact role of Dcp1a S315 phosphorylation on decapping or the activity of Dcp1a remains obscure.

Dcp2 is also a phosphoprotein. In *S. cerevisiae*, Ste20p, a MAPKKKK, phosphorylates Dcp2p at S137 both *in vivo* and *in vitro* under several stress conditions [76]. Although S137 is located adjacent to the catalytic site, neither the S137A nor the S137E mutations alter the *in vitro* decapping activity. Consequently, Dcp2p phosphorylation is unlikely to affect global mRNA decay. Indeed, only a small subset of mRNAs were identified to be up-regulated more than 2-fold in a S137E mutant strain. Phosphorylation of Dcp2 under stress appears to be more important for interactions and localization of the protein rather than the decapping activity itself. In fact, Dcp2p phosphorylation is necessary to maintain localization of Dcp2p

1 Introduction

to P-bodies, optimal formation of stress granules, and for its interaction with the decapping enhancer Dhh1p (see Subsection 1.3.2) [76].

Localization of the decapping complex Similar to the deadenylation complexes PAN2-PAN3 and Ccr4-NOT, the decapping complex Dcp1/Dcp2 localizes to the cytoplasm [70, 68]. Interestingly, the decapping complex shows punctuate localization in the cytoplasm. These foci were shown to contain many proteins involved in mRNA degradation and termed ‘Processing bodies’(see below Section 1.4).

1.3.2 Decapping Enhancers

Decapping enhancers are a group of proteins that stimulate the activity of the Dcp1/Dcp2 decapping complex. They associate with the decapping complex mostly via Dcp1. On Dcp1, the EVH1 PRS-binding site is a conserved patch where the decapping enhancers are suggested to bind [78]. Comparing sequences of 20 proteins that interact with Dcp1p, Borja et al. [81] were able to identify FPRP[S/T][F/W] as a preferred proline rich motif that Dcp1p binds to. Tritschler et al. [83] observed that Dcp1 trimerization mutants fail to interact with Hedls and Dcp2, but the interactions with Edc3 (enhancer of mRNA decapping (Edc)) and Rck are not affected. Therefore, it is possible that Dcp1 forms different subcomplexes, one including Hedls and Dcp2, a second one with Edc3 and Rck, and a third combining both subcomplexes [83]. The general idea is that the decapping enhancers have roles in different steps of messenger ribonucleoprotein (mRNP) assembly and/or rearrangement leading to a decapping compatible mRNP [82]. In addition, the decapping enhancers can be divided into two groups: (1) Proteins that are not rate limiting, but can affect the process of decapping. These include Edc1p, Edc2p and Edc3. (2) Regulatory proteins, whose deletion blocks decapping partially. These proteins are thought to be general activators of decapping and include Lsm1-7, Pat1, Rck and Hedls [64].

Edc1p and Edc2p Edc1p and Edc2p are yeast-specific proteins as their homologs in higher eukaryotes have not been identified yet. In yeast, single or double deletion of *EDC1* and *EDC2* do not show any phenotype. Nevertheless, double deletion of both *EDC1* and *EDC2* genes in a *dcp1* mutant strain abolishes decapping to the levels observed in a *DCP1* deletion strain [62]. Moreover, recombinant Edc1p and Edc2p were shown to stimulate the Dcp1p/Dcp2p decapping complex individually in *in vitro* reactions [65]. Therefore, Edc1p and Edc2p appear to stimulate decapping activity, with Dcp1p being more sensitive to Edc1p and Dcp2p to Edc2p [62].

Edc1p and Edc2p interact with Dcp1p [62, 81]. Edc1p was shown to interact with the Dcp1 PRS-binding site via its C-terminus. Deletion of the Edc1 C-terminus eliminates the ability of the protein to enhance decapping, both *in vitro* and *in vivo* [89]. For both proteins the decapping activation and the Dcp1p binding sites are separate from each other. Nevertheless, mutating residues either on Dcp1p or on Edc proteins that would hinder their interaction, reduces the ability of Edc1p and Edc2p to activate decapping [81]. On the other hand, Dcp1p binding itself is not sufficient for stimulation of decapping. Edc1p and Edc2p both increase the affinity of the decapping complex for RNA and the rate of catalysis [62, 81]. Further analysis by Schwartz et al. [89] showed that Edc1p and Edc2p are indeed RNA-binding proteins. Although the RNA binding activity of Edc proteins is independent of the cap, they are able to overcome the eIF4Ep-mediated inhibition of decapping.

Both Edc1p and Edc2p are basic proteins. This property, although it does not explain the specificity for RNA, might be responsible for Edc1p's RNA binding ability. This is suggested to be the case as RNA binding could not be attributed to any part of the protein [89]. Schwartz et al. [89] showed that Edc1p, but not Edc2p, is important for regulation of gene expression when yeast is switched from fermentative to aerobic respiration. RNA binding properties of Edc1p do not explain why only Edc1p is involved in this regulation. However, RNA binding together with decapping complex association, may enhance the substrate binding by Dcp1p/Dcp2p and/or catalytic activity.

Edc3 Edc3p, also termed Lsm16, was identified as a protein having yeast two hybrid (Y2H) interactions with the decapping complex and decapping enhancers. Like *EDC1* and *EDC2*, deletion of *EDC3* does not affect either the growth of yeast or degradation of reporter mRNAs. The function of Edc3p becomes apparent when its deletion is combined with temperature sensitive yeast mutants in both 5' to 3' and 3' to 5' decay. In this strain background, the turnover rate of MFA2 mRNA is slowed down without a change in the deadenylation rate. Thus, Edc3p is an enhancer of decapping that likely stimulates the Dcp1p/Dcp2p decapping complex [64].

The human homolog of Edc3p was identified by Fenger-Grøn et al. [13] as an interaction partner of human Dcp1a and Dcp1b. For the interaction of ectopically expressed human Dcp2 with Edc3, co-expression of Dcp1a and Hedls are required, while the Rck-Edc3 interaction does not depend on co-expression of any other factor. In addition, association between Edc3 and TTP was also observed, indicating its involvement in ARE-mediated mRNA decay [13].

In the yeast Edc3 protein three domains have been identified: (1) a divergent Sm Like (Lsm) domain at the N-terminus, (2) a FDF domain in the middle, and (3) a Yjef-N domain at the C-terminus. The Lsm and FDF domains mediate the interaction with Dcp2p N-terminus [90, 91, 92]. The FDF domain also associates with C-terminal domain of Dhh1p (*S. cerevisiae* homolog of Rck). Surprisingly, the YjeF-N domain interacts with itself, thereby mediating Edc3p self-interaction [90]. Like Dcp2 and the other enhancer proteins, Edc3 localizes to P-bodies [64, 13]. Different from the other decapping enhancers, an active role for Edc3p in P-body assembly has been proposed. Although Edc3p is not required for P-body formation. Decker et al. [90] suggested that Edc3p acts as a scaffolding protein that supports the formation of microscopically visible P-bodies via its interaction with other proteins and self-interaction. Hence, a possible explanation for the decapping enhancement seen by Edc3p is the ability of the protein to form P-bodies, thus increasing the local concentration of mRNA substrates and decapping factors. On the other hand, an Edc3p mutant protein lacking the YjeF-N domain could still rescue the growth and mRNA degradation defects resulting from *EDC3* deletion in cells defective in both 5' to 3' and 3' to 5' decay pathways [90]. Along the same lines, deletion of residues in Dcp2p that are required for Edc3p interaction reduces Dcp2p activity [91]. Furthermore, Nissan et al. [92] showed that recombinant Edc3p stimulates Dcp2p in the absence of Dcp1p, and the Edc3-Lsm domain is sufficient for this. Together, these data indicate that Edc3p enhances decapping both by stimulating P-body formation and directly affecting the activity of Dcp1p/Dcp2p. Genetic interactions between *EDC3* and *SCD6* point towards the possibility of redundancy between the two proteins, which might explain the subtle effect seen in the *edc3* Δ strain [93].

In an attempt to find mRNAs that are differentially regulated by Edc3p, only one single mRNA coding for yeast ribosomal protein RPS28B was identified. Rps28p autoregulates its

1 Introduction

own mRNA via binding to a conserved hairpin structure in the 3' UTR. Edc3p appears to be important for destabilization of this mRNA together with Rps28p itself [94]. In addition, Edc3p is also implicated in the cytosolic decay of YRA1 pre-mRNA that escapes to the cytoplasm without being spliced [95]. Edc3p recognizes and binds to an element in the 5' half of the YRA1 intron. Since abolishing the interaction of Edc3p with the decapping complex does not affect Edc3p-mediated YRA1 pre-mRNA degradation, it is not yet clear how Edc3p induces mRNA decay [96, 91].

Hedls Hedls (human enhancer of decapping large subunit), also termed Edc4 or Ge-1, was identified by Fenger-Grøn et al. [13] as another protein interacting with Dcp1a. Unlike other decapping enhancers, Hedls does not have a yeast homolog. Requirement for Hedls in decapping emerges from the fact that human Dcp1 and Dcp2 do not interact directly with each other. All three proteins are needed to form the trimeric complex as neither Dcp2 nor Hedls interact with Dcp1a alone [13, 97].

In addition to stimulating decapping via complex formation, Hedls also enhances the catalytic activity of Dcp2. An ARE-containing reporter mRNA that was found to associate with Hedls was preferentially deadenylated [13]. Hedls localizes to P-bodies. In *Drosophila*, the conserved C-terminal part of the protein is necessary and sufficient for P-body localization [97]. Hedls is an essential P-body protein, and both the number and size of the P-bodies increases when Hedls is overexpressed [13]. Structural analysis of the C-terminal conserved domain of the *Drosophila* protein indicated that in the context of the full length protein, it can lead to oligomerization [97]. Hedls-mediated oligomerization may then support P-body formation.

p54/Rck p54/Rck belongs to the family of DEAD-box RNA helicases, which possess RNA-dependent ATPase activity. In *Xenopus* and *Drosophila* early oogenesis, the Rck homologs, Xp54 and Me31B respectively, were implicated in translational suppression [98, 99, 100]. In *Xenopus* oocytes, Xp54 was shown to be part of cytoplasmic, translationally silenced mRNPs that contain polyA tails [98]. The data on the effect of Xp54 on translation are rather confusing. Xp54 was shown to suppress the translation of a tethered, *in vitro* transcribed and capped mRNA. The efficiency of translational suppression by Xp54 is reduced when the reporter mRNA has a polyA tail [99]. Confusing the situation even further, mutating residues that disturb the Xp54 helicase activity (either inhibiting the ATPase or the RNA binding activities) enhanced translation of the non-adenylated reporter. The mutant proteins did not affect on translation of the adenylated reporter mRNA. It is possible that Rck-mediated translational suppression is regulated *in vivo* by the polyA tail length [99]. Likewise, the *Drosophila* homolog, Me31B, was also shown to be required for translational inhibition of maternal mRNAs while they are transported from nurse cells to the oocyte [100]. The yeast protein, Dhh1p, is also indicated as a general suppressor of translation under stress conditions [101]. Overexpression of Dhh1p is sufficient to disassemble polysomes. On the other hand, single deletion of *DHH1* does not lead to detectable changes in translation. When combined with a *pat1*Δ strain, *DHH1* deletion fails to block translation upon glucose starvation. This points towards redundant roles of Dhh1p and Pat1p in regulation of translation under stress. Moreover, the mechanism of suppression does not depend on the cap structure, as suppression was also observed on reporter mRNAs containing internal ribosome entry sites (IRESs) from several viruses [101].

Fischer and Weis [102] provided evidence that the yeast protein, Dhh1p, has a role in mRNA decapping. Deletion of *DHH1* alone leads to stabilization of several mRNAs although their deadenylation takes place normally. These stabilized mRNAs are still capped. In addition, Dhh1p interacts with Dcp2p, Xrn1p and Pat1p, supporting its role in 5' to 3' mRNA decay [102, 90]. Strikingly, Dcp1p purified from a *dhh1* Δ strain was less able to enhance decapping [102]. Direct interaction of Dhh1p with Dcp2p, through the N-terminus of Dcp2p, was reported by Nissan et al. [92]. Nevertheless, the authors failed to detect a stimulation of the decapping complex by recombinant Dhh1p *in vitro*. The human homolog, Rck or DDX6, was also found to interact with human Dcp2, Dcp1a and Edc3 [13].

Given the above data, Dhh1p more likely acts on mRNA degradation as a suppressor of translation rather than directly affecting the catalytic activity of decapping. In turn, Dhh1p might positively stimulate decapping by increasing the fraction of non-translating mRNPs, making them substrates for decapping.

DEAD-box RNA helicases contain a core of two RecA-like domains flanked by N- and C-terminal extensions. Cheng et al. [103] solved the crystal structure of the helicase core of the yeast Dhh1p protein. The structure confirmed the presence of two RecA-like domains in Dhh1p although the domain arrangement is unique to Dhh1p, with several inhibitory interactions between the two domains. The N-terminal RecA-like domain is implicated in ATP binding and hydrolysis. RNA binding requires residues from both N- and C-terminal domains. This implies that the RNA binding surface can be rearranged according to the orientations of the two domains. A cycle of conformational changes has been proposed for Dhh1p function. ATP binding and hydrolysis would induce conformational changes that could alter RNA binding, ATP hydrolysis leading to the release of RNA [103, 104]. The structure of the C-terminal RecA-like domain of human Rck, bound to the FDF peptide of Edc3, was solved by Tritschler et al. [105]. Mutational analysis of the *Drosophila* protein showed that Edc3 interaction is important both for translational suppression and P-body localization of Me31B. The C-terminal RecA-like domain of Xp54 was also shown to be sufficient for inhibition of translation of tethered mRNAs. The same domain mediates P-body localization of the human protein, but conserved residues essential for the proposed helicase activity are also required [106].

Biochemical characterization of Dhh1p revealed low ATPase activity and no detectable dsRNA unwinding activity [104]. Although low, the ATPase activity is important for *in vivo* mRNA destabilization by Dhh1p. One possible function of Dhh1p might be the transport of bound mRNAs into P-bodies for translational suppression and decay. Stimulation of the ATPase activity by P-body proteins would then cause the release of mRNA in P-bodies and recycling of Dhh1p from P-bodies [104]. Therefore, it has been suggested that the C-terminal RecA-like domain of Rck mediates the interactions of the protein and that the ATPase (and the potential helicase) activity mediates RNP remodeling [106]. Supporting this idea, the C-terminal part, including the RecA-like domain, of *Drosophila* Me31B was shown to interact with Lsm1, Edc3 and HPat (Pat1p *Drosophila* homolog) [107].

Chu and Rana [108] showed that human Rck forms a complex with Ago2, an important component of RNAi-mediated gene silencing. The Ago2-Rck interaction does not depend on RNA, and Rck mediates the localization of Ago2 to P-bodies. In addition, Rck was needed to suppress both general and miRNA-mediated translation. Nevertheless, knockdown of Rck did not affect siRNA-mediated gene silencing. Thus, the authors suggested that miRNAs use the general translation suppression property of Rck and recruit the protein to target mRNAs [108].

1 Introduction

The Lsm1-7 complex Lsm1p was identified by Boeck et al. [109] as a protein, which when mutated caused accumulation of capped but deadenylated mRNAs. The first hints that the Lsm proteins form heptameric complex(es) came from interaction analysis using Lsm proteins as baits. Fromont-Racine et al. [110] detected several interactions among the Lsm proteins in Y2H screens. In addition, association of Lsm1p with Lsm proteins 2p to 7p were seen by co-immunoprecipitation assays [111, 112]. Importantly, the yeast Lsm proteins 1p to 7p form a complex that is functionally distinct from Lsm2p-8p, which associates with and stabilizes U6 small nuclear RNA (snRNA). Mutations in the yeast Lsm proteins 1p, 2p, 5p, 6p and 7p lead to slower decay rates of reporter mRNAs, with increased levels of full length mRNAs and decreased levels of decay intermediates [109, 111, 112, 113]. In contrast, mutations in Lsm8p did not affect the decay rates of the same reporter mRNAs. In fact, Lsm1p and Lsm8p seem to compete with each other for complex formation with the Lsm 2p-7p proteins [114]. The defect in mRNA decay in Lsm mutants is less pronounced than that in *dcp1* Δ or *dcp2* Δ strains, as is the case for many decapping enhancer proteins [112]. Moreover, Lsm proteins 1p-7p, but not Lsm8p, interact with Dcp1p/Dcp2p and Xrn1p in Y2Hs and in pull-down assays [109, 112, 110, 111]. Therefore, the Lsm1p-7p complex represents yet another decapping enhancer.

The Lsm1p-7p complex associates with mRNAs that are targeted for degradation. Several lines of evidence support this idea. First, the Lsm1p-7p associated mRNAs are deadenylated but still capped [109, 112, 63]. Second, 5' to 3' degradation products are enriched in Lsm1p pull-downs, also indicating that the Lsm1p-7p complex remains on the 3' UTR of the RNA during degradation. Third, interaction of Lsm1p with Dcp2p depends on RNA. While Lsm1p-7p binding to RNA does not require either the decapping complex or Pat1p, the Lsm1p-7p complex does increase the affinity of the decapping complex for mRNA substrates [112, 63]. Still, Lsm1p-7p and Pat1p are likely to work together in mRNA degradation as the double deletion of both genes gives a similar results to the single deletion strains, with respect to mRNA degradation [101].

The Lsm1p-7p complex-Pat1p interaction was reported several times by Y2H, by *in vivo* and by *in vitro* co-immunoprecipitation assays [109, 115, 112, 110, 111]. Therefore it has been suggested that Lsm1p-7p proteins form a tight complex with Pat1p, and exert their effect(s) on mRNA degradation as a complex. The Lsm1p-7p/Pat1p complex was suggested to bind the 3' end of mRNAs with short polyA tails and protect the mRNA from further trimming [109, 116]. Heptameric rings formed by Sm or Lsm proteins are known to bind RNA 3' ends, with preference for oligoA or oligoU stretches. Reporter mRNAs that are shorter than the fully deadenylated species were observed in an *lsm1* Δ strain [109]. Further analysis showed that the same mRNA species accumulate also in a *pat1* Δ strain [116]. Interestingly, trimming of mRNA 3' ends was not detected in strains with *DCP1* deletion. This implies that trimming is not a cause of defective decapping, which is also observed in *lsm1* Δ or *pat1* Δ strains [116]. In addition, the Lsm1-7 complex was found to bind the unusual 5' polyA sequence in poxvirus mRNA, which is capped and polyadenylated, and to stabilize the mRNA [117]. Thus, it is tempting to speculate that the Lsm1-7/Pat1 complex binds to the remaining 3' oligoA tail after deadenylation and prevents its degradation from the 3' end while stimulating decapping and 5' to 3' decay.

Formation of a mammalian complex similar to yeast Lsm1p-7p was confirmed by Ingelfinger et al. [118]. Interestingly, Lsm1-7 proteins were found to co-localize with the decapping proteins Dcp1/Dcp2 in P-bodies in the cytoplasm. The yeast Lsm1p-7p complex also localizes to cytoplasmic P-bodies, unlike the Lsm2p-8p complex which localizes to the nucleus [114].

As an exception among the Lsm proteins, Lsm4p contains an additional glutamine/asparagine (Q/N)-rich prion like domain. This aggregation-prone domain was suggested to participate actively in P-body formation, especially in the absence of Edc3p [90].

Scd6 Genetic interaction between SCD6 (also termed Lsm14, Rap55, TraI, or CAR-1) and EDC3 indicated a role for Scd6p in mRNA degradation. In agreement with this, Scd6p was found to interact with Edc3p, Dcp1p, Dcp2p and Dhh1p in Y2H screens. Although single deletion of *SCD6* does not affect mRNA decay, double deletion of *SCD6* and *EDC3* blocked 5' to 3' degradation of deadenylated mRNAs [93]. These results suggest redundancy between Scd6p and Edc3p. Recombinant Scd6p was also shown to interact with Dcp2p but not with Dcp1p [92]. However, recombinant Scd6p failed to stimulate Dcp1p/Dcp2p activity *in vitro*. Nissan et al. [92] showed that Scd6p represses translation initiation by interfering with 48S translation initiation complex formation, regardless of the cap structure on the mRNA. Thus, Scd6p is likely to enhance decapping activity by increasing the availability of substrate mRNAs for the decapping enzyme, similar to the activity of Dhh1p.

1.3.3 Nudt16, an Alternative to Mammalian Dcp2?

It came as a surprise that Dcp2 is not uniformly expressed, even being absent in some mouse tissues, when Jiao et al. [119] analyzed the distribution of Dcp2. This was true both for protein and mRNA levels. In addition, only modest effects were seen on mRNA half lives upon disruption of Dcp2 gene expression in mouse embryonic fibroblasts. These data strongly imply the presence of a second cytoplasmic decapping enzyme. Nudt16 was known to decap the U8 small nucleolar RNA (snoRNA) in *Xenopus*. Although this protein is nucleolar in *Xenopus*, it represents a potential candidate. Indeed, Jiao et al. [119] showed that Nudt16 is a cytoplasmic protein, with small amounts detectable in the nuclear fraction of mammalian cells. Moreover, Nudt16 is expressed in all mouse tissues tested. Recombinant Nudt16 possess *in vitro* decapping activity, and its knockdown stabilized some of the tested mRNAs [119].

The existence of two cytoplasmic decapping proteins raises the question which one is more important in mRNA decay. A recent analysis by Li et al. [120] using single or double knockdown of Dcp2 and Nudt16 shed light on this question. Dcp2 appears to be the enzyme utilized in NMD as its absence stabilizes reporter mRNAs containing premature termination codon (PTC), while there is no effect of Nudt16 knockdown. miRNA-mediated gene silencing uses both enzymes, making them redundant for this decay pathway. Utilization of the decapping enzymes in ARE-mediated mRNA decay is transcript-specific. Some mRNAs containing AREs are effected by the loss of Dcp2, others by the loss of Nudt16, while for some Dcp2 and Nudt16 appear to be redundant [120].

1.4 Processing Bodies

P-bodies are cytoplasmic foci where proteins involved in deadenylation and 5' to 3' mRNA degradation are enriched. They are small, spherical structures, 100-300 nm in diameter in mammalian cells [121]. Although mammalian cells possess only few P-bodies per cell at resting state, their number and size increase under stress conditions. P-bodies in *S. cerevisiae* are hardly visible unless the cells are stressed, or expression of certain P-body components is modified. P-bodies do not contain ribosomal proteins or translation factors, with the

1 Introduction

exception of eIF4E, indicating the presence of non-translating mRNPs only. Translationally suppressed mRNAs can also return from P-bodies to polysomes when translation is activated [122]. Nevertheless, there are several lines of evidence suggesting that P-bodies have an active role in mRNA degradation rather than being solely storage sites for translationally silenced mRNPs. First, all proteins that function in 5' to 3' decay co-localize to P-bodies, including the deadenylase Ccr4-NOT complex, the decapping complex Dcp1/Dcp2, the exonuclease Xrn1, and the decapping enhancers Lsm1-7, Rck, Edc3, Pat1 and Hedls [118, 13, 123, 124, 27] (refer to Kulkarni et al. [125] for a broader list of proteins localized to P-bodies). Second, Sheth and Parker [126] were able to demonstrate the presence of 5' to 3' decay intermediates in yeast P-bodies. Moreover, depletion of Dcp2 or Xrn1 causes the accumulation of mRNAs in P-bodies, while Dcp2 overexpression leads to their loss. It was also shown that trapping mRNAs in polysomes, which inhibits mRNA decay, abolishes P-bodies.

In addition, components of several cytoplasmic pathways that repress gene expression, either via translational inhibition or mRNA degradation, are present in P-bodies. Initial recognition of the substrate mRNAs is thought to occur diffusely in the cytoplasm. At later steps of regulation, the mRNA substrates and the associated regulatory proteins of NMD, RNAi-mediated gene silencing, and AMD are recruited to P-bodies [20, 123]. For example, the P-body protein GW182 is required for miRNA-mediated mRNA degradation and helps to recruit Ago proteins and the mRNA targets to P-bodies [20]. Nonetheless, inhibition of visible P-body assembly by depleting Lsm1 or Rck leads to a diffuse localization of Ago2 in the cytoplasm, but does not abolish RNAi-mediated gene silencing [108]. This observation points to the possibility that P-bodies are a consequence rather than a cause of the RNAi mechanism [108, 127]. P-bodies also accommodate both protein factors and mRNA targets of AMD [13, 128]. As in the case of RNAi-mediated mRNA degradation, visible P-bodies are not required for AMD to take place, indicating that the 5' to 3' degradation machinery is also active outside the P-bodies. In fact, Franks and Lykke-Andersen [128] demonstrated that TTP and BRF1 can nucleate P-bodies in HeLa cells when the decay machinery is limiting. In this case, P-bodies seem to accumulate the translationally arrested mRNPs. This result further supports the idea that P-bodies become visible when large amounts of mRNA are translationally stalled or targeted for decay, as is the case in *dcp1*Δ or *xrn1*Δ strains [90]. Even if visible P-bodies are not essential, they may still provide an optimal environment for regulation to take place [90].

P-bodies are dynamic structures that continuously exchange their protein and mRNA components with the cytoplasm [129]. Moreover, P-bodies are found to be very motile structures by real-time fluorescence imaging [129, 130]. Kedersha et al. [129] showed that the motile P-bodies frequently touch stress granules (SG), suggesting that there is an exchange of factors between two structures. This observation further supports the hypothesis that SG are sites of mRNA triage from where mRNAs can be routed to P-bodies for degradation [59, 90, 121, 131, 58].

A step-wise model for P-body assembly has been suggested based on interaction data and the careful observation of P-body assembly in *S. cerevisiae*. According to this model, the first step is the formation of a repressed mRNP by the recruitment of the Dcp1p, Dcp2p, Edc3p and Dhh1p decapping complex on the target mRNA after deadenylation. In the next step, the decapping coactivators Pat1p and Lsm1p-7p, possibly together with Xrn1p, are supposed to join the mRNP. Lastly, microscopically visible P-bodies form when many mRNP complexes aggregate via the self-interacting YjeF-N domain of Edc3p and/or the prion-like C-terminal domain of Lsm4p [124, 90, 91]. In fact, most of the P-body proteins contain aggregation-prone

regions, suggesting that self- or co-aggregation is a general mechanism driving P-body assembly [125].

1.5 Pat1

Pat1 was first identified in *Xenopus* oocytes [132], where the regulation of stage-dependent protein expression is mainly post-transcriptional. This makes Pat1 (named as P100 in the original paper) a good candidate for such a regulatory protein in the cell. In a genetic screen in *S. cerevisiae*, two genes named MRT1 and MRT3 (mRNA turnover (MRT)) were found to have a role in the turnover of unstable mRNAs and to be required for efficient decapping [133, 134]. Mutations in these genes suppress the lethality of *PABP* deletion by slowing down the rate of deadenylation-dependent decapping in this strain [133]. Further analysis in *S. cerevisiae* by Tharun et al. [112] revealed that MRT1 and PAT1 are the same gene, and that it interacts with Lsm1p-7p. Pat1p was initially identified as a topoisomerase II interacting protein, and its deletion was found to slow the growth rate of yeast [135]. Finding that the Lsm1p-7p complex also interacts with Dcp1p, Dcp2p and Xrn1p in addition to Pat1p strengthened the idea that Pat1p plays a role in mRNA turnover [112]. Bonnerot et al. [115] found that the Pat1p-Lsm1p interaction is RNA-independent, and observed the association of both proteins with free mRNPs, monosomes and polysomes in polysome profiles. Interestingly, the interaction of Lsm1p with polysomes was dependent on Pat1p. In addition, the authors also detected that the short lived MFA2 transcript is stabilized in a *pat1*Δ strain. The stabilized MFA2 mRNA accumulated as full length mRNA without any decay intermediates visible [115]. Moreover, mRNAs trimmed at the 3' end were detected in both *pat1*Δ and *lsm1*Δ strains [109, 116]. This suggests that Lsm1p-7p and Pat1p, likely as a complex, protect the 3' end of deadenylated mRNAs from endo- or exoribonucleases. These studies indicated that yeast Pat1p is an enhancer of decapping and acts after deadenylation [115].

In yeast, the translation initiation factors eIF4E_p, eIF4G_p, and PABP_p bind Pat1p in an RNA-dependent manner. It is interesting that Lsm1p, as a marker of the Lsm1p-7p complex, does not co-immunoprecipitate with these proteins, and appears to interact only with deadenylated mRNAs. In contrast, Pat1p was found to bind to polyA⁺ mRNAs, which places Pat1p before Lsm1p in the sequence of mRNP rearrangements that lead to mRNA degradation. Nevertheless, the Lsm1p-7p complex does not require Pat1p for its recruitment to mRNA since its interaction with mRNA still occurs in a *pat1*Δ strain. On the other hand, the efficiency of Lsm1p-Dcp2p co-immunoprecipitation was significantly reduced in *pat1*Δ cells. Moreover, the interaction of Dcp2p with mRNA was decreased several fold in *pat1*Δ and *lsm1*Δ strains, supporting the idea that the Lsm1p-7p/Pat1p complex is an enhancer of decapping [63]. In line with this idea, stabilization of the full length reporter mRNA was observed both in *pat1*Δ and *lsm1*Δ strains. Sheth and Parker [126] reported that Pat1p localizes in P-bodies, and that P-bodies are smaller in a *pat1*Δ strain [112]. In contrast, the number of P-bodies was increased in an *lsm1*Δ strain. This observation is consistent with the differential association of Pat1p and Lsm1p with translation initiation factors, and strengthens the argument that Pat1p and Lsm1p-7p activate decapping via different mechanisms [126].

Inhibition of translation is another function that is attributed to Pat1. Although recent data provides solid evidence that Pat1p suppresses translational, earlier studies claimed that Pat1p enhances translation. Wyers et al. [136] suggested that Pat1p enhances translation initiation, before or during the recruitment of the 43S pre-initiation complex. A study by

1 Introduction

Noueiry et al. [137] supports this hypothesis by showing that translation of the brome mosaic virus genomic RNA requires the Lsm1p-7p/Pat1p complex in yeast. Surprisingly, Noueiry et al. [137] failed to see an effect of *PAT1* deletion on polysome profiles, while there was a clear change in the data from Wyers et al. [136]. So far, these reports have not been confirmed by other studies. In a later study, Collier and Parker [101] demonstrated that Pat1p and the helicase Dhh1p function actively as a general repressors of translation. They also show that Pat1p and Dhh1p act independently of the cap structure and, probably, independently of each other. As a result of this repressive mechanism, mRNPs are sorted into P-bodies and are eventually decapped. It was also suggested that Pat1p/Dhh1p compete with the translation apparatus under normal conditions, and the equilibrium may be shifted towards suppression of translation under certain conditions like glucose deprivation or amino acid starvation. In support of Pat1p being a translational repressor, its overexpression was observed to inhibit growth, decrease polysomes, and cause an accumulation of P-bodies [101].

Teixeira and Parker [124] provided important clues as to the functions of several proteins in P-body assembly in *S. cerevisiae*. They reported that the recruitment of Dcp1p and Lsm1p to P-bodies is dependent on Dcp2p and Pat1p, respectively. Interestingly, a *pat1* Δ strain showed reduced numbers of P-bodies, even during glucose deprivation, although repression of translation was not diminished. This observation suggests that Pat1p plays a role in the early steps of P-body assembly. Furthermore, the authors proposed that the previously observed decapping enhancer effect of Pat1p can be explained by the fact that the Lsm1p-7p complex depends on Pat1p in order to be recruited to P-bodies. Pat1p was claimed to have a scaffolding role which allows Xrn1p to interact with the Lsm1-7p complex. The Lsm1-7p complex may function later in P-body assembly, since deletion of its subunits results in accumulation of mRNPs in larger P-bodies. Another interesting observation was that Pat1p shuttles between the nucleus and the cytoplasm, and that Lsm1p may regulate nuclear-cytoplasmic localization of Pat1p [124].

Deletion studies suggested that yeast Pat1p has two distinct domains with separate roles. The C-terminal half of the protein was shown to mediate repression of translation and localization of Pat1p in P-bodies. This domain was also required for recruiting Lsm1p and Dcp2p to P-bodies. This finding is not easy to explain since it is not the C-terminal domain (aa 422 to 763), but a central domain (aa 254 to 422), that interacts with Lsm1p in a Y2H assay. Deletion of the central domain causes a defect in mRNA decapping as strong as deletion of the entire coding region of Pat1p. Pat1 is thought to promote decapping by rearrangement of mRNPs in P-bodies, generating mRNPs that are more susceptible to decapping. Although Pat1p does not have any recognizable RNA-binding domains, the authors clearly show that recombinant Pat1p binds RNA *in vitro*, with a preference for polyU [88].

For a long time it was thought that there is no homolog of yeast Pat1 in mammals since database searches did not reveal any sequences with significant homology. Through more careful analysis, however, we were able to identify two human complementary DNAs (cDNAs) with a limited homology to yeast Pat1p [138]. In parallel, Scheller et al. [139] identified the same proteins as human homologs of Pat1p. They showed that one of the Pat1p homologs, which they name PatL1, co-localize with Lsm1, Rck and Dcp1 in P-bodies. They further reported that P-body numbers decrease when HeLa cells were treated with an siRNA against PatL1 [139].

1.6 Aim of the Study

The goal of my PhD project was to characterize the newly identified human homologs of the yeast protein Pat1p, Pat1a and Pat1b, with respect to their localization, interactions and functions in cytoplasmic mRNA decay. During my Master's studies, I showed that Pat1b localizes to P-bodies and interacts with several P-body proteins. In my PhD thesis, I wanted to include the second human homolog, Pat1a, in the analysis, and compare it to Pat1b. Since no domains have yet been attributed to Pat1b, I focused on describing the role of individual domains in determining the localization, interactions and functions of Pat1b.

2 Results

2.1 Previous Work on Pat1b

During my Master's studies, I started working on the characterization of human homolog of yeast Pat1p, Pat1b. According to careful basic local alignment search tool (BLAST) searches made by Georg Stoecklin, there are two homologs of Pat1 in mammals, named Pat1a and Pat1b. We were kindly provided with the cDNA clone (accession number: DKFZp451I053) by Stefan Wiemann, DKFZ Heidelberg. By that time there was no cDNA available for Pat1a, and cloning proved difficult. Consequently, I began working on Pat1b.

In summary, during my Master's thesis I was able to achieve the following results:

(1) I cloned the Pat1b cDNA from the original pdEYFP-N1gen vector into pcDNA3-HA and pcDNA3-YFP vectors (N-terminal Hemagglutinin (HA) or yellow fluorescent protein (YFP) tags, respectively). In addition, 6 deletion constructs of Pat1b were also cloned in the pcDNA3-HA vector. The deletion constructs include the N-terminal part of Pat1p until the homology region (AN, aa 1-388), the centrally located homology region (H, aa 389-348), the C-terminal part of Pat1b (C, aa 449-770) and combinations of these (see Figure 2.1 for schematic representation of Pat1b domains).

(2) I showed that HA-Pat1b localizes to P-bodies in several mammalian cell lines. To mark P-bodies, I did immunofluorescence (IF) staining against several proteins that are known to be present in P-bodies. Pat1b showed co-localization with endogenous Hedls, Xrn1, Rck, Lsm1, Upf1, and exogenously expressed RFP-Dcp1a.

(3) Localization studies of Pat1b fragments gave three main results. The HA-tagged full length protein and Pat1b-dH (homology domain deletion) localized to P-bodies and increased the number of P-bodies per cell. This implies, first, that although it is highly conserved, the homology domain is not required for P-body localization, and second, that Pat1b is able to stimulate P-body formation. Individual domains of Pat1b did not show P-body localization, suggesting N- and C-terminal parts of the protein are needed for P-body localization of Pat1b.

(4) Interaction studies with overexpressed HA-Pat1b demonstrated that Pat1b interacts with endogenous Xrn1, Hedls, Rck and Lsm1, but not with eIF3 or eIF4G. Having a C-terminal YFP tag did not change these results. In addition, I was able to confirm these interactions by pulling on the interacting partner, i.e. immunoprecipitation of endogenous Xrn1, Hedls, and Rck also brought down HA-Pat1b. Moreover, Pat1b-AN was necessary and sufficient for the Rck interaction, while the C-terminus mediated the interactions with the other proteins. I tested the RNA dependency of these interactions and showed that they are all resistant to RNase A treatment.

In conclusion, the data of my Master's thesis confirmed that Pat1b is the human homolog of yeast Pat1p, and suggested that it may behave as a scaffolding protein that assembles P-body proteins, and hence, helps in the formation of P-bodies [138].

2.2 Pat1b, but not Pat1a, Is a P-body Protein

As mentioned above, there appear to be two homologs of yeast Pat1p in mammals. We termed the human proteins Pat1a and Pat1b, PatL2 and PatL1 according to the nomenclature suggested by Scheller et al. [139]. The sequence that we identified as Pat1a differs from PatL2 at the N-terminus, Pat1a having an extension compared to PatL2. Pat1a and Pat1b share 25.2% identity and 37.9% similarity in the amino acid level. In addition, Pat1a and Pat1b share high homology in the homology domain (H, 56.2% identity and 67.2% similarity) and in the C-terminal domain (C, 32.8% identity and 54.0% similarity) (Figure 2.1). Scheller et al. [139] failed to detect the PatL2 mRNA on northern blots and concluded that the protein may have a tissue- or development-specific expression pattern. Consequently, they excluded PatL2 from their analysis. I started my analysis by comparing the localization and interactions of Pat1a and Pat1b.

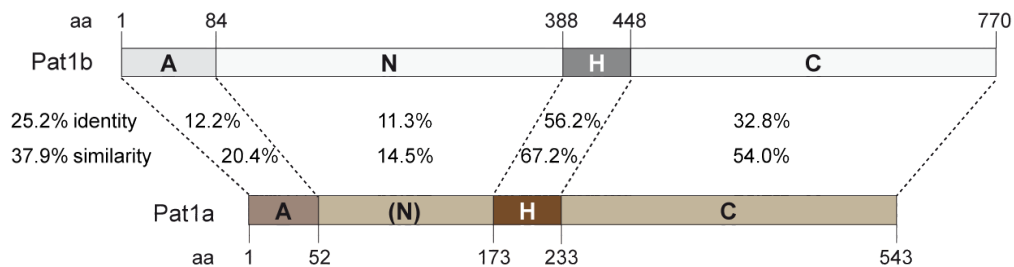


Figure 2.1. Schematic representation of Pat1b domains, and amino acid sequence conservation between Pat1b and Pat1a. A, acidic domain; N, N-terminal aggregation-prone domain; H, homology domain; C, C-terminal domain. Identity and similarity scores between the full length Pat1a and Pat1b, as well as between the corresponding domains are indicated (calculated with the Ebi, EMBOSS Needle pairwise alignment tool). Note that the region of Pat1a corresponding to Pat1b-N is not enriched in aggregation-prone residues, therefore it is depicted as (N).

2.2.1 Cloning of Pat1a

Oksana Seibert and Jochen Kreth in Georg Stoecklin's lab cloned the coding region of human Pat1a using cDNA from HeLa cells. The coding region was subdivided into three parts for polymerase chain reaction (PCR) amplification. After PCR, the fragments were ligated together and cloned into pEYFP and pcDNA3-HA vectors, keeping the tags N-terminal. Please refer to Section 4.2.1 for further details of cloning. It is worth noting that we failed to get PCR products using cDNA generated from several cell lines. This may be due to low expression level of Pat1a in these cells lines.

2.2.2 Comparison of Pat1a and Pat1b Localization

Since Pat1a was identified as a homolog of yeast Pat1p, which localizes to P-bodies, and Pat1b is also known as a P-body protein, I wanted to check the localization of human Pat1a in mammalian cells. For this purpose, I transfected COS7, HeLa or U2OS cells (see Section 4.2.2 for definitions of cell lines) with YFP-Pat1a. I fixed the cells 24 hrs after transfection, immunostained P-bodies with an antibody against Hedls, and analyzed the localization of YFP-Pat1a with regard to Hedls. As can be seen in Figure 2.2, in contrast to the punctate

2 Results

localization of YFP-Pat1b in P-bodies, YFP-Pat1a has a diffuse cytoplasmic localization. Figure 2.2 depicts the localization of YFP-tagged proteins in COS7 cells, as an example. Quantification of P-bodies per cell in transfected cells is given in Figure 2.2-D. Overexpression of the YFP tag alone does not influence the number of P-bodies per cell. A slight decrease in P-body numbers is observed in YFP-Pat1a transfected cells. In contrast, YFP-Pat1b overexpression strongly increases the number of P-bodies per cell.

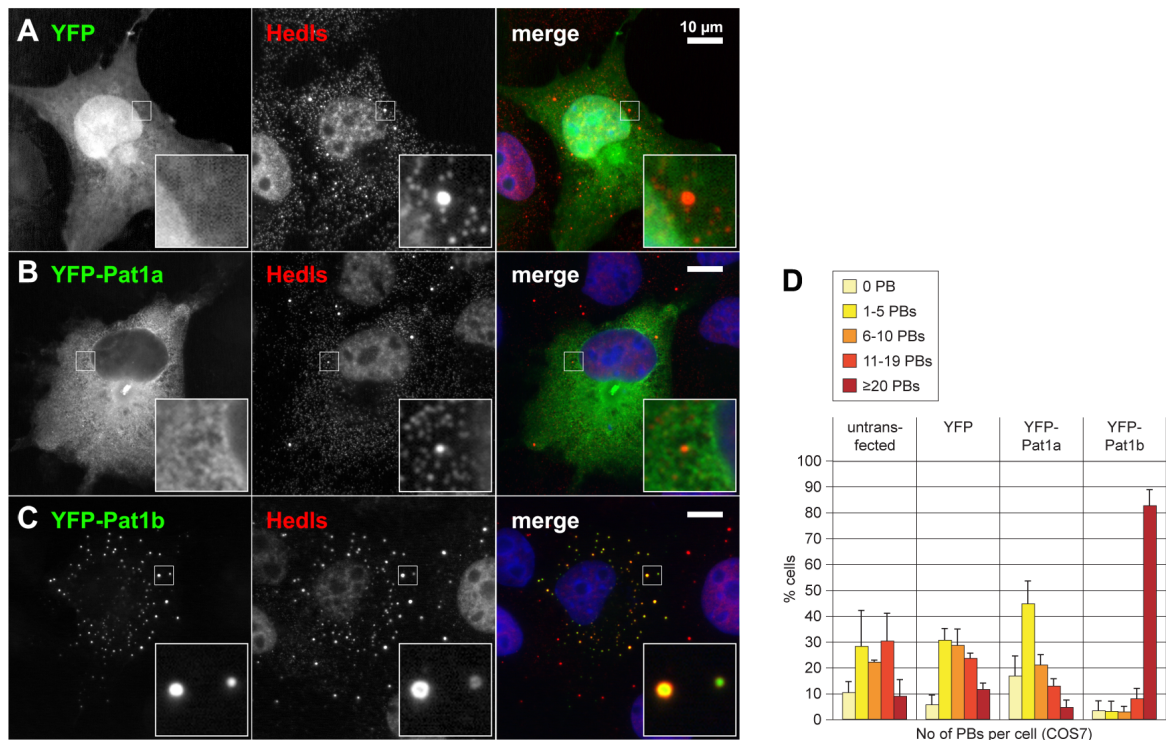


Figure 2.2. Localization of (A) YFP, (B) YFP-Pat1a and (C) YFP-Pat1b in COS7 cells. Cells were transfected with plasmids coding for the indicated YFP-tagged proteins, and fixed 24 hrs post-transfection. Endogenous Hedls was co-stained to mark P-bodies. (D) Number of P-bodies in transfected cells was counted, and the average distribution is presented in the graph. Error bars show standard deviations (SD) based on three independent experiments. Quantification of P-bodies in untransfected cells is shown as a control. Green: YFP-tagged proteins, Red: Hedls, Blue: Hoechst 33342.

2.2.3 Comparison of Pat1a and Pat1b Interactions

Next, I wanted to compare the interactions of Pat1a to that of Pat1b, and check whether Pat1a also interacts with proteins known to localize to P-bodies. To this end, I transfected HEK293 cells with pcDNA3-HA-Pat1a and collected the cells 24 hrs after transfection. An antibody against the HA tag was used for immunoprecipitation (IP) of the interacting protein complexes. After resolving the input and IP samples by sodium dodecyl sulfate polyacrylamide gel electrophoresis (SDS-PAGE), western blot (WB) analysis was used to detect the HA-tagged proteins and potential endogenous interaction partners. The HA tag alone was used as a negative control. Figure 2.3 represents such an analysis and shows that HA-Pat1a interacts with Lsm1, and very weakly with Lsm4 and Xrn1. Therefore, Pat1a is likely to bind to “free”

2.3 Role of Pat1b in P-body Assembly

Lsm1 that is not associated with the other Lsm proteins or Xrn1. Sequestration of Lsm1 from the Lsm1-7 complex by the overexpressed Pat1a may be the reason for the small decrease in P-body numbers observed in YFP-Pat1a transfected cells. In comparison to HA-Pat1a, HA-Pat1b interacts with Rck, Hedls, Xrn1, Lsm1 and Lsm4. WB shows that eIF3B does not interact with either Pat1a or Pat1b. Thus, the interactions observed are specific. As a result of the localization and interaction studies, I concluded that Pat1a is not a P-body protein.

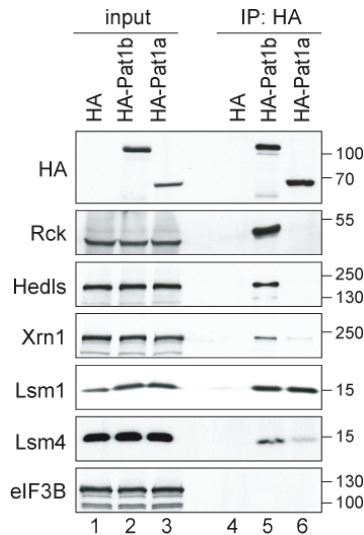


Figure 2.3. Interactions of Pat1a. HEK293 cells transiently transfected with HA, HA-Pat1b or HA-Pat1a were lysed 24 hrs after transfection and used for IP with anti-HA antibody. WBs against HA, Rck, Hedls, Xrn1, Lsm1, Lsm4 and eIF3B are depicted.

2.3 Role of Pat1b in P-body Assembly

Pat1b is a P-body protein. Its deletion in yeast *S. cerevisiae* leads to smaller P-bodies in glucose deprivation [124], implying the requirement of Pat1 for proper P-body assembly. In mammalian cell culture, overexpression of Pat1b leads to an increased number of P-bodies per cell (see Figure 2.2-D for quantification). These findings suggest an active role for Pat1b in P-body formation. Therefore, I conducted experiments to test this hypothesis.

2.3.1 Pat1b Is Essential for P-body Formation

First, I wanted to test if Pat1b is required for P-body assembly. To answer this question, I employed a knockdown strategy. If Pat1b is required for P-body formation, its knockdown should negatively affect P-body formation. Since my aim was to characterize the human protein, I switched to human osteosarcoma (U2OS) cells in this experiment.

To knockdown Pat1b, I used two siRNAs directed against the coding region, siRNAs T2 and T3. As controls, I transfected H₂O or the unspecific siRNA D0. U2OS cells were transfected twice with 100 nM final concentration of siRNAs over 5 days. RNA was isolated from the transfected cells to check the knockdown efficiency. Pat1b mRNA levels were analyzed by quantitative real time PCR (qPCR), and were found to be reduced to 5% and 6% in T2 and T3 transfected cells, respectively, compared to the mRNA levels in D0 transfected cells (Figure 2.4-A). After confirming the knockdown levels, I repeated the transfection and prepared the cells for IF. Cells were stained with an anti-Hedls antibody to detect endogenous Hedls as a marker of P-bodies. Figure 2.4-B depicts examples of cells after H₂O or siRNA transfection,

2 Results

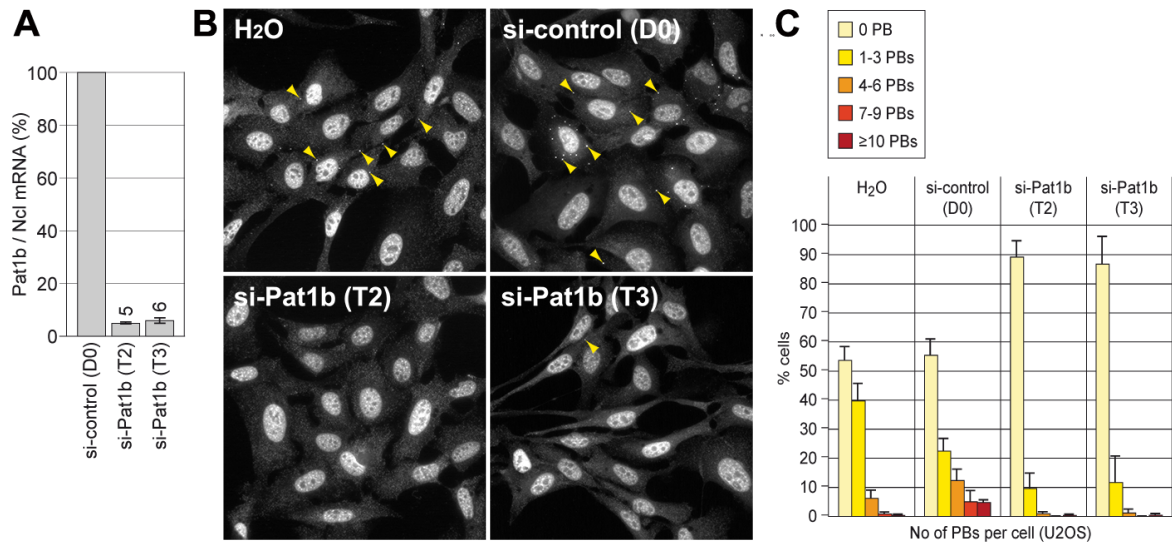


Figure 2.4. Pat1b is an essential P-body protein. U2OS cells were transfected with H₂O, control siRNA (D0) or with two different siRNAs against Pat1b (T2 and T3). (A) Endogenous Pat1b mRNA levels were quantified by qPCR and normalized to nucleolin (Ncl) mRNA levels. Value in D0 transfected cells was taken as 100%. (B) IF staining of U2OS cells after transfection with indicated siRNAs. P-bodies are visualized as bright foci in the cytoplasm after immunostaining against endogenous Hedls. Yellow arrows point towards individual P-bodies. (C) Quantification of P-bodies per cell. Error bars show standard deviations (SD) based on three independent experiments.

showing that the number of cells with P-bodies dropped considerably in cells transfected with siRNAs targeting Pat1b. I also quantified this effect by counting the P-body numbers per cell in control or si-Pat1b transfected cells. Quantification shows that the percentage of cells lacking P-bodies increased from ~55% in water or control siRNA transfected cells to ~90% in si-Pat1b transfected cells (Figure 2.4-C). Hence, I concluded that Pat1b is essential for P-body formation.

2.3.2 Localization of Pat1b Deletion Constructs

Knowing that Pat1b overexpression increases P-body numbers, and that endogenous Pat1b is required for P-body formation, the next question was whether these functions can be attributed to any domain(s) of Pat1b. During my Master's studies, I had examined the localization of deletion constructs of HA-tagged Pat1b. Those data suggested that the entire protein, except for the homology domain, is needed for proper P-body localization. Since detection of the HA tag depends on immunostaining, the signal quality was not always very good. Therefore, I wanted to readdress this question with YFP-tagged deletion constructs. I subdivided Pat1b into four domains: (1) A, the acidic domain enriched in acidic residues, aa 1-84; (2) N, the aggregation-prone domain enriched in glutamine, asparagine and proline residues, aa 85-388, (3) H, the homology domain, aa 389-448, (4) and C, the C-terminal part, aa 449-770. Figure 2.5 shows a scheme of the Pat1b domains and localization of selected deletion constructs. In addition to single domains, I also analyzed combinations of these domains.

Once again, I used endogenous Hedls as a P-body marker. Deletion of the homology domain (Pat1b-dH) does not have an effect on P-body localization of YFP-Pat1b, or its ability to

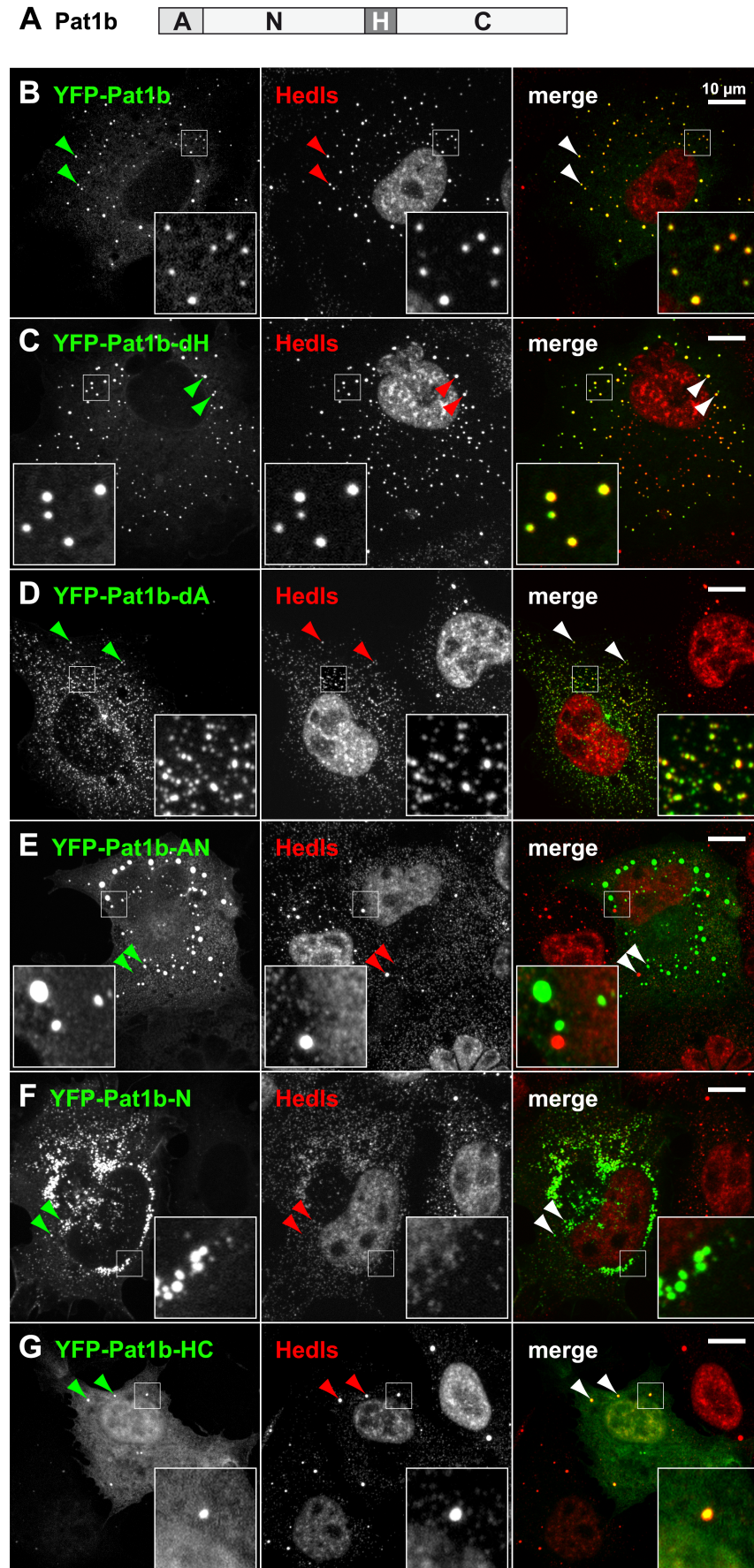


Figure 2.5. Localization of Pat1b deletion constructs. (A) Schematic representation of Pat1b domains. A, acidic domain; N, amino-terminal aggregation-prone domain; H, homology domain; C, carboxy-terminal region. COS7 cells were transiently transfected with (B) YFP-Pat1b, (C) YFP-Pat1b-dH, (D) YFP-Pat1b-dA, (E) YFP-Pat1b-AN, (F) YFP-Pat1b-N, or (G) YFP-Pat1b-HC, and processed for immunofluorescence microscopy. P-bodies in the cytoplasm were counterstained in red using an antibody against Hedls. Images were acquired by spinning-disc confocal microscopy; maximum projections of z-stacks are depicted. Merged images are shown on the right; arrowheads point toward P-bodies. Size bar, 10 μ m.

2 Results

induce P-body numbers per cell. Surprisingly, deletion of the acidic domain (Pat1b-dA) leads to formation of numerous, yet smaller foci. These YFP-Pat1b-dA induced foci correspond to proper P-bodies since Hedls and Rck (data not shown) co-localize in these foci. YFP-Pat1b-AN mostly had cytoplasmic diffuse localization, sometimes with irregular patches in the cytoplasm (data not shown). Interestingly, YFP-Pat1b-AN formed large, bright and round foci in some of the transfected cells, as shown in Figure 2.5-E. These foci are probably protein aggregates that do not correspond to P-bodies since there is no Hedls or Rck (data not shown) detected in most of them. These foci may be explained by the self-aggregation of the Pat1b-N domain, which is enriched in aggregation-prone residues (also see paragraph *Pat1b interacts with itself*). In line with the suggested self-aggregation ability of the Pat1b-N domain, its overexpression also leads to formation of aggregates. YFP-Pat1b-N aggregates are smaller than the ones formed by YFP-Pat1b-AN construct. This observation, together with smaller P-bodies observed in YFP-Pat1b-dA overexpressing cells, implies that Pat1b-A is important for P-body size. Nonetheless, YFP-Pat1b-A alone has a diffuse localization with a stronger nuclear signal, similar to the localization of the YFP tag alone. Lastly, YFP-Pat1b-HC diffusely localizes both to the cytoplasm and the nucleus, and in some cells it was observed weakly in P-bodies. As a conclusion of the localization data, I suggest that in the context of full length protein, Pat1b-N can nucleate P-body formation and Pat1b-A can control the size of P-bodies.

2.3.3 Pat1b Induced P-bodies Are Resistant to Cycloheximide

Next, I wanted to check whether Pat1b induced P-bodies would disappear after cycloheximide (CHX) treatment. CHX blocks translation elongation and traps mRNAs in polysomes. CHX treatment was also shown to rapidly inhibit P-body assembly [140], presumably by hindering P-body compatible mRNP formation. If Pat1b overexpression nucleates P-bodies via its aggregation capacity, these P-bodies should resist CHX treatment. To test this hypothesis, I treated the YFP-Pat1b or YFP-Pat1b-AN overexpressing cells with 5 $\mu\text{g}/\text{ml}$ CHX for 2 hrs before fixation. I immunostained the samples with antibodies against the P-body proteins Hedls, Rck, Xrn1 and Lsm4. Microscopic analyses of the cells treated with CHX showed clearly that there were almost no P-bodies in untransfected cells, while in transfected cells, YFP-Pat1b or YFP-Pat1b-AN bodies were not affected. In fact, YFP-Pat1b bodies still co-localized with Hedls and Rck (also with Xrn1 and Lsm4, data not shown), indicating that these foci correspond to P-bodies. In YFP-Pat1b-AN bodies, which did not co-localize with other P-body proteins most of the time anyway, there was no detectable Hedls. Nevertheless, there was low Rck signal detectable in some YFP-Pat1b-AN bodies. This finding is in line with the data showing that the A domain of Pat1b interacts with Rck.

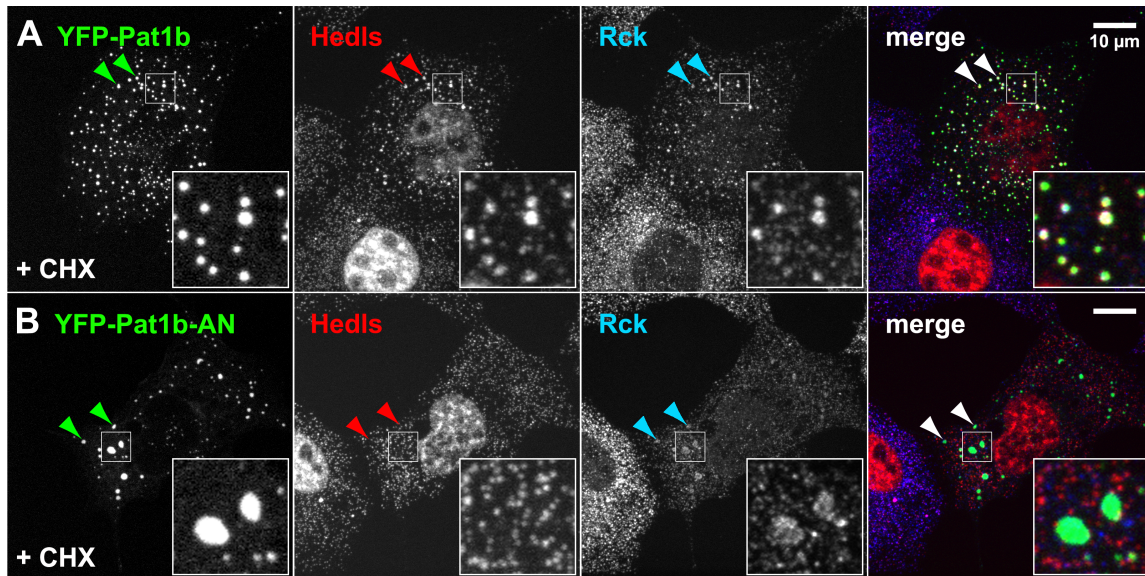


Figure 2.6. Localization of Pat1b in presence of cycloheximide (CHX). COS7 cells were transiently transfected with (A) YFP-Pat1b or (B) YFP-Pat1b-AN, and treated with 5 $\mu\text{g/ml}$ CHX for 2 hours prior to fixation. By immunofluorescence microscopy, P-bodies in the cytoplasm were counterstained using antibodies against Hedls and Rck. Images were acquired by spinning-disc confocal microscopy; maximum projections of z-stacks are depicted. Merged images are shown on the right; arrowheads point toward P-bodies. Size bar, 10 μm .

2.4 Interactions of Pat1b

Pat1b is an essential P-body protein (Section 2.3.1) and interacts with the decapping enhancers Rck, Hedls, Lsm1 and Lsm4, and with the exoribonuclease Xrn1 (see Section 2.2). These data suggest that Pat1 is involved in the 5' to 3' mRNA decay pathway. Therefore, I aimed to determine potential interactions of Pat1b with the Ccr4-NOT deadenylation and the Dcp1/Dcp2 decapping complexes. In order to characterize Pat1b further, I also included the domains of Pat1b in the interaction analyses.

2.4.1 Interactions of Pat1b with Decapping Enhancers

Strength of Pat1b interactions with decapping enhancers and Xrn1 Before analyzing potential interactions of Pat1b with other P-body proteins, I wanted to gain some information about the stability of the interactions with the decapping enhancers and Xrn1. Ideally, one would purify recombinant proteins from bacteria and look for direct associations. Taking the high number of interaction partners of Pat1b and the problems that occurred during bacterial expression and purification of Pat1b into consideration, I had to look for an alternative strategy. Increasing the salt concentrations in the washes of the IP protocol will challenge electrostatic interactions between the proteins and provide an idea about the strength of the interactions. Therefore, I repeated the anti-HA IP using HA-Pat1b transfected cells, divided the IP into 4 samples before washing, and used different sodium chloride (NaCl) concentrations in the wash buffer. Afterwards, I followed the regular protocol for elution with Laemmli buffer, SDS-PAGE

2 Results

and WB analysis. Figure 2.7 shows the results of such an IP.

Increasing the salt concentration to 500 mM NaCl did not interfere with the amount of the HA-Pat1b that is pulled down. Lsm1 appears to be the strongest interactor of Pat1b as the amount of protein co-purifying with HA-Pat1b was not affected by the high salt concentration. Interestingly, although assumed to represent the same complex, Lsm1-7, the Lsm4 interaction is weakened already at 300 mM NaCl. This finding suggests that Lsm1 is likely to be the direct interacting partner of Pat1b, that links the Lsm1-7 complex to Pat1b. There is also a significant amount of Rck co-precipitating with Pat1b at 500 mM NaCl, indicating a tight interaction between Rck and Pat1b. However, it is also possible that Lsm1 and Rck interact with Pat1b via hydrophobic surfaces that would not be affected by high salt concentrations. On the other hand, the Pat1b interactions with Hedls, Edc3 and Xrn1 were already lost at 300 mM NaCl. These proteins are possibly interacting with Pat1b through other proteins making it easier to challenge their association with Pat1b.

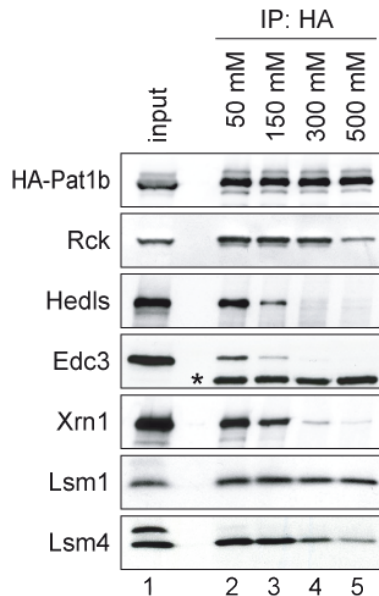


Figure 2.7. Salt resistance of Pat1b interactions. HEK293 cells were transiently transfected with HA-Pat1b. After 1 day, cytoplasmic lysate (input) was prepared for IP with anti-HA antibody. Before washes, the IP samples were divided equally into 4, and each aliquot was subjected to washes with indicated NaCl concentrations. HA-Pat1b, endogenous Rck, Hedls, Edc3, Xrn1, Lsm1 and Lsm4 were detected by western blotting. *, immunoglobulin heavy chain.

Domain analysis of Pat1b interactions with decapping enhancers Next, I wondered if it is possible to attribute these interactions to Pat1b domains. During my Master's studies, I had subdivided the protein into N- and C-terminal parts, taking the N-terminus of the homology domain (H) as the border (these results are shown in Figure 2.8-B). To complete this analysis, I repeated the anti-HA IPs including all domains of Pat1b, in HEK293 cells. For the washes, I used 150 mM NaCl unless otherwise stated.

Figure 2.8-B shows that the interactions of Rck and Lsm1 with Pat1b do not depend on RNA, as incubation with RNase A did not abolish the interactions. Although in WB shown in Figure 2.8-B RNase A treatment seems to enhance the interactions of Rck and Lsm1 with Pat1b, this observation was not reproducible. The Hedls and Edc3 interactions may be strengthened by RNase A treatment, implying the presence of RNA interferes with the Hedls and Edc3 interactions of Pat1b. On the other hand, the Xrn1 interaction seems to be negatively affected by RNase A treatment, suggesting that this interaction is supported by RNA (see Figure S7 in Ozgur et al. [141]). Figure 2.8-B also shows that the Rck interaction is

mediated by the AN fragment of Pat1b, while the other decapping enhancers, here exemplified by Lsm1, associate with the HC fragment. To determine if the A or N domain of Pat1b is necessary for the Rck interaction, I did the IP with HA-dA, HA-AN, HA-N, and HA-A. Although HA-A is not detectable on the WB due to its small size, it is necessary and sufficient to interact with Rck (Figure 2.8-C). In order to find out which domain, H or C, is required for the Pat1b C-terminal interactions, I repeated a similar IP with HA-dH, HA-HC, HA-C, and HA-ANH. Because HA-H is not detected on WB due to its small size, I employed HA-ANH as a control to check if H is sufficient for the Lsm1 interaction. This analysis indicates that neither H nor C alone is sufficient for the Lsm1 interaction, but both are needed. Unlike Lsm1, Hedls and Lsm4 interact with Pat1b-C, but these interactions are stronger with Pat1b-HC, implying that Pat1b-H has a positive effect on the Pat1b-C interactions.

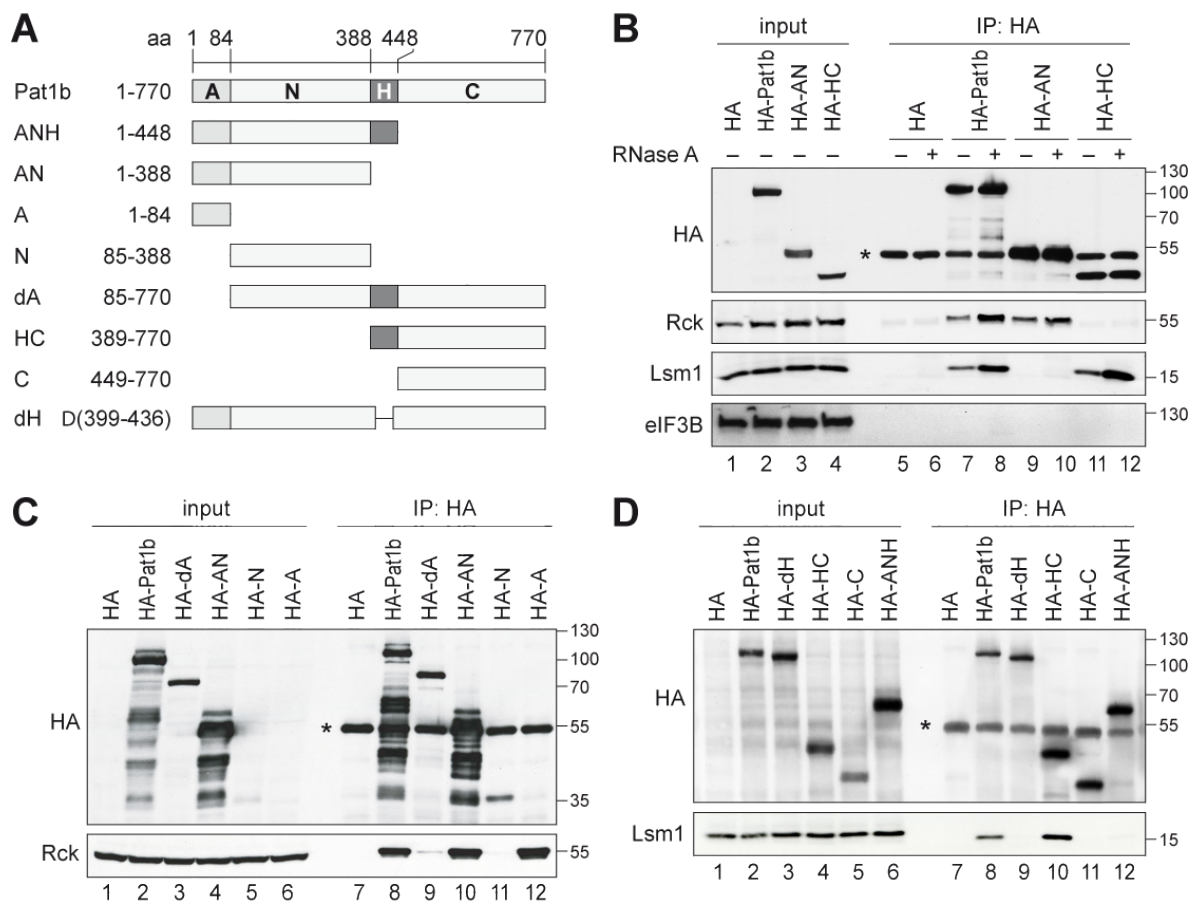


Figure 2.8. Separate interaction domains within Pat1b. (A) Schematic representation of Pat1b fragments. A, acidic domain; N, amino-terminal region; H, homology domain; C, carboxy-terminal region. (B-D) HEK293 cells were transiently transfected with vector alone, full-length HA-Pat1b, or the Pat1b deletion constructs indicated on top of the WB images. After 1 day, cytoplasmic lysates (input) were prepared for IP with anti-HA antibody. The HA-tagged proteins as well as endogenous Rck, Lsm1, and eIF3B were detected by western blotting. Where indicated, RNase A (0.1 mg/ml) was added during IP. *, immunoglobulin heavy chain. The sizes of the molecular weight markers (in kDa) are indicated on the right.

2.4.2 Pat1b Interacts with the Decapping Complex

The above analysis shows that different domains of Pat1b mediate interactions with different proteins. This implies that Pat1b might work as a scaffolding protein which might connect decapping enhancers to the decapping complex. Subsequently, I tested the association of Pat1b with the Dcp1/Dcp2 decapping complex.

At this point I switched to GFP-binder as means of immunoprecipitation since it has been shown as a powerful tool to pull down GFP- or YFP-tagged proteins [142]. We were kindly provided with the plasmid encoding 6xHis-GFP-binder protein by Elmar Schibel (ZMBH, University of Heidelberg). I purified the recombinant protein from *E. coli* BL21-DE3 Codon plus cells, and coupled it to the NHS-activated sepharose beads (GE Healthcare).

To determine the interaction of Pat1b with the decapping complex, I overexpressed YFP-Pat1b together with Flag-Dcp1a or Flag-Dcp2 in HEK293 cells. 24 hrs after transfection I collected the cells and proceeded with IP protocol for GFP-binder. As can be seen in Figure 2.9, Pat1b interacts with both Flag-Dcp1a and Flag-Dcp2. These interactions are resistant to RNase A treatment and 1 M NaCl (Figure 2.9-B). Supporting the suggested scaffolding function of Pat1b, Flag-Dcp2 (Figure 2.9-C) and Flag-Dcp1a (data not shown)

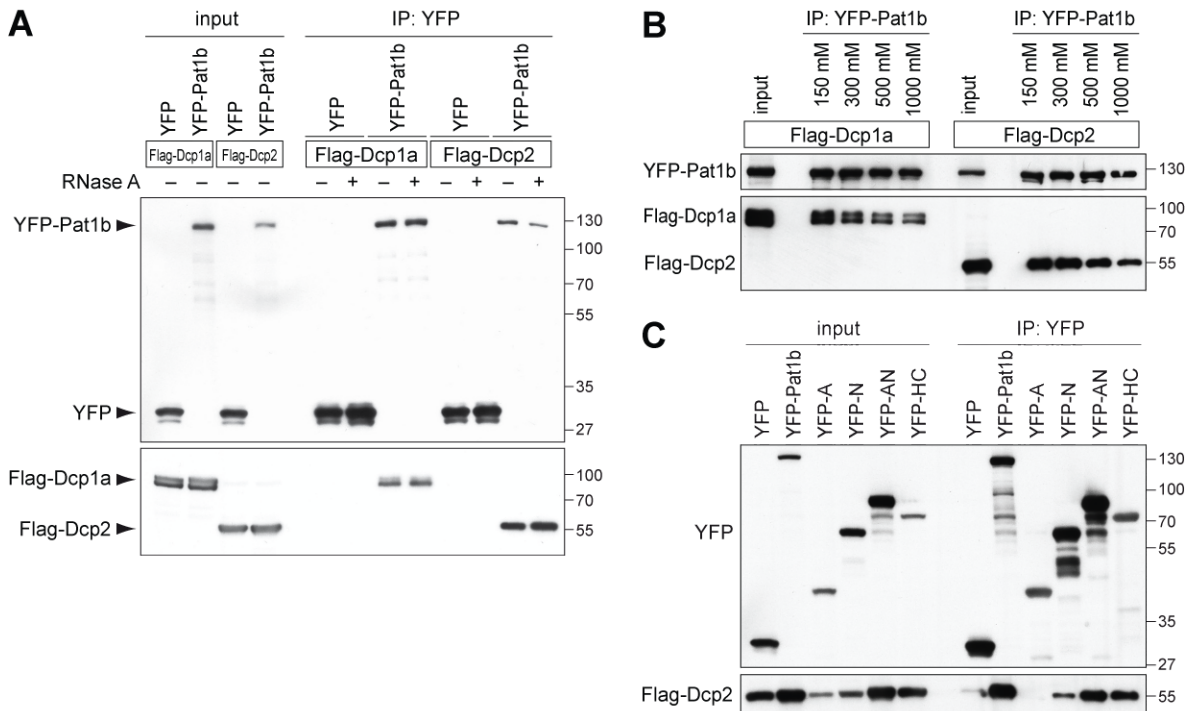


Figure 2.9. Pat1b interacts with Dcp2 and Dcp1a. (A-B) HEK293 cells were transiently transfected with YFP, YFP-Pat1b Flag-Dcp2 or Flag-Dcp1a. GFP-binder was used for IP, and western blot analysis was carried out with anti-GFP and anti-Flag antibodies. The sizes of the molecular weight markers (in kDa) are indicated on the right. Where indicated, RNase A was added during IP. (B) IPs were carried out with GFP-binder and subjected to increasing NaCl concentrations prior to elution. (C) HEK293 cells were transiently transfected with YFP, YFP-Pat1b, YFP-A, YFP-N, YFP-AN, or YFP-HC together with Flag-Dcp2. IP and WB detection was done as described for (A) and (B).

come down with both Pat1b-N and HC domains. As observed with the deadenylation complex, Pat1b-AN interacts with the decapping complex more strongly than Pat1b-N alone, even though Pat1b-A alone does not show detectable interactions.

2.4.3 Pat1b Interacts with the Ccr4-NOT Deadenylation Complex

The data from yeast Pat1p suggest that Pat1p acts at an early step in mRNA degradation. Although the yeast data do not indicate a role for Pat1p in mRNA deadenylation, I wanted to test if Pat1b also interacts with the Ccr4-NOT deadenylation complex, and possibly bridges it to the decapping proteins.

Since the Ccr4-NOT complex is a multi-subunit complex and not many antibodies against its components are available, I chose tagged CNOT1, Caf1a, Caf1b and Ccr4 (data not shown) as

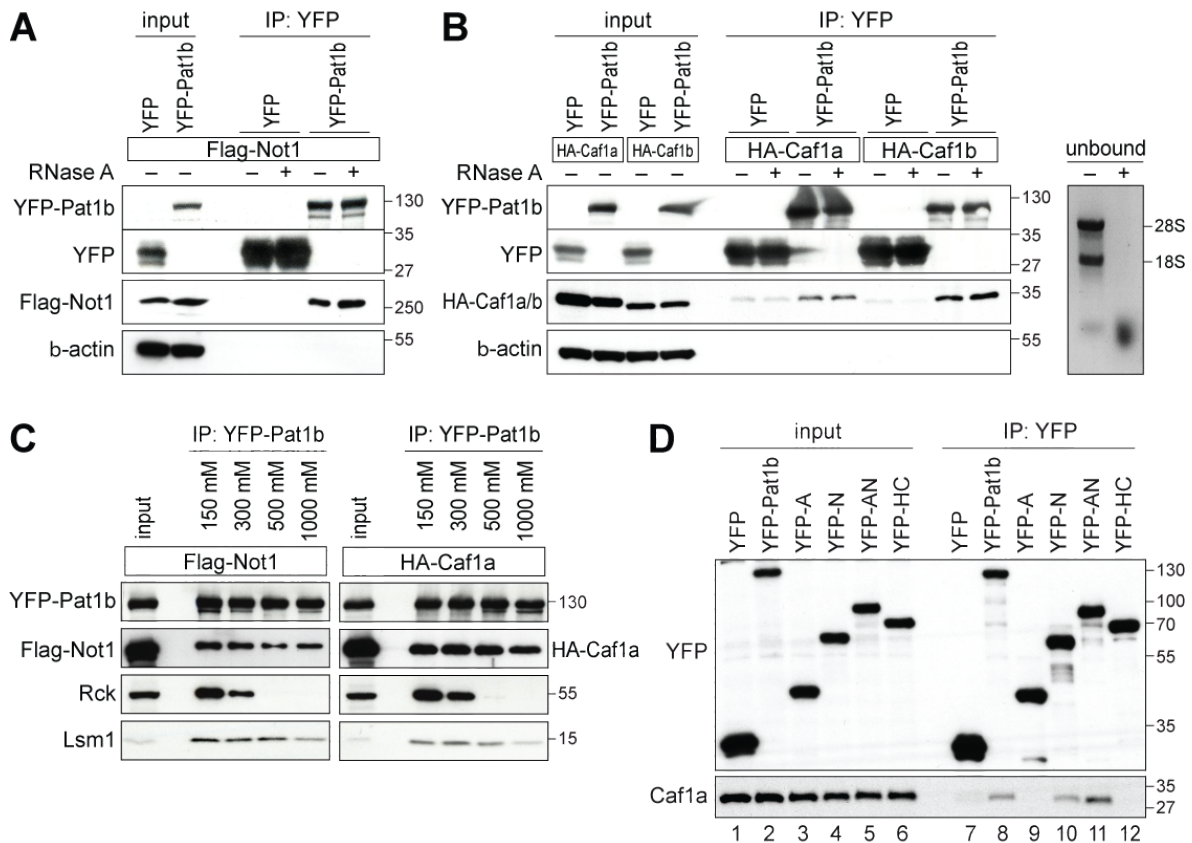


Figure 2.10. Pat1b interacts with the Ccr4-NOT complex. (A-C) HEK293 cells were transiently transfected with YFP or YFP-Pat1b together with the proteins indicated on top of the WB images. GFP-binder was used for IP, and western blot analysis was carried out with anti-GFP, anti-Flag and anti-HA antibodies. The sizes of the molecular weight markers (in kDa) are indicated on the right. Where indicated, RNase A was added during IP. On the right side of panel (B) RNA extracted from unbound fractions and stained with ethidium bromide is shown. (C) After binding to GFP-binder samples were divided into 4 equal aliquots and subjected to increasing NaCl concentrations prior to elution. (D) HEK293 cells were transiently transfected with YFP, YFP-Pat1b, YFP-A, YFP-N, YFP-AN, or YFP-HC and processed for IP with GFP-binder. The YFP-tagged proteins and endogenous Caf1a were detected by WB.

2 Results

markers of the deadenylation complex. I transiently transfected HEK293 cells with YFP-Pat1b (or its fragments) together with Flag-CNOT1 or HA-Caf1a or HA-Caf1b and pulled down the YFP tag using GFP-binder. In order to test the RNA dependency of the interactions, I also added RNase A during the IP where indicated. Figure 2.10 shows that YFP-Pat1b interacts with an RNA-independent manner with Flag-NOT1, HA-Caf1a and HA-Caf1b (Figure 2.10-A and B) and myc-Ccr4 (data not shown). Surprisingly, these interactions (Figure 2.10-C) were resistant to 1 M NaCl. At this salt concentration Rck falls off Pat1b, and the Lsm1 interaction is also significantly weakened. Next, I conducted IPs with the Pat1b domains to determine which domain of Pat1b mediates the interaction of Pat1b with the deadenylation complex (Figure 2.10-D). The aggregation-prone N domain of Pat1b is sufficient for the interaction with endogenous Caf1a, yet the acidic domain, A, appears to enhance the interaction. There is no interaction between endogenous Caf1a and Pat1b-HC. On the other hand, Flag-NOT1 and myc-Ccr4 interact with Pat1b-AN. I did also observe a weak interaction of Pat1b-HC with Flag-NOT1 and myc-Ccr4 (Figure S9 in Ozgur et al. [141]).

2.4.4 Pat1b Enhances the Interaction between Dcp2 and Caf1a

Since Pat1b interacts both with the deadenylation and the decapping complexes, it is appealing to speculate that Pat1b can connect these two important steps of mRNA degradation. To confirm this idea, I examined if Pat1b has an effect on the interaction between the deadenylation and the decapping complexes. For this purpose, I transfected HEK293 cells with GFP-Caf1 together with Flag-Dcp2. In one of the samples I also included HA-Pat1b in the transfection. After 24 hrs, I collected the cells and continued with IP using GFP-binder. In the absence of additional Pat1b overexpression, a faint Flag-Dcp2 band is visible after pull down on GFP-Caf1a. Interestingly, the Flag-Dcp2 band became much stronger when HA-Pat1b was also overexpressed in the cells. In conclusion, this experiment indicates that Pat1b binds to the deadenylation and decapping complexes simultaneously, and may thereby connect the two complexes (Figure 2.11).

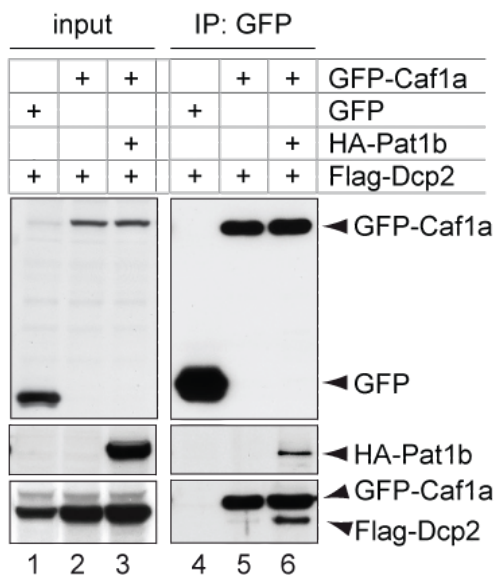


Figure 2.11. Pat1b enhances the interaction between Dcp2 and Caf1a. HEK293 cells were transiently transfected with Flag-Dcp2 together with either GFP alone, GFP-Caf1a alone, or GFP-Caf1a together with HA-Pat1b. Cytoplasmic lysates were processed for IP with GFP-binder and then subjected to WB analysis. In the IP samples, the Flag antibody cross-reacted with GFP-Caf1a.

2.4.5 Other Interactions of Pat1b

During my PhD studies I have also observed several other interactions of Pat1b. While I was trying to understand the role of Pat1b in mRNA degradation, I have also considered the option that Pat1b is involved in mRNA-specific decay pathways like ARE-mediated decay or RNAi. As a quick way to gain information that would support or disprove this possibility, I tested whether Pat1b interacts with proteins known to have roles in these mRNA decay pathways.

Pat1b interacts with proteins involved in ARE-mediated mRNA decay TTP is a well known RNA-binding protein that mediates fast decay of its target mRNAs containing AREs. BRF1 belongs to the same family as TTP. Therefore, I chose these two proteins as representers of protein involved in AMD. Overexpression of YFP-Pat1b and HA-TTP or HA-BRF1, followed by GFP-binder pull down, revealed an RNA-independent interaction of Pat1b with TTP and BRF1. Both of the proteins interacted with the aggregation-prone N domain of Pat1b (Figure 2.12).

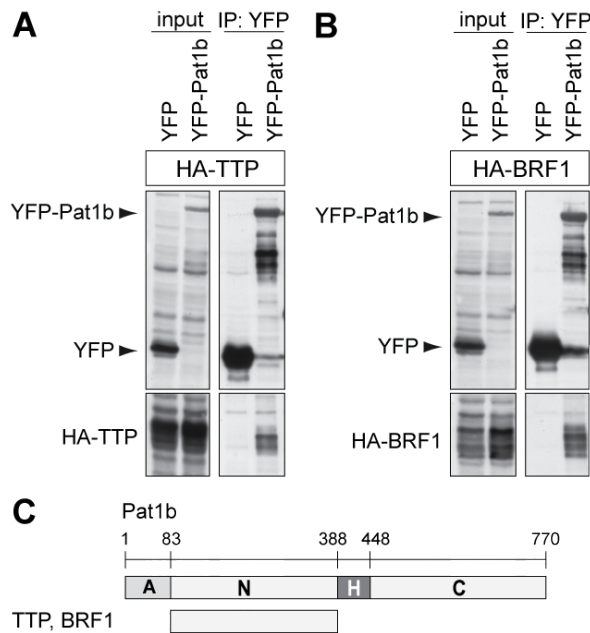


Figure 2.12. Pat1b interacts with TTP and BRF1. HEK293 cells were transiently transfected with YFP or YFP-Pat1b together with (A) HA-TTP or (B) HA-BRF1. After 24 hrs of expression, cytoplasmic lysates were processed for IP with GFP-binder and then subjected to WB analysis with GFP and HA antibodies. Where indicated, RNase A was added to the samples during IP. (C) Schematic summary of the Pat1b domains that mediate the interactions with the proteins indicated on the left.

Pat1b interacts with proteins of RNAi pathway RNAi targets mRNAs for translational suppression or for degradation via RISC, which includes Ago proteins and GW182. In humans there are three homologs of the *Drosophila* GW182 protein, and these proteins are termed TNRC6A, TNRC6B and TNRC6C. Recently, PABP was also indicated in si/miRNA-mediated gene silencing [143]. Hence, I examined if Pat1b would interact with Ago2, Ago4 (data not shown), TNRC6B, TNRC6C or PABP. To this end, I again employed transient transfection of HEK293 cells with YFP-Pat1b together with the Flag-tagged versions of the proteins mentioned. Immunoprecipitation with GFP-binder showed that Pat1b, interacts with Flag-Ago2, Flag-Ago4, Flag-PABP, and Flag-TNRC6B, independently of RNA, and with Flag-TNRC6C via RNA. Nevertheless, these IPs were done only once in the presence of RNase A, and need to be repeated to confirm the RNA dependency of the TNRC6C interaction.

2 Results

Domain analysis of these interactions revealed that both Pat1b-N and Pat1b-HC domains interact with Ago2 and Ago4, while TNRC6 proteins require Pat1b-AN for Pat1b interaction. PABP can associate with Pat1b via Pat1b-N domain alone (see Figure 2.13).

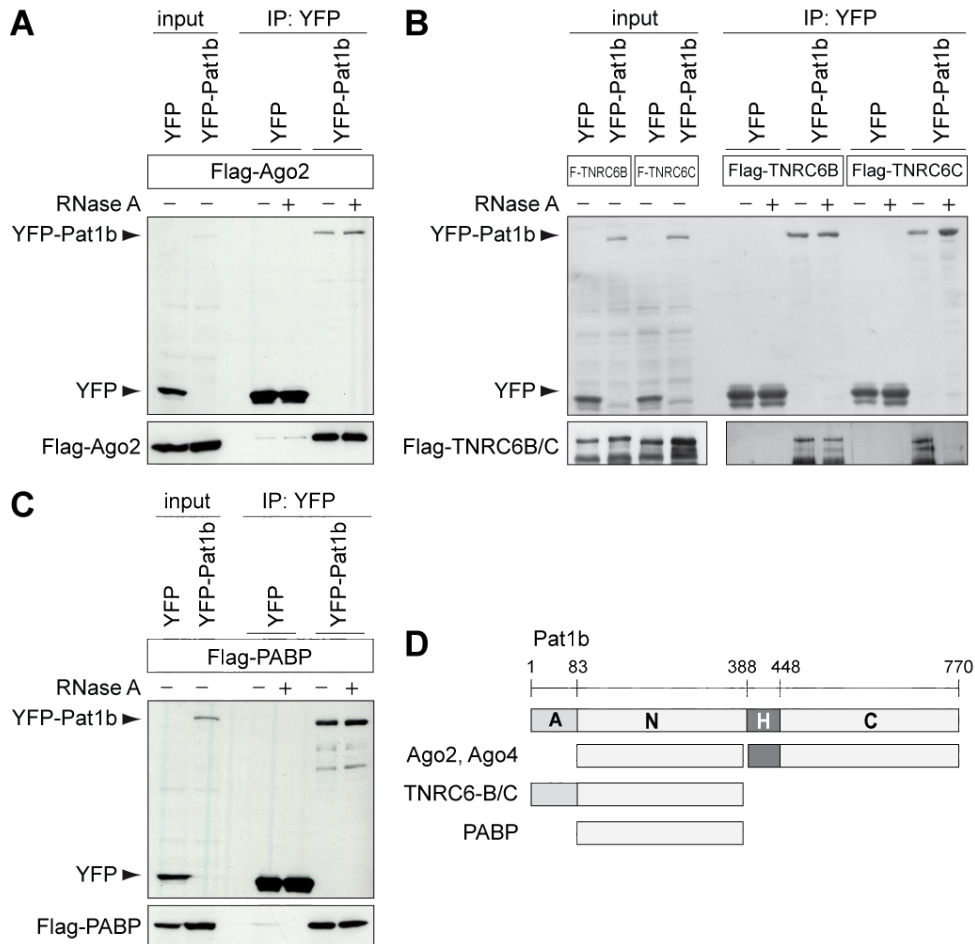


Figure 2.13. Pat1b interacts with effector proteins of RNAi. (A-C) HEK293 cells were transiently transfected with YFP or YFP-Pat1b together with the Flag-tagged proteins indicated on the WB images. Cytoplasmic lysates were processed for IP with GFP-binder and then subjected to WB analysis with GFP and Flag antibodies. Where indicated RNase A was added to the sampled during IP. (D) Schematic summary of the Pat1b domains that mediate the interactions with the proteins indicated on left.

Pat1b interacts with itself Localization data indicates that Pat1b can nucleate P-body assembly. One possible mechanism for Pat1b to induce P-body formation is self-interaction. I showed already that Pat1b interacts with many proteins which have roles in different aspects of mRNA degradation. Hence, Pat1b may act as a scaffolding protein in P-body formation by interacting with other P-body proteins and putting them closer to each other via self-interaction. To test this hypothesis, I co-expressed HA-Pat1b together with YFP-Pat1b, and after pulling down the YFP tag, I looked for HA-Pat1b. Figure 2.14 shows that YFP-Pat1b brought down HA-Pat1b. Except for YFP-Pat1b-A, all other fragments of YFP-Pat1b were

able to interact with HA-Pat1b. The strongest interaction was observed between HA-Pat1b and all YFP-tagged fragments of Pat1b that contain the Pat1b-N domain (data not shown).

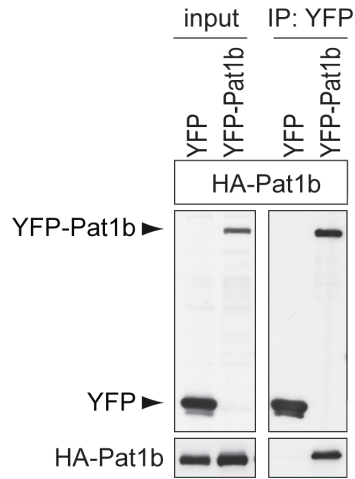


Figure 2.14. Pat1b interacts with itself. HEK293 cells were transiently transfected with YFP or YFP-Pat1b together with HA-Pat1b. 24 hrs after transfection, cytoplasmic lysates were processed for IP with GFP-binder and then subjected to WB analysis with GFP and HA antibodies.

Mass Spectrometry analysis of the Pat1b interactome In order to obtain a more complete picture of Pat1b interacting proteins, I decided to carry out a mass spectrometry (MS) analysis of proteins that co-purify with Pat1b. Since the efficiency of GFP-binder pull-down is very high, I chose to use YFP-Pat1b as bait. I also included YFP-Pat1b-A in the analysis, hoping to find proteins other than Rck that interact with the acidic domain. I transfected HEK293 cells either with YFP, YFP-Pat1b or YFP-Pat1b-A, using two 15 cm dishes per transfection. After 24 hrs, I collected the cells and performed the IP with GFP-binder. In order to increase the specificity of the interacting proteins I washed the beads with 300 mM NaCl prior to elution. Samples were run into SDS-polyacrylamide gel for only 1-2 cm. The gel was stained with colloidal coomassie and given to the ZMBH Core Facility for Mass Spectrometry and Proteomics for analysis. Each sample lane was cut into four pieces, and proteins were identified by HPLC-MS/MS.

Several proteins were found to be enriched in YFP-Pat1b and/or YFP-Pat1b-A compared to YFP alone (see Table 5.1 for the complete list of enriched proteins). Many proteins that I previously found to associate with Pat1b are also included in the list (depicted in *italic* on Table 5.1), supporting that the proteins identified by MS are valid. Specifically, I found both Dcp1a and Dcp2, as well as the decapping enhancers Hedls, Rck, Edc3, and all components of the Lsm1-7 complex except for Lsm5 in the MS data. In addition, PABP1 and Xrn1 were also included in the list. Although the Pat1b interactions with the decapping complex and the decapping enhancers are well represented, only CNOT1 among the Ccr4-NOT complex components was detected by MS. Other proteins that I could show to interact with Pat1b when expressed exogenously, like the Argonaute proteins or TTP, were not identified by the MS analysis either. It is possible that these interactions are enhanced when the proteins are expressed exogenously in high amounts. On the other hand, the MS data is unlikely to cover all the interacting partners of Pat1b.

There are a large number of ribosomal proteins (72 including mitochondrial ribosomal proteins) among the proteins identified to interact with Pat1b. It would be important to confirm these interactions since ribosomal proteins are known as common contaminants in MS analysis. Also, it would be important to determine if the ribosomal proteins interact

2 Results

Pat1b via mRNA (or RNA in general). There are also several RNA-binding proteins in the list, including RNA helicases and heterogeneous nuclear ribonucleoproteins (HNRPs). I chose a few candidates from the list of Pat1b interacting proteins for confirmation via western blot analysis. Figure 2.15 shows that G3BP1, IMP1 and IMP2 do interact with YFP-Pat1b. G3BP1 and IMP1 appear to associate with Pat1b via RNA, while the IMP2 interaction is resistant to RNase A treatment.

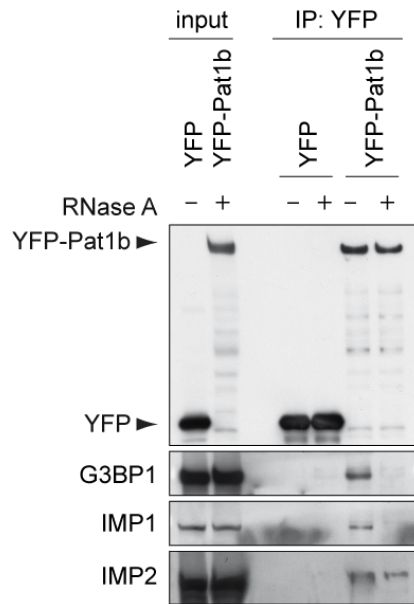


Figure 2.15. Confirmation of novel Pat1b interacting proteins. HEK293 cells were transiently transfected with YFP or YFP-Pat1b. 24 hrs after transfection, cytoplasmic lysates were processed for IP with GFP-binder. WB analysis against YFP, endogenous G3BP1, IMP1 and IMP2 was done with specific antibodies. Where indicated, RNase A was added to the samples during IP.

Rck is represented with the highest number of unique peptides in the list of proteins that were identified to interact with Pat1b-A. There are several HNRPs among the Pat1b-A interacting proteins. A few examples with high numbers of unique peptides among the Pat1b-A interacting proteins are RACK1, which localizes to stress granules, Peflin, which is a Ca^{2+} -binding protein, and CDK2, a Ser/Thr protein kinase required for G1/S transition. It will be important to validate these interactions before drawing any conclusions.

2.4.6 Summary of Pat1b Interactions

My co-IP analyses showed that Pat1b interacts with the Ccr4-NOT deadenylation complex, the Dcp1/Dcp2 decapping complex, the decapping enhancers Rck, Hedls, Edc3, Lsm1-7, and the exoribonuclease Xrn1. In addition, Pat1b interacts with TTP and BRF1, which are involved in ARE-mediated mRNA decay, and Argonaute and TNRC6 proteins, which are involved in miRNA-mediated mRNA decay. These interactions are mediated via different domains of Pat1b. The acidic domain, Pat1b-A, mediates the interaction with Rck, and contributes to the interaction of Pat1b-N with the deadenylation and decapping complexes. Interestingly, the decapping and the deadenylation complexes, as well as the Argonaute proteins, interact with both the N and C domains. Moreover, Pat1b-N mediates the interactions with TTP, BRF1 and PABP, while the AN domain is required for the interaction with TNRC6 proteins. The C-terminal domain of Pat1b connects Pat1b to the decapping enhancers and Xrn1. Although no interactions have been attributed to the homology domain, it strengthens the Pat1b-C interactions. A schematic summary of the Pat1b interactions identified to this point is depicted in Figure 2.16.

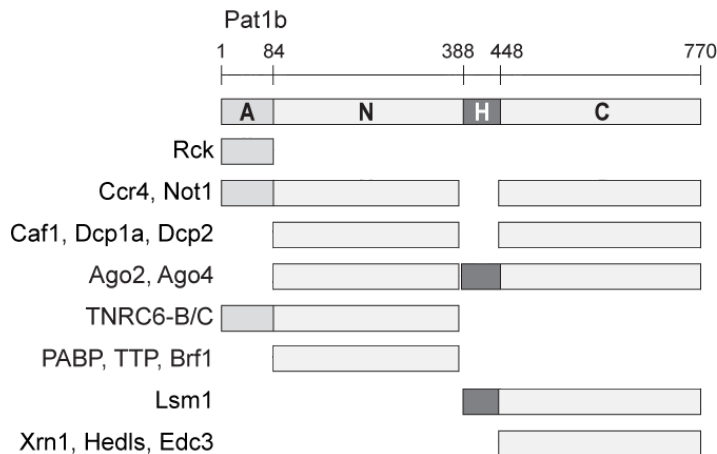


Figure 2.16. Summary of Pat1b interactions. Grey bars represent the domains of Pat1b that mediate interactions with the proteins indicated on the left.

2.5 Function of Pat1b

Localization and interaction data strongly suggest that Pat1b is involved in mRNA turnover. In addition, yeast Pat1p was found to be a translational suppressor (see Section 1.5). To address the function of human Pat1b, I first tested if knockdown of the human protein would have an effect on translational control or mRNA half lives. Moreover, I probed the function of Pat1b using the tethering assays. The results of these functional assays are summarized below.

2.5.1 Pat1b as a Suppressor of Translation?

I used radioactive labeling to determine the effect of Pat1b knockdown on global translation. ^{35}S (radioactive sulfur isotope) labeled methionine and cysteine added to the growth medium are utilized by the cells for protein synthesis. Therefore, ^{35}S labeling enables the quantification of the newly synthesized proteins in the cell. To determine if Pat1b is required for translational control, I employed ^{35}S labeling after siRNA-directed knockdown of Pat1b, in comparison with cells transfected with control siRNAs. In yeast, Pat1p and Dhh1p have redundant functions in suppressing translation under conditions of glucose deprivation. Thus, I also included double knockdown of Rck together with Pat1b. To achieve the knockdown, cells were transfected twice with siRNAs over 5 days. On the fifth day, cells were labeled with ^{35}S -Met/Cys for 30 min after they had been starved of methionine and cysteine for 2 hrs in depletion medium. After lysis, radioactivity incorporated into precipitable proteins was measured by scintillation counting, and normalized to total protein measured by Bradford assay.

Figure 2.17 shows the knockdown efficiency by qPCR (A) and WB (B), and the results of the ^{35}S labeling after Pat1b and/or Rck knockdown. If Pat1b was a suppressor of translation, one would expect to see an increase in ^{35}S -Met/Cys incorporation after its knockdown. Although the knockdown both for Pat1b and Rck worked fairly well, there is no effect on global translation. I was also not able to detect consistent differences in translation upon Pat1b and/or Rck knockdown after exposing cells to different stress conditions like glucose deprivation (data not shown). From these experiments I concluded that Pat1b does not have an effect on general translation.

2 Results

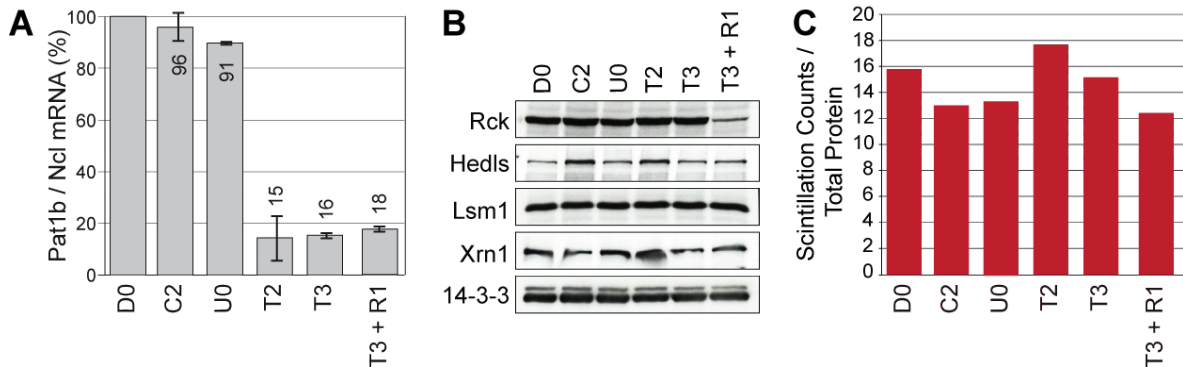


Figure 2.17. Pat1b does not affect general translation. U2OS cells were transfected with control siRNAs (D0, C2, and U0), or with siRNAs against Pat1b (T2, T3), or with siRNAs against Pat1b (T3) and Rck (R1) at 50 nM final concentration. (A) Endogenous Pat1b mRNA levels were quantified by qPCR and normalized to nucleolin (Ncl) mRNA levels. The value in D0 transfected cells was taken as 100%. (B) Western blot analysis shows the Rck protein levels after siRNA transfection. WBs against Hedls, Lsm1 and Xrn1 are also shown. WB against 14-3-3 serves as loading control. (C) siRNA transfected cells were labeled with ^{35}S -Met/Cys for 30 min. Scintillation counts of precipitated total protein were normalized to total protein levels, shown are arbitrary units.

2.5.2 Pat1b as an Essential Protein in mRNA Degradation?

In order to determine whether Pat1b is required for mRNA degradation, I again used siRNA-directed Pat1b knockdown. Since there are no known targets of Pat1, I tested reporter mRNAs with short half lives. These reporters contain either 2 target sites for the miRNA let-7A (7B-lin41), or the TNF α -ARE sequence (7B-ARE) in the 3' UTR of a rabbit β -globin minigene. The reporters were stably transfected in HeLa-Tet-On cells, and their expression can be induced by addition of Doxycycline (Dox) to the cell culture medium. Cells were transfected twice either with water, control siRNA (D0) or one of the 4 siRNAs against Pat1b, at 50 nM final concentration over 5 days. Transcription of the reporters was induced for 16 hrs before sample collection. Transcription was inhibited by addition of actinomycin D (ActD), and total RNA was isolated at 0, 1, 2 and 3 hrs after inhibition. Such an ActD chase experiment enables the estimation of mRNA half lives since, after transcriptional blockage, only the decay rates determine changes in mRNA levels.

As can be seen in Figure 2.18-A, the 7B-ARE reporter mRNA is stabilized upon knock down of Pat1b with siRNAs T3 and s37, but not with T2 and s38. With all siRNAs against Pat1b, endogenous Pat1b mRNA levels were reduced down to approximately 20% (as measured by qPCR) compared to the levels in D0 transfected cells (data not shown). If the stabilization of the 7B-ARE reporter mRNA was a result of reduced Pat1b protein levels, it should have been seen with all 4 siRNAs against Pat1b. Consequently, the stabilization seen with T3 and s37 siRNAs is likely to be due to off-target effects of these siRNAs. No significant change in the decay of the miRNA target, 7B-lin41 mRNA, was observed upon Pat1b knockdown regardless of the siRNA used. In conclusion, Pat1b does not seem to be essential for the decay of either the ARE or the miRNA reporter mRNAs.

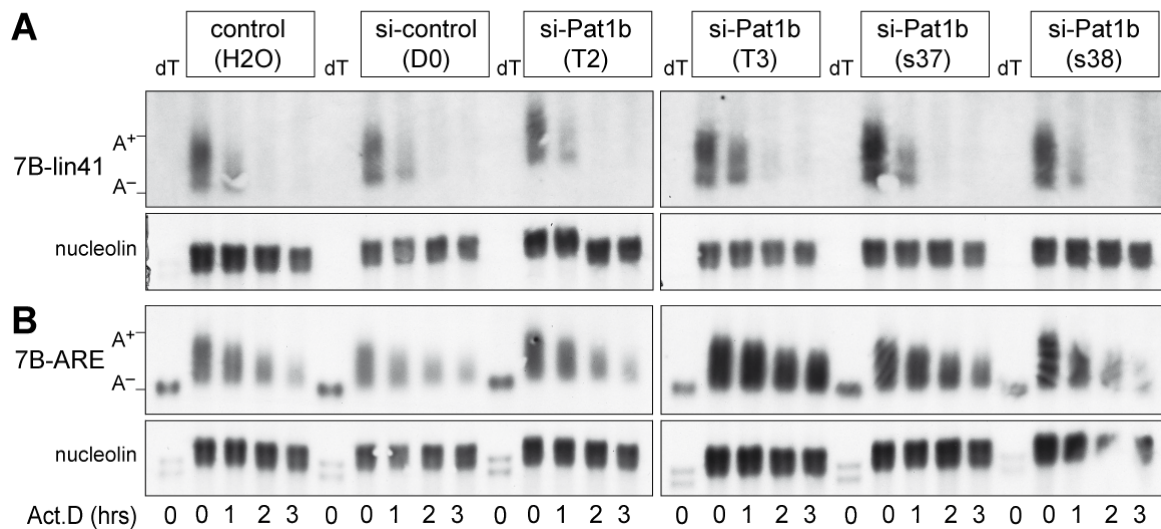


Figure 2.18. Pat1b knockdown does not affect degradation of reporter mRNAs. HeLa-Tet-On cells were transfected either with water, control siRNA (D0), or with siRNAs against Pat1b (T2, T3, s37, s38) at 50 nM final concentration. Transcription of miRNA (7B-lin41) and ARE (7B-ARE) reporter mRNAs was induced by 5 $\mu\text{g}/\text{ml}$ doxycycline for 16 hrs before sample collection. Transcription was blocked by addition of actinomycin D (ActD), and total RNA was isolated at indicated time points. RNA samples were run in 1.6% agarose gel and northern blotting was done to detect the reporter mRNAs in addition to the endogenous nucleolin mRNA, which serves as loading control. Where labeled with "dT", the polyA tail of the reporter mRNAs were digested by RNase H treatment after being incubated with oligo(dT). (A) miRNA reporter 7B-lin41, (B) ARE reporter 7B-ARE.

2.5.3 Pat1b Tethering Assay

Since no substantial differences were detectable in general translation and selected reporter mRNA half lives upon knockdown of Pat1b, I decided to change the experimental approach. I used a tethering assay, whereby bringing Pat1b in close proximity of the reporter mRNA. The tethering strategy that I used is based on an RNA-protein interaction of the *Pseudomonas aeruginosa* bacteriophage PP7 [144]. The PP7 coat protein (cp) binds as a dimer with high affinity to a stem loop in the bacteriophage RNA, the PP7 binding site (bs). To be able to measure both protein and mRNA levels of the reporter gene, I cloned firefly luciferase (FL) at the 5' end of the rabbit β -globin minigene. In the 3' UTR of this reporter gene (termed FLB), I cloned six copies of the PP7bs (FLB-PP7bs). In addition, I introduced the PP7cp between the HA tag and Pat1b. When the two plasmids are co-expressed in cells, Pat1b will be in close proximity of the reporter mRNA using this strategy (Figure 2.19-A).

Pat1b tethering suppresses mRNA expression levels First, I wanted to make sure that the tethering system is working. As the binding of PP7cp to PP7bs is of high affinity, it should be possible to detect the RNA-protein interaction after IP with antibody against the HA tag on the HA-PP7cp-Pat1b fusion protein. I transfected HeLa cells with plasmids encoding for FLB or FLB-PP7 together with HA-PP7cp, HA-PP7cp-Pat1b or HA-Pat1b. 24 hrs after transfection, I collected the cells and conducted the anti-HA IP. Before elution, I split the

2 Results

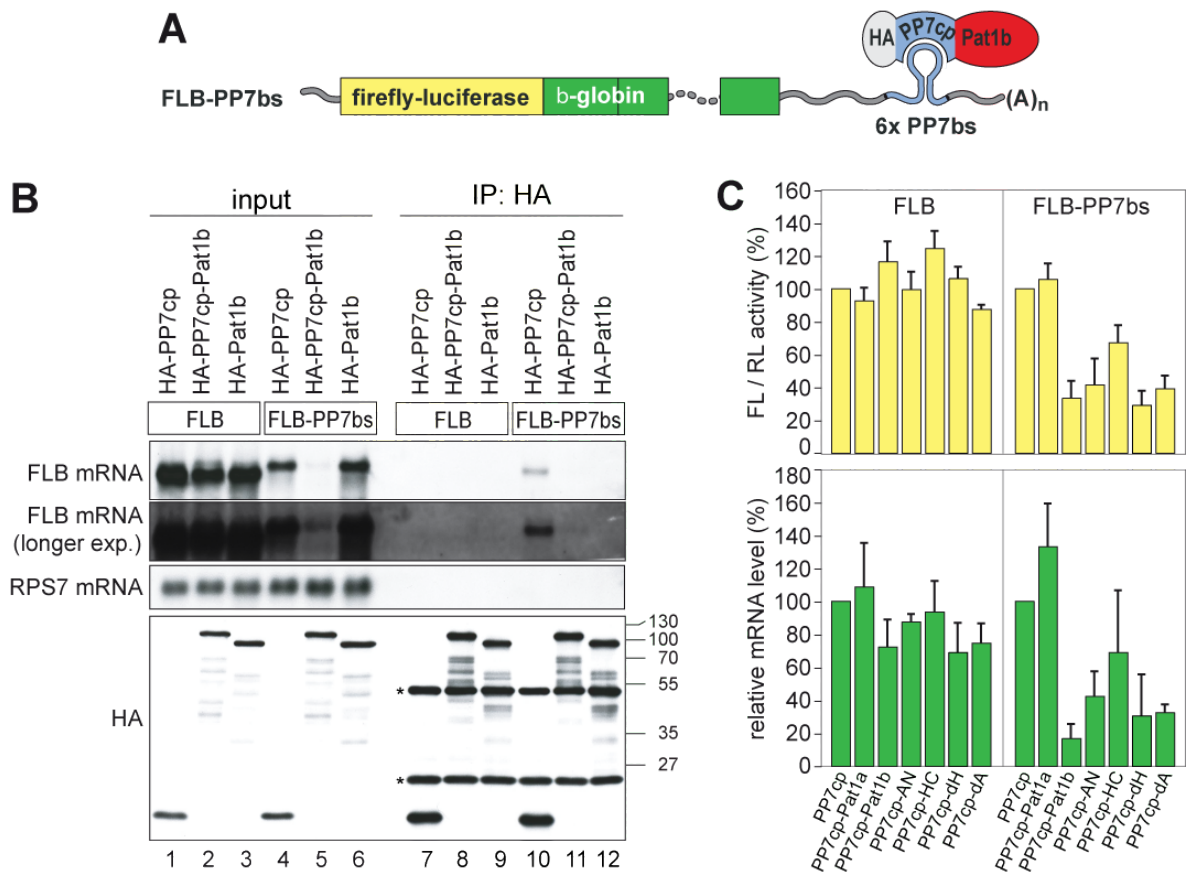


Figure 2.19. Pat1b tethering reduces mRNA levels. (A) Schematic representation of the FLB-PP7bs reporter containing firefly luciferase fused to rabbit β -globin mRNA. 6 copies of the PP7 binding sites (PP7bs) were cloned in the 3' UTR of the FLB reporter. The PP7 coat protein was fused to Pat1b C-terminal to the HA tag (HA-PP7cp-Pat1b). (B) HeLa cells were transfected with FLB or FLB-PP7bs reporter together with either HA-PP7cp, HA-PP7cp-Pat1b, or HA-Pat1b. HA-tagged proteins were immunoprecipitated with anti-HA antibody. RNA and protein were extracted from both the input and IP samples, and analyzed by northern (top two panels) and western (bottom) blotting. A longer exposure of the northern blot against the FLB mRNA is also shown. The sizes of the molecular weight markers (in kDa) are indicated on the right. *, immunoglobulin heavy and light chains. Ribosomal protein S7 (RPS7) mRNA serves as RNA loading control. (C) HeLa cells were transiently transfected with FLB or FLB-PP7bs reporter together with a Renilla luciferase (RL) reporter and either HA-PP7cp, HA-PP7cp-Pat1a, HA-PP7cp-Pat1b, or HA-PP7cp fused to fragments of Pat1b. Cells were collected 24 hrs after transfection. One third of the cells were used for luciferase assay, and total RNA was isolated from two thirds. FLB mRNA levels were determined by northern blot analysis, normalized to RPS7 mRNA, and quantified. Average values together with error bars showing SD from three repeat experiments were plotted in the graph.

beads into 2 samples, and isolated both RNA and protein. Figure 2.19-B shows the results of such an anti-HA IP. As expected, the reporter mRNA lacking the PP7bs did not co-IP with any of the proteins. Interestingly, overexpression of HA-PP7cp-Pat1b strongly reduced the mRNA levels of FLB-PP7bs (lane 5), but not of the FLB (lane 2). As can be seen in Figure 2.19-B lane 7, HA-PP7cp did in fact bring down FLB-PP7bs mRNA. Although this mRNA should

also bind HA-PP7cp-Pat1b, there is no FLB-PP7bs mRNA detectable in HA-PP7cp-Pat1b pull down. This is probably due to the low mRNA levels. HA-Pat1b alone without the PP7cp did not pull down any FLB-PP7bs mRNA although the protein itself was immunoprecipitated as efficiently as HA-PP7cp.

Figure 2.19-C represents the normalized protein and mRNA levels after tethering of the constructs (all HA-tagged) indicated at the bottom of the panel. In this experiment, I also included Pat1a. Tethering of HA-PP7cp-Pat1a leads to a slight increase in FLB-PP7bs mRNA levels, although a large error bar makes the significance of this results questionable. On the other hand, tethering of HA-PP7cp-Pat1b results in a clear suppression of mRNA and protein levels derived from the FLB-PP7bs reporter. Since the low mRNA levels correlated well with the low protein levels, I concluded that the primary effect of Pat1b tethering is on mRNA levels. Tethering of the Pat1b fragments AN, HC, dH and dA indicates that Pat1b-AN is responsible for the observed mRNA suppression. Pat1b-AN probably exerts its effect independently of the acidic domain, since its deletion (Pat1b-dA) did not abrogate the ability of Pat1b to suppress mRNA and protein levels.

Pat1b tethering causes mRNA degradation The observed decrease in mRNA levels upon tethering of Pat1b can be explained either by an increased mRNA turnover rate or by an indirect effect on transcription. In order to make sure that the effect of Pat1b tethering is posttranscriptional, transcriptional pulse-chase experiments were conducted by Jochen Kreth. In these experiments, a reporter mRNA without the firefly luciferase (7B-PP7bs) was used. HeLa cells were transfected with 7B-PP7bs together with HA, HA-PP7cp, HA-PP7cp-Pat1b or HA-Pat1b. 24 hrs after transfection, transcription was inhibited by ActD and RNA was isolated 0, 1, 2, and 3 hrs following ActD addition. Northern blot analysis of the 7B-PP7bs mRNA together with that of endogenous nucleolin mRNA, which serves as loading control, is depicted in Figure 2.20-A. This experiment clearly shows that the low reporter mRNA levels seen after Pat1b tethering are due to an increased mRNA decay rate. Co-expression of HA, HA-PP7cp or HA-Pat1b did not affect the stability of the reporter mRNA. Quantification of mRNA half lives is given in Figure 2.20-C. Careful analysis of the northern blot after HA-PP7cp-Pat1b tethering enables detection of two bands corresponding to adenylated and deadenylated mRNA. The adenylated species disappear as early as 1 h after transcriptional inhibition. To determine the change in polyA tail length more clearly, I quantified the northern blot signal along the vertical axis for all time points (Figure 2.20-B). This quantification indicates that Pat1b tethering first induces mRNA deadenylation followed by the decay of the mRNA body. This finding is in line with the interaction of Pat1b with the Ccr4-NOT deadenylation complex shown in Section 2.4.3.

2.5.4 Pat1b-Mediated mRNA Decay Utilizes Dcp2 and Caf1a

The finding that Pat1b tethering induces mRNA deadenylation suggests that the interaction of Pat1b with the Ccr4-NOT deadenylation complex is functionally significant. Keeping in mind that Pat1b also interacts with the Dcp1/Dcp2 decapping complex, I wanted to analyze the importance of both these interactions for Pat1b-mediated mRNA decay. For this purpose, I utilized previously published dominant negative mutants of Caf1a (similar to the mutant described by Zheng et al. [27]) and Dcp2 [70, 68]. These mutations, Caf1a D40A/E42A (Caf1a-AA) and Dcp2 E147A/E148A (Dcp2-AA) disturb the metal ion binding of Caf1a and Dcp2, and, hence, abolish the deadenylation and decapping activities. I repeated the

2 Results

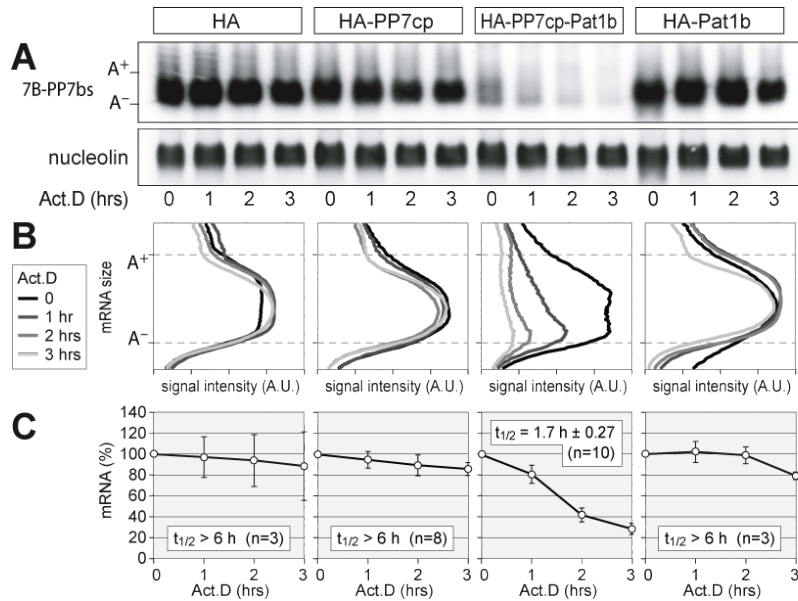


Figure 2.20. Pat1b tethering induces mRNA decay. HeLa cells were transiently transfected with a T7-tagged β -globin reporter containing 6 copies of PP7bs (7B-PP7bs) together with either the HA tag alone, HA-PP7cp, HA-PP7cp-Pat1b, or HA-Pat1b. Total RNA was extracted at 1 h intervals after blocking transcription with actinomycin D (5 μ g/ml). (A) The reporter mRNA was detected by northern blot analysis; nucleolin mRNA serves as loading control. (B) Deadenylation was visualized by quantifying the signal intensity (in arbitrary units, A.U.) of 7B-PP7bs mRNA along the length of the signal and plotting it as a function of mRNA size. (C) The overall signal intensity of 7B-PP7bs mRNA was quantified and normalized to that of nucleolin mRNA. Average values were plotted as a percentage of the initial time point. Error bars indicate standard errors (SE). Experiment repeat numbers used for quantification are shown in each panel.

tethering assays including overexpression of Caf1a-AA and/or Dcp2-AA, and ran the RNA samples in high percentage agarose gels to better visualize the polyA tail length (Figure 2.21). Overexpression of Caf1a-wt slightly enhances the degradation of Pat1b tethered reporter mRNA (7B-PP7bs). The Caf1a-AA dominant negative mutant inhibits deadenylation (note the size of the reporter mRNA in Figure 2.21-C), but does not significantly stabilize the mRNA. This indicates that Pat1b is capable of triggering mRNA decay in the absence of deadenylation activity, even though it clearly triggers Caf1a-mediated deadenylation. I did not observe a significant change in the reporter mRNA half life after overexpression of Dcp2-wt. Dcp2-AA, on the other hand, leads to accumulation of deadenylated mRNA (Figure 2.21-E). The deadenylated reporter mRNA accumulated even more when Caf1a-wt and Dcp2-AA were overexpressed at the same time. Thus, Pat1b also utilizes Dcp2-mediated decapping to trigger the degradation of tethered mRNA. Similar to overexpression of Caf1a-AA alone, mRNA persists in its adenylated form when Dcp2-wt is co-expressed together with Caf1a-AA. The Pat1b tethered reporter mRNA was completely stabilized when both deadenylation and decapping was blocked by overexpression of both Caf1a and Dcp2 dominant negative mutants (Figure 2.21-H). From these results, I concluded that Pat1b triggers both Caf1a-mediated deadenylation and Dcp2-mediated decapping of the tethered mRNA, thereby increasing the degradation rate.

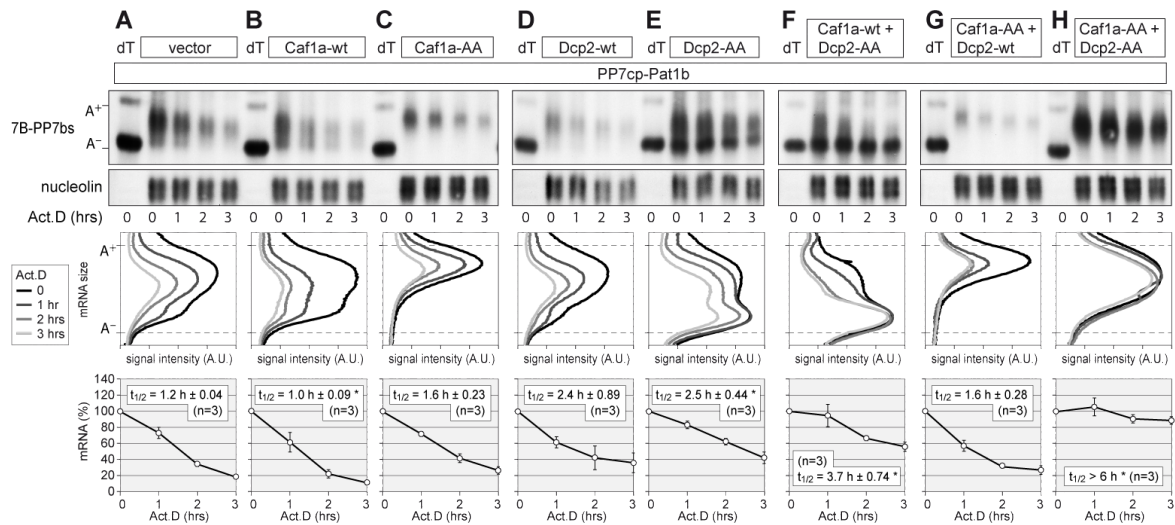


Figure 2.21. mRNA decay induced by Pat1b tethering utilizes Caf1a and Dcp2. HeLa cells were transiently transfected with a T7-tagged β -globin reporter containing 6 copies of PP7bs (7B-PP7bs) together with (A) HA-PP7cp-Pat1b and vector alone, (B) Caf1a-wt, (C) dominant negative Caf1a-AA (D40A/E42A), (D) Dcp2-wt, (E) dominant negative Dcp2-AA (E147A/E148A), (F) Caf1a-wt plus Dcp2-AA, (G) Caf1a-AA plus Dcp2-wt, and (H) Caf1a-AA plus Dcp2-AA. Total RNA was extracted at 1 h intervals after blocking transcription with actinomycin D (5 μ g/ml). The reporter mRNA was detected by northern blot analysis; nucleolin mRNA served as a loading control. RNA samples marked dT were treated with oligo(dT) and RNase H, and serve as a size marker for deadenylated (A^-) reporter mRNA. In the middle panels, deadenylation was visualized by quantifying the signal intensity of 7B-PP7bs mRNA along the length of the signal and plotting it as a function of mRNA size. In the bottom panels, the overall signal intensity of 7B-PP7bs mRNA was quantified and normalized to nucleolin mRNA. Average values were plotted as a percentage of the initial time point. Error bars indicate standard errors (SE). An asterisk indicates a significant difference in the mRNA half-life ($t_{1/2}$) ($P < 0.05$ by two-tailed Student's t test) as compared to the vector control depicted in panel A. Experiment repeat numbers used for quantification are shown in each panel.

2.5.5 Pat1-N Is Necessary and Sufficient for Pat1b Function

In order to determine which domain(s) of Pat1b is required for triggering degradation of tethered mRNA, I cloned PP7cp into HA-Pat1b deletion constructs, and repeated the tethering assay. As can be seen in Figure 2.21, the aggregation-prone Pat1b-N domain is sufficient to induce mRNA decay by tethering. Having the acidic domain together with the N domain appears to increase the mRNA degradation rate. On the other hand, the acidic domain on its own lacks the ability to trigger mRNA decay. Tethering the HC domain does not induce mRNA decay either. Interestingly, C-terminal domain of Pat1b appears to have an inhibitory role in Pat1b activity. Although Pat1b-N alone is sufficient to induce mRNA decay in the tethering assay, it is not fully active in the context of HA-PP7cp-dH or HA-PP7cp-dA. It is possible that the A and H domains of Pat1b act as inducers of Pat1b-N, and their deletion impairs the Pat1b activity. Because Pat1b-N is active on its own, such stimulatory effect(s) does not explain the low activity of HA-PP7cp-dH or HA-PP7cp-dA in the tethering assays, unless the activity of Pat1b-N is inhibited by the Pat1b-C domain. It is likely that the negative effect of Pat1b-C is regulated by the Pat1b-A and/or Pat1b-H domains since the inhibitory

2 Results

effect of Pat1b-C is not detectable in the full length protein.

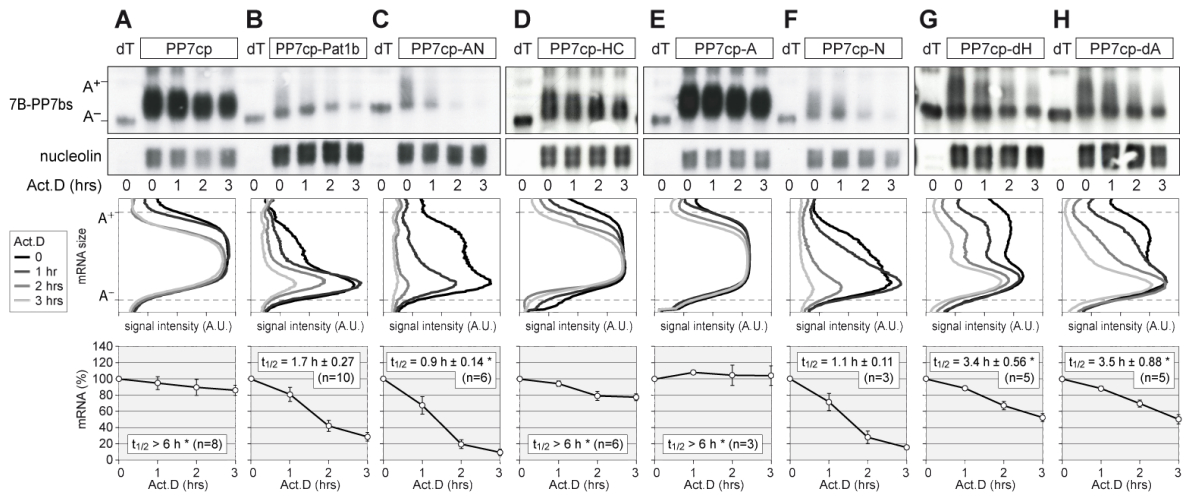


Figure 2.22. Tethering of Pat1b fragments. HeLa cells were transiently transfected with the 7B-PP7bs reporter and (A) HA-tagged PP7cp, (B) PP7cp-Pat1b, (C) PP7cp-AN, (D) PP7cp-HC, (E) PP7cp-A, (F) PP7cp-N, (G) PP7cp-dH, or (H) PP7cp-dA. Degradation of the reporter mRNA was analyzed and quantified as described in the legend to Figure 2.21. Average values \pm SE were plotted as a percentage of the initial time point. An asterisk indicates a significant difference in the mRNA $t_{1/2}$ ($P < 0.05$ by two-tailed Student's *t* test) compared to tethering of PP7cp-Pat1b depicted in panel B.

2.5.6 Is Pat1b Required for Caf1a Activity or Coupling of Deadenylation and Decapping?

Pat1b tethering indicates that Pat1b can recruit Caf1a to the tethered mRNA to mediate deadenylation. However, this assay does not tell us whether Pat1b is required for Caf1a activity. Nor does it provide an idea if Pat1b is needed for coupling of the deadenylation step with decapping in mRNA degradation. In order to test these possibilities, I tethered Caf1a on the mRNA under normal and Pat1b knockdown conditions, and looked for a change in mRNA deadenylation and degradation rates. I also included the knockdown of Rrp40, an exosome core component, to block 3' to 5' decay [145]. This would make mRNA decay entirely dependent on the 5' to 3' pathway, thereby making the potential effect of Pat1b on Caf1a activity and/or decapping more visible. If Pat1b is required for Caf1a activity, adenylated mRNA species should accumulate after Pat1b knockdown. On the other hand, if Pat1b is required for coupling deadenylation to decapping, then deadenylated mRNA should accumulate after Pat1b knockdown. Tethering of Caf1a after control siRNAs transfection led to rapid mRNA degradation (Figure 2.23). Knockdown of Pat1b or Rrp40 alone did not change the mRNA half life or the polyA tail length. Double knockdown of Pat1b together with Rrp40 stabilized Caf1a tethered mRNA slightly, but this effect was statistically not significant (tested by the Student's *t*-test). The distribution of polyA tail length was not changed by double knockdown of Pat1b and Rrp40. In conclusion, according to this experiment, Pat1b does not seem to be needed for Caf1a activity or the coupling of deadenylation and decapping.

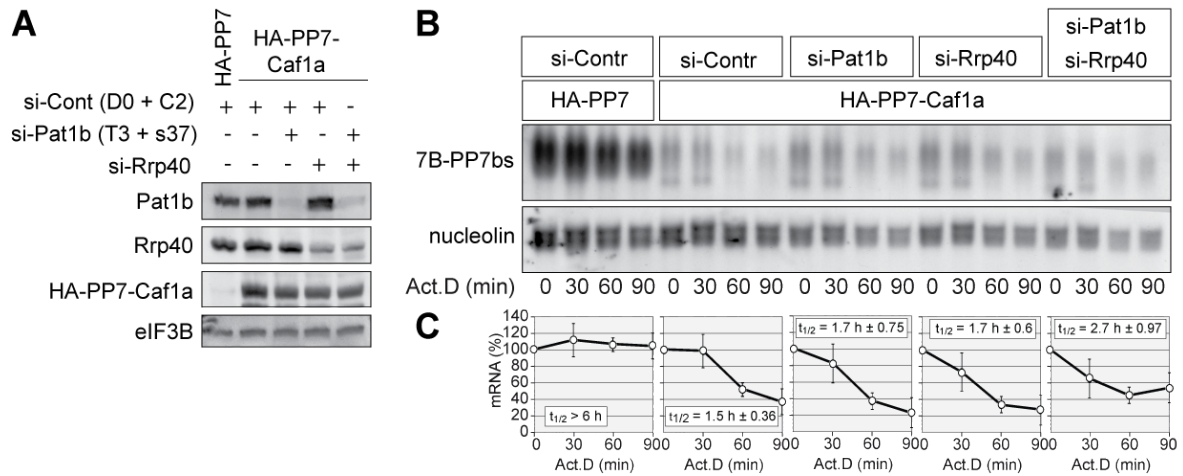


Figure 2.23. Effect of Pat1b knockdown on Caf1a activity. HeLa cells were transfected with control siRNAs (D0 and C2), siRNAs against Pat1b (T3 and s37) and control siRNAs, si-Rrp40 and control siRNAs, or si-Pat1b (T3 and s37) and si-Rrp40 (all at 50 + 50 nM), twice over a period of 4 days. In the second siRNA transfection, plasmids encoding for the 7B-PP7bs reporter and HA-PP7cp or PP7cp-Caf1a were also included in the transfection mix. (A) Western blots against Pat1b, Rrp40, HA tag and eIF3B (as loading control) are shown. (B) After transcriptional block with actinomycin D (5 μ g/ml), total RNA was isolated at 30 min intervals. The reporter mRNA was detected by northern blot analysis; nucleolin mRNA served as a loading control. (C) Quantification of the total signal, normalized to nucleolin mRNA. Average values \pm SD were plotted as a percentage of the initial time point. Average mRNA half lives, together with \pm SD, as indicated in each graph (n=3).

2.6 Endogenous mRNA Targets of Pat1b

The data that I have shown so far indicate that Pat1b is involved in 5' to 3' mRNA decay. Firstly, Pat1b localizes to and is required for formation of P-bodies, where other proteins involved in deadenylation and 5' to 3' decay are concentrated. Secondly, Pat1b interacts with the Ccr4-NOT deadenylation complex, several decapping enhancers, the decapping complex and the 5' to 3' exoribonuclease Xrn1. And lastly, tethering of Pat1b to a reporter mRNA leads to rapid mRNA degradation. Despite these strong data, knockdown of Pat1b by four different siRNAs did not lead to a significant change in the decay of ARE and miRNA reporter mRNAs. It is possible that Pat1b acts on some target mRNAs that do not fit to same criteria as the reporters that I used so far. In order to determine such potential targets and learn more about the physiological function of Pat1b in the cell, I decided to analyze genome wide mRNA expression levels after knockdown of Pat1b by microarray analysis.

2.6.1 Strategy and Quality Control of Samples

With all 4 siRNAs I tested, the Pat1b knockdown was very efficient. Therefore, I hypothesized that any potential target of Pat1b should be up-regulated after a 5 day long siRNA treatment. In order to avoid off-target effects of individual siRNAs, I combined all four siRNAs against Pat1b in equal ratios for transfection. Likewise, I also made a pool of three control siRNAs. As Pat1b and Rck are close interaction partners and were proposed to share roles in translational suppression, I also included Rck knockdown in the experiment. Overall, I had four knockdown

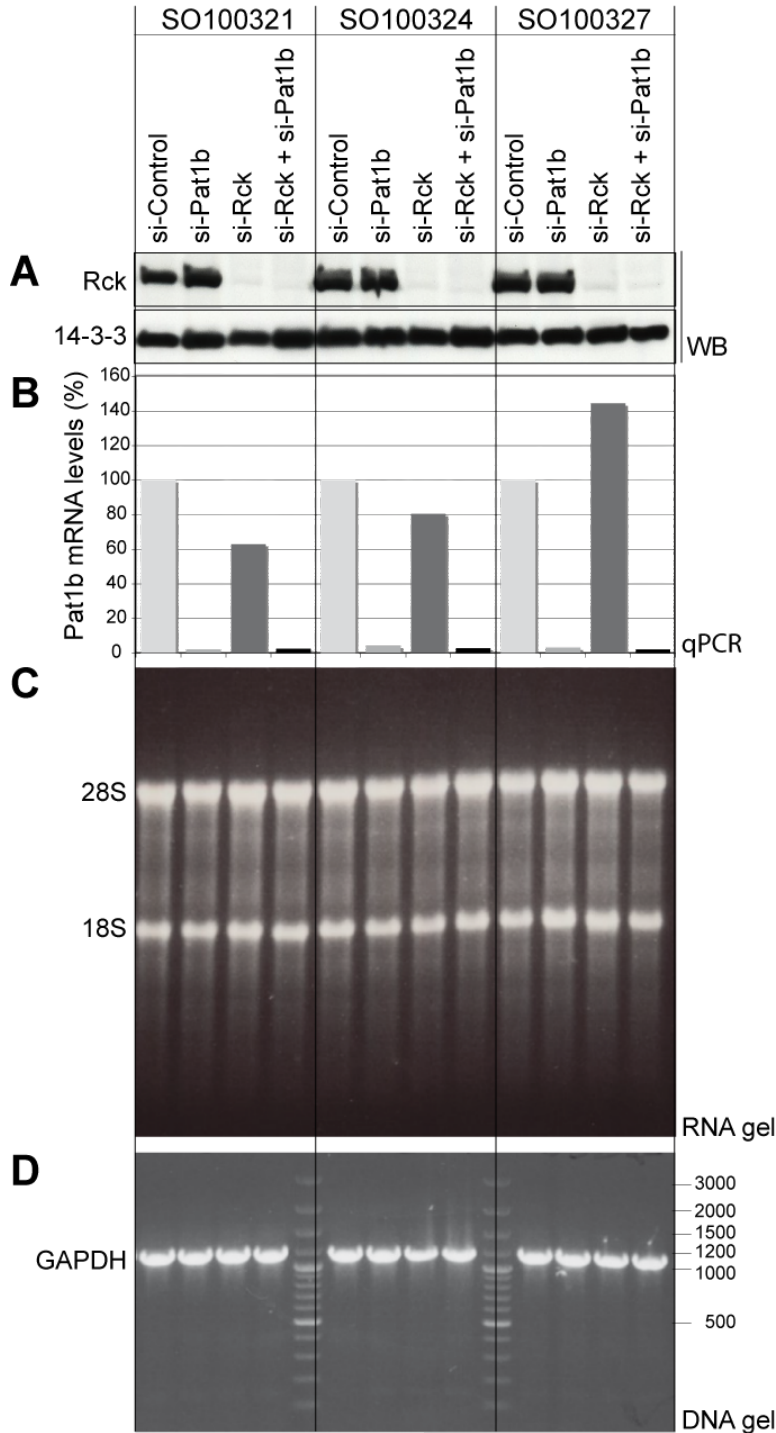


Figure 2.24. Quality control of Rck and Pat1b knockdown levels and integrity of RNA samples for microarray analysis. U2OS-TREX cells were transfected with control siRNAs (1:1:1 mixture of D0, C2 and U0, at 100 nM combined), a pool of siRNAs against Pat1b (1:1:1:1 mixture of T2, T3, s37 and s38, at 80 nM combined, together with 20 nM of si-Control mix), a pool of si-Rck (1:1 mixture of R1 and s28, at 20 nM combined plus 80 nM of si-Control mix) and the si-Pat1b pool together with the si-Rck pool (80 nM plus 20 nM, respectively). siRNA transfection was done twice over five days. One fifth of the cells (harvested from 10 cm dish) were lysed in Laemmli buffer for protein analysis, and total RNA was isolated from the rest of the cells. RNA samples were treated with DNase RQ1 before any further analysis. In total, three repeat experiments were done (SO100321, SO100324 and SO100327). (A) Western blot analysis with anti-Rck and anti-14-3-3 antibodies. (B) qPCR analysis of endogenous Pat1b mRNA levels, normalized to nucleolin mRNA. (C) Ethidium bromide staining of 1 μ g total RNA resolved by denaturing agarose gel. (D) Ethidium bromide staining of PCR amplified (oligos G1862 and G1863) GAPDH cDNA. DNA size of the major marker bands is indicated on the right, in bp.

conditions: (1) si-Control, pool of D0, C2 and U0 siRNAs, mixed equally, at 100 nM final concentration; (2) si-Pat1b, pool of T2, T3, s37 and s38, mixed equally, at 80 nM final concentration, plus 20 nM si-Control pool to have 100 nM final siRNA concentration; (3) si-Rck, pool of R1 and s28 siRNAs against Rck, mixed equally, at 20 nM final concentration combined with 80 nM final concentration of si-Control; (4) mixture of si-Pat1b pool, at 80 nM final concentration, and si-Rck pool, at 20 nM final concentration. I chose to use the U2OS-TREX cell line in the microarray experiment, for several reasons: (1) it is a human cell line; (2) it has a large cytoplasm, hence it is convenient for microscopy; (3) U2OS-TREX cells stably expressing GS-Pat1b were already present.

I transfected the U2OS-TREX cells with siRNAs twice over 5 days, made total lysates from one fifth of the cells (from 10 cm dish) to check protein levels, and isolated total RNA from the rest. I then treated the RNA samples with DNase RQ1 to remove potential DNA contamination. I repeated the experiment three times so that there will be biological repeats included. Rck knockdown was confirmed by western blot analysis (Figure 2.24-A). In order to determine Pat1b knockdown efficiency, I measured the endogenous Pat1b mRNA levels via qPCR (Figure 2.24-B). Both Rck and Pat1b were efficiently suppressed. Before proceeding with microarray analysis, I tested the quality of the RNA. First, I ran 1 μ g total RNA in a denaturing agarose gel to detect possible degradation of the RNA samples. Figure 2.24-C shows that there is no significant degradation. Secondly, I tested the integrity of RNA samples via PCR amplifying cDNAs longer than 1 kb. After reverse transcription with oligo(dT) primer, PCR was done to amplify cDNAs of GAPDH (oligos G1862 and G1863) and nucleolin (oligos G1864 and G1865) mRNAs. Figure 2.24-D shows that the GAPDH cDNA was successfully amplified by PCR at the expected size (PCR for nucleolin mRNA is not shown).

2.6.2 Data Analysis

Total RNA samples from three repeat experiments were given to the EMBL Genomics Core Facility for microarray analysis. cDNA was prepared with random hexamers, and GeneChip Human Gene 1.0 ST Arrays from Affymetrix were used. The GeneChip Human Gene 1.0 ST Array employs 25-mer probes against sense strand. The array offers whole-transcript coverage, with each of the 28,869 genes being represented on the array by approximately 26 probes spread across the full length of the transcript. I analyzed the expression data provided by the EMBL Genomics Core Facility using Chipster software. The data was normalized using RMA algorithm. The data was filtered by 1 SD eliminating the genes that have smallest standard deviations. The rationale is that the genes with lowest standard deviations (standard deviation is calculated for every gene, from all samples, without taking the biological grouping into account) are the ones that do not show differences in expression levels. Filtering by 1 SD removes 67% of the genes. Student's t-test, with Benjamini-Hochberg correction on P-values, was employed to test the statistical significance of the differences in expression levels compared to the si-Control transfected cells.

Table 5.2 shows the genes which were up- or down-regulated at least 2-fold in si-Pat1b, si-Rck and si-Pat1b plus si-Rck transfected cells compared to the si-Control. Despite the strong effect of Pat1b on tethered mRNAs, there are only 59 mRNAs whose expression levels change more than 2-fold upon Pat1b knockdown.

2.6.3 Data Verification

In order to verify the microarray data, I picked 8 up-regulated and 9 down-regulated transcripts from si-Pat1b list, and 6 up-regulated and 5 down-regulated transcripts from si-Rck list (among these selected targets, those with fold changes above 2 are depicted in italics in Table 5.2). I designed qPCR primers for the selected target mRNAs to test if the microarray can be confirmed by qPCR (see Table 4.1 for qPCR primers). Using the same RNA samples that were also used for microarray analysis, I was able to confirm the microarray data. However, when I repeated the siRNA transfections with a new batch of cells, using siRNAs individually instead of in mixtures, I had strong fluctuations in the data. In the end, it appeared that the effects observed by microarray were, due to single siRNAs. Even though comparable knockdown levels of Pat1b and Rck were achieved by individual siRNAs and by the siRNA pools, the targets tested did not respond similarly to individual siRNAs. Two examples are represented in Figure 2.25. *SLITRK6* mRNA is up-regulated 2.5-fold according to the microarray data. This effect can be reproduced by using the RNA samples from experiments 100321, 100324 and 100327 (which were used for the microarrays) but not with RNA samples isolated from later experiments. T2 can be the siRNA responsible for the fold change detected for *SLITRK6* mRNA by microarray analysis. Likewise, down-regulation of *PXDN* mRNA can be confirmed with RNA samples used for microarray, but not with RNA isolated from further repeat experiments. siRNA s37 seems to be a major reason for the observed effect. The same problem holds true also for the Rck targets. In summary, the fold changes determined by microarray analysis appear to be due to off-target effects of individual siRNAs.

2.7 A Closer Look at the Pat1b-Rck Interaction

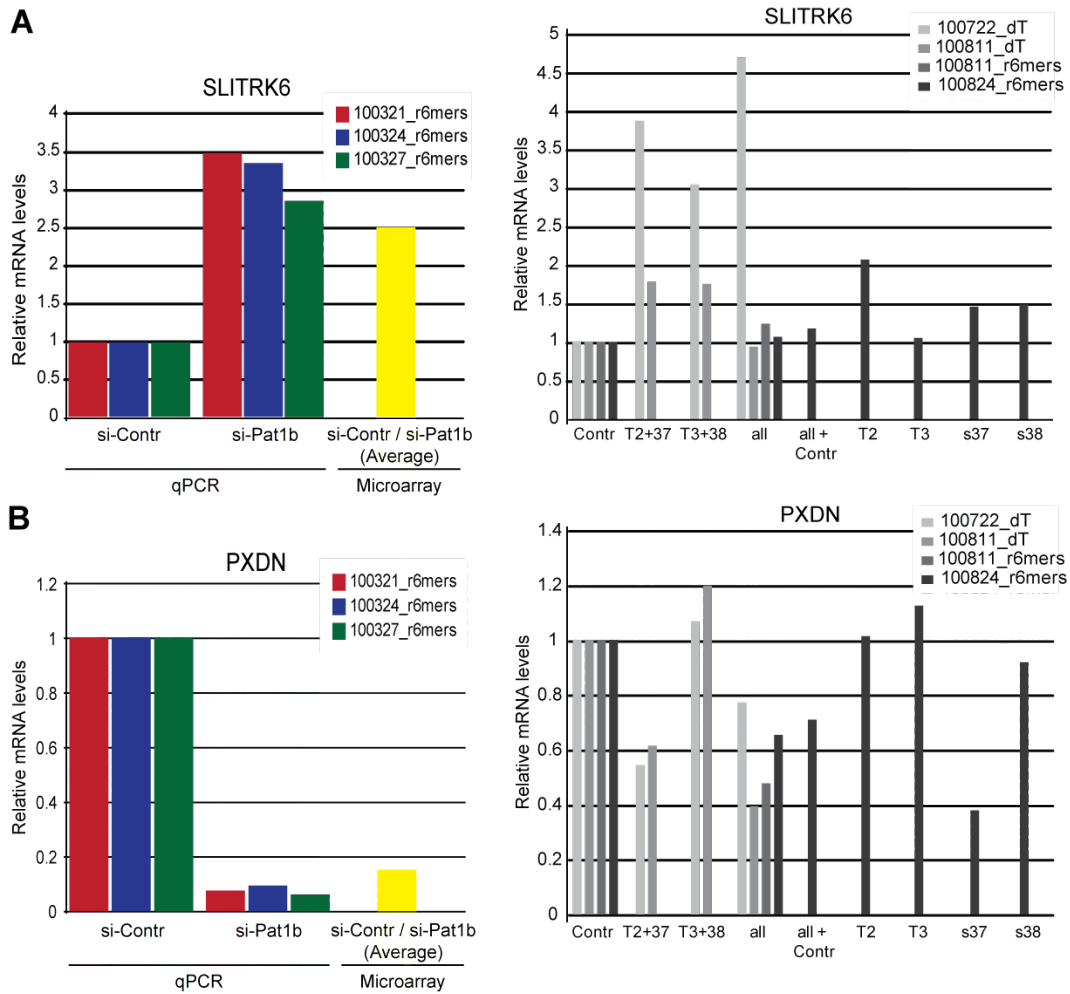


Figure 2.25. qPCR analysis of two putative Pat1b targets identified by microarray. RNA samples were prepared as described in the legend of Figure 2.24. RNA samples from experiments 100321, 100324 and 100327 are the same as the samples used for microarray analysis. Experiments 100722, 100811 and 100824 represent further repeats with siRNA transfections as indicated on the X-axis. Individual siRNAs against Pat1b were transfected at 80 nM final concentration. Contr, pool of control siRNAs D0, C2 and U0, at 80 nM combined; all, pool of si-Pat1b (T2, T3, s37 and s38) at 80 nM combined; all+Contr, si-Pat1b mixture (80 nM) plus si-Control mixture (20 nM); dT, cDNA prepared with oligo(dT) primer; r6mers, cDNA prepared with random hexamers. mRNA levels were normalized to GAPDH mRNA levels.

2.7 A Closer Look at the Pat1b-Rck Interaction

In yeast, Pat1p and Dhh1p were shown to suppress translation under stress conditions, their action being redundant (see Section 1.5). My data also showed that Pat1b and Rck interact tightly in human cells. Therefore, I wanted to analyze the importance of this interaction for Pat1b localization and function in more detail.

2.7.1 Pat1b and Rck Interaction Mutants

I aimed at identifying mutations that would abrogate the interaction between Pat1b and Rck. On the Pat1b side, I showed that the acidic domain is required for Rck interaction (Figure 2.8-C). Alignment of the N-terminal acidic domains of Pat1b from different species points to a conserved DDTF motif (see Figure 2.26-A) [107]. I mutated these amino acids to alanines, and termed the mutant protein Pat1b-4A. The Pat1b-4A mutant does not interact with Rck (Figure 2.26-C).

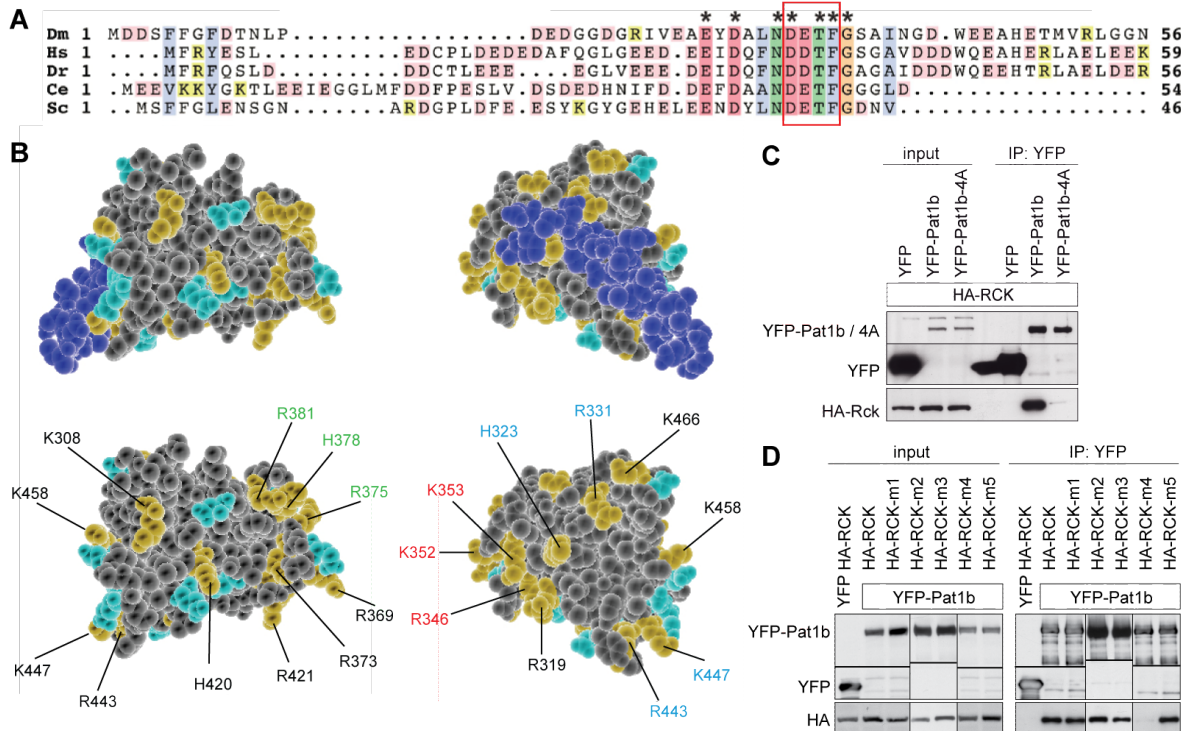


Figure 2.26. Pat1b and Rck interaction mutants. (A) Alignment of Pat1b N-terminal domains from *D. melanogaster*, Dm; *Homo sapiens*, Hs; *Danio rerio*, Dr. *Caenorhabditis elegans*, Ce; and *S. cerevisiae*, Sc. (B) C-terminal RecA-like domain of human Rck together with FDF peptide of Edc3 (blue) [83]. Positively (yellow) and negatively (cyan) charged surface residues are indicated. Residues that were mutated to alanines are pointed in color. The same color was used for marking residues mutated as a group. (C) HEK293 cells were transiently transfected with YFP, YFP-tagged Pat1b or Pat1b-4A together with HA-tagged Rck. (D) HEK293 cells were transiently transfected with YFP or YFP-Pat1b together with HA-tagged Rck wild type or mutants. 24 hrs after transfection, cell lysates were prepared for IP of the YFP tag with GFP-binder. Western blot analyses with antibodies against YFP and HA tags are shown.

On the Rck side, it is the C-terminal RecA-like domain that interacts with Pat1b (data not shown). Since Rck interacts with the negatively charged acidic domain of Pat1b, I reasoned that the positively charged residues on the surface of Rck could mediate Pat1b interaction. The structure of the Rck C-terminal RecA-like domain was published by Tritschler et al. [83]. After visualizing the positively charged residues on the Rck surface (Figure 2.26-B) I mutated them in groups to alanines (residues mutated together are depicted in the same color). Mutation of residues R346, K352 and K353 to alanines in Rck, termed Rck-m4, abolished the

interaction of Rck with Pat1b (Figure 2.26-C).

2.7.2 Rck Binding Is not Required for Pat1b-Mediated mRNA Degradation

Lastly, I wanted to test whether the Rck interaction is important for Pat1b function in the tethering assay. I cloned HA-PP7cp-Pat1b-4A and repeated the tethering assay as described above (subsection 2.5.3). I utilized the FLB reporter, with or without the PP7bs, to measure the protein and mRNA levels. Figure 2.27-A shows FL activity, while panel B shows the mRNA levels. As expected, the FLB reporter without the PP7 binding sites did not show a significant change, neither in protein nor in mRNA levels, upon co-expression of HA-PP7cp-Pat1b or HA-PP7cp-Pat1b-4A. FLB-PP7bs, on the other hand, was equally suppressed by HA-PP7cp-Pat1b and HA-PP7cp-Pat1b-4A tethering. Protein levels were reduced to 30% compared to HA-PP7cp tethered reporter, and the mRNA levels were reduced to ~40%. In conclusion, the Rck interaction is not required for Pat1b function in the tethering assay.

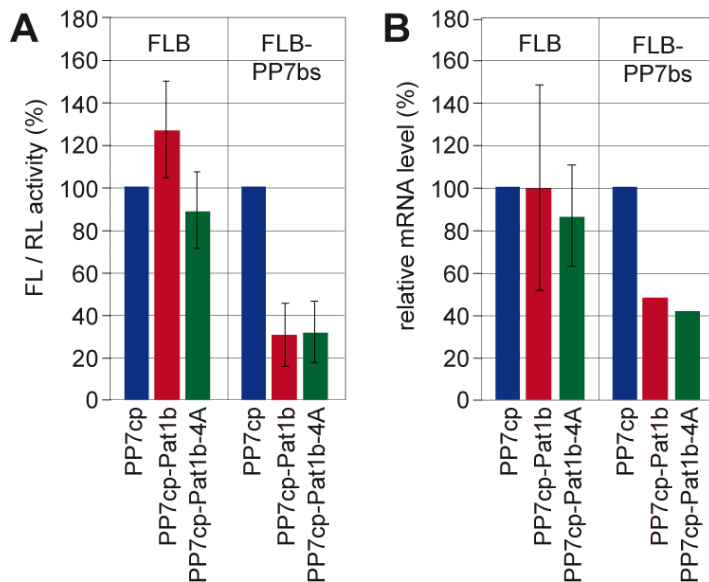


Figure 2.27. Rck is dispensable for the activity of Pat1b in a tethering assay. HeLa cells were transfected with FLB or FLB-PP7bs reporters together with a Renilla luciferase (RL) reporter and either HA-PP7cp, HA-PP7cp-Pat1b or HA-PP7cp-Pat1b-4A. Cells were collected 24 hrs after transfection. One third of the cells were used for luciferase activity measurement, and total RNA was isolated from two thirds. FLB mRNA levels were determined by northern blot analysis, normalized to RPS7 mRNA, and quantified. Average values \pm SD were plotted in the graph. (A) Protein levels, $n=3$. (B) mRNA levels, $n=3$ for FLB reporter and $n=2$ for FLB-PP7bs reporter.

2.7.3 Rck Requires Pat1b Binding for P-body Localization and Formation

Deletion of the Pat1b acidic domain leads to formation of small but numerous P-bodies. Among the many interaction partners of Pat1b, only Rck interacts with Pat1b-A. Hence, I hypothesized that the Rck-Pat1b interaction may be important for controlling P-body size. If this hypothesis holds true, overexpression of the YFP-Pat1b-4A mutant, which does not interact with Rck, should lead to formation of small P-bodies as seen in YFP-Pat1b-dA overexpression. To test this hypothesis, I transfected HeLa cells with YFP-Pat1b-4A and analyzed P-body size and numbers. As can be seen in Figure 2.28-A, P-bodies formed in YFP-Pat1b-4A expressing cells look more like the P-bodies formed in wild type YFP-Pat1b expressing cells. Thus, loss of Rck interaction in Pat1b-dA is not enough to explain the formation of small P-bodies in YFP-Pat1b-dA expressing cells. I have also tested the requirement of Rck binding for Pat1b-mediated P-body formation. Under normal conditions, transfected YFP-Pat1b-4A can interact with endogenous Pat1b and thereby be recruited

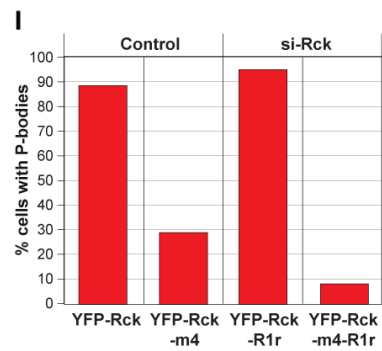
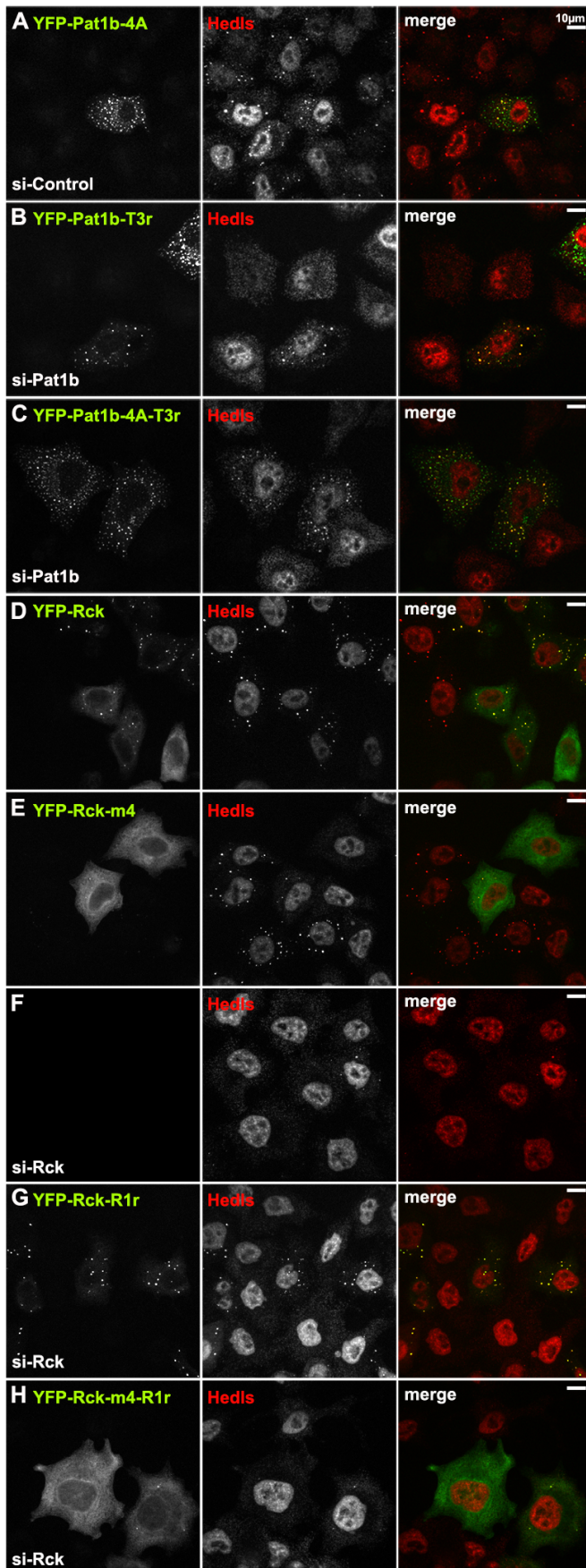
2 Results

to P-bodies passively. siRNA-mediated knockdown of Pat1b inhibits P-body formation as shown in Section 2.3. If the Pat1b-4A mutant depends on endogenous Pat1b for P-body formation, it should not be able to form P-bodies in si-Pat1b transfected cells. To be able to do this experiment, I introduced silent mutations in YFP-Pat1b and YFP-Pat1b-4A, termed YFP-Pat1b-T3r and YFP-Pat1b-4A-T3r, that would make the Pat1b mRNA resistant to cleavage by siRNA T3. Figure 2.28-C shows that, like YFP-Pat1b, YFP-Pat1b-4A can still lead to Pat1b formation, as determined by Hedls localization, after Pat1b knockdown. These results indicate that Pat1b does not depend on Rck for P-body formation.

Next, I tested if Rck needs Pat1b for P-body localization. Overexpression of YFP-Rck in HeLa cells shows accumulation of Rck in P-bodies with some diffuse staining in the cytoplasm. On the other hand, YFP-Rck-m4 has a more diffuse localization in the cytoplasm with only one third of the cells showing YFP-Rck-m4 in P-bodies. I also checked the ability of Rck and Rck-m4 to rescue P-body assembly in cells transfected with si-Rck. Like Pat1b, Rck is an essential P-body protein, whose knockdown results in inhibition of P-body formation. I introduced silent mutations into YFP-Rck and YFP-Rck-m4, termed YFP-Rck-R1r and YFP-Rck-m4-R1r, that render the Rck mRNA resistant to si-Rck R1. Overexpression of YFP-Rck in si-Rck transfected cells leads to P-body formation as judged by Hedls localization. In contrast, YFP-Rck-m4 failed to rescue P-body assembly after Rck knockdown (Figure 2.28-H), with only 8% of the YFP-Rck-m4 transfected cells showing few P-bodies. These results indicate that Rck needs to bind to Pat1b in order to localize in P-bodies and to promote P-body formation.

Figure 2.28. (Next page) Localization of YFP-Pat1b-4A and YFP-Rck-m4. HeLa cells were transfected with (A) control siRNA (D0) and YFP-Pat1b-4A, (B) si-Pat1b (T3) and YFP-Pat1b, which is resistant to siRNA T3, (C) si-Pat1b (T3) and T3 resistant YFP-Pat1b-4A-T3r, (D) YFP-Rck, (E) YFP-Rck-m4, (F) siRNA against Rck (R1), (G) R1 siRNA and YFP-Rck-R1r resistant to R1, and (H) R1 siRNA and R1 resistant YFP-Rck-m4-R1r. siRNAs were transfected twice, at 50 nM final concentration, over 5 days. Plasmids were included in the second siRNA transfection. After 4% formaldehyde fixation, cells were stained with an antibody against endogenous Hedls to mark P-bodies. Images were acquired by spinning-disc confocal microscopy with 60x objective; maximum projections of z-stacks are depicted. Merged images are shown on the right; size bar, 10 μm . (I) Quantification of number of cells with P-bodies in YFP-Rck or YFP-Rck-m4 transfected cells under control conditions or after si-Rck transfection. n=1.

2.7 A Closer Look at the Pat1b-Rck Interaction



3 Discussion

During my PhD studies, I explored the human homolog of the yeast decapping enhancer Pat1p. In the yeast and *Drosophila* genomes, only one homolog of Pat1 has been identified [112, 107]. In contrast, two homologs of Pat1 were found in *Xenopus* and mammalian genomes [146, 139, 141, 147]. The fungal and metazoan proteins share sequence conservation in the N-terminal 50-70 aa long acidic stretch and in the homology domain located in the middle of the proteins. The human proteins Pat1a and Pat1b share high homology throughout their protein sequence. The major difference between Pat1a and Pat1b is the lack of a ~150 aa long portion following the acidic region in the Pat1a protein sequence. This N-terminal portion of Pat1b is enriched in aspartate, glutamine and proline residues.

I started my analysis by investigating whether both of the mammalian Pat1 proteins, Pat1a (PatL2) and Pat1b (PatL1), represent the functional homologs of the yeast protein in human somatic cells. Pat1b localizes to P-bodies and interacts with P-body proteins. In contrast, Pat1a localizes diffusely in the cytoplasm of transfected cells, and no apparent co-localization with P-body markers was observed (Figure 2.2). In order to determine if Pat1a interacts with P-body proteins, I overexpressed Pat1a in human HEK293 cells and carried out immunoprecipitation experiments. Unlike Pat1b, which co-IPs with endogenous Rck, Hedls, Xrn1, Lsm1 and Lsm4, HA-Pat1a interacts only with Lsm1 and very weakly with Lsm4 and Xrn1 (Figure 2.3). Taken together, these data imply that Pat1a is not a P-body protein in the mammalian somatic cell lines tested (COS7, HeLa, U2OS, HEK293).

In fact, the available data suggest that Pat1a is expressed at very low levels in somatic cells. First, it was difficult to amplify the Pat1a cDNA by PCR from several human somatic cell lines. Second, Scheller et al. [139] failed to detect PatL2 mRNA in somatic tissues via northern blot analysis. Third, Marnef et al. [146] and Nakamura et al. [148] showed that xPat1a is expressed in *Xenopus* oocytes, degraded during meiotic maturation, and no longer detected in somatic tissues. Fourth, global microarray expression data shows that Pat1a is expressed at levels close to background in most human and mouse somatic tissues, with modest expression levels in mouse placenta, mast cells and the embryonic stem cell lines V26-2-p16 and Bruce4-p13 [149]. xPat1b, on the other hand, starts to be expressed at low levels towards the end of oogenesis, and remains to be expressed throughout *Xenopus* embryogenesis in somatic tissues. In mammals, global microarray expression data shows that Pat1b is expressed in most mouse somatic tissues with highest expression levels in lymphocytes and macrophages [149]. In conclusion, Pat1a homologs appear to be expressed only during oogenesis, and are not associated with somatic P-bodies.

3.1 Role of Pat1b in P-body Formation

Pat1b is clearly a P-body protein. During my Master's studies, I showed that Pat1b forms several bright cytoplasmic foci, and that Pat1b co-localizes with endogenous Hedls, Xrn1, Rck, Lsm1, Upf1 and overexpressed RFP-Dcp1a in these foci. The localization data mark Pat1b foci as P-bodies. I also examined the localization of endogenous Pat1b with an anti-Pat1b

3.1 Role of Pat1b in P-body Formation

antibody, which was kindly provided by Marina Chekulaeva from Witold Filipowicz's lab, FMI Basel. The anti-Pat1b antibody, termed Ab387, results in a punctuate staining (see Figure S4 and Figure 1 in Ozgur et al. [141] for validation of the antibody and for IF with Ab387, respectively). Among many smaller dots, there are bright and big foci that co-localize with Hedls and Lsm1 (please refer to Ozgur et al. [141] for IF pictures). P-body localization of Pat1b in mammalian cell lines was also confirmed by Scheller et al. [139], Braun et al. [147], and Marnef et al. [146]. Haas et al. [107] showed that HPat, the *Drosophila* homolog of Pat1, also localizes to P-bodies in *Drosophila* S2 cells.

Pat1b is an essential protein for P-body formation. siRNA-mediated knockdown of Pat1b leads to loss of P-bodies in mammalian cell lines (Figure 2.4) [139, 146]. In *S. cerevisiae*, *PAT1* deletion does not abolish P-body formation completely, but P-bodies formed in this strain are smaller and their numbers are reduced, even under stress conditions [126, 124]. These observations indicate that Pat1b is not a passive resident in P-bodies, but plays a critical role in P-body assembly. In fact, overexpression of HA- or YFP-tagged Pat1b increases both the numbers and the size of P-bodies. Quantification of P-bodies formed in YFP-Pat1b transfected cells (Figure 2.2-D) shows that the number of P-bodies per cell increases above 20 in 90% of the transfected cells, while YFP transfected cells have 9 P-bodies per cell on average. Indeed, many of the HA-Pat1b or YFP-Pat1b transfected cells had 50 or more P-bodies per cell. The ability to increase P-body numbers so dramatically upon overexpression seems to be a unique feature of Pat1b, since no other protein has yet been reported to have such an effect. Interestingly, some of these numerous Pat1b foci, in particular the small ones at the periphery of the cell, did not co-localize with other P-body proteins. This suggests that Pat1b is able to aggregate autonomously and nucleate P-body assembly.

Depletion or overexpression of several proteins affect P-body size and numbers. For example, in *S. cerevisiae*, deletion of *XRN1* or *DCP1* leads to dramatic increases in both size and number of P-bodies [126]. The reason for these observations is suggested to be the accumulation of mRNA decay intermediates, rather than a direct effect of Xrn1p or Dcp1p on P-body formation. In this regard, Pat1b is important, since the data suggest an active role for Pat1b in P-body assembly. Supporting the idea that Pat1b can nucleate P-bodies, Pat1b interacts with itself (Figure 2.14). In addition, Pat1b interacts with the Ccr4-NOT deadenylation complex, the decapping complex and several decapping enhancers via its different domains. Therefore, Pat1b may induce P-body formation by providing an interaction platform for the other P-body proteins it interacts with. Thereby, Pat1b self-interaction might allow smaller mRNPs to assemble and form microscopically visible P-bodies. In line with this idea, Pat1b-induced foci do not disassemble in the presence of CHX. CHX is an inhibitor of the translation elongation step in protein synthesis. Treatment of cells with CHX was proposed to trap mRNAs in ribosomes, and thereby inhibit P-body formation [140]. YFP-Pat1b bodies resisted CHX treatment as long as 6 hrs, while non-transfected cells did not have any P-bodies after 2 hrs (Figure 2.6). Although I did not check for the presence of mRNA in YFP-Pat1b foci after CHX treatment, the P-body proteins Hedls, Rck, Xrn1 and Lsm4 were still present in these foci. This indicates that YFP-Pat1b foci are not solely non-specific aggregates of Pat1b, but that Pat1b can stabilize protein-protein interactions that lead to proper P-body formation.

Although I could show that Pat1b co-IPs with several proteins in an RNA-independent manner, it is not known which of these interactions are direct. In yeast, recombinant Pat1p was shown to interact with the recombinant Dhh1p, Scd6p, Xrn1p, Lsm1p, Dcp1p and Dcp2p. In addition, the Pat1p-C domain interacts directly with the Pat1p-M and C domains [88]. In *Drosophila*, recombinant Edc3-FDF peptide was able to compete with the HPat for Me31B

3 Discussion

interaction. This suggests that HPat probably interacts with Me31B directly. For human Pat1b, the most likely direct interaction partners are Rck (Figure 2.26), Dcp2, Hedls, and Lsm1 [147], because the interaction of Pat1b with these proteins was abolished by mutating Pat1b residues. Although these mutations may abolish other interactions that are needed for Rck, Dcp2, Hedls and Lsm1 to associate with Pat1b, it is more likely that these interactions are direct protein-protein interactions. My analysis of the strength of Pat1b interactions with increasing salt concentrations showed that the association of Hedls, Edc3 and Xrn1 is almost lost at 300 mM NaCl (Figure 2.7). These data indicate that Pat1b forms weak electrostatic interactions with Hedls, Edc3 and Xrn1, which may still be direct. My analysis also showed that the Pat1b interaction with Lsm1, the decapping and the deadenylation complex proteins are resistant to 1 M NaCl. Although such strong associations may be due to hydrophobic interactions, this observation suggests that these interactions are likely to be direct. Altogether, these data argue in favor of Pat1b being a scaffolding protein that probably interacts directly with several P-body proteins. However, the precise architecture of the Pat1b associated complex will only become clear after analysis of these interactions using recombinant proteins.

Localization studies of Pat1b deletion constructs resulted in two important findings. First, in line with the ability of Pat1b to initiate P-body formation, the N and AN domains form autonomous aggregates, which do not correspond to P-bodies, when overexpressed. The N domain of Pat1b is enriched in glutamine, asparagine and proline residues, which typically occur in aggregation-prone proteins. In addition, the N and AN domains show the strongest self-interaction with Pat1b. Thus, in the full length Pat1b protein, the N domain can mediate Pat1b self-interaction and lead to P-body formation. Interestingly, aggregation-prone Q/N-rich domains are found in several P-body proteins [125]. This highlights the importance of Q/N-rich domains in protein-protein interactions that are needed for P-body assembly. For example, Decker et al. [90] showed that the Q/N-rich C-terminal domain of Lsm4p provides an alternative way for P-body assembly when Edc3p is absent. As a proof that it is the aggregation property of Lsm4 Q/N-rich tail which is important for P-body assembly, the C-terminus of Lsm4p can be functionally replaced by the prion domain of Rnq1p. P-bodies formed in cells expressing a Lsm4-Rnq1 fusion protein were bigger and brighter compared to P-bodies formed by wild-type Lsm4. This observation indicates that the Rnq1 prion domain interferes with the dynamic properties of P-bodies. The aggregation-prone C-terminal domain of Lsm4p is not conserved in the human Lsm4 protein. This puts Pat1b in a more critical position for P-body formation in human cells. It is worth mentioning that overexpression of the N and AN domains suppress P-body formation in transfected cells (see Table S2 in Ozgur et al. [141]). It is likely that N and AN domains sequester endogenous Pat1b into their autonomous aggregates and therefore have a dominant negative effect on P-body assembly.

The second finding is that Pat1b-A controls the size of P-bodies. Deletion of the Pat1b acidic domain leads to formation of higher number of P-bodies that are smaller in size. Similarly, the aggregates formed by the N domain are much smaller than those formed by the AN domain (Figure 2.5). Although Pat1b-A has a diffuse localization when expressed alone, the A domain contributes to the fusion of smaller mRNPs into larger P-bodies in the context of the full length Pat1b. The only interaction partner of Pat1b-A identified so far is Rck. Therefore, I hypothesized that the loss of the Rck interaction in Pat1b-dA might be the reason for the small P-bodies observed in Pat1b-dA overexpressing cells. I introduced four alanine mutations in the Pat1b acidic domain (mutant construct named Pat1b-4A) that abolish the Rck interaction. Overexpression of the YFP-Pat1b-4A mutant led to the formation of P-bodies that resemble

P-bodies induced by YFP-Pat1b, but not YFP-Pat1b-dA (Figure 2.28). Moreover, YFP-Pat1b-4A-T3r, just like YFP-Pat1b-T3r, rescued P-body formation when overexpressed in cells that were transfected with the anti-Pat1b siRNA T3. Furthermore, I observed that YFP-Pat1b and YFP-Pat1b-4A can induce P-body formation in si-Rck transfected cells (data not shown, n=1). Altogether, these data indicate that Pat1b can form P-bodies regardless of the Rck interaction, and that Pat1b-A controls P-body size independently of Rck. There is no other P-body protein among the proteins identified by mass spectrometry to interact with Pat1b-A. In the list of Pat1b-A interacting proteins, RACK1 is the only one known to localize to stress granules [150]. Since P-bodies and stress granules have dynamic contacts [129], RACK1 might be the factor through which Pat1b-A controls P-body size. An alternative hypothesis is that Pat1b-A contributes to the size of P-bodies via its negative charge. It is possible that the A domain interacts with positively charged residues on other P-body proteins, thereby bridging small mRNPs to P-bodies.

Rck seems to depend on the Pat1b interaction for P-body localization. The Rck-m4 mutant, which does not interact with Pat1b, mostly localizes diffusely in the cytoplasm, and only one third of the transfected cells showed YFP-Rck-m4 in P-bodies (Figure 2.28). In contrast, YFP-Rck localizes to P-bodies in ~90% of the transfected cells. In addition, unlike YFP-Rck-R1r, YFP-Rck-m4-R1r could not rescue P-body formation after Rck knockdown. Therefore, despite the ability of Pat1b to form P-bodies independently of Rck, Rck seems to depend on Pat1b to localize to P-bodies.

3.2 Role of Pat1b in mRNA Degradation

In yeast, Pat1p was shown to suppress translation upon glucose starvation [101]. Pilkington and Parker [88] found that the C-terminal domain of Pat1p (aa 422-763) is required for translational suppression. Interestingly, overexpression of Pat1p is sufficient to suppress translation by ~50% under normal conditions. Nissan et al. [92] showed that the recombinant Pat1p-M+C domain efficiently suppresses translation of luciferase mRNA in an *in vitro* assay. (Refer to Figure 3.1 for comparison of Pat1 domains from different species and studies.) The authors demonstrated that the Pat1p-M+C domain reduces 48S translation initiation complex formation on MFA2 reporter mRNA, and suggested that Pat1p inhibits the association of the 43S pre-initiation complex with mRNA. Despite these strong data for yeast Pat1p, I could not detect a significant effect of Pat1b knockdown on translation in mammalian cells, neither under control conditions nor upon stress. Since Dhh1p and Pat1p were shown to be redundant suppressors of translational, I also included a double knockdown of Pat1b and Rck in my analysis. Nevertheless, I could not record any translational up-regulation in the double knockdown either. Marnef et al. [146] detected that xPat1b suppresses translation of tethered luciferase mRNA when injected in *Xenopus* oocytes. In these experiments, the authors used capped but non-polyadenylated mRNAs and did not observe a difference in mRNA levels. The lack of changes in mRNA levels is not surprising given the fact that in oocytes, mRNA degradation does not take place. Although the data are convincing, the system employed is somewhat artificial since xPat1b is not expressed in *Xenopus* oocytes. It is also possible that in the course of evolution, Pat1b lost its ability to suppress translation.

Pat1b interacts with decapping enhancers, which points towards a role of Pat1b in mRNA degradation. Tethering Pat1b on the FLB reporter mRNA results in a clear reduction of mRNA levels, which is also reflected by low reporter protein expression. Actinomycin D chase

3 Discussion

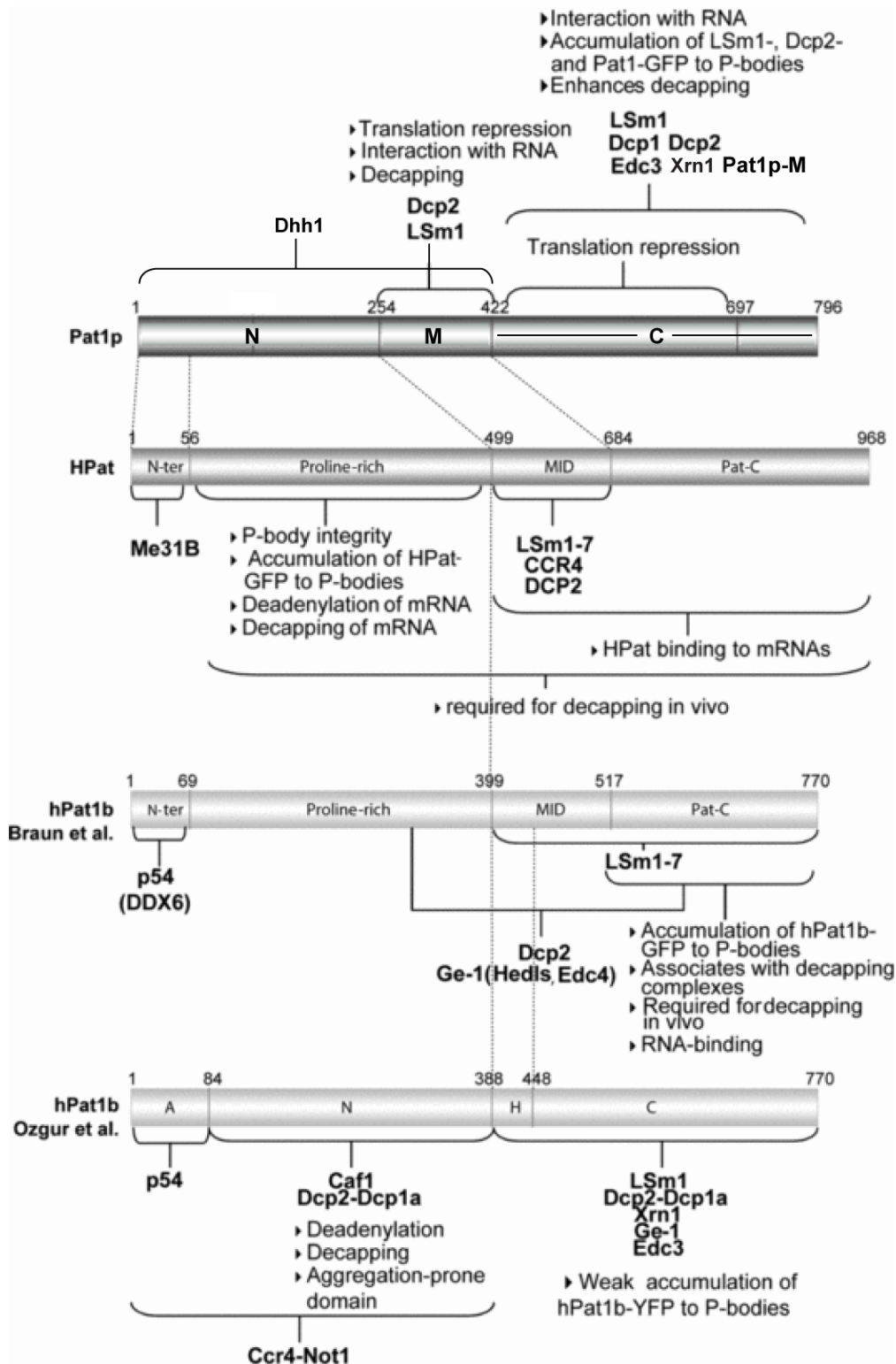


Figure 3.1. Summary of Pat1 interactions and functional domains. Pat1 data from different species are compared. Boundaries of domains used in different studies are also indicated, not to scale. Figure was reproduced from Marnef and Standart [151].

3.2 Role of Pat1b in mRNA Degradation

experiments showed that the low levels of Pat1b tethered mRNA are due to an increased mRNA decay rate. mRNA decay induced by Pat1b tethering is fast. The Pat1b tethered 7B-PP7bs mRNA has a half life of $1.7 \text{ h} \pm 0.27$, while the half life of HA-PP7cp tethered mRNA is more than 6 hrs (Figure 2.20). Since no domain with potential enzymatic activity can be identified in Pat1b sequence, Pat1b is likely to induce mRNA decay via interacting proteins. In fact, Pat1b interacts with the Ccr4-NOT deadenylation and the Dcp1/Dcp2 decapping complexes. Supporting a role of deadenylation in Pat1b tethered mRNA degradation, the adenylated 7B-PP7bs mRNA disappears faster in transcriptional chase experiments. In order to test whether Pat1b-mediated mRNA decay depends on deadenylation and/or decapping, I used dominant negative mutants of the deadenylase Caf1a and the decapping enzyme Dcp2. Overexpression of the Caf1a-AA dominant negative mutant in Pat1b tethering experiments inhibits deadenylation. Interestingly, although mRNA deadenylation is blocked, the mRNA is still degraded with a half life comparable to transfection of vector alone (Figure 2.21). On the other hand, transfection of the Dcp2-AA dominant negative mutant in the Pat1b tethering assay, causes accumulation of deadenylated mRNA species, yet again does not inhibit mRNA decay completely. The Pat1b tethered mRNA is stabilized only in cells overexpressing both Caf1a-AA and Dcp2-AA. Therefore, Pat1b tethering causes mRNA deadenylation and decapping independently.

The Pat1b tethered reporter mRNA is stabilized by 2-fold in cells co-expressing Dcp2-AA, compared to the half life of Pat1b tethered mRNA in cells co-transfected with vector alone. This finding indicates that decapping is a critical step in Pat1b-mediated mRNA decay. By comparing the effect of deadenylation inhibition to the effect of decapping inhibition, it appears that Pat1b-mediated mRNA decay depends on decapping more than deadenylation. Although Totaro et al. [152] suggested that Pat1b induces deadenylation of c-fos mRNA, the effect of Pat1b knockdown they observed is rather subtle. I also did not see a significant effect of Pat1b knockdown on decay of Caf1a tethered mRNA. This observation indicates that Pat1b is unlikely to stimulate deadenylation by Caf1a (Figure 2.23). My data are in line with the decapping enhancer activity attributed to yeast Pat1p. In fact, the recombinant yeast Pat1p N, M and C domains were recently shown to stimulate Dcp1p/Dcp2p in an *in vitro* decapping assay [92]. Pat1p-M and Pat1p-C interact with the N-terminal part of Dcp2p, at aa 100-300 which was used to test this interaction. This implies that the Pat1p-Dcp2p interaction is necessary for Pat1p to enhance decapping. Nevertheless, Pat1p-M+C, which does not interact with Dcp2-(aa 100-300), also enhances decapping, although to a lesser extent than Pat1-C. It is possible that Pat1p-M+C binds to the C-terminal part of Dcp2p, or to Dcp1, to enhance decapping. Alternatively, it might activate decapping via influencing substrate availability to the decapping complex. Despite the results from the *in vitro* assay, it was shown that Pat1p-M is necessary for *in vivo* stimulation of decapping in yeast [88]. Haas et al. [107] showed that in *Drosophila* S2 cells, the HPat Mid and C-terminal domains are required for *in vivo* decapping. The authors reached this result indirectly: they used GW182 tethered mRNA whose degradation is dependent on decapping. They could show that HPat rescues decay, and therefore decapping, of GW182 tethered mRNA in an HPat/ME31B double knockdown background. Braun et al. [147] were able to detect decapping activity with GFP-Pat1b immunoprecipitated from human cells on an *in vitro* synthesized mRNA. This activity seems to depend on Dcp2 that is pulled down together with GFP-Pat1b, because Pat1b mutants and Pat1b N-terminal domains, which do not bind Dcp2, failed to show any decapping activity. Therefore, although the yeast Pat1p can clearly enhance decapping by recombinant Dcp1p/Dcp2p, the ability of the *Drosophila* and human Pat1 proteins to stimulate

3 Discussion

decapping is not clear.

A possible role of Pat1b in mRNA degradation is to connect the two critical steps of mRNA degradation: deadenylation and decapping. Pat1b is likely to interact with the Ccr4-NOT and the Dcp1/Dcp2 complexes simultaneously. I conducted experiments to determine whether there is a competition between the two complexes for Pat1b binding. I tried to compete out Dcp1 or Dcp2 with overexpression of Ccr4-NOT complex components, but could not observe any competition between the deadenylation and the decapping complexes (data not shown). Although it is possible that I did not see any competition because I did not use the direct interaction partners of Pat1b, these results suggest that both complexes bind Pat1b at the same time. Moreover, the Pat1b self-interaction provides another way for Pat1b to bring the deadenylation and the decapping complexes together. My results show that Pat1b interacts with the Ccr4-NOT and the Dcp1/Dcp2 complexes both through the N and C domains. This strongly indicates that Pat1b acts as a scaffolding protein. The most convincing evidence for Pat1b being a physical link between the deadenylation and the decapping complex came from the following experiment (Figure 2.11). When immunoprecipitated, GFP-Caf1a brings down very small amounts of co-expressed Flag-Dcp2. When HA-Pat1b is also expressed in the same cells, the amount of Flag-Dcp2 co-IPed with GFP-Caf1a increases significantly. Hence, Pat1b increases the association between Caf1a, which served as a marker for the deadenylation complex, and Dcp2 used as a marker of the decapping complex. If Pat1b has decapping enhancing activity, it would then further stimulate decapping in addition to complex formation with the Ccr4-NOT deadenylation complex.

My deletion analysis showed that the aggregation-prone N domain of Pat1b is necessary and sufficient to induce decay of tethered mRNA. Tethering of AN or N resulted in faster mRNA decay than tethering of full length Pat1b. The N and AN domains of Pat1b interact with the deadenylation and the decapping complexes. Thus, Pat1b-N appears to induce degradation of the tethered mRNA by recruiting the deadenylation and the decapping complexes. Supporting the role of Pat1b-N in mRNA decay, Haas et al. [107] showed that the P-rich region of HPat, which corresponds to Pat1b-N, is also sufficient to induce decay of tethered mRNA in *Drosophila* S2 cells. Interestingly, although Pat1b-HC also interacts with the Ccr4-NOT and the Dcp1/Dcp2 complexes, its tethering does not lead to mRNA decay. The association of Pat1b-HC with the deadenylation and the decapping complexes is weaker than that of Pat1b-N. Nevertheless, this is not sufficient to explain the difference observed in the tethering assay. Actually, Pat1b-HC interacts with most of the decapping enhancers and, hence, would be expected to have higher activity than Pat1b-N or Pat1b-AN. One possible explanation is that by interacting with the endogenous full length Pat1b, Pat1b-(A)N can induce formation of a complex with higher activity. On the other hand, Pat1b-C appears to have an inhibitory role in Pat1b-mediated mRNA decay. Although Pat1b-N alone is active in mRNA degradation, its activity is repressed in Pat1b-dH and Pat1b-dA mutants, which include the C domain. Tethering of Pat1b-dH or Pat1b-dA leads to accumulation of deadenylated reporter mRNA species, implying that the decapping step is inhibited (Figure 2.22). Inhibition of HPat activity in a tethering assay was also observed after deletion of HPat-N (which corresponds to Pat1b-A) in *Drosophila* S2 cells. It is possible that Pat1b-C negatively regulates Pat1b activity by interfering with the interactions of Pat1b-N. The inhibitory effect of Pat1b-C might be balanced by Pat1b-A and/or Pat1b-H in full length Pat1b. In fact, the crystal structure of the Pat1b C-terminal domain (aa 517-767) shows that the surface of this domain is enriched in positively charged residues [147]. One may speculate that the negatively charged Pat1b-A domain interacts with the positively charged surface of Pat1b-C and thereby provides a self

regulatory mechanism for Pat1b activity. The negative effect of Pat1b-C would be antagonized by its interaction with Pat1b-A. It would be interesting to test the proposed hypothesis by overexpressing the A domain in the tethering assay together with PP7cp-Pat1b-dA. The overexpressed A domain should interact with the C domain of Pat1b-dA and relieve the inhibition on the N domain. Alternatively, if the suggested regulation depends on electrostatic interactions, replacing the A domain with another negatively charged protein sequence should not affect Pat1b activity in the tethering assay, while replacing the A domain with a positively charged protein sequence should reduce Pat1b activity.

Despite its strong effect in tethering assays, the physiological role of Pat1b in mRNA degradation is not clear. Pat1 binds RNA and this property seems to be evolutionarily conserved. In yeast, the Pat1p M and C domains are individually able to bind polyU, but not polyC, RNA [88]. In *Drosophila*, HPat was shown to pull down reporter mRNA independently of Lsm1 [107]. Marnef et al. [146] showed that *in vitro* translated xPat1b as well as human Pat1b binds to polyU and polyG RNA. Weaker binding to polyA RNA was also detected with human Pat1b by Marnef et al. [146], while no interaction with polyA and poly(dU) was observed by Braun et al. [147]. Since AREs are U-rich sequences, it is possible that Pat1b may have a role in ARE-mediated mRNA decay via binding to AU-rich elements. I tried to determine whether Pat1b is required for ARE-mediated or miRNA-mediated mRNA decay via Pat1b knockdown. I used four different siRNAs against Pat1b in these assays and achieved comparable knockdown levels by the individual siRNAs. It appeared that reporter mRNA stabilization, which I observed with two different siRNAs, is due to off-target effects of the two siRNAs. Likewise, I could not reproduce the effect of Pat1b knockdown on potential Pat1b target mRNAs identified by microarray analysis using individual siRNAs. One possible reason for the lack of a significant effect of Pat1b knockdown may be the redundancy between decapping enhancers in mammalian cells. In *Drosophila*, at least two decapping enhancers need to be co-depleted to inhibit decapping [107]. Redundancy is also supported indirectly by the fact that Pat1b interacts with protein components of both the ARE-mediated and the miRNA-mediated mRNA decay pathways.

3.3 Summary

During my PhD thesis, I showed that human Pat1b is an essential P-body protein that has an active role in P-body formation. Moreover, Pat1b interacts with the Ccr4-NOT deadenylation complex, the Dcp1/Dcp2 decapping complex, several decapping enhancers, the 5' to 3' exoribonuclease and many other proteins with roles in mRNA decay. These interactions have functional implications as Pat1b induces degradation of a reporter mRNA when tethered. Pat1b-mediated mRNA decay utilizes both Caf1a induced deadenylation and Dcp2-mediated decapping. In fact, Pat1b increases the association of the deadenylation complex with the decapping complex. Pat1b interacts with the above mentioned proteins via its different domains mostly in an RNA-independent manner. Therefore, Pat1b is likely to act as a scaffolding protein and provide a platform for the formation of degradation compatible mRNPs. Pat1b may further stimulate mRNA degradation by clustering these mRNPs in P-bodies by means of Pat1b self-interaction. I suggest that Pat1b is recruited to the mRNA via its interaction with the Ccr4-NOT deadenylation complex, and that it then bridges the deadenylation complex with the decapping complex, thereby enhancing mRNA decay. In addition, Pat1b may also stimulate the decapping step itself. The association of Pat1b with

3 Discussion

proteins involved in ARE- and miRNA-mediated mRNA decay further suggests that Pat1b is a general factor in 5' to 3' mRNA decay. As it was not possible to detect any effect of Pat1b knockdown on tested reporter mRNAs, Pat1b possibly shares redundant functions with other decapping enhancers.

3.4 Possible Future Directions

My data suggest that Pat1b is a rather general factor in mRNA decay because there was no significant effect of Pat1b knockdown on reporter mRNAs, and because the microarray results could not identify reliable Pat1b target mRNAs. It is still possible that Pat1b is not only a general factor, but required for the decay of a subset of mRNAs under certain conditions. As a future experiment, it would be important to have one more attempt to identify Pat1b targets. Instead of using a knockdown strategy, crosslinking followed by immunoprecipitation and microarray or RNA-sequencing methodology is more likely to identify mRNAs that preferentially interact with Pat1b. The suggested experiment can be repeated under several stress conditions to cover possible conditions under which Pat1b activity might be more essential.

One possibility is that Pat1b stimulates the activity of Dcp2 directly. The yeast data clearly shows that Pat1p induces decapping, but there is no data showing direct stimulation of Dcp2 activity by human Pat1b. An *in vitro* decapping assay is probably more challenging in mammalian systems since formation of a decapping complex is known to require at least Hedls. Lykke-Andersen [61] was able to set up an *in vitro* decapping assay using proteins purified from HEK293 cells. Considering the tight interaction of Pat1b with Dcp2, such an assay would not be conclusive unless the purity of proteins is assured. Moreover, purification of full length Pat1b from bacteria is not straightforward. For the yeast protein, individual domains of Pat1p are sufficient for significant increase in decapping activity by recombinant Dcp1p/Dcp2p. It might be possible to conduct a reliable experiment with recombinant Dcp2 and recombinant domains of Pat1b. An alternative to the proposed *in vitro* decapping assay might be to test the effect of Pat1b knockdown on decapping *in vivo*. Splinted-ligation RT-PCR assay was used by Hu et al. [153] to measure the levels of endogenous decapped mRNAs in *S. cerevisiae*. This assay depends on the knowledge of the exact transcription start site, and it would be necessary to determine the 5' end of the transcript(s) of interest, for example by 5' RACE. Considering the redundancy of Pat1b with other decapping enhancers, it would be important to test double knockdown of Pat1b with other decapping enhancers, and to conduct rescue assays. The splinted-ligation RT-PCR assay may provide evidence whether Pat1b is required to stimulate decapping *in vivo*.

In addition to the interactions that I detected by immunoprecipitation experiments, Pat1b interacts with many more proteins identified by mass spectrometry. I was able to confirm that Pat1b interacts with G3BP1, for which only 2 peptides were detected in MS analysis. Therefore, it is likely that many of the proteins identified by MS indeed associate with Pat1b. Among these proteins, there are several RNA-binding and ribosomal proteins. One interesting candidate is Stau1 which is known to bind dsRNA and induce mRNA decay by an unknown mechanism. Pat1b may be required for Stau1-induced mRNA decay. On the other hand, it is worth exploring the interaction of Pat1b with ribosomal proteins. If the association can be confirmed, they may provide a mechanism for Pat1b to be recruited to mRNAs.

4 Materials and Methods

4.1 Materials

Lists of DNA and RNA oligos, antibodies, technical equipment, chemicals and enzymes, and disposable materials and kits used in this work are given in the following.

4.1.1 DNA and RNA Oligos

Table 4.1. DNA oligos used in this study. DNA oligoes were purchased from Invitrogen or Eurofins MWG. F, forward primer; R, reverse primer.

Oligo	Sequence	Description	Restriction site
G18	ACATTCGGCCGGGTCGACCACTG	β -globin F	SalI
G19	AATTGATATCCACCATGGCCAGCATGACCGGCGGC CAGCAGATGGCGTGCATCTGTCCAG	β -globin R	EcoRV
G78	GGTGGTCGGAAAAGCTATC	NB probe for RPS7 F	
G83	TTACAAAGTCACTCAGGATG	NB probe for nucleolin F	
G85	AGCTTACCACCATGTACCCATACGATGTTCCAGAT TACGCTGGTACCGGATCCG	HA oligo F	
G86	AATTCGGATCCGGTACCAGCGTAATCTGGAACATC GTATGGGTACATGGTGGTA	HA oligo R	
G243	ATATAAGCTTCCACCATGGTGAG	YFP F	HindIII
G244	ATATGGTACCCTTGTACAGCTCG	YFP R	KpnI
G1000	GTGCATCTGTCCAGTG	NB probe for β -globin F	
G1001	GCCGATTTAGGTGACACTATAGAATACCCTGAAGT TCTC	NB probe for β -globin R	
G1008	GCCGATTTAGGTGACACTATAGAATACTATAGACA CCAG	NB probe for RPS7 R	
G1009	GCCGATTTAGGTGACACTATAGAATACTTAGCGTC TTCG	NB probe for nucleolin R	
G1198	TTAATCTAGATCAGTAAATCCAGGCAAACCTCC	Pat1a C-term (2nd PCR) R	XbaI
G1219	GCCAAGATGAATTCGCTTGAAG	Pat1a N-term (1st PCR) F	
G1221	ACTGCTTGCAGCTTCTATATCC	Pat1a mid R	Pat1a D
G1222	GTCTGATGATTCAACTTCC	Pat1a C-term (1st PCR) R	
G1225	ATATGGTACCATGTTCCGCTACGAG	Pat1b-AN F	KpnI
G1226	TATACTCGAGTTAGTGACTTCTCTATCTCC	Pat1b-AN R	XhoI
G1227	ATATGGTACCCGGAGCAGTCATCAAG	Pat1b-H F	KpnI
G1228	TATACTCGAGTTATTCTTCAGCAGCTGAC	Pat1b-H R	XhoI
G1229	ATATGGTACCATACAAGGTGATGGC	Pat1b-C F	KpnI
G1230	TATACTCGAGTTATCGTATCCCCTGAAC	Pat1b-C R	XhoI
G1243	TGTTGGTAGTCCACTTGC	Pat1b Internal Primer	
G1253	ATATCTCGAGTTAACCCCTGTACAGC	Pat1b-YFP R	XhoI
G1256	ATATAAGCTTCCACCATGGAAGACGCC	Fluc F	HindIII
G1257	ATATGGTACCCACGGCGATCTTTC	Fluc R	KpnI
G1268	ATATGGATCCATGTTCCGCTACGAG	Pat1b cloning into p2434 F	BamHI
G1269	GCCTCAGAACTTCAGATCC	Pat1b cloning into p2434 R	
G1270	TTGGGGATCCAGCTGTACTT	Pat1a qPCR (UPL) F	
G1271	CATACCAGGGCCTTGACT	Pat1a qPCR (UPL) R	
G1272	CACCAGCACTCTCCAATCCT	Pat1b qPCR (UPL) F	
G1273	AGCAGTGACAGGCCAAACTT	Pat1b qPCR (UPL) R	
G1295	CTCCAGTTTTTCAAACCTTTCGGAGATG	Pat1b homology domain deletion R	

Continued on Next Page...

4 Materials and Methods

Oligo	Sequence	Description	Restriction site
G1296	CATCTCCGAAAGTTTAAAACTGGAG	Pat1b homology domain deletion F	
G1302	ATCACTCGAGTTAAGGTTTCTCATCTTCTAC	Rck R aa 483	XhoI
G1315	CTTCTGAGGAGGAGCTGGTGTCTG	Pat1a mid F	
G1332	CTCGCCGAGCTATTGATGC	Pat1a C-term (1st and 2nd PCR) F	
G1340	CAAGGAGGCAAGTGACATTC	Pat1a N-term (1st and 2nd PCR) R	
G1353	ATATGGATCCGAATTCATGAATTGCCTTGAAGGGC	Pat1a N-term (2nd PCR) F	BamHI, EcoRI
G1377	TAGTGGATCCATGAGCACGGCCAGACAGAGAACC CTGTTATAATGGTCTGTCCAGTC	Rck synthetic primer for aa 1-11 F	BamHI
G1408	ATATGGTACCAATCTGGCAGAAAAGG	Pat1b-dA F	KpnI
G1425	TATACTCGAGTTACTCCTCATGGTCACC	Pat1b acidic domain R	XhoI
G1501	ATATGGTACCATGTCCAAAACCATC	PP7cp F	KpnI
G1502	ATATGGTACCACGGCCAGCGGCAC	PP7cp R	KpnI
G1777	ACCCAGAAGACTGTGGATGG	GAPDH qPCR F	
G1778	CAGTGAGCTTCCCGTTCCAG	GAPDH qPCR R	
G1784	CAGAAGTAATGTTTATGGCAACACGAGAAC	Pat1b T3 resistant mutant F	
G1785	ATAAACATTACTTCTGTCCACTGATTATTTTG	Pat1b T3 resistant mutant R	
G1816	GAATATGCTTTGCCCTCAGAGGC	Pat1b qPCR F	
G1817	CGGACACAGAATCTGTTGGGTG	Pat1b qPCR R	
G1862	CAGCCTCCCGCTTCGCTCTC	hGAPDH F	
G1863	TGGCAGGGACTCCCCAGCAG	hGAPDH R	
G1864	CAGCCAAAGCAGTTACCACA	hNCL F	
G1865	TTCCAAGGAGACCACAGGAC	hNCL R	
G1883	CAGGGGTACCTAGCAAAATCAGG	Dcp2-E147Q,E148Q F	KpnI
G1884	CTTTGATATCAAAACAGTTGCTGCAAAGACCTCTC	Dcp2-E147Q,E148Q R	EcoRV
G2047	TTGAAGGCCAAAGACATGGCAGCAG	TAGLN qPCR F	
G2048	TCCACGGTAGTGCCCATCTTCTT	TAGLN qPCR R	
G2049	AACACTTTCCTGCTCCTCTCTGTGTC	ACTA2 qPCR F	
G2050	CGAGTCAGAGCTTTGGCTAGGAAT	ACTA2 qPCR R	
G2077	GCACTGCACAGATGGCTGGTTT	Myocardin qPCR F	
G2078	TCTGTGACTCCGGGTCATTTCG	Myocardin qPCR R	
G2079	TCATGAATTCCTATTGTCAG	RCK F	EcoRI
G2080	AATTGCTAGCCAAGAAGATTCTC	RCK F	NheI
G2081	CTTGGCTAGCAATTCAACTCG	RCK R	NheI
G2082	CGCCAAAAGTAGCCTGCCTCAACACTTTTCTCC GGCTTCAGATA	RCK-H323A,R331A (m1) F	
G2083	TATCTGAAGCGCGGAGAAAAGTGTGTTGAGGCAGGC TACTTTTTGGCG	RCK-H323A,R331A (m1) R	
G2084	CATATGATGATGCCTTCAACCTGGCAAGTATTGAGG	RCK-R443A,K447A (m2) F	
G2085	CCTCAATACCTGGCAGGTTGAAGGCATCATCATATG	RCK-R443A,K447A (m2) R	
G2086	GATCAATTCATGCTGCTGCAGCTGGGTCAGGTG	Pat1b-4A F	
G2087	CACCTGACCCAGCTGCAGCAGCATTGAATTGATC	Pat1b-4A R	
G2088	CTCCTCTCAGGCAGTTGAATTGCTAGCCGCGCGGAT TTCTCAAC	RCK-R346A,K352A,K353A (m4) F	
G2089	GTTGAGAAATCGCCGCGGCTAGCAATCAACTGCCT GAGAGGAG	RCK-R346A,K352A,K353A (m4) R	
G2090	GGAACATCGAAATGCTGTATTTGCTGATTTGCGAAA TGGCTTATGC	RCK-R375A,H378A,R381A (m5) F	
G2091	GCATAAGCCATTTGCGAAATCAGCAAATACAGCATT TCGATGTTCC	RCK-R375A,H378A,R381A (m5) R	
G2098	CAGCTCACTCAGCCACACACACC	ACTG2 qPCR F	
G2099	CCACCATCACACCTGGTGGCGA	ACTG2 qPCR R	
G2104	TTCCGGTCTCCAGCTCGACCC	PXDN qPCR F	
G2105	AAAGCCCGCCAGAAGGCGTG	PXDN qPCR R	
G2106	CCCTATAAACTGAAAAGGAGAAGGAGCTG	PPP2R5D qPCR F	
G2107	CGTTGAGTCTGCCCCTTCA	PPP2R5D qPCR R	
G2108	CACAGTCGAGCAGTGCTTTGGTG	CYFIP1 qPCR F	
G2109	GCCGCTGCTGCCAAGAAGTA	CYFIP1 qPCR R	
G2110	CACTACCAGCGGGCGGACTTC	FKBP8 qPCR F	
G2111	TCCTCCTCGAACGTCATGTCCACTTTGG	FKBP8 qPCR R	
G2114	GCCGCCGAGGAAACCTTGAT	CALM3 qPCR F	
G2115	GGAGAAGGCCTCCTTGAACCTGTGCA	CALM3 qPCR R	
G2116	TCGGAGCTACACTTGCTGTGCT	APOBEC3B qPCR F	
G2117	GAGGCTTGAATACACTGGCCTCG	APOBEC3B qPCR R	

Continued on Next Page. . .

Oligo	Sequence	Description	Restriction site
G2118	GCGAGTAGAACCGCTGAGGCG	PARN qPCR F	
G2119	TCACTGATTCTCTGAAAACTCCCATCGA	PARN qPCR R	
G2120	TGCGGAAGGAGAAATGCACGAG	IPO5 qPCR F	
G2121	GTCCACAGTCTCCAGAAGTCTGT	IPO5 qPCR R	
G2122	TGTGCTGCCGTAGCAAATTGGA	NCBP1 qPCR F	
G2123	TCACTTCGCCGTTTGTGTTGCCT	NCBP1 qPCR R	
G2126	ACTCAGAGGAGGCGCCATGTGAGA	CDKN1A qPCR F	
G2127	AGCCCGCCATTAGCGCATCAC	CDKN1A qPCR R	
G2128	TCTGCAGCCCGAGCTAGGATAGA	RCAN2 qPCR F	
G2129	TCTCTGGAGTCTGAACCTGTGCAAA	RCAN2 qPCR R	
G2130	GCGAGGCAATCGTCCGGTGT	G3BP2 qPCR F	
G2131	GCTGCACAATGTCAAATGCTAGAGG	G3BP2 qPCR R	
G2132	ACGAACACCTGTGAGCCCAAGTCAA	RPS6KB1 qPCR F	
G2133	GGTGCCGATGCTTCCCCTC	RPS6KB1 qPCR R	
G2134	GGAAGAGTCTCTGCTTTACAGAATCGG	SLITRK6 qPCR F	
G2135	AGCCTCTGGATGAGAGCACTGGA	SLITRK6 qPCR R	
G2136	CCTGCCTGGAGAGGCCAAAGAGT	RGS16 qPCR F	
G2137	GCTCAGCAGCAGGTCGAACGAC	RGS16 qPCR R	
G2138	TGCATCGTCTTTCAAGGTGCCA	SLC7A11 qPCR F	
G2139	ACGCAGGACTCCAGTCAGAGT	SLC7A11 qPCR R	
G2142	GACCCACCCATTGACCTGGGA	AMTN qPCR F	
G2143	TAGTGCCCTGGGCTCCAAGTTGT	AMTN qPCR R	
G2169	TGCACTGCAACCATGAGTGAGAACA	IFIT2 qPCR F	
G2170	GCCAGTAGGTTGCACATTGTGGC	IFIT2 qPCR R	
G2171	CCATCCTCTTTGGCGCTGCGT	RNPEP qPCR F	
G2172	GTGTCGCGGTCACACGCTG	RNPEP qPCR R	
G2173	TCTACAAGCCAAGGGGAAAGCAAG	RANBP2 qPCR F	
G2174	CGGCTGACTGGGTTCCGACTG	RANBP2 qPCR R	
G2175	AGTCTGAGCAGTTGGCGGA	ROCK1 qPCR F	
G2176	TGCTTCTTCAAGCCGACTAACAGTG	ROCK1 qPCR R	
G2177	CCGGGACCTTCGCGACACAC	BRF1 qPCR F	
G2178	TTGTTACCCTTGCATAAAACTTCGCTCA	BRF1 qPCR R	
G2179	AAACAAGGATCGTCCAGCGATGC	UPF3B qPCR2 F	
G2180	TGGTGCTGTATCAGGGGACA	UPF3B qPCR2 R	
G2264	TCATGAATTCCTTTCaCaAAgCCaTAcGAaATT AACCTGATGGAGG	RCK-R1 resistant mutant F	EcoRI

Table 4.2. List of siRNAs used in this study. siRNAs were synthesized by Ambion (sense strand), and purchased from Applied Biosystems or Eurofins MWG.

No	Target	Acc. #	1st nt in CDS	Sequence
D0 (s002)	unspec.			GCAUUCACUUGGAUAGUAAdTdT
C2 (s014)	unspec.			GGUCCGGCUCSCCAAAUGdTdT
U0 (s015)	unspec.			GAAUGCUCUUGUUGAAUCAdTdT
T1 (s009)	hPat1a	NM_001145112	955	GAGGAAGGCUGGAAGUAUAdTdT
T2 (s010)	hPat1b	NM_152716	259	GCAGAAAGGCUCAGUAAGAdTdT
T3 (s011)	hPat1b	NM_152716	2141	GGACGGAGGUGAUGUUAUdTdT
s037	hPat1b 3'UTR	NM_152716	3738 in mRNA	AGGGACAGGUUAUGUUAUUdTdT
s038	hPat1b	NM_152716	1167	GAGCAGUCAUCAAGAUCAUdTdT
R1 (s008)	hRck	NM_004397	876	GCAGAAACCCUAUGAGAUUUdTdT
s028	hRCK	NM_004397	968	UCUCCAGGCUUCAGAUAAAAdTdT
s041	hRRP40	AF281132.1	59	CACGCACAGUACUAGGUCAdTdT

4.1.2 List of Antibodies**Table 4.3.** Antibodies used in this study. IP, immunoprecipitation; WB, western blotting; IF, immunofluorescence.

Antibody	Clonality	Species	Method	Dilution / Amount	Source (order nr.)
14-3-3	polyclonal	rabbit	IP WB	1 μ g 1:2000	Santa Cruz Biotechnology (sc-629)
Caf1a	monoclonal	rabbit	WB	1:1000	Ann-Bin Shyu, Uni. of Texas, Houston, TX
eIF3B	polyclonal	goat	IP WB	1 μ g 1:1000	Santa Cruz Biotechnology (sc-16377)
eIF4G	polyclonal	mouse	IF IP WB	1:500 1 μ g 1:500	Cell Signaling(NEB) (#2498)
eIF4E (P-2)	monoclonal	mouse	IP WB	1 μ g 1:500	Santa Cruz Biotechnology (sc-9976)
FLAG M2	monoclonal	mouse	WB	1:500	Sigma F 3165
G3BP1(TT-Y)	monoclonal	mouse	WB	1:10000	Santa Cruz sc-81940
GFP	polyclonal	rabbit	WB	1:10000	Abcam ab290
IMP1 (E-20)	polyclonal	goat	WB	1:500	Santa Cruz Biotechnology (sc-21026)
IMP2 (P-16)	polyclonal	rabbit	WB	1:500	Santa Cruz Biotechnology (sc-99464)
HA.11	monoclonal	mouse	IP WB	1 μ g 1:500	Covance Innovative Antibodies (MMS-101P)
HA-Y11	polyclonal	rabbit	IF	1:500	Santa Cruz Biotechnology (sc805)
Lsm1	polyclonal	chicken	IP WB	1 μ g 1:2000	Genway (15-288-22100F)
Lsm4	polyclonal	chicken	IF WB	1:500 1:2000	Abcam (19101)
p-S6K (Hedls)	monoclonal	mouse	IP WB	1 μ g 1:500	Santa Cruz Biotechnology (sc8416)
Pat1b (Ab387)	monoclonal	rabbit	IF	1:500	Witek Filipowicz, FMI, Basel, Switzerland
Pat1b	monoclonal	rabit	WB	1:2000	Tillmann Achsel, VWB, Leuven, Belgium
RCK	polyclonal	rabbit	IP WB	1 μ g 1:10000	BETHYL (A300-461A)
Rrp40		rabbit	IF	1:1000	
Xrn1	polyclonal	rabbit	WB IP WB	1:2000 1 μ g 1:500	Georg Stoecklin BETHYL (A300-443A-1)
mouse-HRP		donkey	WB	1:10000	Jackson ImmunoResearch (715-035-150)
rabbit-HRP		donkey	WB	1:10000	Jackson ImmunoResearch (711-035-152)
chicken-HRP		donkey	WB	1:10000	Jackson ImmunoResearch (703-035-155)
goat-HRP		donkey	WB	1:10000	Jackson ImmunoResearch (705-035-147)
Cy2-rabbit		donkey	IF	1:500	Jackson ImmunoResearch (711-225-152)
Cy3-mouse		donkey	IF	1:500	Jackson ImmunoResearch (715-165-150)
DyLigth 649-rabbit		donkey	IF	1:500	Jackson ImmunoResearch (711-495-152s)

4.1.3 Technical Equipment

Table 4.4

Equipment	Company
Freezer -20°C	Liebherr
Freezer -80°C	Liebherr
Fridge 4°C	Liebherr
Cell Culture Incubator	Binder
Centrifuge (5417R)	Eppendorf
Centrifuge (J2-MC, rotor JA-17)	Beckman
Centrifuge (Labofuge M)	Heraeus Sepatech
Centrifuge (Multifuge 1S)	Thermo
Centrifuge (Pico17)	Thermo
Film Development Apparatus (HyperProcessor)	Amersham
GeneAmp PCR System 9700	Applied Biosystems
Heating Block (neoBlock 1)	NeoLab
Intelli-mixer	NeoLab
Laminar Flow Cabinet	NUAIRE
Magnetic Stirrer (MR3001)	NeoLab
Micropipettes	Gilson
Microwave	Privileg
Mini Protean 3 Cell	BIORAD
Mini Trans Blot Cell	BIORAD
Nanodrop ND 1000	PeQLab
pH Meter (766 Calimetic)	Knick
Poly-Prep column	Biorad
Power Supply (powerpack300)	Biorad
Scale (440-47N)	Kern
Shaker (DOS-20S)	NeoLab
Shaker (PMR-30)	Grant-bio
Sorvall Discovery 90SE	Thermo Scientific
Speedvac	Eppendorf Concentrator
TurboBlotter (northern blotting)	Whatman
UV Gel Documentation	System Raytest IDA
UV Table (TVL-312A)	Spektroline
Vortex	NeoLab
Waterbath	GFL

4.1.4 Chemicals and Enzymes

Table 4.5

Chemical/Enzyme	Company
10x Taq Polymerase Buffer	QIAGEN
10x NB blocking solution	Roche
10x RNaseH Buffer	New England Biolabs
2-Mercaptoethanol (2-ME, β -ME)	Sigma
5x Transcription Buffer	Promega
Acetic Acid	Fluka
Actinomycin D	AppliChem
Adenosine triphosphate (ATP)	Fermentas
Agar	Roth
Agarose	Biozym Scientific GmbH
Ammonium acetate	Fluka
Ammoniumsulfate	Roth
Ammoniumpersulfate	AppliChem
Ampicillin	Applichem
Bradford	Sigma-Aldrich
Bromphenol blue	Applichem
Bovine Serum Albumin (BSA)	New England Biolabs
Calf Intestine Phosphatase (CIP)	New England Biolabs
Chloroform	VWR
Complete Protease Inhibitor Cocktail Tablets, EDTA-free	Roche
Coomassie Brilliant Blue R250	ROTH
Coomassie Brilliant Blue R250	AppliChem
Desoxyadenosine triphosphate (dATP)	Fermentas
Desoxycytidine triphosphate (dCTP)	Fermentas
Desoxyguanosine triphosphate (dGTP)	Fermentas
Desoxythymidine triphosphate (dTTP)	Fermentas
DH5 α competent E. coli cells	Invitrogen
DIG easy hyb solution	Roche
DIG labelling mix	Roche
Dithiothreitol (DTT)	Applichem
Dimethylsulfoxid (DMSO)	Serva Electrophoresis
Disodiumhydrogenphosphate	Roth
Doxycycline	AppliChem
Ethanol	Riedel-de-Haen
Ethidium bromide (EtBr)	Applichem
Ethylenediaminetetraacetic acid (EDTA)	Roth
Formaldehyde	Merck
Formamide	AppliChem
Gene Ruler 1kb Ladder Plus	Fermentas

Continued on Next Page...

Chemical/Enzyme	Company
Glycerol	Roth
Glycine	Gerbu
Heparin sulfate	Sigma
HEPES	Roth
IgG sepharose	GE Healthcare
Isopropanol	Sigma-Aldrich
Kanamycinesulfate	Roth
Lipofectamine 2000	Invitrogen
L-glutamine	PAN
Magnesium chloride	Merck
Maleic acid	Fluka
Methanol	Fluka
Milk powder	Roth
MOPS	Roth
NEG-772 EASYTAG express protein labeling mix, ³⁵ S-Cys/Met	PerkinElmar
Nonidet P-40 (NP-40)	US Biological
Ocadaic acid	Sigma-Aldrich
O'GeneRuler 100bp Plus DNA Ladder	Fermentas
O-phosphoric acid	Roth
PageRuler Prestained Protein Ladder	Fermentas
Paraformaldehyde	AppliChem
Polyethyleneimine (PEI)	Polysciences Europe
Penicillin-streptomycin	PAN
Ponceau S	MD
Potassiumacetate	Roth
Potassiumchloride	Roth
Potassiumdihydrogenphosphate	Roth
Puromycin	AppliChem
Protein A/G Ultra Link Resin	Thermo Scientific
Random hexamers	Fermentas
Restriction Enzymes	New England Biolabs
RNase A	Genomed
RNase H	New England Biolabs
RNase inhibitor RNasin	Promega
Rotiphorese Acrylamide Solution	Roth
RQ1 DNase	Promega
Sodium arsenite	Fluka
Sodium azide	AppliChem
Sodium chloride	Sigma-Aldrich
Sodiumdihydrogenphosphate	Riedel de Haen
Sodium dodecyl sulphate (SDS)	Gerbu
Sodiumfluoride	Sigma-Aldrich
Sodium hydroxide pellets	Riedel-de-Haen

Continued on Next Page...

4 Materials and Methods

Chemical/Enzyme	Company
Sodiumvanadate	Sigma-Aldrich
SP6 polymerase	Fermentas
Streptavidin sepharose	GE Healthcare
T4 DNA Ligase	Fermentas
T4 DNA Polymerase	New England Biolabs
T4 Polynucleotide Kinase	Promega
Taq Polymerase	QIAGEN
TEMED	AppliChem
Thermo polymerase buffer	New England Biolabs
Transcriptor reverse transcriptase	Roche
Transcriptor reverse transcriptase 5x reaction buffer	Roche
Trifast	PeQLab
Trisodiumcitrate	VWR
Triton-X-100	Appllichem
Trizma base	Sigma-Aldrich
Trypsin/EDTA	PAN
Tryptone	AppliChem
Tween-20	Sigma-Aldrich
Vent DNA Polymerase	New England Biolabs
Xylenecyanol	Appllichem
Yeast Pyrophosphatase	Sigma
Yeast tRNA	Ambion

4.1.5 Disposable Materials and Kits

Table 4.6

Material	Company
1.5 ml, 2 ml Reaction Tubes	Eppendorf
15 ml, 50 ml Falcon Tubes	Falcon, Greiner, Nunc
2 ml Cryotubes	Nunc
Filter tips	StarLab
Filter paper Whatman 3MM	Whatman
Cellscraper	CoStar Corning Inc.
CellStar Tissue culture flasks (T75, T25)	Greiner Bio-One
CellStar Tissue culture dishes (6, 10, 15cm)	Greiner Bio-One
CellStar Cell culture plates (6-well, 12-well, 24-well)	Greiner Bio-One
DIG labelling Kit	Ambion
Gloves	Meditrade
Mini quick spin RNA columns	Roche
Pipette tips	Steinbrenner, Starlab
PureYield Plasmid Midi Prep System	Promega
PureLink HiPure Plasmid Midiprep Kit	Invitrogen
PureLink HiPure Plasmid Maxiprep Kit	Invitrogen
QIAquick Gel Extraction Kit	QIAGEN
QIAprep Spin Miniprep Kit	QIAGEN
QIAquick PCR Purification Kit	QIAGEN
QIAquick Nucleotide Removal Kit	QIAGEN
Rapid DNA Ligation Kit	Fermentas
RNeasy Plus Mini Kit	QIAGEN
RNA Isolation Kit	EURx, Roboklon
Transcriptor First Strand cDNA Synthesis Kit	Roche

4.2 Methods

All kits and reagents were used according to the manufacturer's instructions, unless otherwise stated.

4.2.1 Plasmids and Cloning

The following plasmids have been described previously: pCMV-FLAG-NOT1 [154], pcDNA3-Myc-Ccr4, pcDNA3-Flag-Dcp1a and pcDNA3-Flag-Dcp2 [9], pCIneo-RL [155]. To generate pcDNA3-HA (p2003), oligos G85 / G86 were annealed and cloned into the HindIII - EcoRI sites of pcDNA3 (Invitrogen).

For pcDNA3-YFP (p2168), YFP was amplified with oligos G243 / G244 and then ligated into the HindIII - KpnI sites of pcDNA3-HA (p2003), thereby replacing the HA tag. For plasmid pEYFP-Pat1a (p2639), the human Pat1a coding sequence was amplified in three portions from cDNA of HeLa cells and ligated sequentially into the BglII-XbaI sites of pEYFP-C1 (Clontech / BD Biosciences). The following primer pairs were used: G1332 / G1222 (1st PCR) and G1332 / G1198 (2nd PCR) for the Pat1a C-terminal portion, ligated as a KpnI - XbaI fragment; G1315 / G1221 for the middle portion, ligated as a BglII - KpnI fragment; G1219 / G1340 (1st PCR) and G1353 / G1340 (2nd PCR) for the Pat1a N-terminal portion, ligated as a BamHI - BglII fragment and thereby introducing an EcoRI site upstream of the start codon. For pcDNA3-HA-Pat1a (p2638), the human Pat1a coding sequence was excised from pEYFP-Pat1a (p2639) as an EcoRI - XbaI fragment, and cloned into the same sites of pcDNA3-HA (p2003).

A human Pat1b cDNA clone (DKFZp451I053) fused at the C-terminus to YFP was kindly provided by Stefan Wiemann (German Cancer Research Center, Heidelberg). In order to generate HA-tagged Pat1b constructs, fragments were amplified by PCR from human Pat1b cDNA and inserted into the KpnI - XhoI sites of pcDNA3-HA (p2003). The following primers were used: G1225 / G1230 for pcDNA3-HA-Pat1b (p2516), G1225 / G1226 for pcDNA3-HA-Pat1b-AN (p2511), G1225 / G1228 for pcDNA3-HA-Pat1b-ANH (p2514), G1227 / G1228 for pcDNA3-HA-Pat1b-H (p2512), G1227 / G1230 for pcDNA3-HA-Pat1b-HC (p2515), G1229 / G1230 for pcDNA3-HA-Pat1b-C (p2513), G1225 / G1425 for pcDNA3-HA-Pat1b-A (p2591), G1408 / G1226 for pcDNA3-HA-Pat1b-N (p2592) and G1408 / G1230 for pcDNA3-HA-Pat1b-dA (p2675). For pcDNA3-HA-Pat1b-dH (p2542), the N- and C-terminal regions of Pat1b were first amplified as separate fragments with primers G1225 / G1295 and G1296 / G1230, respectively. The PCR products were then aligned, Pat1b lacking the H domain was amplified with primers G1225 / G1230, and the PCR product was cloned into the KpnI - XhoI sites of pcDNA3-HA (p2003).

pcDNA3-YFP-Pat1b full length (p2521), pcDNA3-YFP-Pat1b-A (p2630), pcDNA3-YFP-Pat1b-AN (p2626), pcDNA3-YFP-Pat1b-N (p2627), pcDNA3-YFP-Pat1b-ANH (p2522), pcDNA3-YFP-Pat1b-H (p2632), pcDNA3-YFP-Pat1b-C (p2628), pcDNA3-YFP-Pat1b-HC (p2629), pcDNA3-YFP-Pat1b-dA (p2631) and pcDNA3-YFP-Pat1b-dH (p2633) were generated by replacing the HA tag in the corresponding HA-tagged Pat1b constructs with YFP excised as a HindIII - KpnI fragment from pcDNA3-YFP (p2168). For pcDNA3-HA-Pat1b-YFP (p2520), Pat1b-YFP was amplified by PCR with primers G1225 - G1253 using clone DKFZp451I053 as template, and inserted into the KpnI - XhoI sites of pcDNA3-HA-Pat1b (p2516).

In order to generate pcDNA3-HA-PP7cp-Pat1b (p2634), pcDNA3-HA-PP7cp-Pat1b-AN (p2658), pcDNA3-HA-PP7cp-Pat1b-HC (p2659), pcDNA3-HA-PP7cp-Pat1b-dA (p2663),

pcDNA3-HA-PP7cp-Pat1b-dH (p2660), pcDNA3-HA-PP7cp-Pat1b-A (p2747), pcDNA3-HA-PP7cp-Pat1b-N (p2748), and pcDNA3-HA-PP7cp-Pat1a (2661), PP7cp [144] was amplified by PCR using primers G1501 - G1502 and inserted into the KpnI site of corresponding pcDNA3-HA-Pat1b constructs and pcDNA3-HA-Pat1a (p2638). Orientation of the insert was verified by sequencing. pcDNA3-HA-PP7cp-Caf1a was cloned by Sahil Sharma (unpublished work).

For pcDNA3-Bgl (p2001), the BglIII site in pcDNA3 (Invitrogen) was removed by digestion with BglIII and blunt-end religation, thereby introducing a novel ClaI site. pcDNA3-7B (p2308) expressing a T7-tagged rabbit β -globin gene was subsequently generated by amplifying β -globin by PCR with primers G18 / G19 from plasmid puroMXbglobin [156]. The fragment was digested with EcoRV and Sall, and ligated into the BamHI/blunt - XhoI sites of pcDNA3-Blg. For pcDNA3-7B-PP7bs (p2314), six repeats of the PP7 binding site were excised as a BamHI - BglIII fragment from pSP73-6xPP7bs [144] and introduced into the BglIII site of pcDNA3-7B (p2308). For pFLB (p2524), firefly luciferase cDNA was amplified by PCR using primers G1256 / G1257 from pGL3-Control (Promega) and cloned into the HindIII - KpnI sites of pcDNA3-7B (p2308). From there, the 6xPP7bs repeats were cloned as an EcoRI - BglIII fragment from pcDNA3-7B-PP7bs (p2314) into the corresponding sites of pFLB (p2524) to generate pFLB-PP7bs (p2646).

For TOpuro-Caf1a-mycSG (p2485), the human Caf1a cDNA was amplified by RT-PCR using primers G1122 and G1123 and cloned as into the BamHI - XhoI sites of TOpuro-mycSG (p2484). For pTOpuro-Caf1a-AA-mycSG (p2737) containing the D40A/E42A mutation, a fragment amplified by PCR with primers G1730 and G1731 was inserted into the KpnI - EcoRI sites of TOpuro-Caf1a-mycSG (p2485). For pEGFP-TEV-Caf1a (p2793), Caf1a cDNA was cloned as a BamHI - XhoI fragment into the BglIII - XhoI sites of pEGFP-N1 containing a TEV cleavage site. To generate pcDNA3-Flag-Dcp2-AA (p2798), the E147A/E148A mutation was introduced into the KpnI - EcoRV sites of pcDNA3-Flag-Dcp2 [9] using a PCR fragment amplified with primers G1883 and G1884.

Rck coding sequence was PCR amplified with oligos G1377 / G1302 using cDNA from HeLa cells as template, and was inserted into BamHI-XhoI sites of pcDNA3-HA (p2003). Point mutations were introduced into pcDNA3-HA-Rck (p2570) and pcDNA3-YFP-Pat1b-A (p2630) by PCR. 5' and 3' regions flanking the mutation sites (including mutations) were PCR amplified with oligos G2079 / G2083 (5') and G2082 / G2081 (3') for pcDNA3-HA-Rck-m1 (p2839), G2080 / G2085 (5') and G2084 / G1302 (3') for pcDNA3-HA-Rck-m2 (p2840), G2079 / G2089 (5') and G2988 / G1302 (3') for pcDNA3-HA-Rck-m4 (p2842), G2080 / G2091 (5') and G2090 / G1302 (3') for pcDNA3-HA-Rck-m5 (p2843), G1225 / G2087 (5') and G2086 / G1425 (3') for pcDNA3-YFP-Pat1b-A-4A (p2844), and G1225 / G2085 (5') and G2086 / G1269 (3') for pcDNA3-YFP-Pat1b-4A (p2845). The 5' and 3' PCR fragments were aligned and mutant Rck and Pat1b fragments were PCR amplified for second time with oligos G2079 / G2081 for pcDNA3-HA-Rck-m1 (p2839), G2080 / G1302 for pcDNA3-HA-Rck-m2 (p2840), G2079 / G1302 for pcDNA3-HA-Rck-m4 (p2842), G2080 / G1302 for pcDNA3-HA-Rck-m5 (p2843), G1225 / G1425 for pcDNA3-YFP-Pat1b-A-4A (p2844), and G1225 / G1269 for pcDNA3-YFP-Pat1b-4A (p2845). Second PCR product carrying m1 mutation was digested with NheI - EcoRI, second PCR product carrying m2 mutation with NheI - XhoI, second PCR product carrying m4 mutation with EcoRI - XhoI and inserted into the same sites of pcDNA3-HA-Rck (p2570). Second PCR product of oligos G1225 / G1425 carrying 4A mutation was digested with KpnI and XhoI and inserted at the same sites of pcDNA3-YFP-Pat1b-A (p2630). For pcDNA3-YFP-Pat1b-4A (p2845), second PCR product was digested with

4 Materials and Methods

KpnI - EcoRI and inserted into the same sites of pcDNA3-YFP-Pat1b (p2521). To generate pcDNA3-HA-Rck-m3 (p2841), fragment containing m2 mutation was cut out by NheI - XhoI from pcDNA3-HA-Rck-m2 (p2840), and inserted into the same sites of pcDNA3-HA-Rck-m1 (p2839). In order to generate YFP-tagged Rck wt and mutants, pcDNA3-Flag-YFP-Rck (p2680), pcDNA3-Flag-YFP-Rck-m1 (p2865), pcDNA3-Flag-YFP-Rck-m2 (p2866), pcDNA3-Flag-YFP-Rck-m3 (p2867), pcDNA3-Flag-YFP-Rck-m4 (p2868), pcDNA3-Flag-YFP-Rck-m5 (p2869), Rck coding sequences were cut out of the corresponding HA plasmids with BamHI - XhoI restriction digestion, and ligated into the same sites of pcDNA3-Flag-YFP (p2679) [157].

For pcDNA3-HA-PP7cp-Pat1b-4A (p2909), PP7cp was cut out from pcDNA3-HA-PP7cp-Pat1b (p2634) by KpnI digestion and ligated at the KpnI site of pcDNA3-HA-Pat1b-4A (p2846). Orientation of the insert was verified by sequencing.

YFP-Pat1b sequence resistant to T3 siRNA was generated by introducing silent mutations in two RCR steps into Pat1b coding region. The first 5' and 3' regions flanking the mutations were PCR amplified with oligos G1785 / G1229 (5') and G1784 / G1230 (3'). PCR products were aligned and second PCR was done with G1229 / G1230. PCR product was digested with XcmI - XhoI, and inserted into the same sites of pcDNA3-HA-Pat1b (p2516). After sequencing, the fragment carrying the mutations was digested with XcmI - XhoI out of pcDNA3-HA-Pat1b-T3r (p2749) and inserted at the same sites of pcDNA3-YFP-Pat1b (p2521) to generate pcDNA3-YFP-Pat1b-T3r (p2750), and of pcDNA3-YFP-Pat1b-4A (p2845) to generate pcDNA3-YFP-Pat1b-4A-T3r (p2950). Rck sequence resistant to siRNA R1 was generated by introducing silent mutations by PCR with oligos G2264 / G2081. PCR product was digested with EcoRI - NheI, and inserted into the same sites of pcDNA3-Flag-YFP-Rck (p2680) to generate pcDNA3-Flag-YFP-Rck-R1r (p2900), and of pcDNA3-Flag-YFP-Rck-m4 (p2868) to generate pcDNA3-Flag-YFP-Rck-m4-R1r (p2908).

Plasmids pCMV-3xFlag-Ago4 (p2098) and pcDNA3-Flag-Ago2 (p2093) was kindly provided by J. Han. Plasmids pcDNA3-HA-hTTP (p2131), pcDNA3-HA-hBrl1 (p2113) and pcDNA3-Flag-PABP (p2022) were received from P. Anderson. Plasmids pENTR4-TNRC6B (p2757) and pENTR4-TNRC6C (p2758) were received from Thomas Tuschl.

Gateway entry clones pENTR4-TNRC6B (p2757) and pENTR4-TNRC6C (p2758) were kindly provided by Thomas Tuschl. pFLAG-TNRC6-B (p2764) and pFLAG-TNRC6-C (p2765) were cloned into Gateway destination vector pFLAG-CMV-D11 (p2586) (received from Bernhard Korn) with LR Clonase (Invitrogen).

TOpuroGS-Pat1b (p2534) was generated in two steps. First 5' 400 nt of Pat1b coding region was PCR amplified with oligos G1268 / G1269 and inserted into BamHI - EcoRI sites of TOPuroGS (p2434) (cloned by Heike Sandler [11]). At the second step Pat1b nt 401-2310 were cut out of pcDNA3-HA-Pat1b (p2516) with EcoRI - XhoI and inserted at the same sites of TOpuroGS-Pat1b(1-400 nt).

4.2.2 Cell Culture and Transfection

HeLa, U2OS, HEK293 and COS7 cells were cultured in Dulbecco's Modified Eagle's Medium (DMEM) containing 10% fetal bovine serum (Biochrom), 2 mM L-glutamine, 100 U/ml penicillin and 0.1 mg/ml streptomycin (all PAN Biotech) at 37°C / 5% CO₂. HeLa-Tet-On-7B-TNF-ARE, HeLa-Tet-On-lin41, U2OS-TREX-GS and U2OS-TREX-GS-Pat1b cells were cultured under the same conditions except with DMEM containing 10% Tetracyclin negative foetal bovine serum (PAA Laboratories). Expression of 7B-TNF-ARE, 7B-lin41, GS and GS-Pat1b was induced by addition of 1 µg/ml doxycycline to the medium.

Plasmids were transfected with Lipofectamine 2000 (Invitrogen) for protein interaction studies, or with Fugene HD (Roche) for immunofluorescence analysis according to the manufacturer's recommendations. Alternatively, polyethyleneimine (Polysciences Europe, 1 mg/ml, pH 7.0) was also used as transfection reagent for interaction and functional studies. siRNAs were transfected at a concentration of 100 nM with Lipofectamine 2000 twice over a time period of 4 or 5 days. Where indicated, cells were treated for 2 hours with 5 μ g/ml cycloheximide (Roth).

Table 4.7. Cell lines used in this study.

Cell Line	Comment (ATCC Number)
COS7	African green monkey (<i>Cercopithecus eathiops</i>) kidney fibroblast-like cell line (CRL-1651)
HEK293	Hypotriploid human embryonic kidney cell line (CRL-1573)
HeLa	Human ephitalial cervical adenocarcinoma cell line (CCL-2)
HeLa-YFP	Stable cell line, mass culture. HeLa cells were transfected with pcDNA3-YFP (p2168) using PEI, and selection was done with G418.
HeLa-YFP-Pat1a	Stable cell line, mass culture. HeLa cells were transfected with pEYFP-Pat1a (p2639) using PEI, and selection was done with G418.
HeLa-YFP-Pat1b	Stable cell line, mass culture. HeLa cells were transfected with pcDNA3-YFP-Pat1b (p2521) using PEI, and selection was done with G418.
HeLa-Tet-On-7B-TNF-ARE	Stable cell line, regulated expression of 7B-TNR-ARE upon tetracycline or doxycycline addition to cell culture media, recieved from Jochen Kreth, Georg Stoecklin lab
HeLa-Tet-On-7B-lin41	Stable cell line, regulated expression of 7B-lin41 upon tetracycline or doxycycline addition to cell culture media, recieved from Jochen Kreth, Georg Stoecklin lab
U2OS	Chromosomally highly altered, human osteosarcoma cell line (HTB-96)
U2OS-TREX	U2OS cells which stably expressing Tet repressor, which enables regulated gene expression upon tetracycline or doxycycline addition to cell culture media.
U2OS-TREX-GS	Stable cell line, single colony. U2OS-TREX cells were transfected with TOPuroGS (p2434) using FuGENE, and selection was done with puromycin.
U2OS-TREX-GS-Pat1b	Stable cell line, single colony. U2OS-TREX cells were transfected with TOPuroGS-Pat1b (p2534) using FuGENE, and selection was done with puromycin.

4.2.3 Immunofluorescence Microscopy

24 hours after transient transfection, cells grown on glass coverslips were fixed in 4% paraformaldehyde for 10 minutes at room temperature. Cell membranes were then permeabilized in -20°C cold methanol for 10 minutes. Phosphate buffered saline (PBS) containing 0.1% sodium-azide and 5% horse serum was used for blocking and antibody dilution. DNA was visualized using Heochst dye (#33342, Sigma, 1 $\mu\text{g}/\text{ml}$). After washing in PBS, cells were mounted onto glass slides using a solution of 14% polyvinol-alcohol (P8136, Sigma) and 30% glycerol in PBS. P-bodies were counted on an upright epi-fluorescence microscope (BX60, Olympus). Images were acquired at the Nikon Imaging Center, Heidelberg, either on an upright epi-fluorescence microscope (90i, Nikon) or by spinning disc confocal microscopy (Ultraview ERS, Perkin Elmer, on a TE2000 inverted microscope, Nikon) using a EM-CCD camera (Hamamastu).

4.2.4 Co-IP and Western Blot Analysis

24 hours after transient transfection, HEK293 cells from a confluent 10-cm dish were collected and lysed in 400 μl ice cold hypotonic lysis buffer (10 mM Tris pH 7.5, 10 mM NaCl, 10 mM M EDTA, 0.5% Triton-X100 with freshly added Complete protease inhibitors, Roche). Nuclei were removed by centrifugation at 500 g for 5 minutes at 4°C. The cytoplasmic lysate was precleared by the addition of 30 μl protein A/G agarose beads (Pierce or Santa Cruz) for 1 hour at 4°C and incubated with 1 μg of antibody for 2 hours. 30 μl of protein A/G beads were added for additional 2 hours and washed 6 times in NET2 buffer (50 mM Tris pH 7.5, 150 mM NaCl, 0.5% Triton-X100). Protein complexes were eluted with 25 μl SDS sample buffer with or without 100 mM DTT. Where indicated, RNase A (Sigma, 0.1 mg/ml) was added to the lysates after preclearing. Proteins were resolved on 10 or 12% polyacrylamide gels and transferred onto 0.2 μm pore size nitrocellulose membrane (PepLab) for Western blotting. Horseradish peroxidase-coupled secondary antibodies (Jackson ImmunoResearch) in combination with Western Lightning enhanced chemiluminescence substrate (Perkin Elmer) were used for detection. The GFP-binder was used for IP of YFP-tagged proteins as described [142].

4.2.5 Northern Blot Analysis

For RNA decay experiments, actinomycin D (Applichem) was added to cell cultures at 5 $\mu\text{g}/\text{ml}$, and total RNA was extracted using the Genematrix Total RNA purification kit (Eurx, Roboklon). For RNase H digestion, 20 μg RNA samples were first annealed with oligo(dT) (4 μl of 1 nmol/ μl oligo(dT), 4 μl of 1 mM EDTA in 35 μl final volume) by incubation at 26°C for 15 min. After annealing, 4 μl of 10x RNase H reaction buffer and 5 U of RNase H (New England Biolabd) were added, and the reaction mixture was incubated at 37°C for 15 min. Phenol/chloroform/isoamylalcohol extraction was done to purify the RNase H digested RNA. 5-20 μg of RNA was resolved by 1.1% agarose / 2% formaldehyde / MOPS gel electrophoresis and blotted overnight with 8x SSC onto Hybond-N+ Nylon membranes (Amersham, GE). Membranes were hybridized overnight with digoxigenin-labeled RNA probes at 55°C, washed twice with 2x SSC / 0.1% SDS for 5 minutes, and twice with 0.5x SSC / 0.1% SDS for 20 minutes at 65°C. Alkaline phosphatase-labeled anti-DIG Fab fragments and CDP-Star substrate (both Roche) were used for detection according to the manufacturer's instructions. The following primers were used to generate templates for Sp6 probes by PCR: G78 / G1001

for the probe against exon 1 and 2 of rabbit β -globin; G78 / G1008 for the probe against human RPS7; and G083 / G1009 for the probe against nucleolin.

4.2.6 Quantitative Real Time PCR

Possible DNA contamination in RNA samples was eliminated with RQ1 DNase (Promega) according to manufacturer's protocol (1U enzyme per μ g of RNA). RNA was precipitated with ammonium-acetate and dissolved in RNase free water. cDNA was generated from 1 μ g total RNA by reverse transcription using oligo(dT₁₈) or random hexamers as primer and transcriptase reverse transcriptase (Roche). The reaction mixture contained the following components: 1 μ g total RNA, 4 μ l 5x reverse transcription buffer (Promega), 2 μ l 10 mM dNTPs (dATP, dGTP, dTTP, dCTP), 2.5pmol oligo(dT₁₈) or 0.01 μ g random hexamer primer, 0.5 μ l RNase inhibitor (Promega), 10 U transcriptase reverse transcriptase (Roche). Reaction mixture was incubated at 55°C for 30 min for cDNA synthesis and the enzyme was inactivated at 85°C for 5 min.

cDNA was prepared fresh for each run of SYBR Green 480 (Roche) quantitative real time PCR (qPCR). The qPCR reaction was performed in a total volume of 10 μ l containing 2.5 μ l cDNA (1:5 diluted in PCR grade water), 4 pmol target-specific forward and reverse primers plus 5 μ l SYBR Green Mastermix (2x). Primers G1576 / G1577 against human nucleolin, or G1777 / G1778 against human GAPDH (for verification of microarray analysis) were used as control for internal normalization. Quantitative real time PCR (Light Cycler 480, Roche) was carried out according to the manufacturer's instructions with modified PCR program as presented in table 4.8.

Table 4.8. Light Cycler Program.

Program	Target (°C)	Aquisition Mode	Hold	Ramp Rate
Pre-Incubation	95	none	5 min	4.4
Amplification	95	none	10 sec	4.4
	55	none	15 sec	2.5
	72	single	25 sec	4.8
Melting curve	95	none	5 sec	4.8
	60	none	1 min	2.5
	97	continuous	-	0.11
Cooling	40	none	10 sec	2

4.2.7 ³⁵S-Methionine/Cysteine Metabolic Labeling and Autoradiography

U2OS or HeLa cells were seeded in 6-well plates on the second day of siRNA transfection. When needed, the cells were incubated overnight in glucose-free medium before labeling, for these cells glucose-free medium was used in the following steps also. 2 hrs before labeling, the medium was replaced with cysteine/methionine-free DMEM containing 10% dialysed FBS (dialysed against 1X PBS twice overnight, 4°C, and filter sterilized). Cells were metabolically labelled with 55 μ Ci/ml final concentration for 30 min. Cells were trypsinized, and lysed

4 Materials and Methods

in 200 μ l lysis buffer (15 mM Tris-HCl pH 7.4, 15 mM MgCl₂, 300 mM NaCl, 1% Triton-X 100, protease inhibitors, Roche). Nuclei were pelleted by centrifugation (2000 rpm, 2 min) and 100 μ l of the supernatant was precipitated on ice for at least 30 min after adding 100 μ l 20% TCA. The precipitated proteins were then bound to glass microfibre filters in vacuum, washed 3x with ice cold 20% TCA and then 3x with ice cold acetone. Filters were dried and ³⁵S incorporation was subsequently measured in 4 ml Econofluor-2 operating a liquid scintillation counter. Another aliquot of the supernatant was used for determining the total amount of proteins with Bradford Assay Kit (Sigma-Aldrich) according to the manufacturer's instructions.

4.2.8 Luciferase Assay

One third of a 6-cm dish of transiently transfected HeLa cells was lysed in 150 μ l of passive lysis buffer (Dual-Luciferase Reporter Assay System, Promega) and frozen at -20°C. After thawing, nuclei were removed by centrifugation for 2 minutes at 13,000 rpm at 4°C. 20 μ l of the supernatant was mixed with 50 μ l of 1:3 diluted substrates from the Dual-Luciferase Reporter Assay System. Firefly and Renilla luciferase activities were measured on a Fluostar Optima (BMG Labtech) plate reader.

Acronyms

aa	amino acid
ActD	actinomycin D
Ago	Angonaute
AMD	ARE-mediated mRNA decay
ARE-BP	ARE-binding protein
ARE	AU-rich element
BLAST	basic local alignment search tool
CBP80	cap-binding protein 80
cDNA	complementary DNA
CHX	cycloheximide
Dcp	mRNA decapping enzyme
Dox	Doxycycline
dsRNA	double stranded RNA
Edc	enhancer of mRNA decapping
eIF4E	eukaryotic translation initiation factor 4E
EVH1	Enabled/VASP homology 1
HA	Hemagglutinin
Hedls	human enhancer of decapping large subunit
HNRP	heterogeneous nuclear ribonucleoprotein
IF	immunofluorescence
IP	immunoprecipitation
IRES	internal ribosome entry site
JNK	c-Jun N-terminal kinase
LRR	leucine-rich repeat
Lsm	Sm Like
m⁷GDP	7-methylated guanosine diphosphate
m⁷G	7-methylated guanosine cap
Mg²⁺	magnesium
miRNA	microRNA
Mn²⁺	manganese
mRNA	messenger RNA
mRNP	messenger ribonucleoprotein
MRT	mRNA turnover
NaCl	sodium chloride
NMD	nonsense-mediated mRNA decay
NMR	nuclear magnetic resonance
NTD	Residues N-terminal to Dcp2p NudiX domain
nt	nucleotide
NudiX	Nucleotide diphosphate linked to an X moiety
P-bodies	Processing bodies

4 *Materials and Methods*

PABP polyA-binding protein
PAN polyA nuclease
PARN polyA-specific ribonuclease
PCR polymerase chain reaction
polyA poly adenosine
polyG poly guanosine
PRS proline-rich sequence
PTC premature termination codon
qPCR quantitative real time PCR
RISC RNA-induced silencing complex
RNAi RNA interference
RNase ribonuclease
RRM RNA-recognition motif
SDS-PAGE sodium dodecyl sulfate polyacrylamide gel electrophoresis
SG stress granules
siRNA small interfering RNA
snoRNA small nucleolar RNA
snRNA small nuclear RNA
ssRNA single stranded RNA
TTP tristetraproline
U-tract uridine tract
UTR untranslated region
WB western blot
wt wild type
Y2H yeast two hybrid
YFP yellow fluorescent protein

Acknowledgement

Many thanks to...

...Dr. Georg Stoecklin for creating such a wonderful group and pleasant atmosphere and giving me the opportunity to be a part of his group, for his invaluable guidance, for his motivation, time and patience, and for his kind invitations and delicious food.

...Jochen Kreth for his technical assistance, for always finding what I looked for and did not see, for his cheerful singing and dancing and for the delicious food on his annual BBQs.

...Sarah Hofmann for being more than a colleague and such a nice room mate even at the other end of the world, and for her critical reading of this work.

...Milan Spasic for his time that he spent on my technical questions and for the beers that he invited me to.

...Heike Sandler for sharing her experience and helping with L^AT_EX, Kathrin Leppek and Meeta Kulkarni for their critical reading of this work.

...former and current members of the Stoecklin group, Frederic Bethke, Julia Luther, Janine Philip, Sonja Reitter, Johanna Schott, Oksana Seibert and Sahil Sharma, beside those already mentioned, for making the lab and the office a great and friendly working environment.

...Gizem Ölmezer, Moritz Haneklaus and Till Michels for their collaboration during their practical studies.

...Dr. Ulrike Engel and all members of Nikon Imaging Center at the University of Heidelberg for their help and support with microscopy.

...Dr. Sven Diederichs and his group for their input and fruitful discussions during my joint lab meetings.

...Dr. Stefan Wiemann for providing us with the Pat1b clone.

...Dr. Marina Chekulaeva and Dr. Tilmann Achsel for providing us with Pat1b antibodies.

...Prof. Dr. Christine Clayton, Dr. Sven Diederichs and Prof. Dr. Matthias Hentze for their support and ideas they gave me during my TAC meetings.

...Prof. Dr. Christine Clayton, Prof. Dr. Michael Brunner and Prof. Dr. Oliver Gruss for their time and participation in the examination of this thesis.

...Daniel Brüderle for sharing his expertise on L^AT_EX, for his time and unconditioned support, and for sharing his life with me.

...bana her zaman güç ve destek veren aileme sonsuz teşekkürler.

Bibliography

- [1] Carolyn J. Decker and Roy Parker. A turnover pathway for both stable and unstable mRNAs in yeast: evidence for a requirement for deadenylation. *Genes and Development*, 7:1632–1643, 1993.
- [2] Denise Muhlrاد, Carolyn J. Decker, and Roy Parker. Turnover mechanisms of the stable yeast PGK1 mRNA. *Molecular and Cellular Biology*, 15(4):2145–2156, 1995.
- [3] Cecilia L. Hsu and Audrey Stevens. Yeast cells lacking 5'->3' exoribonuclease 1 contain mRNA species that are poly(A) deficient and partially lack the 5' cap structure. *Molecular and Cellular Biology*, 13(8):4826–4835, 1993.
- [4] Denise Muhlrاد, Carolyn J. Decker, and Roy Parker. Deadenylation of the unstable mRNA encoded by the yeast MFA2 gene leads to decapping followed by 5' to 3' digestion of the transcript. *Genes and Development*, 8:855–866, 1994.
- [5] Nicole L. Garneau, Jeffrey Wilusz, and Carol J. Wilusz. The highways and byways of mRNA decay. *Nature Reviews Molecular Cell Biology*, 8:113–126, 2007.
- [6] Luc Barreau, Carine adn Paillard and H. Beverley Osborne. AU-rich elements and associated factors: are there unifying principles? *Nucleic Acids Research*, 33(22): 7138–7150, 2005.
- [7] Carol J. Wilusz and Jeffrey Wilusz. Bringing the role of mRNA decay in the control of gene expression into focus. *TRENDS in Genetics*, 20(10):491–497, 2004.
- [8] Xiaokan Zhang, Anders Virtanen, and Frida E. Kleiman. To polyadenylate or to deadenylate. *Cell Cycle*, 9(22):4437–4449, 2010.
- [9] Jens Lykke-Andersen and Eileen Wagner. Recruitment and activation of mRNA decay enzymes by two ARE-mediated decay activation domains in the proteins TTP and BRF-1. *Genes and Development*, 19:351–361, 2005.
- [10] Georg Stoecklin and Paul Anderson. In a tight spot: ARE-mRNAs at processing bodies. *Genes and Development*, 21:627–631, 2007.
- [11] Heike Sandler, Jochen Kreth, H. Th. Marc Timmers, and Georg Stoecklin. Not1 mediates recruitment of the deadenylase Caf1 to mRNAs targeted for degradation by tristetraprolin. *Nucleic Acids Research*, 39(10):4373–4386, 2011.
- [12] Georg Stoecklin, Thomas Mayo, and Paul Anderson. ARE-mRNA degradation requires the 5'-3' decay pathway. *EMBO Reports*, 7(1):72–77, 2006.
- [13] Martin Fenger-Grøn, Christy Fillman, Bodil Norrild, and Jens Lykke-Andersen. Multiple processing body factors and the ARE binding protein TTP activate mRNA decapping. *Molecular Cell*, 20:905–915, 2005.

Bibliography

- [14] Lin He and Gregory J. Hannon. MicroRNAs: small RNAs with a big role in gene regulation. *Nature Reviews Genetics*, 5(7):522–531, 2004.
- [15] Guiliang Tang. siRNA and miRNA: an insight into RISCs. *TRENDS in Biochemical Sciences*, 30(2):106–114, 2005.
- [16] Ana Eulalio, Eric Huntzinger, and Elisa Izaurralde. GW182 interaction with argonaute is essential for miRNA-mediated translational repression and mRNA decay. *Nature Structural and Molecular Biology*, 15(4):346–353, 2008.
- [17] Jr-Shiuan Yang and Eric C. Lai. Alternative miRNA biogenesis pathways and the interpretation of core miRNA pathway mutants. *Molecular Cell*, 43:892–903, 2011.
- [18] Gyorgy Hutvagner and Martin J. Simard. Argonaute proteins: key players in RNA silencing. *Nature Reviews Molecular Cell Biology*, 9(1):22–32, 2008.
- [19] Jan Rehwinkel, Isabelle Behm-Ansmant, David Gatfield, and Elisa Izaurralde. A crucial role for GW182 and the DCP1:DCP2 decapping complex in miRNA-mediated gene silencing. *RNA*, 11:1640–1647, 2005.
- [20] Isabelle Behm-Ansmant, Jan Rehwinkel, Tobias Doerks, Alexander Stark, Peer Bork, and Elisa Izaurralde. mRNA degradation by miRNAs and GW182 requires both CCR4:NOT deadenylase and DCP1:DCP2 decapping complexes. *Genes and Development*, 20:1885–1898, 2006.
- [21] Jidong Lui. Control of protein synthesis and mrna degradation by microRNAs. *Current Opinion in Cell Biology*, 20:214–221, 2008.
- [22] Marc R. Fabian, Geraldine Mathonnet, Thomas Sundermeier, Hansruedi Mathys, Jakob T. Zipprich, Yuri V. Svitkin, Fabiola Rivas, Martin Jinek, James Wohlschlegel, Jennifer A. Doudna, Chyi-Ying A. Chen, Ann-Bin Shyu, John R. Yates III, Gregory J. Hannon, Witold Filipowicz, Thomas F. Duchaine, and Nahum Sonenberg. Mammalian miRNA RISC recruits CAF1 and PABP to affect PABP-dependent deadenylation. *Molecular Cell*, 35:868–880, 2009.
- [23] Ana Eulalio, Eric Huntzinger, and Elisa Izaurralde. Getting to the root of miRNA-mediated gene silencing. *Cell*, 132:9–14, 2008.
- [24] Ligang Wu and Joel G. Belasco. Let me count the ways: Mechanisms of gene regulation by miRNAs and siRNAs. *Cell*, 29:1–7, 2008.
- [25] Akio Yamashita, Tsung-Cheng Chang, Yukiko Yamashita, Wenmiao Zhu, Zhenping Zhong, Chyi-Ying A Chen, and Ann-Bin Shyu. Concerted action of poly(A) nucleases and decapping enzyme in mammalian mRNA turnover. *Nature Structural and Molecular Biology*, 12(12):1054–1063, 2005.
- [26] Yuji Funakoshi, Yusuke Doi, Nao Hosoda, Naoyuki Uchida, Masanori Osawa, Ichio Shimada, Masafumi Tsujimoto, Tsutomu Suzuki, Toshiaki Katada, and Shin-ichi Hoshino. Mechanism of mRNA deadenylation: evidence for a molecular interplay between translation termination factor eRF3 and mRNA deadenylases. *Genes and Development*, 21:3135–3148, 2007.

- [27] Dinghai Zheng, Nader Ezzeddine, Chyi-Ying A. Chen, Wenmiao Zhu, Xiangwei He, and Ann-Bin Shyu. Deadenylation is prerequisite for P-body formation and mRNA decay in mammalian cells. *Journal of Cell Biology*, 182(1):89–101, 2008.
- [28] Christof G. Körner and Elmar Wahle. Poly(A) tail shortening by a mammalian poly(A)-specific 3'-exoribonuclease. *Journal of Biological Chemistry*, 272(16):10448–10456, 1997.
- [29] Nikolaos A. A. Balatsos, Per Nilsson, Catherine Mazza, Stephen Cusack, and Anders Virtanen. Inhibition of mRNA deadenylation by the nuclear cap binding complex (CBC). *Journal of Biological Chemistry*, 281(7):4517–4522, 2006.
- [30] Min Gao, David T. Fritz, Lance P. Ford, and Jeffrey Wilusz. Interaction between a poly(A)-specific ribonuclease and the 5' cap influences mRNA deadenylation rates *in vitro*. *Molecular Cell*, 5:479–488, 2000.
- [31] Philip Mitchell and David Tollervey. mRNA stability in eukaryotes. *Current Opinion in Genetics and Development*, 10:193–198, 2000.
- [32] Niklas Henriksson, Per Nilsson, Mousheng Wu, Haiwei Song, and Anders Virtanen. Recognition of adenosine residues by the active site of poly(A)-specific ribonuclease. *Journal of Biological Chemistry*, 285(1):163–170, 2010.
- [33] Ronald Boeck, Salvador Z. Jr. Tarun, Michael Riegeri, Julie A. Deardorff, Silke Muller-Auer, and Alan B. Sachs. The yeast Pan2 protein is required for poly(A)-binding protein-stimulated poly(A)-nuclease activity. *Journal of Biological Chemistry*, 271(1):432–438, 1996.
- [34] Christine E. Brown, Salvador Z. Jr. Tarun, Ronald Boeck, and Alan B. Sachs. PAN3 encodes a subunit of the Pab1p-dependent poly(A) nuclease in *Saccharomyces cerevisiae*. *Molecular and Cellular Biology*, 16(10):5744–5753, 1996.
- [35] Joanna E. Lowell, David Z. Rudner, and Alan B. Sachs. 3'-UTR-dependent deadenylation by the yeast poly(A) nuclease. *Genes and Development*, 6:2088–2099, 1992.
- [36] Christine E. Brown and Alan B. Sachs. Poly(A) tail length control in *Saccharomyces cerevisiae* occurs by message-specific deadenylation. *Molecular and Cellular Biology*, 18(11):6548–6559, 1998.
- [37] David A. Mangus, Matthew C. Evans, Nathan S. Agrin, Mandy Smith, Preetam Gongidi, and Allan Jacobson. Positive and negative regulation of poly(A) nuclease. *Molecular and Cellular Biology*, 24(12):5521–5533, 2004.
- [38] Naoyuki Uchida, Shin-ichi Hoshino, and Toshiaki Katada. Identification of a human cytoplasmic poly(A) nuclease complex stimulated by poly(A)-binding protein. *Journal of Biological Chemistry*, 279(2):1383–1391, 2004.
- [39] Ewan F. Dunn, Christopher M. Hammell, Christine A. Hodge, and Charles N. Cole. Yeast poly(A)-binding protein, Pab1, and PAN, a poly(A) nuclease complex recruited by Pab1, connect mRNA biogenesis to export. *Genes and Development*, 19:90–103, 2005.

Bibliography

- [40] Junji Chen, Juri Rappsilber, Yueh-Chin Chiang, Pamela Russell, Matthias Mann, and Clyde L. Denis. Purification and characterization of the 1.0 MDa CCR4-NOT complex identifies two novel components of the complex. *Journal of Molecular Biology*, 314(4): 683–694, 2001.
- [41] Martine A. Collart. Global control of gene expression in yeast by the Ccr4-Not complex. *Gene*, 313:1–16, 2003.
- [42] Martine A. Collart and H. Th. Marc Timmers. The eukaryotic Ccr4-Not complex: A regulatory platform integrating mRNA metabolism with cellular signaling pathways? *Progress in Nucleic Acid Research and Molecular Biology*, 77:289–322, 2004.
- [43] Morgan Tucker, Marco A. Valencia-Sanchez, Robin R. Staples, Junji Chen, Clyde L. Denis, and Roy Parker. The transcription factor associated Ccr4 and Caf1 proteins are components of the major cytoplasmic mRNA deadenylase in *Saccharomyces cerevisiae*. *Cell*, 104:377–386, 2001.
- [44] Claudia Temme, Lianbing Zhang, Elisabeth Kremmer, Christian Ihling, Aymeric Chartier, Andrea Sinz, Martine Simonelig, and Elmar Wahle. Subunits of the *Drosophila* CCR4-NOT complex and their roles in mRNA deadenylation. *RNA*, 16:1356–1370, 2010.
- [45] Claudia Temme, Sophie Zaessinger, Sylke Meyer, Martine Simonelig, and Elmar Wahle. A complex containing the CCR4 and CAF1 proteins is involved in mRNA deadenylation in *Drosophila*. *EMBO Journal*, 23(14):2862–2871, 2004.
- [46] Nga-Chi Lau, Annemieke Kolkman, Frederik M. A. van Schaik, Klaas W. Mulder, W. W. M. Pim Pijnappel, Albert J. R. Heck, and H. Th. Marc Timmers. Human Ccr4-Not complexes contain variable deadenylase subunits. *Biochemical Journal*, 422:443–453, 2009.
- [47] Thomas K. Albert, Marc Lemaire, Nynke L. van Berkum, Reiner Gentz, Martine A. Collart, and H. Th. Marc Timmers. Isolation and characterization of human orthologs of yeast CCR4-NOT complex subunits. *Nucleic Acids Research*, 28(3):809–817, 2000.
- [48] Thomas K. Albert, Hiroyuki Hanzawa, Yvonne I.A. Legtenberg, Marjolein J. de Ruwe, Fiona A. J. van den Heuvel, Martine A. Collart, Rolf Boelens, and H. Th. Marc Timmers. Identification of a ubiquitin-protein ligase subunit within the CCR4-NOT transcription repressor complex. *EMBO Journal*, 21(3):355–364, 2002.
- [49] Olesya Panasenko, Emilie Landrieux, Marc Feuermann, Andrija Finka, Nicole Paquet, and Martine A. Collart. The yeast Ccr4-Not complex controls ubiquitination of the nascent-associated polypeptide (NAC-EGD) complex. *Journal of Biological Chemistry*, 281(42):31389–31398, 2006.
- [50] Lyudmila N. Dimitrova, Kazushige Kuroha, Tsuyako Tatematsu, and Toshifumi Inada. Nascent peptide-dependent translation arrest leads to Not4p-mediated protein degradation by the proteasome. *Journal of Biological Chemistry*, 284(16):10343–10352, 2009.
- [51] Junji Chen, Yueh-Chin Chiang, and Clyde L. Denis. CCR4, a 3' to 5' poly(A) RNA and ssDNA exonuclease, is the catalytic component of the cytoplasmic deadenylase. *EMBO Journal*, 21(6):1414–1426, 2002.

- [52] Palaniswamy Viswanathan, Junji Chen, Yueh-Chin Chiang, and Clyde L. Denis. Identification of multiple RNA features that influence CCR4 deadenylation activity. *Journal of Biological Chemistry*, 278(17):14949–14955, 2003.
- [53] Morgan Tucker, Robin R. Staples, Marco A. Valencia-Sanchez, Denise Muhlrud, and Roy Parker. Ccr4p is the catalytic subunit of a Ccr4p/Pop2p/Notp mRNA deadenylase complex in *Saccharomyces cerevisiae*. *EMBO Journal*, 21(6):1427–1436, 2002.
- [54] Angela Schwede, Louise Ellis, Julia Luther, Mark Carrington, Georg Stoecklin, and Christine Clayton. A role for Caf1 in mRNA deadenylation and decay in trypanosomes and human cells. *Nucleic Acids Research*, 36(10):3374–3388, 2008.
- [55] Masahiro Morita, Toru Suzuki, Takahisa Nakamura, Kazumasa Yokoyama, Takashi Miyasaka, and Tadashi Yamamoto. Depletion of mammalian CCR4b deadenylase triggers elevation of the p27Kip1 mRNA level and impairs cell growth. *Molecular and Cellular Biology*, 27(13):4980–4990, 2007.
- [56] Takbum Ohn, Yueh-Chin Chiang, Darren J. Lee, Gang Yao, Chongxu Zhang, and Clyde L. Denis. CAF1 plays an important role in mRNA deadenylation separate from its contact to CCR4. *Nucleic Acids Research*, 35(9):3002–3015, 2007.
- [57] Palaniswamy Viswanathan, Takbum Ohn, Yueh-Chin Chiang, Junji Chen, and Clyde L. Denis. Mouse CAF1 can function as a processive deadenylase/3′–5′-exonuclease *in vitro* but in yeast the deadenylase function of CAF1 is not required for mRNA poly(A) removal. *Journal of Biological Chemistry*, 279(23):23988–23995, 2004.
- [58] Roy Parker and Ujwal Sheth. P bodies and the control of mRNA translation and degradation. *Molecular Cell*, 25(5):635–646, 2007.
- [59] Paul Anderson and Nancy Kedersha. Stress granules: the Tao of RNA triage. *Trends in Biochemical Sciences*, 33(3):141–150, 2008.
- [60] Clare A. Beelman, Audrey Stevens, Giordano Caponigro, Thomas E. LaGrandeur, Lianna Hatfield, David M. Fortner, and Roy Parker. An essential component of the decapping enzyme required for normal rates of mRNA decapping. *Nature*, 382:642–646, 1996.
- [61] Jens Lykke-Andersen. Identification of a human decapping complex associated with hUpf proteins in nonsense-mediated decay. *Molecular and Cellular Biology*, 22(23):8114–8121, 2002.
- [62] Travis Dunckley, Morgan Tucker, and Roy Parker. Two related proteins, Edc1p and Edc2p, stimulate mRNA decapping in *Saccharomyces cerevisiae*. *Genetics*, 157:27–37, 2001.
- [63] Sundaresan Tharun and Roy Parker. Targeting an mRNA for decapping: Displacement of translation factors and association of the Lsm1p–7p complex on deadenylated yeast mRNAs. *Molecular Cell*, 8:1075–1083, 2001.
- [64] Meenakshi Kshirsagar and Roy Parker. Identification of Edc3p as an enhancer of mRNA decapping in *Saccharomyces cerevisiae*. *Genetics*, 166:729–739, 2004.

Bibliography

- [65] Michelle Steiger, Anne Carr-Schmid, David C. Schwartz, Megerditch Kiledjian, and Roy Parker. Analysis of recombinant yeast decapping enzyme. *RNA*, 9:231–238, 2003.
- [66] Christopher Piccirillo, Richie Khanna, and Megerditch Kiledjian. Functional characterization of the mammalian mRNA decapping enzyme hDcp2. *RNA*, 9:1138–1147, 2003.
- [67] Travis Dunckley and Roy Parker. The DCP2 protein is required for mRNA decapping in *Saccharomyces cerevisiae* and contains a functional MutT motif. *EMBO Journal*, 18(19):5411–5422, 1999.
- [68] Erwin van Dijk, Nicolas Cougot, Sylke Meyer, Sylvie Babajko, Elmar Wahle, and Bertrand Seraphin. Human Dcp2: a catalytically active mRNA decapping enzyme located in specific cytoplasmic structures. *EMO Journal*, 21(24):6915–6924, 2002.
- [69] Thomas E. LaGrandeur and Roy Parker. Isolation and characterization of Dcp1p, the yeast mRNA decapping enzyme. *EMBO Journal*, 17(5):1487–1496, 1998.
- [70] Zuoren Wang, Xinfu Jiao, Anne Carr-Schmid, and Megerditch Kiledjian. The hDcp2 protein is a mammalian mRNA decapping enzyme. *PNAS*, 99(20):12663–12668, 2002.
- [71] Richie Khanna and Megerditch Kiledjian. Poly(A)-binding-protein-mediated regulation of hDcp2 decapping *in vitro*. *EMBO Journal*, 23:1968–1976, 2004.
- [72] Mandar V. Deshmukh, Brittnee N. Jones, Duc-Uy Quang-Dang, Jeremy Flinders, Stephen N. Floor, Candice Kim, Jacek Jemielity, Marcin Kalek, Edward Darzynkiewicz, and John D. Gross. mRNA decapping is promoted by an RNA-binding channel in Dcp2. *Molecular Cell*, 29:324–336, 2008.
- [73] You Li, Man-Gen Song, and Megerditch Kiledjian. Transcript-specific decapping and regulated stability by the human Dcp2 decapping protein. *Molecular and Cellular Biology*, 28(3):939–948, 2008.
- [74] Jonathan Houseley, John LaCava, and David Tollervey. RNA-quality control by the exosome. *Nature Reviews Molecular Cell Biology*, 7:529–539, 2006.
- [75] You Li, Eric S. Ho, Samuel I. Gunderson, and Megerditch Kiledjian. Mutational analysis of a Dcp2-binding element reveals general enhancement of decapping by 5'-end stem-loop structures. *Nucleic Acids Research*, 37(7):2227–2237, 2009.
- [76] Je-Hyun Yoon, Eui-Ju Choi, and Roy Parker. Dcp2 phosphorylation by Ste20 modulates stress granule assembly and mRNA decay in *Saccharomyces cerevisiae*. *Journal of Cell Biology*, 189(5):813–827, 2010.
- [77] Katharina Rzeczowski, Knut Beuerlein, Helmut Müller, Oliver Dittrich-Breiholz, Heike Schneider, Daniela Kettner-Buhrow, Helmut Holtmann, and Michael Kracht. c-Jun N-terminal kinase phosphorylates DCP1a to control formation of P bodies. *Journal of Cell Biology*, 194(4):581–596, 2011.
- [78] Meipei She, Carolyn J. Decker, Kumar Sundramurthy, Yuying Liu, Nan Chen, Roy Parker, and Haiwei Song. Crystal structure of Dcp1p and its functional implications in mRNA decapping. *Nature Structural and Molecular Biology*, 11(3):249–256, 2004.

- [79] Meipei She, Carolyn J. Decker, Dmitri I. Svergun, Adam Round, Nan Chen, Denise Muhlrud, Roy Parker, and Haiwei Song. Structural basis of Dcp2 recognition and activation by Dcp1. *Molecular Cell*, 29:3367–349, 2008.
- [80] Stephen N. Floor, Brittnee N. Jones, Gail A. Hernandez, and John D. Gross. A split active site couples cap recognition by Dcp2 to activation. *Nature Structural and Molecular Biology*, 17(9):1096–1102, 2010.
- [81] Mark S. Borja, Kirill Piotukh, Christian Freund, and John D. Gross. Dcp1 links coactivators of mRNA decapping to Dcp2 by proline recognition. *RNA*, 17:278–290, 2011.
- [82] Stephen N. Floor, Brittnee N. Jones, and John D. Gross. Control of mRNA decapping by Dcp2. *RNA Biology*, 5(4):189–192, 2008.
- [83] Felix Tritschler, Joerg E. Braun, Carina Motz, Catia Igreja, Gabrielle Haas, Vincent Truffault, Elisa Izaurralde, and Oliver Weichenrieder. DCP1 forms asymmetric trimers to assemble into active mRNA decapping complexes in metazoa. *PNAS*, 106(51):21591–21596, 2009.
- [84] Giordano Caponigro and Roy Parker. Multiple functions for the poly(A)-binding protein in mRNA decapping and deadenylation in yeast. *Genes and Development*, 9:2421–2432, 1995.
- [85] Carol J. Wilusz, Min Gao, Charles L. Jones, Jeffrey Wilusz, and Stuart W. Peltz. Poly(A)-binding proteins regulate both mRNA deadenylation and decapping in yeast cytoplasmic extracts. *RNA*, 7:1416–1424, 2001.
- [86] David C. Schwartz and Roy Parker. mRNA decapping in yeast requires dissociation of the cap binding protein, eukaryotic translation initiation factor 4E. *Molecular and Cellular Biology*, 20(21):7933–7942, 2000.
- [87] Man-Gen Song and Megerditch Kiledjian. 3' terminal oligo U-tract-mediated stimulation of decapping. *RNA*, 13:2356–2365, 2007.
- [88] Guy R. Pilkington and Roy Parker. Pat1 contains distinct functional domains that promote P-body assembly and activation of decapping. *Molecular and Cellular Biology*, 28(4):1289–1312, 2008.
- [89] David Schwartz, Carolyn J. Decker, and Roy Parker. The enhancer of decapping proteins, Edc1p and Edc2p, bind RNA and stimulate the activity of the decapping enzyme. *RNA*, 9:239–251, 2003.
- [90] Carolyn J. Decker, Daniela Teixeira, and Roy Parker. Edc3p and a glutamine/asparagine-rich domain of Lsm4p function in processing body assembly in *Saccharomyces cerevisiae*. *Journal of Cell Biology*, 179(3):437–449, 2007.
- [91] Yuriko Harigaya, Brittnee N. Jones, Denise Muhlrud, John D. Gross, and Roy Parker. Identification and analysis of the interaction between Edc3 and Dcp2 in *Saccharomyces cerevisiae*. *Molecular and Cellular Biology*, 30(6):1446–1456, 2010.

Bibliography

- [92] Tracy Nissan, Purusharth Rajyaguru, Meipei She, Haiwei Song, and Roy Parker. Decapping activators in *Saccharomyces cerevisiae* act by multiple mechanisms. *Molecular Cell*, 39:773–783, 2010.
- [93] Laurence Decourty, Cosmin Saveanu, Kenza Zemam, Florence Hantraye, Emmanuel Frachon, Jean-Claude Rousselle, Micheline Fromont-Racine, and Alain Jacquier. Linking functionally related genes by sensitive and quantitative characterization of genetic interaction profiles. *PNAS*, 105(15):5821–5826, 2008.
- [94] Allan Jacobson. Regulation of mRNA decay: Decapping goes solo. *Molecular Cell*, 15:1–2, 2004.
- [95] Shuyun Dong, Chunfang Li, Daniel Zenklusen, Robert H. Singer, Allan Jacobson, and Feng He. YRA1 autoregulation requires nuclear export and cytoplasmic Edc3p-mediated degradation of its pre-mRNA. *Molecular Cell*, 25(4):559–573, 2007.
- [96] Shuyun Dong, Allan Jacobson, and Feng He. Degradation of YRA1 pre-mRNA in the cytoplasm requires translational repression, multiple modular intronic elements, Edc3p, and Mex67p. *Plos Biology*, 8(4), 2010.
- [97] Martin Jinek, Ana Eulalio, Andreas Lingel, Sigrun Helms, Elena Conti, and Elisa Izaurralde. The C-terminal region of Ge-1 presents conserved structural features required for P-body localization. *RNA*, 14:1991–1998, 2008.
- [98] Michael Ladomery, Eleanor Wade, and John Sommerville. Xp54, the *Xenopus* homologue of human rna helicase p54, is an integral component of stored mRNP particles in oocytes. *Nucleic Acids Research*, 25(5):965–973, 1997.
- [99] Nicola Minshall, George Thom, and Nancy Standart. A conserved role of a DEAD box helicase in mRNA masking. *RNA*, 7:1728–1742, 2001.
- [100] Akira Nakamura, Reiko Amikura, Kazuko Hanyu, and Satoru Kobayashi. Me31B silences translation of oocyte-localizing RNAs through the formation of cytoplasmic RNP complex during *Drosophila* oogenesis. *Development*, 128:3233–3242, 2001.
- [101] Jeff Collier and Roy Parker. General translational repression by activators of mRNA decapping. *Cell*, 122:875–886, 2005.
- [102] Nicole Fischer and Karsten Weis. The DEAD box protein Dhh1 stimulates the decapping enzyme Dcp1. *EMBO Journal*, 21(11):2788–2797, 2002.
- [103] Zhihong Cheng, Jeff Collier, Roy Parker, and Haiwei Song. Crystal structure and functional analysis of DEAD-box protein Dhh1p. *RNA*, 11:1258–1270, 2005.
- [104] Arnob Dutta, Suting Zheng, Deepti Jain, Craig E. Cameron, and Joseph C. Reese. Intermolecular interactions within the abundant DEAD-box protein Dhh1 regulate its activity *in Vivo*. *Journal of Biological Chemistry*, 286(31):27454–27470, 2011.
- [105] Felix Tritschler, Joerg E. Braun, Ana Eulalio, Vincent Truffault, Elisa Izaurralde, and Oliver Weichenrieder. Structural basis for the mutually exclusive anchoring of P body components EDC3 and Tral to the DEAD box protein DDX6/Me31B. *Molecular Cell*, 33:661–668, 2009.

- [106] Nicola Minshall, Michel Kress, Dominique Weil, and Nancy Standart. Role of p54 RNA helicase activity and its C-terminal domain in translational repression, P-body localization and assembly. *Molecular Biology of the Cell*, 20:2464–2472, 2009.
- [107] Gabrielle Haas, Joerg E. Braun, Cátia Igreja, Felix Tritschler, Tadashi Nishihara, and Elisa Izaurralde. HPat provides a link between deadenylation and decapping in metazoa. *Journal of Cell Biology*, 189(2):289–302, 2010.
- [108] Chia-ying Chu and Tariq M. Rana. Translation repression in human cells by microRNA-induced gene silencing requires RCK/p54. *PLOS Biology*, 4(7):1122–1136, 2006.
- [109] Ronald Boeck, Bruno Lapeyre, Christine E. Brown, and Alan B. Sachs. Capped mRNA degradation intermediates accumulate in the yeast *spb8-2* mutant. *Molecular and Cellular Biology*, 18(9):5062–5072, 1998.
- [110] Micheline Fromont-Racine, Andrew E. Mayes, Adeline Brunet-Simon, Adeline Rain, Alan Colley, Ian Dix, Laurence Decourty, Nicolas Joly, Florence Ricard, Jean D. Beggs, and Pierre Legrain. Genome-wide protein interaction screens reveal functional networks involving Sm-like proteins. *Yeast*, 17:59–110, 2000.
- [111] Emmanuelle Bouveret, Guillaume Rigaut, Anna Shevchenko, Matthias Wilm, and Bertrand Seraphin. A Sm-like protein complex that participates in mRNA degradation. *EMBO Journal*, 19(7):1661–1671, 2000.
- [112] Sundaresan Tharun, Weihai He, Andrew E. Mayes, Pascal Lennertz, Jean D. Beggs, and Roy Parker. Yeast Sm-like proteins function in mRNA decapping and decay. *Nature*, 404:515–518, 2000.
- [113] Ben Lehner and Christopher M. Sanderson. A protein interaction framework for human mRNA degradation. *Genome Research*, 14:1315–1323, 2004.
- [114] Michael P. Spiller, Martin A. M. Reijns, and Jean D. Beggs. Requirements for nuclear localization of the Lsm2-8p complex and competition between nuclear and cytoplasmic Lsm complexes. *Journal of Cell Science*, 120:4310–4320, 2007.
- [115] Claire Bonnerot, Ronald Boeck, and Bruno Lapeyre. The two proteins Pat1p (Mrt1p) and Spb8p interact in vivo, are required for mRNA decay, and are functionally linked to Pab1p. *Molecular and Cellular Biology*, 20(16):5939–5946, 2000.
- [116] Weihai He and Roy Parker. The yeast cytoplasmic LsmI/Pat1p complex protects mRNA 3' termini from partial degradation. *Genetics*, 158:1445–1455, 2001.
- [117] Naomi Bergman, Karen C. M. Moraes, John R. Anderson, Bozidarka Zaric, Christian Kambach, Robert J. Schneider, Carol J Wilusz, and Jeffrey Wilusz. Lsm proteins bind and stabilize RNAs containing 5' poly(A) tracts. *Nature Structural and Molecular Biology*, 14(9):824–831, 2007.
- [118] Dierk Ingelfinger, Donna J. Arndt-Jovin, Reinhard Lührmann, and Tilmann Achsel. The human LSm1-7 proteins colocalize with the mRNA-degrading enzymes Dcp1/2 and Xrn1 in distinct cytoplasmic foci. *RNA*, 8:1489–1501, 2002.

Bibliography

- [119] Xinfu Jiao, Song Xiang, ChanSeok Oh, Charles E. Martin, Liang Tong, and Megerditch Kiledjian. Identification of a quality-control mechanism for mRNA 5'-end capping. *Nature*, 467:608–612, 2010.
- [120] You Li, Mangen Song, and Megerditch Kiledjian. Differential utilization of decapping enzymes in mammalian mRNA decay pathways. *RNA*, 17:419–428, 2011.
- [121] Ana Eulalio, Isabelle Behm-Ansmant, and Elisa Izaurralde. P bodies: at the crossroads of post-transcriptional pathways. *Nature Reviews Molecular Cell Biology*, 8:9–22, 2007.
- [122] Suvendra N. Bhattacharyya, Regula Habermacher, Ursula Martine, Ellen I. Closs, and Witold Filipowicz. Relief of microRNA-mediated translational repression in human cells subjected to stress. *Cell*, 125:1111–1124, 2006.
- [123] Andrew Jakymiw, Kaleb M. Pauley, Songqing Li, Keigo Ikeda, Shangli Lian, Theophany Eystathioy, Minoru Satoh, Marvin J. Fritzler, and Edward K. L. Chan. The role of GW/P-bodies in RNA processing and silencing. *Journal of Cell Science*, 120:1317–1323, 2007.
- [124] Daniela Teixeira and Roy Parker. Analysis of P-body assembly in *Saccharomyces cerevisiae*. *Molecular Biology of the Cell*, 18:2274–2287, 2007.
- [125] Meeta Kulkarni, Sevim Ozgur, and Georg Stoecklin. On track with P-bodies. *Biochemical Society Transactions*, 38(1):242–251, 2010.
- [126] Ujwal Sheth and Roy Parker. Decapping and decay of messenger RNA occur in cytoplasmic processing bodies. *Science*, 300(5620):805–808, 2003.
- [127] Ana Eulalio, Isabelle Behm-Ansmant, Daniel Schweizer, and Elisa Izaurralde. P-body formation is a consequence, not the cause, of RNA-mediated gene silencing. *Molecular and Cellular Biology*, 27(11):3970–3981, 2007.
- [128] Tobias M. Franks and Jens Lykke-Andersen. TTP and BRF proteins nucleate processing body formation to silence mrnas with AU-rich elements. *Genes and Development*, 21(719-735), 2007.
- [129] Nancy Kedersha, Georg Stoecklin, Maranatha Ayodele, Patrick Yacono, Jens Lykke-Andersen, Marvin J. Fritzler, Donalyn Scheuner, Randal J. Kaufman, David E. Golan, and Paul Anderson. Stress granules and processing bodies are dynamically linked sites of mRNP remodeling. *Journal of Cell biology*, 169(6):871–884, 2005.
- [130] Adva Aizer, Yehuda Brody, Lian Wee Ler, Nahum Sonenberg, Robert H. Singer, and Yaron Shav-Tal. The dynamics of mammalian P body transport, assembly, and disassembly *In Vivo*. *Molecular Biology of the Cell*, 19:4154–4166, 2008.
- [131] Paul Anderson and Nancy Kedersha. RNA granules. *Journal of Cell Biology*, 172(6): 803–808, 2006.
- [132] Russell P. Rother, Mark B. Frank, and Patricia S. Thomas. Purification, primary structure, bacterial expression and subcellular distribution of an oocyte-specific protein in *Xenopus*. *European Journal of Biochemistry*, 206:673–683, 1992.

- [133] Lianna Hatfield, Clare A. Beelman, Audrey Stevens, and Roy Parker. Mutations in *trans*-acting factors affecting mRNA decapping in *Saccharomyces cerevisiae*. *Molecular and Cellular Biology*, 16(10), 1996.
- [134] Shuang Zhang, Carol J. Williams, Kevin Hagan, and Stuart W. Peltz. Mutations in VPS16 and MRT1 stabilize mRNAs by activating an inhibitor of the decapping enzyme. *Molecular and Cellular Biology*, 19(11):7568–7576, 1999.
- [135] Xiaoqi Wang, Paul M. Watt, Edward J. Louis, Rhona H. Borts, and Ian D. Hickson. Pat1: a topoisomerase II-associated protein required for faithful chromosome transmission in *Saccharomyces cerevisiae*. *Nucleic Acids Research*, 24(23):4791–4797, 1996.
- [136] Françoise Wyers, Michele Minet, Marie E. Dufour, Le T. Vo, and François Lacroute. Deletion of the *PAT1* gene affects translation initiation and suppresses a *PAB1* gene deletion in yeast. *molecular and Cellular Biology*, 20(10):3538–3549, 2000.
- [137] Amine O. Noueir, Juana Díez, Shaun P. Falk, Jianbo Chen, and Paul Ahlquist. Yeast Lsm1p-7p/Pat1p deadenylation-dependent mRNA-decapping factors are required for brome mosaic virus genomic RNA translation. *Molecular and Cellular Biology*, 23(12):4094–4106, 2003.
- [138] Sevim Özgür. Identification of human Pat1b, a coordinator of translation and mRNA decay. Master thesis, Ruprecht-Karls-Universität Heidelberg, 2008.
- [139] Scheller Scheller, Patricia Resa-Infante, Susana de la Luna, Rui P. Galao, Mario Albrecht, Lars Kaestner, Peter Lipp, Thomas Lengauer, Andreas Meyerhans, and Juana Díez. Identification of PatL1, a human homolog to yeast P body component Pat1. *Biochimica et Biophysica Acta*, 173:1786–1792, 2007.
- [140] Nicolas Cougot, Sylvie Babajko, and Bertrand Seraphin. Cytoplasmic foci are sites of mRNA decay in human cells. *Journal of Cell Biology*, 165(1):31–40, 2004.
- [141] Sevim Ozgur, Marina Chekulaeva, and Stoecklin Georg. Human Pat1b connects deadenylation with mRNA decapping and controls the assembly of processing bodies. *Molecular and Cellular Biology*, 30(17):4308–4323, 2010.
- [142] Ulrich Rothbauer, Kouros Zolghadr, Kouros Muyltermans, Aloys Schepers, M. Cristina Cardoso, and Heinrich Leonhardt. A versatile nanotrap for biochemical and functional studies with fluorescent fusion proteins. *Molecular and Cellular Proteomics*, 7(2):282–289, 2008.
- [143] Eric Huntzinger, Joerg E. Braun, Susanne Heimstadt, Latifa Zekri, and Elisa Izaurralde. Two PABPC1-binding sites in GW182 proteins promote miRNA-mediated gene silencing. *EMBO Journal*, 29(24):4146–4160, 2010.
- [144] Francis Lim, Thomas P. Downey, and David S. Peabody. Translational repression and specific RNA binding by the coat protein of the *Pseudomonas* phage PP7. *Journal of Biological Chemistry*, 276(25):22507–22513, 2001.
- [145] Rafal Tomecki, Maiken S. Kristiansen, Søren Lykke-Andersen, Aleksander Chlebowski, Katja M. Larsen, Roman J. Szczesny, Karolina Drazkowska, Agnieszka Pastula, Jens S.

Bibliography

- Andersen, Piotr P. Stepien, Andrzej Dziembowski, and Torben Heick Jensen. The human core exosome interacts with differentially localized processive RNases: hDIS3 and hDIS3L. *EMBO Journal*, 29:2342–2357, 2010.
- [146] Aline Marnef, Maria Maldonado, Anthony Bugaut, Shankar Balasubramanian, Michel Kress, Dominique Weil, and Nancy Standart. Distinct functions of maternal and somatic Pat1 protein paralogs. *RNA*, 16(11):2094–2107, 2010.
- [147] Joerg E. Braun, Felix Tritschler, Gabrielle Haas, Catia Igreja, Vincent Truffault, Oliver Weichenrieder, and Elisa Izaurralde. The C-terminal α - α superhelix of Pat is required for mRNA decapping in metazoa. *EMBO Journal*, 29(14):2368–2380, 2010.
- [148] Yoriko Nakamura, Kimio J. Tanaka, Maki Miyauchi, Lin Huang, Masafumi Tsujimoto, and Ken Matsumoto. Translational repression by the oocyte-specific protein P100 in *Xenopus*. *Developmental Biology*, 344(1):272–283, 2010.
- [149] The Scripps Research Institute. A free extensible and customizable gene annotation portal, a complete resource for learning about gene and protein function, 2011. URL <http://biogps.org>.
- [150] Kyoko Arimoto, Hiroyuki Fukuda, Shinobu Imajoh-Ohmi, Haruo Saito, and Mutsuhiro Takekawa. Formation of stress granules inhibits apoptosis by suppressing stress-responsive MAPK pathways. *Nature Cell Biology*, 10(11):1324–1332, 2008.
- [151] Aline Marnef and Nancy Standart. Pat1 proteins: a life in translation, translation repression and mRNA decay. *Biochemical Society Transactions*, 38(6):1602–1607, 2010.
- [152] Antonio Totaro, Fabrizio Renzi, Giorgio La Fata, Claudia Mattioli, Monika Raabe, Henning Urlaub, and Tilmann Achsel. The human Pat1b protein: a novel mRNA deadenylation factor identified by a new immunoprecipitation technique. *Nucleic Acids Research*, 39(2):635–647, 2010.
- [153] Wenqian Hu, Thomas J. Sweet, Sangpen Chamnongpol, Kristian E. Baker, and Jeff Collier. Co-translational mRNA decay in *Saccharomyces cerevisiae*. *Nature*, 461(7261):225–229, 2009.
- [154] G. Sebastiaan Winkler, Klaas W. Mulder, Vivian J. Bardwell, Eric Kalkhoven, and H. Th. Marc Timmers. Human Ccr4-Not complex is a ligand-dependent repressor of nuclear receptor-mediated transcription. *EMBO Journal*, 25:3089–3099, 2006.
- [155] Ramesh S. Pillai, Suvendra N. Bhattacharyya, Caroline G. Artus, Tabea Zoller, Nicolas Cougot, Eugenia Basyuk, Edouard Bertrand, and Witold Filipowicz. Inhibition of translational initiation by Let-7 microRNA in human cells. *Science*, 309(5740):1573–1576, 2005.
- [156] Georg Stoecklin, Pascal Stoeckle, Min Lu, Oliver Muehlemann, and Christoph Moroni. Cellular mutants define a common mRNA degradation pathway targeting cytokine AU-rich elements. *RNA*, 7(11):1578–1588, 2001.
- [157] Moritz Haneklaus. Functional analysis of the DEAD-box RNA helicase Rck. Bachelor’s thesis, Ruprecht-Karls-Universitat Heidelberg, 2009.

5 Appendix

5.1 Results of HPLC-MS/MS Analysis

Table 5.1. List of proteins identified to interact with YFP-Pat1b and/or YFP-Pat1b-A by HPCL-MS/MS. Proteins that were shown to interact with Pat1b are depicted in *italics*. Proteins with special interest are depicted in **bold**. Sorted according to the number of unique peptides identified in YFP-Pat1b IP.

Symbol	Description	MW (kDa)	Num. of Unique Peptides		Peptide Ratio		
			YFP-Pat1b	YFP	YFP-Pat1b / YFP	YFP-Pat1b-A / YFP	
<i>PATL1</i>	<i>Protein PAT1 homolog 1</i>	87	65	5	4	13.00	0.80
<i>Hedls</i>	<i>Enhancer of mRNA-decapping protein 4</i>	152	58	1	0	58.00	0.00
SART3	Squamous cell carcinoma antigen recognized by T-cells 3	110	45	0	0		
<i>Rck</i>	<i>Probable ATP-dependent RNA helicase DDX6</i>	54	34	0	43		
NUCL	Nucleolin	77	27	8	9	3.38	1.13
RS3	40S ribosomal protein S3	27	22	0	6		
RS3A	40S ribosomal protein S3a	30	19	0	3		
<i>PABP1</i>	<i>Polyadenylate-binding protein 1</i>	71	19	5	5	3.80	1.00
PRP8	Pre-mRNA-processing-splicing factor 8	274	19	3	12	6.33	4.00
DDX21	Nucleolar RNA helicase 2	87	18	9	16	2.00	1.78
RS4X	40S ribosomal protein S4, X isoform	30	17	0	4		
RS2	40S ribosomal protein S2	31	15	0	7		
IMP1	Insulin-like growth factor 2 mRNA-binding protein 1 IF2B1	63	15	1	1	15.00	1.00
<i>EDC3</i>	<i>Enhancer of mRNA-decapping protein 3</i>	56	15	0	0		
ADT2	ADP/ATP translocase 2	33	14	6	14	2.33	2.33
CBR1	Carbonyl reductase [NADPH] 1	30	14	0	12		
RS7	40S ribosomal protein S7	22	14	2	3	7.00	1.50
<i>DCP1A</i>	<i>mRNA-decapping enzyme 1A</i>	63	14	0	0		
RS6	40S ribosomal protein S6	29	14	0	1		
HNRPR	Heterogeneous nuclear ribonucleoprotein R	71	13	4	10	3.25	2.50
U520	U5 small nuclear ribonucleoprotein 200 helicase	245	13	4	11	3.25	2.75
RACK1	Guanine nucleotide-binding protein subunit beta-2-like 1	35	13	0	9		
ILF3	Interleukin enhancer-binding factor 3	95	13	0	4		
DHX30	Putative ATP-dependent RNA helicase DHX30	134	13	0	0		
HNRH1	Heterogeneous nuclear ribonucleoprotein H	49	12	4	6	3.00	1.50
PTBP1	Polypyrimidine tract-binding protein 1	57	12	5	9	2.40	1.80
CA069	Putative transferase Clorf69, mitochondrial	38	12	5	12	2.40	2.40
CAPZB	F-actin-capping protein subunit beta	31	12	4	9	3.00	2.25
HNRPK	Heterogeneous nuclear ribonucleoprotein K	51	12	5	8	2.40	1.60
H2AY	Core histone macro-H2A.1	40	12	7	4	1.71	0.57
ISOC1	Isochorismatase domain-containing protein 1	32	12	0	7		
CDK2	Cell division protein kinase 2	34	12	0	11		
RS18	40S ribosomal protein S18	18	12	1	3	12.00	3.00
RL7A	60S ribosomal protein L7a	30	12	0	1		
RS8	40S ribosomal protein S8	24	11	2	0	5.50	0.00
HNRPL	Heterogeneous nuclear ribonucleoprotein L	64	11	6	12	1.83	2.00
RL6	60S ribosomal protein L6	33	11	4	1	2.75	0.25
HNRPD	Heterogeneous nuclear ribonucleoprotein D0	38	11	6	3	1.83	0.50
RL3	60S ribosomal protein L3	46	11	6	0	1.83	0.00
RL7	60S ribosomal protein L7	29	11	0	2		
RS19	40S ribosomal protein S19	16	11	0	1		
<i>XRN1</i>	<i>5'-3' exoribonuclease 1</i>	194	11	0	0		
RS9	40S ribosomal protein S9	23	11	2	1	5.50	0.50
MBB1A	Myb-binding protein 1A	149	10	3	11	3.33	3.67
MPCP	Phosphate carrier protein, mitochondrial	40	10	2	9	5.00	4.50
RS5	40S ribosomal protein S5	23	10	1	1	10.00	1.00
RL4	60S ribosomal protein L4	48	10	1	2	10.00	2.00
RL23A	60S ribosomal protein L23a	18	10	2	5	5.00	2.50
DDX5	Probable ATP-dependent RNA helicase DDX5	69	10	1	1	10.00	1.00
PEF1	Pef1in	30	9	1	8	9.00	8.00

Continued on Next Page...

5 Appendix

Symbol	Description	MW (kDa)	Num. of Unique Peptides			Peptide Ratio	
			YFP- Pat1b	YFP	YFP- Pat1b-A	YFP- Pat1b / YFP	YFP- Pat1b-A / YFP
<i>LSM4</i>	<i>U6 snRNA-associated Sm-like protein LSM4</i>	15	9	0	0		
RS13	40S ribosomal protein S13	17	9	2	6	4.50	3.00
RS10	40S ribosomal protein S10	19	9	1	1	9.00	1.00
FHL1	Four and a half LIM domains protein 1	36	9	1	11	9.00	11.00
RS16	40S ribosomal protein S16	16	9	2	3	4.50	1.50
ROAA	Heterogeneous nuclear ribonucleoprotein A/B	36	9	3	1	3.00	0.33
RBM14	RNA-binding protein 14	69	9	0	3		
RL17	60S ribosomal protein L17	21	9	0	0		
G3BP2	Ras GTPase-activating protein-binding protein 2	54	9	0	0		
RS27A	Ubiquitin-40S ribosomal protein S27a	18	8	4	5	2.00	1.25
NUBP2	Cytosolic Fe-S cluster assembly factor NUBP2	29	8	3	7	2.67	2.33
RS15	40S ribosomal protein S15	17	8	0	0		
PSME2	Proteasome activator complex subunit 2	27	8	0	7		
CATD	Cathepsin D	45	8	0	7		
MTAP	S-methyl-5'-thioadenosine phosphorylase	31	8	0	7		
<i>LSM2</i>	<i>U6 snRNA-associated Sm-like protein LSM2</i>	11	8	0	0		
GLO2	Hydroxyacylglutathione hydrolase, mitochondrial	34	8	0	8		
6PGL	6-phosphogluconolactonase	28	8	2	5	4.00	2.50
RL13	60S ribosomal protein L13	24	8	2	3	4.00	1.50
<i>CNOT1</i>	<i>CCR4-NOT transcription complex subunit 1</i>	267	8	5	2	1.60	0.40
RS12	40S ribosomal protein S12	15	8	2	3	4.00	1.50
<i>LSM1</i>	<i>U6 snRNA-associated Sm-like protein LSM1</i>	15	8	0	0		
RL8	60S ribosomal protein L8	28	8	0	2		
CAPR1	Caprin-1	78	8	0	0		
PSME3	Proteasome activator complex subunit 3	30	7	0	9		
PROSC	Proline synthase co-transcribed bacterial homolog protein	30	7	0	6		
NOP56	Nucleolar protein 56	66	7	0	9		
YBOX1	Nuclease-sensitive element-binding protein 1	36	7	0	0		
RL5	60S ribosomal protein L5	34	7	1	2	7.00	2.00
ELAV1	ELAV-like protein 1	36	7	0	6		
SRSF3	Serine/arginine-rich splicing factor 3	19	7	0	3		
RS14	40S ribosomal protein S14	16	7	1	1	7.00	1.00
RS11	40S ribosomal protein S11	18	7	1	3	7.00	3.00
RS17	40S ribosomal protein S17	16	7	1	3	7.00	3.00
SPRE	Sepiapterin reductase	28	6	3	3	2.00	1.00
<i>LSM7</i>	<i>U6 snRNA-associated Sm-like protein LSM7</i>	12	6	0	0		
HNRPQ	Heterogeneous nuclear ribonucleoprotein Q	70	6	1	3	6.00	3.00
RL14	60S ribosomal protein L14	23	6	3	1	2.00	0.33
VIME	Vimentin	54	6	0	4		
RS15A	40S ribosomal protein S15a	15	6	2	2	3.00	1.00
RL15	60S ribosomal protein L15	24	6	0	1		
RS26	40S ribosomal protein S26	13	6	1	1	6.00	1.00
<i>LSM6</i>	<i>U6 snRNA-associated Sm-like protein LSM6</i>	9	6	0	0		
RAN	GTP-binding nuclear protein Ran	24	6	1	2	6.00	2.00
THOC4	THO complex subunit 4	27	6	0	3		
RL10	60S ribosomal protein L10	25	6	1	2	6.00	2.00
RL18A	60S ribosomal protein L18a	21	6	0	1		
DNJA3	DnaJ homolog subfamily A member 3, mitochondrial	52	6	0	0		
SRSF1	Serine/arginine-rich splicing factor 1	28	6	0	2		
RL26	60S ribosomal protein L26	17	6	0	1		
RL24	60S ribosomal protein L24	18	6	1	0	6.00	0.00
RM12	39S ribosomal protein L12, mitochondrial	21	6	0	0		
PRPF3	U4/U6 small nuclear ribonucleoprotein Prp3	78	6	0	0		
PRP4	U4/U6 small nuclear ribonucleoprotein Prp4	58	6	0	0		
GSH0	Glutamate-cysteine ligase regulatory subunit	31	5	2	5	2.50	2.50
NAA38	N-alpha-acetyltransferase 38, NatC auxiliary subunit	10	5	0	0		
RPIA	Ribose-5-phosphate isomerase	33	5	0	8		
RL23	60S ribosomal protein L23	15	5	2	3	2.50	1.50
UCK2	Uridine-cytidine kinase 2	29	5	0	4		
C1QBP	Complement component 1 Q subcomponent-binding protein, mitochondrial	31	5	1	1	5.00	1.00
BCLF1	Bcl-2-associated transcription factor 1	106	5	1	4	5.00	4.00
<i>DCP2</i>	<i>mRNA-decapping enzyme 2</i>	48	5	0	0		
NONO	Non-POU domain-containing octamer-binding protein	54	5	0	4		
KCTD6	BTB/POZ domain-containing protein KCTD6	28	5	0	1		
RL31	60S ribosomal protein L31	14	5	1	1	5.00	1.00
CDK5	Cell division protein kinase 5	33	5	0	4		
RS25	40S ribosomal protein S25	14	5	1	0	5.00	0.00
RT29	28S ribosomal protein S29, mitochondrial	46	5	0	0		
RL11	60S ribosomal protein L11	20	5	1	2	5.00	2.00
RS23	40S ribosomal protein S23	16	5	1	1	5.00	1.00
LC7L2	Putative RNA-binding protein Luc7-like 2	47	5	2	0	2.50	0.00
HNRDL	Heterogeneous nuclear ribonucleoprotein D-like	46	5	0	2		
ROA0	Heterogeneous nuclear ribonucleoprotein A0	31	5	1	1	5.00	1.00

Continued on Next Page...

5.1 Results of HPLC-MS/MS Analysis

Symbol	Description	MW (kDa)	Num. of Unique Peptides			Peptide Ratio	
			YFP- Pat1b	YFP	YFP- Pat1b-A	YFP- Pat1b / YFP	YFP- Pat1b-A / YFP
1433T	14-3-3 protein theta	28	5	0	1		
RT22	28S ribosomal protein S22, mitochondrial	41	5	0	0		
YTDC2	Probable ATP-dependent RNA helicase YTHDC2	160	5	0	0		
UFC1	Ubiquitin-fold modifier-conjugating enzyme 1	19	4	2	5	2.00	2.50
ADT3	ADP/ATP translocase 3	33	4	1	3	4.00	3.00
DDX18	ATP-dependent RNA helicase DDX18	75	4	2	4	2.00	2.00
RL18	60S ribosomal protein L18	22	4	1	2	4.00	2.00
LSM3	U6 snRNA-associated Sm-like protein LSM3	12	4	1	0	4.00	0.00
MSRB2	Methionine-R-sulfoxide reductase B2, mitochondrial	20	4	2	4	2.00	2.00
SAFB1	Scaffold attachment factor B1	103	4	1	6	4.00	6.00
MTNB	Probable methylthioribulose-1-phosphate dehydratase	27	4	0	3		
TFAM	Transcription factor A, mitochondrial	29	4	0	5		
RS27	40S ribosomal protein S27	9	4	2	2	2.00	1.00
WIPI3	WD repeat domain phosphoinositide-interacting protein 3	38	4	0	3		
CHM1A	Charged multivesicular body protein 1a	22	4	0	5		
DDX3X	ATP-dependent RNA helicase DDX3X	73	4	0	1		
RALY	RNA-binding protein Raly	32	4	2	2	2.00	1.00
NH2L1	NHP2-like protein 1	14	4	1	3	4.00	3.00
RL10A	60S ribosomal protein L10a	25	4	0	1		
RUXE	Small nuclear ribonucleoprotein E	11	4	1	1	4.00	1.00
RLA2	60S acidic ribosomal protein P2	12	4	0	1		
RL9	60S ribosomal protein L9	22	4	0	1		
LMNB2	Lamin-B2	68	4	0	1		
CPPED	Calcineurin-like phosphoesterase domain-containing protein 1	36	4	0	2		
RL35	60S ribosomal protein L35	15	4	0	2		
RPF2	Ribosome production factor 2 homolog	36	4	0	1		
LARP1	La-related protein 1	124	4	1	0	4.00	0.00
RL19	60S ribosomal protein L19	23	4	0	0		
PABP4	Polyadenylate-binding protein 4	71	4	0	0		
BAG2	BAG family molecular chaperone regulator 2	24	4	0	0		
RT27	28S ribosomal protein S27, mitochondrial	48	4	0	0		
RCD1	Cell differentiation protein RCD1 homolog	34	4	0	0		
TADBP	TAR DNA-binding protein 43	45	4	0	0		
RM15	39S ribosomal protein L15, mitochondrial	33	4	0	0		
H2AX	Histone H2A.x	15	3	1	3	3.00	3.00
SMD1	Small nuclear ribonucleoprotein Sm D1	13	3	1	2	3.00	2.00
U5S1	116 U5 small nuclear ribonucleoprotein component	109	3	1	6	3.00	6.00
MCM5	DNA replication licensing factor MCM5	82	3	1	8	3.00	8.00
RS24	40S ribosomal protein S24	15	3	1	2	3.00	2.00
PSME1	Proteasome activator complex subunit 1	29	3	0	4		
RL7L	60S ribosomal protein L7-like 1	29	3	1	1	3.00	1.00
RSMB	Small nuclear ribonucleoprotein-associated proteins B and B'	25	3	1	2	3.00	2.00
AIBP	Apolipoprotein A-I-binding protein	32	3	0	2		
IMA2	Importin subunit alpha-2	58	3	0	1		
RS30	40S ribosomal protein S30	7	3	0	1		
RCC1	Regulator of chromosome condensation	45	3	0	2		
RL30	60S ribosomal protein L30	13	3	0	1		
IRS4	Insulin receptor substrate 4	134	3	0	1		
RL21	60S ribosomal protein L21	19	3	1	1	3.00	1.00
SRP14	Signal recognition particle 14 protein	15	3	0	1		
RL22	60S ribosomal protein L22	15	3	0	1		
UPP1	Uridine phosphorylase 1	34	3	0	1		
DKC1	H/ACA ribonucleoprotein complex subunit 4	58	3	0	1		
ZCCHV	Zinc finger CCCH-type antiviral protein 1	101	3	1	0	3.00	0.00
XRCC5	X-ray repair cross-complementing protein 5	83	3	0	1		
RL28	60S ribosomal protein L28	16	3	0	1		
DDX17	Probable ATP-dependent RNA helicase DDX17	72	3	0	0		
RM38	39S ribosomal protein L38, mitochondrial	45	3	0	0		
SRSF5	Serine/arginine-rich splicing factor 5	31	3	0	0		
TRA2A	Transformer-2 protein homolog alpha	33	3	0	0		
ATD3A	ATPase family AAA domain-containing protein 3A	71	3	0	0		
CPVL	Probable serine carboxypeptidase CPVL	54	3	0	0		
H1X	Histone H1x	22	3	0	0		
RL13A	60S ribosomal protein L13a	24	3	0	0		
STPAP	Speckle targeted PIP5K1A-regulated poly(A) polymerase	94	3	0	0		
FUS	RNA-binding protein FUS	53	3	0	0		
TIPRL	TIP41-like protein	31	3	0	0		
RL35A	60S ribosomal protein L35a	13	3	0	0		
COX17	Cytochrome c oxidase copper chaperone	7	2	1	4	2.00	4.00
CYBP	Calcyclin-binding protein	26	2	0	6		
RL38	60S ribosomal protein L38	8	2	1	3	2.00	3.00
AIMP2	Aminoacyl tRNA synthase complex-interacting multifunctional protein 2	35	2	1	2	2.00	2.00

Continued on Next Page...

5 Appendix

Symbol	Description	MW (kDa)	Num. of Unique Peptides			Peptide Ratio	
			YFP- Pat1b	YFP	YFP- Pat1b-A	YFP- Pat1b / YFP	YFP- Pat1b-A / YFP
HMGCL	Hydroxymethylglutaryl-CoA lyase, mitochondrial	34	2	0	2		
DCTP1	dCTP pyrophosphatase 1	19	2	1	3	2.00	3.00
UAP56	Spliceosome RNA helicase BAT1	49	2	1	1	2.00	1.00
H2A2B	Histone H2A type 2-B	14	2	0	2		
RASL2	Ras GTPase-activating protein 4	90	2	1	1	2.00	1.00
CH082	UPF0598 protein C8orf82	24	2	1	1	2.00	1.00
SRSF9	Serine/arginine-rich splicing factor 9	26	2	0	2		
SMRC1	SWI/SNF complex subunit SMARCC1	123	2	0	2		
RUXF	Small nuclear ribonucleoprotein F	10	2	0	2		
RL27	60S ribosomal protein L27	16	2	0	2		
MTCH2	Mitochondrial carrier homolog 2	33	2	0	1		
RUXG	Small nuclear ribonucleoprotein G	8	2	1	1	2.00	1.00
HN1L	Hematological and neurological expressed 1-like protein	20	2	1	1	2.00	1.00
RUVB1	RuvB-like 1	50	2	1	1	2.00	1.00
SFPQ	Splicing factor, proline- and glutamine-rich	76	2	0	2		
RIPK1	Receptor-interacting serine/threonine-protein kinase 1	76	2	1	1	2.00	1.00
EBP2	Probable rRNA-processing protein EBP2	35	2	1	0	2.00	0.00
RRP12	RRP12-like protein	144	2	0	1		
GGH	Gamma-glutamyl hydrolase	36	2	0	1		
DHB12	Estradiol 17-beta-dehydrogenase 12	34	2	0	0		
DHX36	Probable ATP-dependent RNA helicase DHX36	115	2	0	0		
RM21	39S ribosomal protein L21, mitochondrial	23	2	0	0		
NPM3	Nucleoplasm-in-3	19	2	1	0		
DNJC9	DnaJ homolog subfamily C member 9	30	2	0	1		
BYST	Bystin	50	2	0	0		
DDX1	ATP-dependent RNA helicase DDX1	82	2	0	0		
MK671	MK167 FHA domain-interacting nucleolar phosphoprotein	34	2	0	0		
RM19	39S ribosomal protein L19, mitochondrial	34	2	0	0		
SMD2	Small nuclear ribonucleoprotein Sm D2	14	2	0	0		
STAU1	Double-stranded RNA-binding protein Staufen homolog 1	63	2	0	0		
TRA2B	Transformer-2 protein homolog beta	34	2	0	0		
RM28	39S ribosomal protein L28, mitochondrial	30	2	0	0		
RM17	39S ribosomal protein L17, mitochondrial	20	2	0	0		
MAGD1	Melanoma-associated antigen D1	86	2	0	0		
RS29	40S ribosomal protein S29	7	2	0	0		
RBM39	RNA-binding protein 39	59	2	0	0		
BRX1	Ribosome biogenesis protein BRX1 homolog	41	2	0	0		
H2AW	Core histone macro-H2A.2	40	2	0	0		
RCL1	RNA 3'-terminal phosphate cyclase-like protein	41	2	0	0		
RENT1	Regulator of nonsense transcripts 1	124	2	0	0		
SNR40	U5 small nuclear ribonucleoprotein 40 protein	39	2	0	0		
PRC2C	Protein PRC2C	317	2	0	0		
RM03	39S ribosomal protein L3, mitochondrial	39	2	0	0		
KHDR1	KH domain-containing, RNA-binding, signal transduction-associated protein 1	48	2	0	0		
FHL3	Four and a half LIM domains protein 3	31	2	0	0		
DHX37	Probable ATP-dependent RNA helicase DHX37	130	2	0	0		
G3BP1	Ras GTPase-activating protein-binding protein 1	52	2	0	0		
SRSF2	Serine/arginine-rich splicing factor 2	25	2	0	0		
VAPA	Vesicle-associated membrane protein-associated protein A	28	1	0	14		
NU205	Nuclear pore complex protein Nup205	228	1	0	4		
UT14A	U3 small nucleolar RNA-associated protein 14 homolog A	88	1	0	3		
NU160	Nuclear pore complex protein Nup160	162	1	0	2		
HMGA1	High mobility group protein HMG-I/HMG-Y	12	1	0	3		
NPA1P	Nucleolar pre-ribosomal-associated protein 1	254	1	0	3		
BAZ1A	Bromodomain adjacent to zinc finger domain protein 1A	179	1	0	2		
ACYP2	Acylphosphatase-2	11	1	0	2		
RN114	RING finger protein 114	26	1	0	3		
UTP20	Small subunit processome component 20 homolog	318	1	0	2		
HMGN1	Non-histone chromosomal protein HMG-14	11	1	0	2		
MYL6	Myosin light polypeptide 6	17	1	0	2		
HMGN2	Non-histone chromosomal protein HMG-17	9	1	0	2		
ANX11	Annexin A11	54	1	0	2		
NOL11	Nucleolar protein 11	81	1	0	2		
TOP1	DNA topoisomerase 1	91	1	0	2		
FAKD5	FAST kinase domain-containing protein 5	87	1	0	2		

5.2 Results of Microarray Analysis

Table 5.2. List of mRNAs that are up- or down-regulated more than 2-fold, upon siRNA-mediated knockdown of Pat1b, Rck and/or Pat1b together with Rck (Pat1b + Rck). Target mRNAs that were tested with qPCR analysis are depicted in *italics*. FC, fold change.

	Gene ID	Symbol	Description	FC (Linear Scale)		
				si-Pat1b	si-Rck	si-Pat1b + si-Rck
Pat1b only	113791	PIK3IP1	phosphoinositide-3-kinase interacting protein 1	3.26		
	84898	PLXDC2	plexin domain containing 2	2.46		
	158572	LOC158572	hypothetical LOC158572	2.31		
	8140	SLC7A5	solute carrier family 7 (cationic amino acid transporter, y+ system), member 5	2.10		
	4211	MEIS1	Meis homeobox 1	2.05		
	5955	RCN2	reticulocalbin 2, EF-hand calcium binding domain	2.03		
	808	CALM3	calmodulin 3 (phosphorylase kinase, delta)	0.50		
	54741	LEPROT	leptin receptor overlapping transcript	0.49		
	6385	SDC4	syndecan 4	0.49		
	80196	RNF34	ring finger protein 34	0.49		
	338811	FAM19A2	family with sequence similarity 19 (chemokine (C-C motif)-like), member A2	0.47		
	9231	DLG5	discs, large homolog 5 (Drosophila)	0.47		
	1404	HAPLN1	hyaluronan and proteoglycan link protein 1	0.47		
	5577	PRKAR2B	protein kinase, cAMP-dependent, regulatory, type II, beta	0.46		
	4674	NAP1L2	nucleosome assembly protein 1-like 2	0.46		
	8539	API5	apoptosis inhibitor 5	0.44		
	3936	LCP1	lymphocyte cytosolic protein 1 (L-plastin)	0.41		
	9813	KIAA0494	KIAA0494	0.40		
	56938	ARNTL2	aryl hydrocarbon receptor nuclear translocator-like 2	0.39		
	989	SEPT7	septin 7	0.38		
Pat1b & Pat1b + Rck	401138	<i>AMTN</i>	<i>amelotin</i>	<i>4.58</i>		<i>3.60</i>
	23657	<i>SLC7A11</i>	<i>solute carrier family 7, (cationic amino acid transporter, y+ system) member 11</i>	<i>3.13</i>		<i>2.71</i>
	6004	<i>RGS16</i>	<i>regulator of G-protein signaling 16</i>	<i>2.87</i>		<i>3.31</i>
	84189	<i>SLITRK6</i>	<i>SLIT and NTRK-like family, member 6</i>	<i>2.49</i>		<i>2.45</i>
	3887	KRT81	keratin 81	2.42		3.27
	10962	MLLT11	myeloid/lymphoid or mixed-lineage leukemia (trithorax homolog, Drosophila); translocated to, 11	2.36		2.23
	144165	PRICKLE1	prickle homolog 1 (Drosophila)	2.33		2.78
	51647	FAM96B	family with sequence similarity 96, member B	2.26		3.45
	54732	TMED9	transmembrane emp24 protein transport domain containing 9	2.24		2.35
	9652	TTC37	tetratricopeptide repeat domain 37	2.16		2.51
	6744	SSFA2	sperm specific antigen 2	2.15		2.20
	51088	KLHL5	kelch-like 5 (Drosophila)	2.14		3.61
	7286	TUFT1	tuftelin 1	2.13		3.10
	3516	RBPJ	recombination signal binding protein for immunoglobulin kappa J region	2.10		2.36
	2632	GBE1	glucan (1,4-alpha-), branching enzyme 1	2.09		2.58
	51614	ERGIC3	ERGIC and golgi 3	2.07		2.22
	3295	HSD17B4	hydroxysteroid (17-beta) dehydrogenase 4	2.01		2.45
	4591	TRIM37	tripartite motif-containing 37	0.49		0.43
	57687	VAT1L	vesicle amine transport protein 1 homolog (T. californica)-like	0.48		0.45
	51280	GOLM1	golgi membrane protein 1	0.48		0.32
	79794	C12orf49	chromosome 12 open reading frame 49	0.47		0.48
	4893	NRAS	neuroblastoma RAS viral (v-ras) oncogene homolog	0.46		0.47
	10713	USP39	ubiquitin specific peptidase 39	0.44		0.47
	3572	IL6ST	interleukin 6 signal transducer (gp130, oncostatin M receptor)	0.44		0.39
	3925	STMN1	stathmin 1/oncoprotein 18	0.44		0.46
	27248	C2orf30	chromosome 2 open reading frame 30	0.43		0.39
	3397	ID1	inhibitor of DNA binding 1, dominant negative helix-loop-helix protein	0.43		0.40
	6386	SDCBP	syndecan binding protein (syntenin)	0.42		0.45
	3930	LBR	lamin B receptor	0.41		0.45
	55326	AGPAT5	1-acylglycerol-3-phosphate O-acyltransferase 5 (lysophosphatidic acid acyltransferase, epsilon)	0.40		0.31
	10592	SMC2	structural maintenance of chromosomes 2	0.39		0.40
	29940	DSE	dermatan sulfate epimerase	0.38		0.23
	9768	KIAA0101	KIAA0101	0.38		0.37
	7706	<i>TRIM25</i>	<i>tripartite motif-containing 25</i>	<i>0.32</i>		<i>0.36</i>
	23770	<i>FKBP8</i>	<i>FK506 binding protein 8, 38kDa</i>	<i>0.28</i>		<i>0.34</i>
	23191	<i>CYFIP1</i>	<i>cytoplasmic FMR1 interacting protein 1</i>	<i>0.27</i>		<i>0.38</i>
5528	<i>PPP2R5D</i>	<i>protein phosphatase 2, regulatory subunit B, delta isoform</i>	<i>0.16</i>		<i>0.17</i>	
7837	<i>PXDN</i>	<i>peroxidasin homolog (Drosophila)</i>	<i>0.15</i>		<i>0.17</i>	
219988	PATL1	protein associated with topoisomerase II homolog 1 (yeast)	0.09		0.09	

Continued on Next Page...

5 Appendix

				FC (Linear Scale)		
	Gene ID	Symbol	Description	si-Pat1b	si-Rck	si-Pat1b + si-Rck
Rck only	72	ACTG2	<i>actin, gamma 2, smooth muscle, enteric</i>		9.94	
	59	ACTA2	<i>actin, alpha 2, smooth muscle, aorta</i>		7.14	
	6876	TAGLN	<i>transgelin</i>		3.99	
	57381	RHOJ	ras homolog gene family, member J		2.94	
	3897	L1CAM	L1 cell adhesion molecule		2.33	
	3690	ITGB3	integrin, beta 3 (platelet glycoprotein IIIa, antigen CD61)		2.27	
	7414	VCL	vinculin		2.13	
	51704	GPRC5B	G protein-coupled receptor, family C, group 5, member B		2.11	
	10398	MYL9	myosin, light chain 9, regulatory		2.05	
	51199	NIN	ninein (GSK3B interacting protein)		0.42	
	6051	RNPEP	<i>arginyl aminopeptidase (aminopeptidase B)</i>		0.39	
	Rck & Pat1b+Rck	3491	CYR61	cysteine-rich, angiogenic inducer, 61		2.53
143888		KDEL2	KDEL (Lys-Asp-Glu-Leu) containing 2		0.28	0.23
1656		DDX6	DEAD (Asp-Glu-Ala-Asp) box polypeptide 6		0.07	0.09
Pat1b + Rck	55681	SCYL2	SCY1-like 2 (S, cerevisiae)			6.68
	1317	SLC31A1	solute carrier family 31 (copper transporters), member 1			5.10
	148362	C1orf58	chromosome 1 open reading frame 58			4.17
	169200	TMEM64	transmembrane protein 64			3.47
	10026	PIGK	phosphatidylinositol glycan anchor biosynthesis, class K			3.39
	1136	CHRNA3	cholinergic receptor, nicotinic, alpha 3			3.38
	8549	LGR5	leucine-rich repeat-containing G protein-coupled receptor 5			3.10
	79719	FLJ11506	alpha- and gamma-adaptin-binding protein p34			2.98
	1004	CDH6	cadherin 6, type 2, K-cadherin (fetal kidney)			2.96
	54838	C10orf26	chromosome 10 open reading frame 26			2.87
	284119	PTRF	polymerase I and transcript release factor			2.72
	3632	INPP5A	inositol polyphosphate-5-phosphatase, 40kDa			2.69
	8076	MFAP5	microfibrillar associated protein 5			2.63
	4238	MFAP3	microfibrillar-associated protein 3			2.63
	6502	SKP2	S-phase kinase-associated protein 2 (p45)			2.53
	85236	HIST1H2BK	histone cluster 1, H2bk			2.47
	2690	GHR	growth hormone receptor			2.47
	127933	UHMK1	U2AF homology motif (UHM) kinase 1			2.44
	11022	TDRKH	tudor and KH domain containing			2.41
	29101	SSU72	SSU72 RNA polymerase II CTD phosphatase homolog (S, cerevisiae)			2.39
	1000	CDH2	cadherin 2, type 1, N-cadherin (neuronal)			2.39
	586	BCAT1	branched chain aminotransferase 1, cytosolic			2.37
	9802	DAZAP2	DAZ associated protein 2			2.36
	22862	FNDC3A	fibronectin type III domain containing 3A			2.33
	53	ACP2	acid phosphatase 2, lysosomal			2.30
	7052	TGM2	transglutaminase 2 (C polypeptide, protein-glutamine-gamma-glutamyltransferase)			2.28
	1809	DPYSL3	dihydropyrimidinase-like 3			2.23
	55161	TMEM33	transmembrane protein 33			2.22
	5437	POLR2H	polymerase (RNA) II (DNA directed) polypeptide H			2.19
	6302	TSPAN31	tetraspanin 31			2.19
	1718	DHCR24	24-dehydrocholesterol reductase			2.19
	3685	ITGAV	integrin, alpha V (vitronectin receptor, alpha polypeptide, antigen CD51)			2.17
	89970	RSPRY1	ring finger and SPRY domain containing 1			2.17
	79822	ARHGAP28	Rho GTPase activating protein 28			2.16
	9213	XPR1	xenotropic and polytropic retrovirus receptor			2.15
	9929	JOSD1	Josephin domain containing 1			2.15
	3836	KPNA1	karyopherin alpha 1 (importin alpha 5)			2.13
	9520	NPEPPS	aminopeptidase puromycin sensitive			2.13
	10900	RUNDC3A	RUN domain containing 3A			2.13
	4047	LSS	lanosterol synthase (2,3-oxidosqualene-lanosterol cyclase)			2.11
	80146	UXS1	UDP-glucuronate decarboxylase 1			2.10
	10195	ALG3	asparagine-linked glycosylation 3, alpha-1,3- mannosyltransferase homolog (S, cerevisiae)			2.09
	8992	ATP6V0E1	ATPase, H+ transporting, lysosomal 9kDa, V0 subunit e1			2.08
	3678	ITGA5	integrin, alpha 5 (fibronectin receptor, alpha polypeptide)			2.06
	9241	NOG	noggin			2.06
	23196	FAM120A	family with sequence similarity 120A			2.06
	51474	LIMA1	LIM domain and actin binding 1			2.05
9188	DDX21	DEAD (Asp-Glu-Ala-Asp) box polypeptide 21			2.04	
6198	RPS6KB1	ribosomal protein S6 kinase, 70kDa, polypeptide 1			2.03	
51706	CYB5R1	cytochrome b5 reductase 1			2.03	

Continued on Next Page...

5.2 Results of Microarray Analysis

				FC (Linear Scale)			
Gene ID	Symbol	Description			si-Pat1b	si-Rck	si-Pat1b + si-Rck
			si-Pat1b	si-Rck			
523	ATP6V1A	ATPase, H+ transporting, lysosomal 70kDa, V1 subunit A					2.02
8048	CSRP3	cysteine and glycine-rich protein 3 (cardiac LIM protein)					2.02
93663	ARHGAP18	Rho GTPase activating protein 18					2.02
1024	CDK8	cyclin-dependent kinase 8					2.01
81575	APOLD1	apolipoprotein L domain containing 1					0.50
114908	TMEM123	transmembrane protein 123					0.50
3696	ITGB8	integrin, beta 8					0.50
55536	CDCA7L	cell division cycle associated 7-like					0.49
63901	FAM111A	family with sequence similarity 111, member A					0.49
3024	HIST1H1A	histone cluster 1, H1a					0.49
6241	RRM2	ribonucleotide reductase M2 polypeptide					0.49
25945	PVRL3	poliovirus receptor-related 3					0.49
9582	APOBEC3B	apolipoprotein B mRNA editing enzyme, catalytic polypeptide-like 3B					0.48
348235	FAM33A	family with sequence similarity 33, member A					0.48
8787	RGS9	regulator of G-protein signaling 9					0.48
10457	GNPMB	glycoprotein (transmembrane) nmb					0.48
5627	PROS1	protein S (alpha)					0.48
135293	PM20D2	peptidase M20 domain containing 2					0.48
26002	MOXD1	monooxygenase, DBH-like 1					0.48
6364	CCL20	chemokine (C-C motif) ligand 20					0.48
405	ARNT	aryl hydrocarbon receptor nuclear translocator					0.47
3920	LAMP2	lysosomal-associated membrane protein 2					0.47
51514	DTL	denticleless homolog (Drosophila)					0.47
134829	RLBP1L2	retinaldehyde binding protein 1-like 2					0.47
1812	DRD1	dopamine receptor D1					0.47
79598	CEP97	centrosomal protein 97kDa					0.47
28951	TRIB2	tribbles homolog 2 (Drosophila)					0.47
3672	ITGA1	integrin, alpha 1					0.46
142679	DUSP19	dual specificity phosphatase 19					0.46
90381	C15orf42	chromosome 15 open reading frame 42					0.45
23532	PRAME	preferentially expressed antigen in melanoma					0.45
220988	HNRNPA3	heterogeneous nuclear ribonucleoprotein A3					0.45
113146	AHNAK2	AHNAK nucleoprotein 2					0.44
9897	KIAA0196	KIAA0196					0.44
26503	SLC17A5	solute carrier family 17 (anion/sugar transporter), member 5					0.42
23306	TMEM194A	transmembrane protein 194A					0.42
57088	PLSCR4	phospholipid scramblase 4					0.41
53904	MYO3A	myosin IIIA					0.40
51136	RNFT1	ring finger protein, transmembrane 1					0.39
3075	CFH	complement factor H					0.38
93649	MYOCD	myocardin					0.35
57157	PHTF2	putative homeodomain transcription factor 2					0.35
84767	SPRYD5	SPRY domain containing 5					0.34
79365	BHLHE41	basic helix-loop-helix family, member e41					0.32
59084	ENPP5	ectonucleotide pyrophosphatase/phosphodiesterase 5 (putative function)					0.32
6414	SEPP1	selenoprotein P, plasma, 1					0.32
3037	HAS2	hyaluronan synthase 2					0.17

5.3 Publication by Özgür et al.: Human Pat1b Connects Deadenylation with mRNA Decapping and Controls the Assembly of Processing Bodies

The following 29 pages contain a copy of the article specified below, including 13 pages of supplements:

Title: Human Pat1b Connects Deadenylation with mRNA Decapping and Controls the Assembly of Processing Bodies

Authors: Sevim Ozgur, Marina Chekulaeva, Georg Stoecklin

Journal: Molecular and Cellular Biology, Sept. 2010, p. 4308–4323 Vol. 30, No. 17

doi: 10.1128/MCB.00429-10

Human Pat1b Connects Deadenylation with mRNA Decapping and Controls the Assembly of Processing Bodies^{∇†}

Sevim Ozgur,¹ Marina Chekulaeva,² and Georg Stoecklin^{1*}

Helmholtz Junior Research Group Posttranscriptional Control of Gene Expression, German Cancer Research Center, DKFZ-ZMBH Alliance, Im Neuenheimer Feld 280, 69120 Heidelberg, Germany,¹ and Friedrich Miescher Institute for Biomedical Research, Maulbeerstrasse 66, 4058 Basel, Switzerland²

Received 13 April 2010/Returned for modification 27 April 2010/Accepted 11 June 2010

In eukaryotic cells, degradation of many mRNAs is initiated by removal of the poly(A) tail followed by decapping and 5'-3' exonucleolytic decay. Although the order of these events is well established, we are still lacking a mechanistic understanding of how deadenylation and decapping are linked. In this report we identify human Pat1b as a protein that is tightly associated with the Ccr4-Caf1-Not deadenylation complex as well as with the Dcp1-Dcp2 decapping complex. In addition, the RNA helicase Rck and Lsm1 proteins interact with human Pat1b. These interactions are mediated via at least three independent domains within Pat1b, suggesting that Pat1b serves as a scaffold protein. By tethering Pat1b to a reporter mRNA, we further provide evidence that Pat1b is also functionally linked to both deadenylation and decapping. Finally, we report that Pat1b strongly induces the formation of processing (P) bodies, cytoplasmic foci that contain most enzymes of the RNA decay machinery. An amino-terminal region within Pat1b serves as an aggregation-prone domain that nucleates P bodies, whereas an acidic domain controls the size of P bodies. Taken together, these findings provide evidence that human Pat1b is a central component of the RNA decay machinery by physically connecting deadenylation with decapping.

By controlling gene expression at the posttranscriptional level, cells can rapidly induce, suppress, or fine-tune the production of specific proteins. A well-studied example is a class of mRNAs that contain AU-rich elements (AREs) in their 3' untranslated region (UTR), which causes rapid mRNA decay. The degradation of ARE mRNAs can be inhibited by extracellular signals, a mechanism that contributes to the efficient production of cytokines in activated cells of the immune system (37). Another prominent example are mRNAs targeted by microRNAs (miRNAs), which generally cause translational inhibition and/or accelerated mRNA decay (7). The reversible transit of an actively translating mRNA to a state of translational silencing and the irreversible step that elicits mRNA degradation involve crucial rearrangements of the ribonucleoprotein (RNP) composition. In some cases, the transit of an mRNA to a repressed state is associated with its recruitment to processing (P) bodies (3, 14, 35). P bodies are cytoplasmic foci that contain many enzymes of the general mRNA decay pathway, such as the Ccr4-Caf1-Not deadenylase complex and the decapping enzyme Dcp2 together with its activators Dcp1, Edc3, and Hedls, as well as the 5'-3' exoribonuclease Xrn1 that is tightly associated with the heptameric ring of the Lsm1-7 proteins (2, 10, 13, 21, 24, 35, 41, 43, 47).

For most eukaryotic mRNAs, deadenylation is the first step in the decay pathway. Once the poly(A) tail is removed, the mRNA is either degraded in the 3'-5' direction by the exosome

or decapped at the 5' end and subsequently degraded in the 5'-3' direction by Xrn1 (15). Both ARE-mediated mRNA decay and miRNA-mediated mRNA decay make use of this general decay pathway by delivering mRNAs at an accelerated rate to the decay machinery.

An unsolved question is how deadenylation at the 3' end of an mRNA is linked to decapping at the 5' end. Since deadenylated but capped mRNAs are virtually undetectable in wild-type (wt) cells, the two events seem to be coupled very tightly. However, it is not clear which factors physically connect the deadenylation and decapping complexes.

Studies of *Saccharomyces cerevisiae* suggest that Pat1 (protein associated with topoisomerase II, also termed MRT1) might play a role in coupling deadenylation with decapping. On the one hand, yeast mutants lacking Pat1 show reduced rates of mRNA degradation and accumulate deadenylated but capped mRNA (18). Thus, Pat1 was proposed to enhance mRNA decay by activating the decapping reaction. On the other hand, Pat1 was found to interact with the cytoplasmic Lsm1-7 proteins, which form a heptameric ring structure (5, 6). The Lsm1-7-Pat1 complex was shown to preferentially bind to the 3' end of mRNAs that contain short poly(A) tails (8, 42). Since strains lacking Lsm1 or Pat1 generate transcripts that are truncated at the 3' end, the Lsm1-7-Pat1 complex also appears to protect mRNA from further trimming after deadenylation (19). Thus, the Lsm1-7-Pat1 complex was proposed to serve as a linker that recognizes oligo- or deadenylated mRNAs at the 3' end and activates the subsequent step of decapping at the 5' end.

To further pursue the mechanism by which deadenylation is coupled to decapping, we sought to study the function of human Pat1 homologs. For many years, a metazoan counterpart of yeast Pat1 has not been identified since routine BLAST

* Corresponding author. Mailing address: German Cancer Research Center, DKFZ-A200, Im Neuenheimer Feld 280, D-69120 Heidelberg, Germany. Phone: 49-6221-546887. Fax: 49-6221-545891. E-mail: g.stoecklin@dkfz.de.

† Supplemental material for this article may be found at <http://mcb.asm.org/>.

∇ Published ahead of print on 28 June 2010.

analysis does not reveal homologous proteins. In 2007, Scheller et al. identified two human homologs which they termed PatL1 and PatL2 (34). This report showed that human PatL1 localizes to P bodies and that its depletion by small interfering RNA (siRNA) causes loss of P bodies. We have independently identified the same two proteins as possible homologs of yeast Pat1. In accordance with the two orthologs in *Xenopus laevis*, we termed the two proteins Pat1a and Pat1b (Nancy Standard, personal communication). In the present study we provide evidence that human Pat1b (PatL1) physically and functionally connects the deadenylation and decapping machinery. Whereas no function could be attributed to Pat1a (PatL2), we found that Pat1b also controls the assembly of P bodies.

MATERIALS AND METHODS

Plasmids. The following plasmids have been described previously: pCMV-FLAG-NOT1 (45), pcDNA3-Myc-Ccr4, pcDNA3-Flag-Dcp1a, pcDNA3-Flag-Dcp2 (25), and pCIneo-RL (31).

To generate pcDNA3-HA (p2003), oligonucleotides G85/G86 (for primer sequences, see Table S1 in the supplemental material) were annealed and cloned into the HindIII-EcoRI sites of pcDNA3 (Invitrogen). For pcDNA3-YFP (p2168), yellow fluorescent protein (YFP) was amplified with oligonucleotides G243/G244 and then ligated into the HindIII-KpnI sites of pcDNA3-HA (p2003), thereby replacing the hemagglutinin (HA) tag.

For plasmid pEYFP-Pat1a (p2639), the human Pat1a coding sequence was amplified in three portions from the cDNA of HeLa cells and ligated sequentially into the BglII-XbaI sites of pEYFP-C1 (Clontech/BD Biosciences). The following primer pairs were used: G1332/G1222 (1st PCR) and G1332/G1198 (2nd PCR) for the Pat1a C-terminal portion, ligated as a KpnI-XbaI fragment; G1315/G1221 for the middle portion, ligated as a BglII-KpnI fragment; and G1219/G1340 (1st PCR) and G1353/G1340 (2nd PCR) for the Pat1a N-terminal portion, ligated as a BamHI-BglII fragment and thereby introducing an EcoRI site upstream of the start codon. For pcDNA3-HA-Pat1a (p2638), the human Pat1a coding sequence was excised from pEYFP-Pat1a (p2639) as an EcoRI-XbaI fragment and cloned into the same sites of pcDNA3-HA (p2003).

A human Pat1b cDNA clone (DKFZp451I053) fused at the C terminus to YFP was kindly provided by Stefan Wiemann (German Cancer Research Center, Heidelberg, Germany). In order to generate HA-tagged Pat1b constructs, fragments were amplified by PCR from human Pat1b cDNA and inserted into the KpnI-XhoI sites of pcDNA3-HA (p2003). The following primers were used: G1225/G1230 for pcDNA3-HA-Pat1b (p2516), G1225/G1226 for pcDNA3-HA-AN (p2511), G1225/G1228 for pcDNA3-HA-ANH (p2514), G1227/G1228 for pcDNA3-HA-H (p2512), G1227/G1230 for pcDNA3-HA-HC (p2515), G1229/G1230 for pcDNA3-HA-C (p2513), G1225/G1425 for pcDNA3-HA-A (p2591), G1408/G1226 for pcDNA3-HA-N (p2592), and G1408/G1230 for pcDNA3-HA-dA (p2675). For pcDNA3-HA-dH (p2542), the N- and C-terminal regions of Pat1b were first amplified as separate fragments with primers G1225/G1295 and G1296/G1230, respectively. The PCR products were then aligned, Pat1b lacking the H domain was amplified with primers G1225/G1230, and the PCR product was cloned into the KpnI-XhoI sites of pcDNA3-HA (p2003).

pcDNA3-YFP-Pat1b full length (p2521), pcDNA3-YFP-A (p2630), pcDNA3-YFP-AN (p2626), pcDNA3-YFP-N (p2627), pcDNA3-YFP-ANH (p2522), pcDNA3-YFP-H (p2632), pcDNA3-YFP-C (p2628), pcDNA3-YFP-HC (p2629), pcDNA3-YFP-dA (p2631), and pcDNA3-YFP-dH (p2633) were generated by replacing the HA tag in the corresponding HA-tagged Pat1b constructs with YFP excised as a HindIII-KpnI fragment from pcDNA3-YFP (p2168). For pcDNA3-HA-Pat1b-YFP (p2520), Pat1b-YFP was amplified by PCR with primers G1225/G1253, using clone DKFZp451I053 as a template, and inserted into the KpnI-XhoI sites of pcDNA3-HA-Pat1b (p2516).

In order to generate pcDNA3-HA-PP7cp-Pat1b (p2634), pcDNA3-HA-PP7cp-AN (p2658), pcDNA3-HA-PP7cp-HC (p2659), pcDNA3-HA-PP7cp-dA (p2663), pcDNA3-HA-PP7cp-dH (p2660), and pcDNA3-HA-PP7cp-Pat1a (p2661), PP7cp (46) was amplified by PCR using primers G1501/G1502 and inserted into the KpnI site of corresponding pcDNA3-HA-Pat1b constructs and pcDNA3-HA-Pat1a (p2638). Orientation of the insert was checked by sequencing.

For pcDNA3-Bgl (p2001), the BglII site in pcDNA3 (Invitrogen) was removed by digestion with BglII and blunt-end religation, thereby introducing a novel ClaI site. pcDNA3-7B (p2308) expressing a T7-tagged rabbit β -globin gene was sub-

sequently generated by amplifying β -globin by PCR with primers G18/G19 from plasmid puroMX β globin (39). The fragment was digested with EcoRV and Sall and ligated into the BamHI/blunt-XhoI sites of pcDNA3-Bgl. For pcDNA3-7B-PP7bs (p2314), six repeats of the PP7 binding site were excised as a BamHI-BglII fragment from pSP73-6xPP7bs (46) and introduced into the BglII site of pcDNA3-7B (p2308). For pFLB (p2524), firefly luciferase (FL) cDNA was amplified by PCR using primers G1256/G1257 from pGL3-Control (Promega) and cloned into the HindIII-KpnI sites of pcDNA3-7B (2308). From there, the 6 \times PP7bs repeats were cloned as an EcoRI-BglII fragment from pcDNA3-7B-PP7bs (p2314) into the corresponding sites of pFLB (p2524) to generate pFLB-PP7bs (p2646).

For TOPuro-Caf1a-mycSG (p2485), the human Caf1a cDNA was amplified by reverse transcription (RT)-PCR using primers G1122 and G1123 and cloned into the BamHI-XhoI sites of TOPuro-mycSG (p2484). For pTOPuro-Caf1a-AA-mycSG (p2737) containing the D40A/E42A mutation, a fragment amplified by PCR with primers G1730 and G1731 was inserted into the KpnI-EcoRI sites of TOPuro-Caf1a-mycSG (p2485). For pEGFP-TEV-Caf1a (p2793), Caf1a cDNA was cloned as a BamHI-XhoI fragment into the BglII-XhoI sites of pEGFP-N1 containing a tobacco etch virus (TEV) cleavage site. To generate pcDNA3-Flag-Dcp2-AA (p2798), the E147A/E148A mutation was introduced into the KpnI-EcoRV sites of pcDNA3-Flag-Dcp2 (25) using a PCR fragment amplified with primers G1883 and G1884.

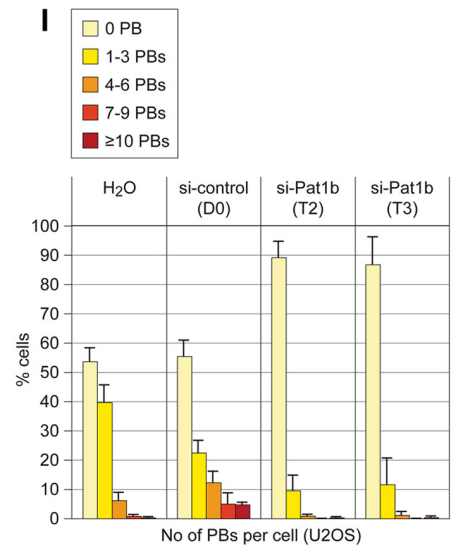
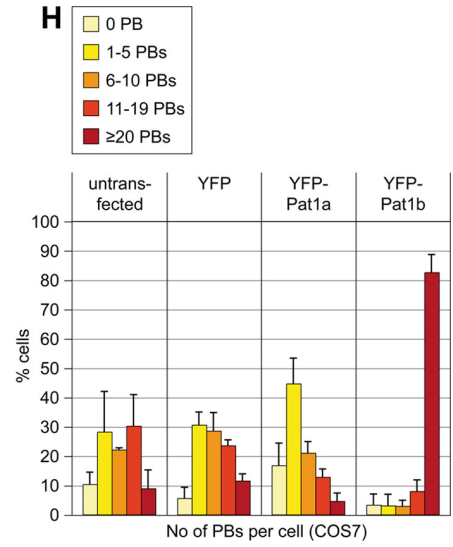
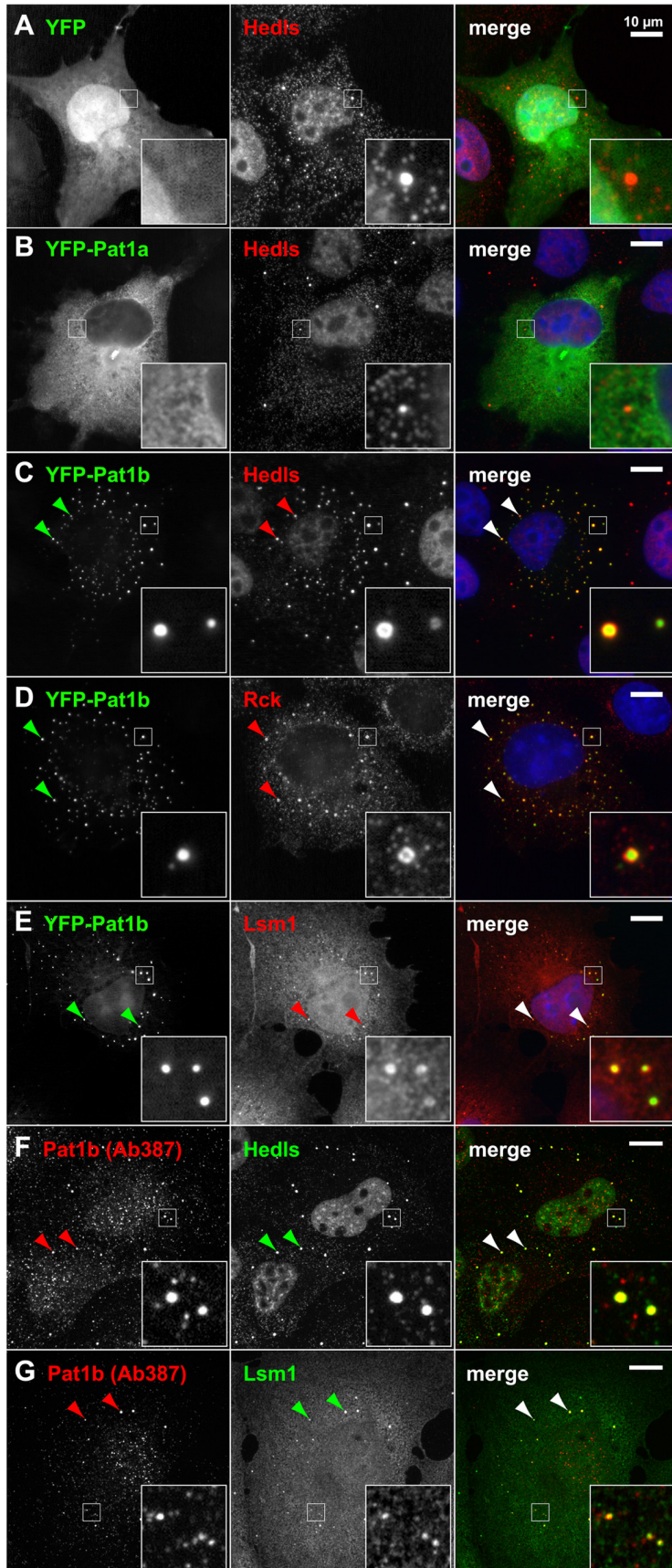
Cell culture and transfection. HeLa, U2OS, HEK293, and COS7 cells were cultured in Dulbecco's modified Eagle medium (DMEM) containing 10% fetal bovine serum (PAA Laboratories), 2 mM L-glutamine, 100 U/ml penicillin, and 0.1 mg/ml streptomycin (all PAN Biotech) at 37°C/5% CO₂. Plasmids were transfected with Lipofectamine 2000 (Invitrogen) for protein interaction studies or with Eugene HD (Roche) for immunofluorescence analysis according to the manufacturer's recommendations. Alternatively, polyethyleneimine (Poly-sciences Europe; 1 mg/ml, pH 7.0) was also used as a transfection reagent for interaction and functional studies. siRNAs were transfected at a concentration of 100 nM with Lipofectamine 2000 twice over a time period of 4 days. Where indicated, cells were treated for 2 h with 5 μ g/ml cycloheximide (Roth).

siRNAs. siRNAs used in this study were synthesized by Ambion against the following sequences (sense strand): D0 (control), 5'-GCAUUCACUUGGAUA GUAAAdTdT-3'; T2 (human Pat1b), 5'-GCAGAAAGGCUCAGUAAGAdTdT-3'; and T3 (human Pat1b), 5'-GGACGGAGGUGAUGUUCAUdTTdT-3'.

Immunofluorescence microscopy. Twenty-four hours after transient transfection, cells grown on glass coverslips were fixed in 4% paraformaldehyde for 10 min at room temperature. Cell membranes were then permeabilized in -20°C cold methanol for 10 min. Phosphate-buffered saline (PBS) containing 0.1% sodium azide and 5% horse serum was used for blocking and antibody dilution. DNA was visualized using Hoechst dye (no. 33342, 1 μ g/ml; Sigma). After washing in PBS, cells were mounted onto glass slides using a solution of 14% polyvinyl alcohol (P8136; Sigma) and 30% glycerol in PBS. P bodies were counted on an upright epifluorescence microscope (BX60; Olympus). Images were acquired at the Nikon Imaging Center, Heidelberg, Germany, either on an upright epifluorescence microscope (90i; Nikon) or by spinning-disc confocal microscopy (Ultraview ERS [Perkin Elmer] on a TE2000 inverted microscope [Nikon]) using an electron-multiplier charge-coupled-device (EM-CCD) camera (Hamamatsu).

Coimmunoprecipitation (co-IP) and Western blot analysis. Twenty-four hours after transient transfection, HEK293 cells from a confluent 10-cm dish were collected and lysed in 400 μ l ice-cold hypotonic lysis buffer (10 mM Tris [pH 7.5], 10 mM NaCl, 10 mM EDTA, 0.5% Triton X-100 with freshly added protease inhibitors [Complete; Roche]). Nuclei were removed by centrifugation at 500 \times g for 5 min at 4°C. The cytoplasmic lysate was precleared by the addition of 30 μ l protein A/G-agarose beads (Pierce or Santa Cruz) for 1 h at 4°C and incubated with 1 μ g of antibody for 2 h. A total of 30 μ l of protein A/G beads was added for an additional 2 h and washed six times in NET2 buffer (50 mM Tris [pH 7.5], 150 mM NaCl, 0.5% Triton X-100). Protein complexes were eluted with 25 μ l SDS sample buffer with or without 100 mM dithiothreitol (DTT). Where indicated, RNase A (Sigma; 0.1 mg/ml) was added to the lysates after preclearing. Proteins were resolved on 10% polyacrylamide gels and transferred onto a 0.2- μ m-pore-size nitrocellulose membrane (Peqlab) for Western blotting. Horseradish peroxidase-coupled secondary antibodies (Jackson ImmunoResearch) in combination with Western Lightning enhanced chemiluminescence substrate (Perkin Elmer) were used for detection. The green fluorescent protein (GFP)-binder was used for immunoprecipitation (IP) of YFP-tagged proteins as described previously (33).

Antibodies. Polyclonal antibody Ab387 against human Pat1b was produced at Eurogentec by immunizing rabbits with peptide QGPEDDRDLSERALPR. The following antibodies were used for IP and Western blotting, and immunofluo-



rescence analysis: mouse monoclonal antibodies anti-HA (HA.11; Covance) and anti-Edc3 (Abcam; ab57780-100); a cross-reacting mouse monoclonal phospho-S6-kinase antibody (sc-8416; Santa Cruz) for detection of Hedls; polyclonal chicken antibodies against Lsm1 (15-288-22100F; Genway Biotech) and Lsm4 (19101; Abcam); polyclonal rabbit antibodies against Xrn1 (A300-461A; Bethyl Laboratories), p54/Rck (A300-443A; Bethyl Laboratories), eIF4G (sc-11373; Santa Cruz), 14-3-3 (sc-629; Santa Cruz), and HA (sc-805; Santa Cruz); and a polyclonal goat antibody against eIF3B (sc-16377; Santa Cruz). Polyclonal rabbit anti-Caf1a was kindly provided by Ann-Bin Shyu (University of Texas, Houston, TX).

Northern blot analysis. For RNA decay experiments, actinomycin D (Applchem) was added to cell cultures at 5 $\mu\text{g/ml}$, and total RNA was extracted using the Genematrix RNA purification kit (Eurz, Roboklon). A total of 7 to 15 μg of RNA was resolved by 1.1 or 1.6% agarose-2% formaldehyde-MOPS (morpholinepropanesulfonic acid) gel electrophoresis and blotted overnight with $8\times$ SSC ($1\times$ SSC is 0.15 M NaCl plus 0.015 M sodium citrate) onto Hybond-N+ Nylon membranes (Amersham, GE). Membranes were hybridized overnight with digoxigenin-labeled RNA probes at 55°C and washed twice with $2\times$ SSC-0.1% SDS for 5 min and twice with $0.5\times$ SSC-0.1% SDS for 20 min at 65°C. Alkaline phosphatase-labeled anti-DIG Fab fragments and CDP-Star substrate (both Roche) were used for detection according to the manufacturer's instructions. The following primers were used to generate templates for Sp6 probes by PCR: G1000/G1001 for the probe against exon 1 and 2 of rabbit β -globin, G78/G1008 for the probe against human RPS7, and G083/G1009 for the probe against nucleolin. Primer sequences are listed in Table S1 in the supplemental material.

Luciferase assay. One third of a 6-cm dish of transiently transfected HeLa cells was lysed in 150 μl of passive lysis buffer (dual-luciferase reporter assay system; Promega) and frozen at -20°C . After thawing, nuclei were removed by centrifugation for 2 min at 13,000 rpm at 4°C. A total of 20 μl of the supernatant was mixed with 50 μl of substrates from the dual-luciferase reporter assay system, diluted 1:3. Firefly and *Renilla* luciferase activities were measured on a Fluostar Optima (BMG Labtech) plate reader.

RESULTS

Identification of two human Pat1 homologs. In order to identify a human homolog of yeast Pat1, we compared Pat1 sequences of different fungi and observed a highly conserved central region of about 40 amino acids (aa), hereinafter termed the homology (H) domain. Using this domain, BLAST analysis was able to identify homologous sequences in various metazoa, including *Caenorhabditis elegans*, *Drosophila melanogaster*, *Danio rerio*, and *Xenopus laevis* (see Fig. S1 in the supplemental material). Two proteins sharing the H domain were found in mice and humans, indicative of a gene duplication in mammals. Outside the H domain, the only detectable sequence conservation between the fungal and metazoan proteins lies in a highly acidic stretch of 50 to 70 aa at the very amino terminus, hereinafter referred to as the acidic domain (A). We termed the two human proteins Pat1a and Pat1b. Pat1b is identical to PatL1 previously identified by Scheller et al. (34). Pat1a matches the partial sequence that was previously sug-

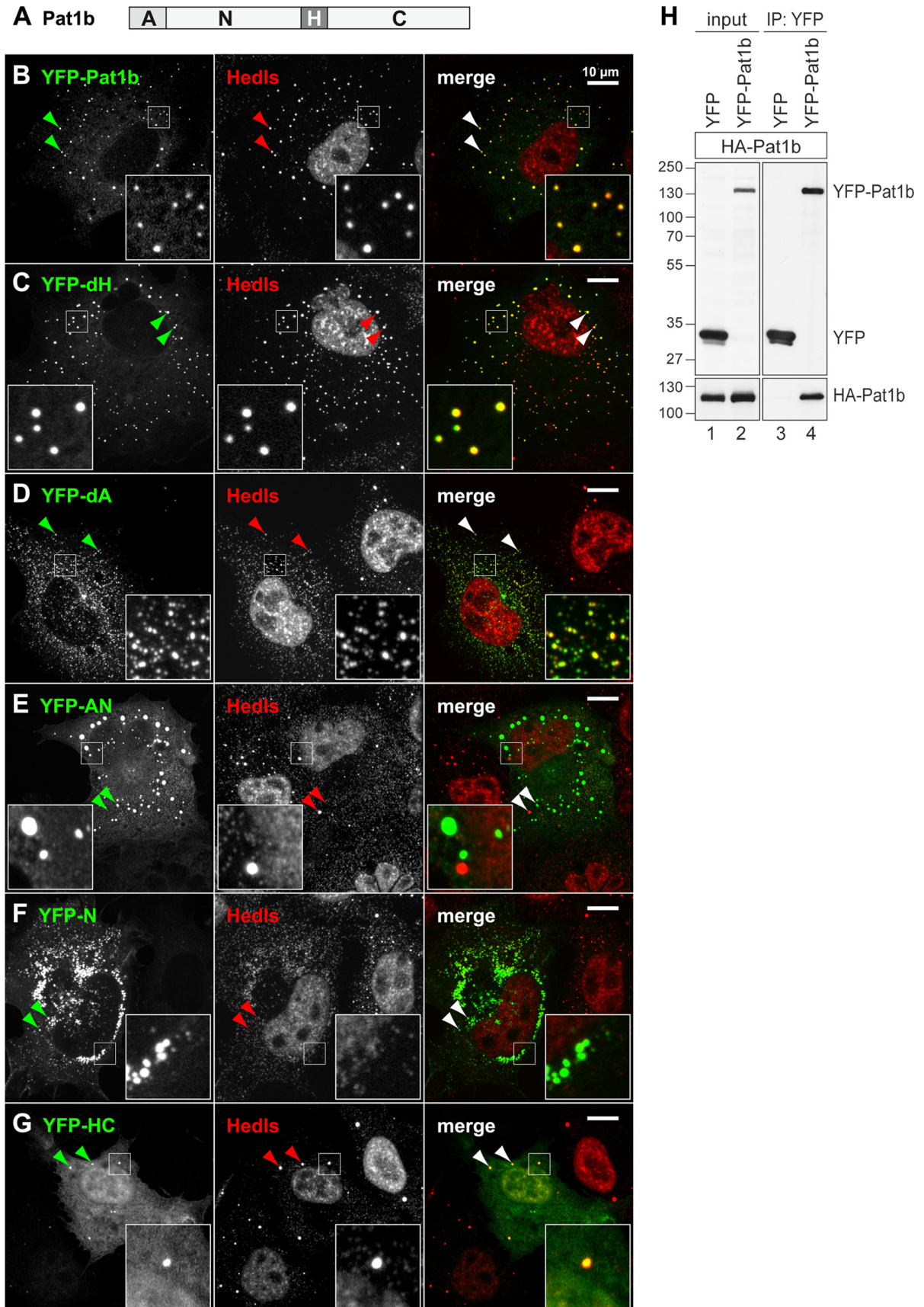
gested as the human Pat1 ortholog (9) and differs from the predicted PatL2 sequence at the N terminus (34). An alignment between the human Pat1a and Pat1b sequence (see Fig. S2 in the supplemental material) shows that Pat1a lacks a region of about 150 aa in the amino-terminal part following the A domain.

Human Pat1b, but not Pat1a, localizes to P bodies. We first examined the localization of human Pat1a and Pat1b by expressing yellow fluorescent protein (YFP)-tagged fusion proteins in COS7 cells. Epifluorescence microscopy showed that YFP-Pat1a is expressed throughout the cytoplasm, where it has a reticular distribution, but does not accumulate in P bodies (Fig. 1B). YFP-Pat1b, however, strongly accumulates in small cytoplasmic foci (Fig. 1C to E). These foci correspond to P bodies as determined by colocalization with different markers, including the enhancer of decapping Hedls (Fig. 1C), the helicase Rck (Fig. 1D), and Lsm1 (Fig. 1E). The localization of Pat1b in P bodies was also observed with a C-terminal fusion of YFP and with N-terminal HA and Flag tags (data not shown). We confirmed the localization of Pat1b in P bodies of human HeLa (data not shown) and U2OS cells (see Fig. S3 in the supplemental material). Thus, human Pat1b, but not Pat1a, localizes in P bodies. This is in line with the previously observed localization of Pat1b (PatL1) in HeLa cells (34).

In order to determine whether endogenous Pat1b would also localize in P bodies, we raised a peptide antibody in rabbit (Ab387). This antibody was able to detect overexpressed Pat1b by Western blot analysis (see Fig. S4A in the supplemental material). By immunofluorescence microscopy, Ab387 gave a punctate staining in both the nucleus and the cytoplasm of untransfected COS7 (Fig. 1F and G) and U2OS cells (see Fig. S3F and G in the supplemental material). The larger foci in the cytoplasm perfectly overlap with Hedls and Lsm1, indicating that endogenous Pat1b also localizes to P bodies.

Human Pat1b induces P-body formation. We noticed that cells transfected with YFP-Pat1b showed strongly increased numbers of P bodies compared to control cells transfected with YFP or YFP-Pat1a (compare Hedls staining in Fig. 1A to C). By counting P bodies using Hedls as a marker, we found that most COS7 cells overexpressing YFP-Pat1b have >20 P bodies per cell compared to an average of about 9 P bodies per cell in untransfected or YFP-expressing cells (Fig. 1H). Overexpression of YFP-Pat1a, however, did not increase the number of P bodies. The strong increase in P-body numbers by Pat1b overexpression was confirmed with an HA-tagged version, and the same was also observed with other cell lines, such as HeLa and

FIG. 1. Intracellular localization of human Pat1a and Pat1b in COS7 cells. COS7 cells were transiently transfected with YFP (A), YFP-Pat1a (B), or YFP-Pat1b (C to E) and processed for immunofluorescence microscopy. P bodies in the cytoplasm were counterstained in red using an antibody against Hedls (A to C), Rck (D), or Lsm1 (E). In addition, cells were stained with Hoechst 33342 in blue to visualize nuclei. Images in panels A to E were acquired by epifluorescence microscopy. Merged images are shown on the right, and the size bar represents 10 μm . Arrowheads point toward P bodies. (F and G) Untransfected COS7 cells were stained in red for endogenous Pat1b with antibody 387 and in green for P bodies using Hedls (F) or Lsm1 (G) as a marker. Images in panels F and G were acquired by spinning-disc confocal microscopy; maximum projections of z-stacks are depicted. (H) COS7 cells transiently transfected with either YFP, YFP-Pat1a, or YFP-Pat1b were fixed and stained for P bodies using an antibody against Hedls. The number of P bodies (PBs) in transfected cells was counted, and the average distribution is represented in the graph. Error bars show the standard deviations (SD) based on three independent repeats. Untransfected COS7 cells serve as an additional control. (I) The expression of Pat1b was knocked down in U2OS cells by transfection of two different siRNAs (T2 and T3) at a concentration of 100 nM. An unspecific siRNA (D0) was transfected as a negative control. The number of PBs per cell was counted after staining for Hedls, and the average distribution is represented in the graph. Error bars show the SD based on three independent repeats.



U2OS (data not shown). Since Pat1b overexpression causes a dramatic amplification of P bodies, many of which are very small, Pat1b may play an active role in nucleating the assembly of P bodies.

To further address the role of Pat1b in P-body assembly, we knocked down endogenous Pat1b in U2OS cells. Two different siRNAs, T2 and T3, reduced Pat1b mRNA levels to 5% and 6%, respectively, compared to the expression level in cells transfected with control siRNA (see Fig. S5A in the supplemental material). Indeed, knockdown of Pat1b led to a nearly complete loss of P bodies (Fig. 1I; see also micrographs shown in Fig. S5B in the supplemental material). This result supports the notion that Pat1b nucleates the assembly of P bodies.

Pat1b domains control P-body assembly. Next, we wanted to examine the contribution of different Pat1b domains, schematically depicted in Fig. 2A, to its intracellular localization. Fragments and deletions of Pat1b were expressed as YFP fusion proteins in COS7 cells and examined by spinning-disc confocal microscopy. Localization data are summarized in Table S2 in the supplemental material, and examples are shown in Fig. 2. As stated above, YFP-Pat1b forms many small- or medium-size foci, reminiscent of a “salt”-like appearance, and these foci colocalize with all P-body markers tested, including Hedls, Rck, Lsm1, and Lsm4 (Fig. 1C to E and 2B; see also Fig. S6E in the supplemental material). Thus, overexpressed Pat1b localizes to and strongly amplifies the number of P bodies. Deletion of the homology domain (YFP-dH) did not change this localization pattern (Fig. 2C). Deletion of the acidic region (YFP-dA), however, caused the protein to localize to much smaller and more numerous foci, reminiscent of a “pepper”-like appearance. These foci colocalize with Hedls (Fig. 2D) and with Rck (data not shown). Thus, YFP-dA triggers the formation of small P bodies, yet deletion of the acidic domain seems to prevent small aggregates from growing or merging into larger P bodies.

Localization of the YFP-AN fragment was very heterogeneous: in about half of the cells, YFP-AN showed a diffuse localization in the cytoplasm, and in these cells endogenous P bodies were strongly suppressed (see Table S2 in the supplemental material). In other cells, YFP-AN formed aggregates apparent as large round foci (Fig. 2E) or irregular patches (not shown). Many of these round foci and patches did not contain other P-body markers, suggesting that the AN fragment had the intrinsic ability to form aggregates. This aggregation-prone behavior was also observed with the YFP-N fragment lacking the A region (Fig. 2F). In contrast, the YFP-A fragment had a diffuse localization indistinguishable from YFP alone (see Table S2). The YFP-HC fragment primarily showed a diffuse localization in the nucleus and the cytoplasm. In some cells, YFP-HC also accumulated weakly in P bodies (Fig. 2G) yet did

not affect the size or number of P bodies. Taken together, these results suggested that the HC fragment is passively recruited to P bodies, whereas the N fragment contains an active aggregation-prone domain. In the context of full-length Pat1b, the N region can strongly promote the formation of P bodies. The idea that Pat1b actively promotes P-body assembly is supported by our observation that Pat1b interacts with itself in a coimmunoprecipitation (co-IP) assay (Fig. 2H).

We then tested whether P bodies induced by YFP-Pat1b would be resistant to treatment with the translation inhibitor cycloheximide (CHX). CHX was shown to inhibit the formation of P bodies (10), presumably because mRNAs are trapped in polysomes by CHX. After 2 h of CHX treatment, P bodies were nearly absent in untransfected cells, whereas large numbers of foci were still present in YFP-Pat1b-expressing cells (see Fig. S6A, D, and F in the supplemental material). Colocalization of Hedls, Rck, Xrn1, and Lsm4 indicated that these structures had the typical composition of P bodies. Interestingly, Pat1b-induced foci persisted even after 6 h of CHX treatment (data not shown). Although we cannot tell whether these P bodies are functional in the presence of CHX, this result indicates that Pat1b not only nucleates P bodies but also stabilizes P bodies once assembled. Aggregates induced by the expression of YFP-AN were also resistant to CHX treatment (see Fig. S6B in the supplemental material). These aggregates showed distinct colocalization with Rck but not with Hedls, suggesting that Rck may interact with the AN fragment.

Tethering of Pat1b accelerates mRNA degradation. Since P bodies have been implicated in the control of both mRNA translation and decay, we went on to test if human Pat1b plays a role in the posttranscriptional control of gene expression. To this end, we tethered Pat1b to a reporter mRNA using a heterologous RNA-protein interaction of the *Pseudomonas aeruginosa* bacteriophage PP7 (23, 46). The PP7 coat protein (cp) binds as a dimer with high affinity to a stem loop in the bacteriophage RNA, the PP7 binding site (bs). We cloned six copies of the PP7bs into the 3' UTR of a rabbit β -globin reporter gene containing firefly luciferase (FL) (FLB-PP7bs). A fusion protein containing an HA tag, PP7cp, and Pat1b, as shown schematically in Fig. 3A, brings Pat1b in close proximity to the reporter mRNA. When expressed together in HeLa cells, HA-PP7cp-Pat1b strongly suppressed the expression level of FLB-PP7bs mRNA compared to HA-PP7cp or HA-Pat1b alone (Fig. 3B, lanes 4 to 6). In contrast, HA-PP7cp-Pat1b had only a very weak effect on the FLB mRNA lacking PP7bs (Fig. 3B, lanes 1 to 3). Similar to HeLa cells used for Fig. 3, Pat1b was also found to suppress the expression of the tethered reporter mRNA in U2OS cells (data not shown).

We then compared the effect of tethering Pat1a, Pat1b, and fragments of Pat1b to the FLB-PP7bs reporter mRNA. We

FIG. 2. Localization of Pat1b subdomains. (A) Schematic representation of Pat1b domains. A, acidic domain; N, amino-terminal region; H, homology domain; C, carboxy-terminal region. COS7 cells were transiently transfected with YFP-Pat1b (B), YFP-dH (C), YFP-dA (D), YFP-AN (E), YFP-N (F), or YFP-HC (G) and processed for immunofluorescence microscopy. P bodies in the cytoplasm were counterstained in red using an antibody against Hedls. Images were acquired by spinning-disc confocal microscopy; maximum projections of z-stacks are depicted. Merged images are shown on the right; arrowheads point toward P bodies. Size bar, 10 μ m. Localization of Pat1b subdomains is also summarized in Table S2 in the supplemental material. (H) HEK293 cells were transiently transfected with HA-Pat1b together with either YFP or YFP-Pat1b. Cytoplasmic lysates (input) were prepared for IP with GFP-binder, and Western blot analysis was carried out to visualize interaction between HA-Pat1b and YFP-Pat1b. The sizes of the molecular weight markers (in thousands) are indicated on the left.

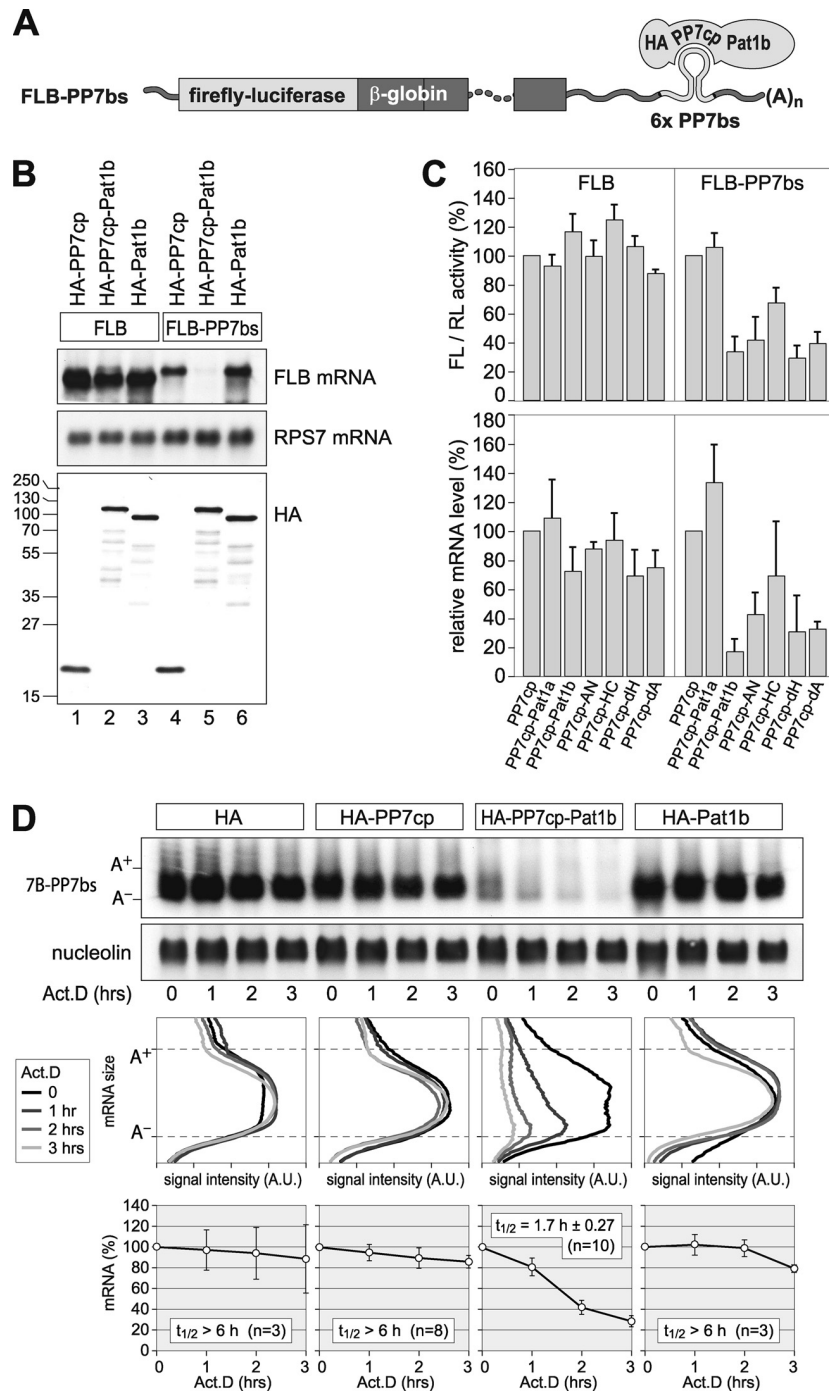


FIG. 3. Tethering of Pat1b accelerates mRNA decay. (A) Schematic representation of the reporter containing firefly luciferase fused to β -globin (FLB). Six copies of the PP7 binding site (bs) were inserted in the 3' UTR for the FLB-PP7bs reporter. An HA-tagged PP7 coat protein (cp) fused to Pat1b specifically binds to the PP7bs RNA. (B) HeLa cells were transiently transfected with FLB or FLB-PP7bs reporter together with either HA-PP7cp, HA-PP7cp-Pat1b, or HA-Pat1b. RNA and protein were extracted and analyzed by Northern (top two panels) and Western (bottom) blotting. The sizes of the molecular weight markers (in thousands) are indicated on the left. Ribosomal protein S7 (RPS7) mRNA serves as RNA loading control. (C) HeLa cells were transiently transfected with FLB or FLB-PP7bs reporter together with a *Renilla* luciferase (RL) reporter and either HA-PP7cp, HA-PP7cp-Pat1a, HA-PP7cp-Pat1b, or HA-PP7cp fused to fragments of Pat1b. Cytoplasmic lysates were prepared after 24 h to measure FL/RL activity. FLB mRNA levels were determined from the same lysates by Northern blot analysis, normalized to RPS7 mRNA, and quantified. Average values \pm SD from three repeat experiments were plotted in the graph. (D) HeLa cells were transiently transfected with a T7-tagged β -globin reporter containing 6 copies of PP7bs (7B-PP7bs) together with either the HA tag alone, HA-PP7cp, HA-PP7cp-Pat1b, or HA-Pat1b. Total RNA was extracted at 1-h intervals after blocking transcription with actinomycin D (5 μ g/ml). The reporter mRNA was detected by Northern blot analysis; nucleolin mRNA serves as loading control. In the middle panels, deadenylation was visualized by quantifying the signal intensity (in arbitrary units [A.U.]) of 7B-PP7bs mRNA along the length of the signal and plotting it as a function of mRNA size. In the bottom panel, the overall signal intensity of 7B-PP7bs mRNA was quantified and normalized to nucleolin mRNA. Average values \pm standard errors (SE) were plotted as a percentage of the initial time point.

measured, as a readout, both firefly luciferase activity and reporter mRNA levels (Fig. 3C). The experiment showed that the tethering of Pat1a had no significant effect compared to PP7cp alone. The tethering of full-length Pat1b had the strongest suppressive effect, reducing FL activity by about 3-fold and mRNA levels by about 5-fold. The tethering of the AN fragment, the dH deletion mutant, or the dA deletion mutant resulted in strong inhibition of the FLB-PP7bs reporter, though at the mRNA level the inhibition was less pronounced than with full-length Pat1b. Since the tethering of the HC fragment had a much weaker effect, the AN fragment of Pat1b appears to be most important for the suppressive effect on reporter mRNA expression. In general, there was good agreement between the relative FL activities and mRNA abundance, indicating that tethered Pat1b acts primarily at the level of mRNA expression.

Next, we wanted to determine whether Pat1b would affect the stability of the tethered mRNA. We expressed a β -globin reporter mRNA containing 6 copies of PP7bs (7B-PP7bs) together with the HA tag alone, HA-PP7cp, HA-PP7cp-Pat1b, or HA-Pat1b in HeLa cells (Fig. 3D). Transcription was blocked by the addition of actinomycin D in order to monitor degradation of the reporter mRNA. The analysis showed that 7B-PP7bs mRNA was stable in the presence of coexpressed HA or HA-Pat1b or when HA-PP7cp alone was tethered to the mRNA. In contrast, the tethering of HA-PP7cp-Pat1b caused rapid degradation of the reporter mRNA. Overall signal intensities were quantified to obtain mRNA half-lives (Fig. 3D, bottom). Measurement of the signal intensity along the length of the reporter mRNA shows that the mRNA was deadenylated as a result of Pat1b tethering (Fig. 3D, middle).

Human Pat1b interacts with Rck, Hedls, Xrn1, and Lsm1. To further explore the connection between human Pat1b and mRNA degradation, we tested whether Pat1b interacts with different mRNA decay factors that localize to P bodies. By expressing HA-tagged Pat1b in HEK293 cells, we found that Pat1b coimmunoprecipitates with the 5'-3' exoribonuclease Xrn1 and with the activators of decapping Rck, Hedls, Lsm1, and Lsm4 (Fig. 4A, lane 5) as well as Edc3 (Fig. 4D). These interactions were also observed with a YFP-tagged form of Pat1b (HA-Pat1b-YFP) (Fig. 4B). eIF3B and eIF4G, translation initiation factors that do not localize in P bodies, did not interact with Pat1b (Fig. 4A and B). As a negative control, the HA tag alone did not co-IP with any of these proteins. Given that mRNAs are also a component of P bodies, we next tested whether the interaction of Pat1b with its partners is RNA dependent. The addition of RNase A to the IP did not affect the interaction of HA-Pat1b with any of its partners (Fig. 4B). RNA extracted from the unbound fraction showed that RNase A treatment had efficiently degraded rRNA (Fig. 4B, lanes 10 and 11). These results suggest that the association of Pat1b with Rck, Hedls, Xrn1, and Lsm1 is based on protein-protein interactions.

Since Pat1b contains an aggregation-prone domain (fragment N) (Fig. 2F), we tested whether Pat1b may aggregate and precipitate unspecifically in our co-IP experiments. From the same HA-Pat1b-containing lysate (input), we carried out the IP procedure with and without the HA antibody (Fig. 4C). In the absence of HA antibody, neither HA-Pat1b nor associated

proteins were precipitated (Fig. 4C, lane 2). This shows that precipitation by the antibody was specific.

To further characterize the binding of Pat1b to its partners, we subjected the complexes to increasing salt concentrations (Fig. 4D). Whereas the interaction with Hedls, Edc3, and Xrn1 was severely reduced at a NaCl concentration of 300 mM, the interaction with Rck and Lsm4 was resistant to 300 mM NaCl. Lsm1-Pat1b was the most stable of these interactions and could not be separated by 500 mM NaCl. This indicates that Lsm1/Lsm4 and Rck are more tightly associated with Pat1b than Hedls, Edc3, and Xrn1. Since Xrn1 forms a stable complex with Lsm1-7 in yeast (6), the interaction of human Xrn1 with Pat1b may occur through Lsm1-7. From these co-IP experiments, however, it is not possible to tell whether Pat1b directly binds to Rck and Lsm1.

Interestingly, Lsm1 co-IPs in similar amounts with Pat1a and Pat1b, yet the association of Lsm4 and Xrn1 with Pat1a is much weaker (Fig. 4A, lane 6). Thus, it is conceivable that Pat1a may preferentially bind to "free" Lsm1 that is not associated with the other Lsm proteins or Xrn1.

To obtain additional evidence for the observed interactions, inverse IPs were carried out in HEK293 cells transiently transfected with HA-Pat1b (Fig. 4E). The Xrn1 antibody was able to co-IP HA-Pat1b and Lsm1 (Fig. 4E, lane 2), the Hedls antibody could co-IP HA-Pat1b, Xrn1, and Lsm1 (lane 3), and the Rck antibody could co-IP HA-Pat1b and Lsm1 (lane 4). The Lsm1 antibody was not suitable for IP (Fig. 4E, lane 5), and a 14-3-3 antibody served as a negative control (lane 6). Taken together, these results confirmed the association of Xrn1, Hedls, and Rck with both Pat1b and Lsm1 and provides evidence for multiple interactions within this group of P-body proteins.

Human Pat1b interacts with enhancers of decapping via separate domains. Since the above analysis revealed that Rck and Lsm1 are tightly associated with Pat1b, we determined which domains of Pat1b are involved in these interactions. To this end, we expressed different fragments of Pat1b as depicted in Fig. 5A. Figure 5B shows that the AN fragment efficiently co-IPs with Rck (lane 9), whereas the carboxy-terminal (HC) fragment co-IPs Lsm1 (lane 11). Similar to Lsm1, the more loosely associated proteins Hedls, Edc3, and Xrn1 were found to be connected to Pat1b via the HC domain (see Fig. S7 in the supplemental material). As shown in Fig. 4B for full-length Pat1b, the interactions mediated by the AN and HC fragments were resistant to RNase A treatment and are thus likely to be RNA independent (Fig. 5B).

We further analyzed the association of Rck with the amino-terminal half of Pat1b (Fig. 5C). Removal of the acidic domain (dA) from full-length Pat1b was sufficient to abrogate the interaction with Rck (Fig. 5C, lane 9). The same was observed when the N fragment was expressed alone in comparison to the AN fragment (Fig. 5C, lanes 10 and 11). Indeed, the HA-tagged acidic domain alone, although not visible by Western blot analysis due to its small size, efficiently co-IPs with Rck (Fig. 5C, lane 12).

We then examined in more detail the association of HC with Lsm1. Deletion of the conserved homology domain H from full-length Pat1b (dH) abolished the interaction with Lsm1 (Fig. 5D, lanes 8 and 9). Similarly, comparison of the HC and C fragments indicated that the H domain is required for asso-

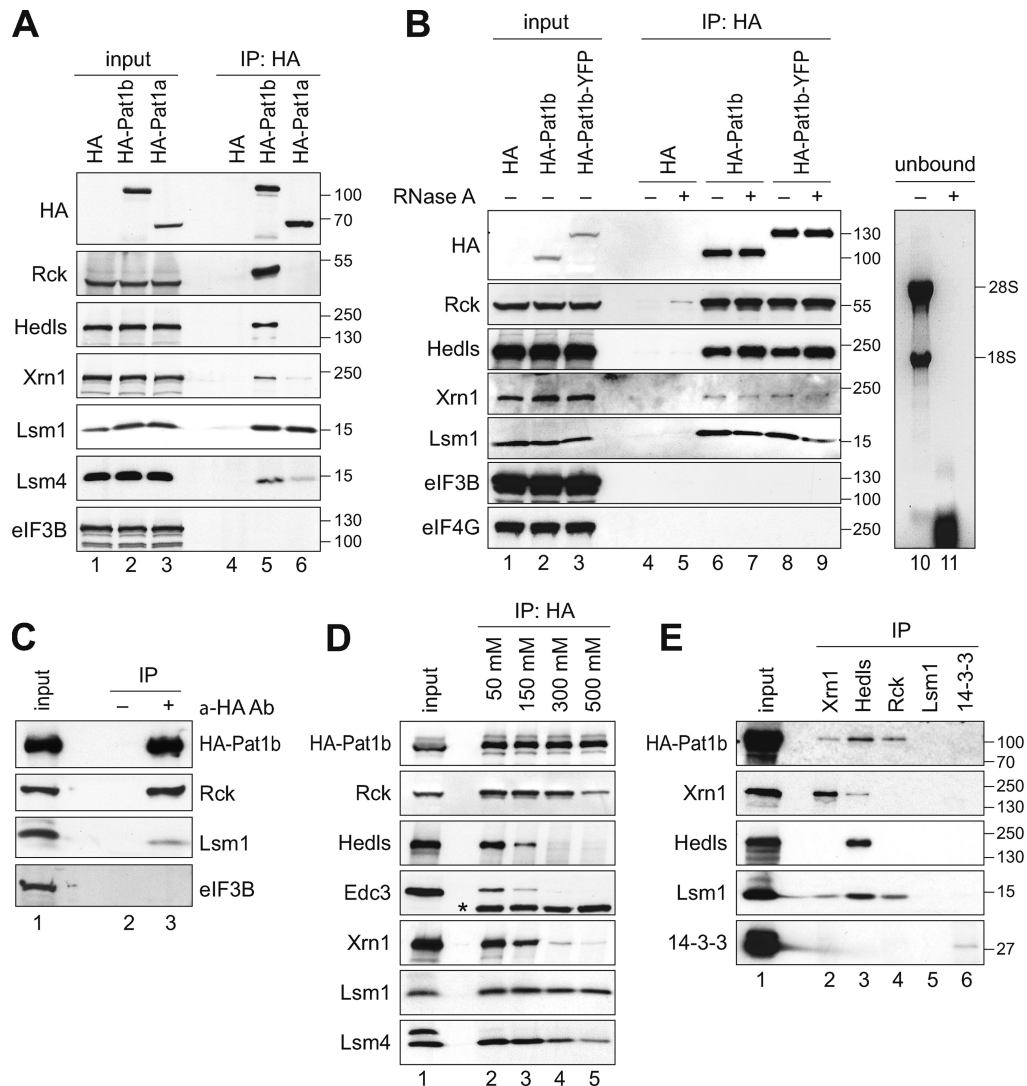


FIG. 4. Pat1b interacts with P-body proteins. (A) HEK293 cells were transiently transfected with vector alone, HA-tagged Pat1b, or HA-tagged Pat1a. After 1 day, cytoplasmic lysates (input) were prepared for IP with anti-HA antibody. The HA-tagged proteins as well as endogenous Rck, Hedls, Xrn1, Lsm1, Lsm4, and eIF3B were detected by Western blotting. The sizes of the molecular weight markers (in thousands) are indicated on the right. (B) HEK293 cells transiently transfected with vector alone, HA-Pat1b, or HA-Pat1b-YFP were used for IP as described in the legend for panel A. Where indicated, RNase A was added to the lysates during IP. Lanes 10 and 11 show RNA extracted from the unbound fraction and stained with ethidium bromide. (C) HA-Pat1b was immunoprecipitated with HA antibody or without antibody as a control for unspecific precipitation. (D) HA-Pat1b was immunoprecipitated and subjected to increasing NaCl concentrations prior to elution of the protein complexes. *, immunoglobulin heavy chain. (E) Endogenous Xrn1, Hedls, Rck, Lsm1, and 14-3-3 were immunoprecipitated from the cytoplasmic lysate of HEK293 cells transiently transfected with HA-Pat1b. The Western blot for Rck is not shown due to an overlapping signal from the immunoglobulin heavy chain.

ciation with Lsm1 (Fig. 5D, lanes 10 and 11). The ANH fragment, however, did not co-IP with Lsm1 (Fig. 5D, lane 12), indicating that the H domain alone is not sufficient to mediate this interaction. We concluded that Lsm1 binding requires both the H and C fragment of Pat1b.

Human Pat1b interacts with the Dcp2-Dcp1a decapping enzyme. Since we found Pat1b to associate with a number of decapping enhancers (Rck, Hedls, Edc3, and Lsm1), we wanted to know if Pat1b would also interact with the decapping enzyme Dcp2 and its closely associated activator Dcp1a. To this end, we switched to YFP-tagged Pat1b proteins, since the use of GFP-binder (33) overcomes detection problems related

to the presence of immunoglobulin in the IP. Full-length Pat1b tagged with YFP was found to co-IP efficiently with Flag-Dcp2 and Flag-Dcp1a (Fig. 6A and B, lanes 8). Interestingly, the two proteins associate with both the N and the HC region of Pat1b (Fig. 6A and B, lanes 10 and 12). The association with Dcp2 and Dcp1a was found to be independent of RNA (see Fig. S8 in the supplemental material). Moreover, the two proteins did not dissociate from Pat1b at 1 M NaCl (Fig. 6C), indicating that Dcp2 and Dcp1a are tightly connected to Pat1b. Taken together, the results show that Pat1b associates with all enhancers of decapping through at least three separate domains: the A fragment associates with Rck, the N fragment with Dcp2

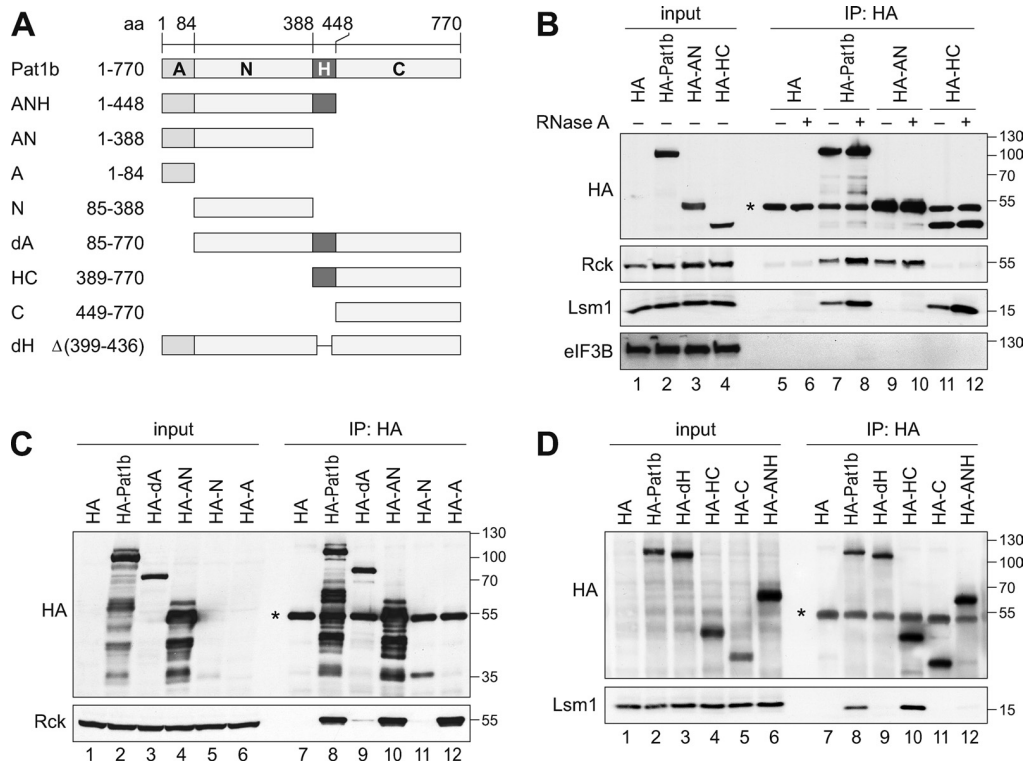


FIG. 5. Separate interaction domains within Pat1b. (A) Schematic representation of Pat1b fragments. A, acidic domain; N, amino-terminal region; H, homology domain; C, carboxy-terminal region. (B) HEK293 cells were transiently transfected with vector alone, full-length HA-Pat1b, HA-AN, or HA-HC. After 1 day, cytoplasmic lysates (input) were prepared for IP with anti-HA antibody. The HA-tagged proteins as well as endogenous Rck, Lsm1, and eIF3B were detected by Western blotting. *, immunoglobulin heavy chain. The sizes of the molecular weight markers (in thousands) are indicated on the right. (C) HEK293 cells transiently transfected with vector alone, HA-Pat1b, HA-dA, HA-AN, HA-N, or HA-A were used for IP as described in the legend for panel B. The HA-tagged proteins and endogenous Rck were detected by Western blotting. (D) HEK293 cells were transiently transfected with vector alone, HA-Pat1b, HA-dH, HA-HC, HA-C, or HA-ANH and used for IP as described in the legend for panel B. The HA-tagged proteins and endogenous Lsm1 were detected by Western blotting.

and Dcp1a, and the HC fragment with Dcp2/Dcp1a, Lsm1/Lsm4, Hedls, and Edc3.

Human Pat1b interacts with the Ccr4-Caf1-Not deadenylation complex. Since we found that the tethering of Pat1b causes mRNA deadenylation (Fig. 3D), we tested for interactions of Pat1b with the Ccr4-Caf1-Not deadenylation complex. Notably, this complex is also concentrated in P bodies (27, 41, 47). Indeed, we found that YFP-Pat1b co-IPs efficiently with Flag-Not1 (Fig. 7A) and myc-Ccr4 (Fig. 7B), as well as HA-Caf1a and HA-Caf1b (Fig. 7C). In all cases, RNase A treatment did not interfere with binding. We then confirmed the interaction of YFP-Pat1b with endogenous Caf1a (Fig. 7D, lane 8). Analysis of subdomains indicated that Caf1a can interact with the N fragment of Pat1b alone (Fig. 7D, lane 10), yet the acidic domain A enhances Caf1a binding (Fig. 7D, lane 11). Interestingly, the A domain was even more important for association with Flag-Not1 and myc-Ccr4 since only the AN fragment showed a robust interaction with these two proteins (see Fig. S9A and B in the supplemental material). Although Flag-Not1 and myc-Ccr4 also co-IP weakly with the HC domain (Fig. S9A and B), we concluded from these experiments that the Ccr4-Caf1-Not complex associates primarily with the AN domain.

By challenging these interactions with increasing salt con-

centrations, we found that Flag-Not1, myc-Ccr4, and HA-Caf1a/b are very stably associated with YFP-Pat1b (Fig. 7E). At a concentration of 1 M NaCl, these proteins remained in a complex with YFP-Pat1b, whereas binding of Lsm1 was reduced and binding of Rck was lost. Thus, it appears that Pat1b associates tightly with the Ccr4-Caf1-Not deadenylase complex and may act as a physical bridge between deadenylases and decapping enzymes.

To provide further evidence for such a bridging function, we tested whether Pat1b would promote the association between Caf1a and Dcp2. By IP of GFP-Caf1a, we found that the co-IP of Flag-Dcp2 is strongly enhanced by coexpression of HA-Pat1b (Fig. 7F, lane 3). This result shows that Pat1b can simultaneously interact with Caf1a and Dcp2 and thereby promote the association between the deadenylation-and-decapping complex.

Tethering of Pat1b causes both deadenylation and mRNA decapping. In order to test whether both deadenylation and decapping activities were associated with Pat1b, we again turned to the tethering assay. A dominant negative Caf1a-AA (D40A/E42A) deadenylase similar to a mutant described by Zheng et al. (47) was generated. In comparison to the vector control, coexpression of Caf1a-wt slightly accelerated the degradation rate of the reporter mRNA tethered to Pat1b (Fig. 8A

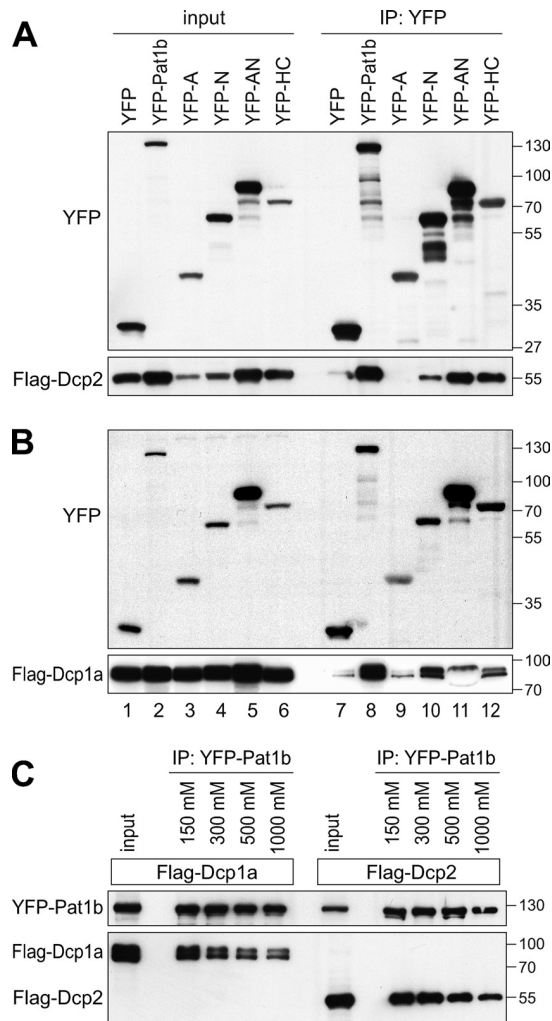


FIG. 6. Pat1b interacts with Dcp2 and Dcp1a. (A) HEK293 cells were transiently transfected with YFP, YFP-Pat1b, YFP-A, YFP-N, YFP-AN, or YFP-HC together with Flag-Dcp2. GFP-binder was used for IP, and Western blot analysis was carried out with anti-GFP and anti-Flag antibody. The sizes of the molecular weight markers (in thousands) are indicated on the right. (B) Same analysis as described in the legend for panel A, except that Flag-Dcp1a was cotransfected. (C) HEK293 cells were transiently transfected with YFP-Pat1b together with either Flag-Dcp1a or Flag-Dcp2. IPs were carried out with GFP-binder and subjected to increasing NaCl concentrations prior to elution.

and B). Quantification of the mRNA decay rates is shown at the bottom of Fig. 8 and summarized in Table S3 in the supplemental material. In contrast to that of Caf1a-wt, coexpression of dominant negative Caf1a-AA prevented deadenylation of the mRNA (Fig. 8C and G). The lack of the A⁻ mRNA population is clearly visible in the middle panels of Fig. 8C and G, in which the signal intensity was quantified along the length of the mRNA. This result suggests that the tethering of Pat1b causes Caf1-dependent mRNA deadenylation. Interestingly, the A⁺ mRNA still underwent degradation without shortening of its size, suggesting that tethered Pat1b could promote decapping of the A⁺ mRNA independently of deadenylation.

To test this possibility, we generated Dcp2-AA (E147A/

E148A) in analogy to a published mutation that inactivates the decapping enzyme Dcp2 (44). Whereas coexpression of Dcp2-wt did not have a significant effect on mRNA degradation (Fig. 8D), Dcp2-AA caused accumulation of the A⁻ mRNA (Fig. 8E). Strong accumulation of A⁻ mRNA was also visible when we cotransfected Caf1a-wt and Dcp2-AA (Fig. 8F). From this we concluded that the tethering of Pat1b also leads to Dcp2-dependent mRNA decapping. Only by coexpressing both Caf1a-AA and Dcp2-AA did we achieve full stabilization of the Pat1b-tethered mRNA (Fig. 8H). Taken together, these experiments demonstrate that Pat1b is tightly associated with both deadenylation and decapping activities in the cell.

N is the primary effector domain of Pat1b. To determine which domain of Pat1b mediates deadenylation and decapping, we tested the effect of tethering Pat1b fragments to the reporter mRNA. The tethering of AN (Fig. 9C) or the N domain alone (Fig. 9F) very efficiently caused mRNA deadenylation and decapping, comparable to the effect of tethering full-length Pat1b (Fig. 9B). The mRNA decay rates are quantified in Fig. 9, bottom, and summarized in Table S4 in the supplemental material. In contrast to that of AN or N, the tethering of the HC fragment (Fig. 9D) or the A domain (Fig. 9E) did not induce mRNA decay and was similar to the tethering of PP7cp alone (Fig. 9A). These data suggest that N is the most potent fragment of Pat1b, and its tethering causes both deadenylation and decapping. This is in good agreement with our observation that the N fragment interacts with both Caf1a (Fig. 7D) and Dcp2 (Fig. 6A). We finally tested the effect of removing the A and the H domain (Fig. 9G and H). Compared to full-length Pat1b, the tethering of either the dA or dH mutant led to a significantly reduced mRNA decay rate. Both mutants caused mRNA deadenylation but resulted in the accumulation of A⁻ mRNA. This suggests that the A domain, possibly by interacting with Rck (Fig. 5C), and the H domain, possibly by enhancing the binding of Lsm1 (Fig. 5D), activate decapping of the tethered mRNA. These enhancing activities require the presence of the N domain since the A and HC fragments on their own were inactive in the tethering assay.

DISCUSSION

In this study we provide evidence that human Pat1b connects two major steps in mRNA degradation: deadenylation and decapping. In yeast, the major pathway by which mRNA is degraded is deadenylation-dependent decapping followed by 5'-3' exonucleolytic decay (15, 29). While this pathway has been established through numerous genetic experiments, the entity that physically connects the deadenylation with the decapping step has not been identified. Pat1 and the Lsm1-7 complex were likely suspects since both are activators of decapping and were found to be preferentially associated with oligoadenylated mRNAs (5, 8, 18, 42). Our analysis reveals that human Pat1b is tightly associated with both deadenylation and decapping enzymes. By co-IP experiments, we found that Pat1b interacts with the Ccr4-Caf1-Not deadenylase complex (Fig. 7), with the decapping enzyme Dcp2 and its enhancers Dcp1a, Rck, Lsm1, Lsm4, Hedls, and Edc3, and with the exoribonuclease Xrn1 (Fig. 4 and 6). Thus, the entire deadenylation-decapping-5'-3' decay machinery appears to be con-

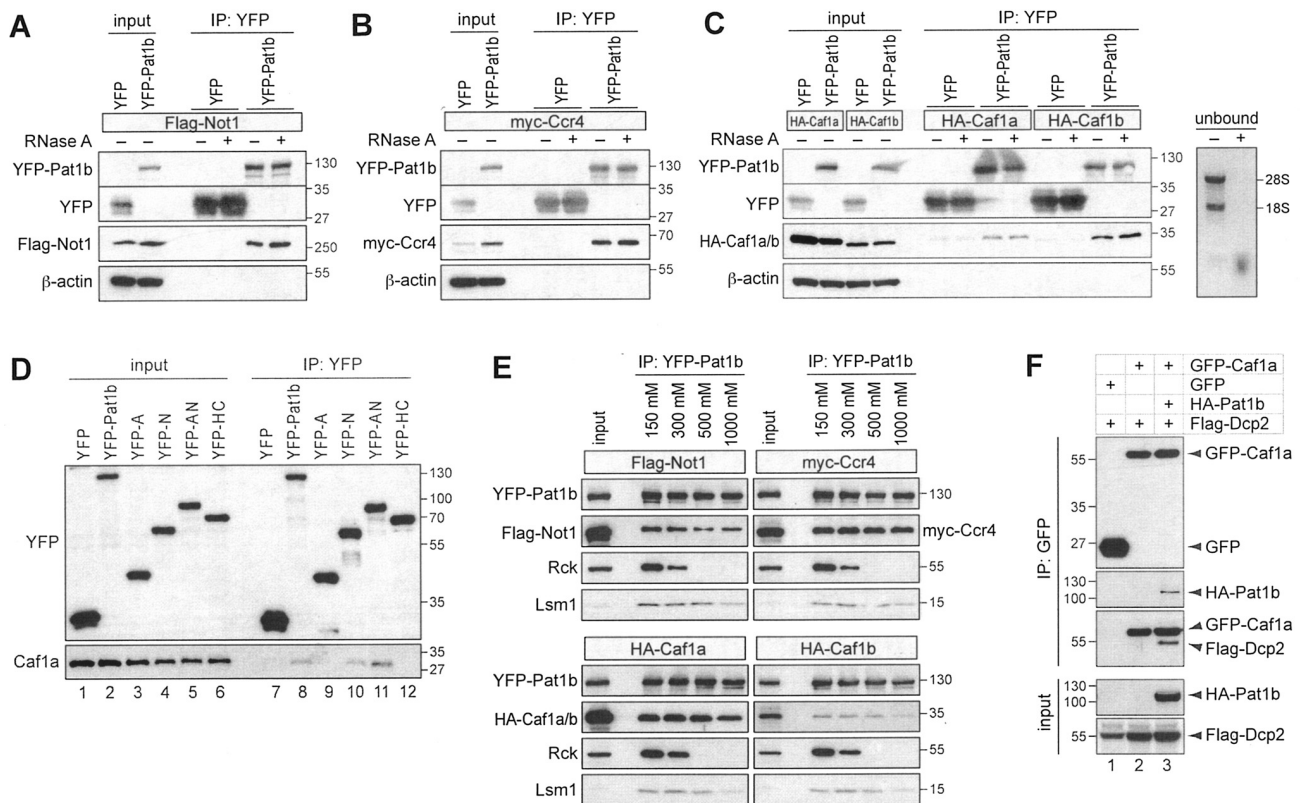


FIG. 7. Pat1b interacts with the Ccr4-Caf1-Not complex. (A) HEK293 cells were transiently transfected with YFP or YFP-Pat1b together with Flag-Not1. GFP-binder was used for IP, and Western blot analysis was carried out with anti-GFP and anti-Flag antibody. The sizes of the molecular weight markers (in thousands) are indicated on the right. Where indicated, RNase A was added during IP. (B) IP was carried out as described in the legend for panel A using YFP or YFP-Pat1b together with myc-Ccr4; anti-myc was used for Western blot analysis. (C) IP was carried out as described in the legend for panel A using YFP or YFP-Pat1b together with HA-Caf1a or HA-Caf1b; anti-HA was used for Western blot analysis. On the right side, RNA was extracted from unbound fractions and stained with ethidium bromide. (D) HEK293 cells were transiently transfected with YFP, YFP-Pat1b, YFP-A, YFP-N, YFP-AN, or YFP-HC and processed for IP with GFP-binder. The YFP-tagged proteins and endogenous Caf1a were detected by Western blotting. (E) HEK293 cells were transiently cotransfected with YFP-Pat1b together with either Flag-Not1, myc-Ccr4, HA-Caf1a, or HA-Caf1b. IPs were carried out with GFP-binder and subjected to increasing NaCl concentrations prior to elution. (F) HEK293 cells were transiently transfected with Flag-Dcp2 together with either GFP alone, GFP-Caf1a alone, or GFP-Caf1a together with HA-Pat1b. Cytoplasmic lysates were processed for IP with GFP-binder and then subjected to Western blot analysis. In the IP samples, the Flag antibody cross-reacted with GFP-Caf1a.

nected to Pat1b. These interactions are functional within a cell since tethering of Pat1b to a reporter mRNA caused both rapid deadenylation and decapping (Fig. 8). By challenging these interactions with increasing salt concentrations, we observed that Pat1b binds most tightly to Ccr4-Caf1-Not1 and to Dcp2/Dcp1a followed by Lsm1/Lsm4 and Rck. Although co-IP experiments cannot provide conclusive evidence for direct binding, our data suggest that Pat1b is in close proximity to the Ccr4-Caf1-Not complex, Dcp2/Dcp1a, the Lsm1-7 heptamer and to Rck. Association with Xrn1, Hedls, and Edc3 was much weaker and is likely to be indirect.

Within this complex, Pat1b appears to have a scaffold function since it interacts with its partners through at least three different domains (summarized in Fig. 10A). The first interaction domain is the very amino-terminal A region of Pat1b that mediates binding to Rck (Fig. 5C). Given that this domain has an astonishing number of 32 acidic amino acids within its 84 residues and a net charge of -27.7 at pH 7.0, it will be inter-

esting to determine whether the Pat1b A domain has an influence on the nucleotide binding or helicase activity of Rck.

The N region that follows the acidic A domain mediates interaction with Dcp2 and Dcp1a (Fig. 6) as well as Caf1a (Fig. 7). Interestingly, Ccr4 and Not1 do not interact with Pat1b through the N region alone but also require the A domain (see Fig. S9 in the supplemental material). Although binding of all the deadenylation complex components appeared to be very tight, as estimated by their resistance to salt, this difference may suggest that Caf1a is positioned particularly close to the N domain of Pat1b. Importantly, the N domain is also the fragment that can potently induce deadenylation and decapping in the tethering assay (Fig. 9F).

On the carboxy-terminal half of Pat1b, HC co-IPs efficiently with Lsm1, Dcp2, and Dcp1a (Fig. 5 and 6), whereas the interaction of HC with Not1, Ccr4, Xrn1, Hedls, and Edc3 is weaker and possibly indirect (see Fig. S7 and S9 in the supplemental material). The H domain that shows the highest

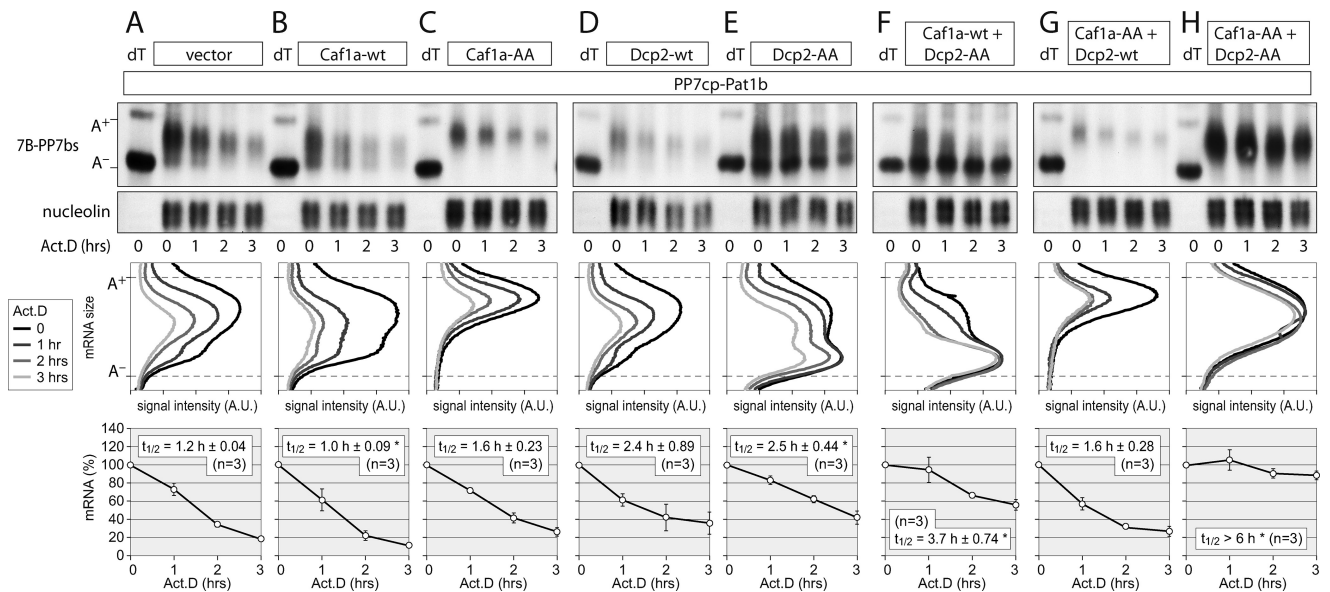


FIG. 8. Tethering of Pat1b causes mRNA deadenylation and decapping. HeLa cells were transiently transfected with the T7-tagged β -globin reporter containing 6 copies of the PP7bs (7B-PP7bs) together with HA-PP7cp-Pat1b and vector alone (A), Caf1a-wt (B), dominant negative Caf1a-AA (D40A/E42A) (C), Dcp2-wt (D), dominant negative Dcp2-AA (E147A/E148A) (E), Caf1a-wt plus Dcp2-AA (F), Caf1a-AA plus Dcp2-wt (G), and Caf1a-AA plus Dcp2-AA (H). Total RNA was extracted at 1-h intervals after blocking transcription with actinomycin D (5 μ g/ml). The reporter mRNA was detected by Northern blot analysis; nucleolin mRNA served as a loading control. RNA samples marked dT were treated with oligo(dT) and RNase H and served as a size marker for deadenylated (A^-) reporter mRNA. In the middle panels, deadenylation was visualized by quantifying the signal intensity of 7B-PP7bs mRNA along the length of the signal and plotting it as a function of mRNA size. In the bottom panels, the overall signal intensity of 7B-PP7bs mRNA was quantified and normalized to nucleolin mRNA. Average values \pm SE were plotted as a percentage of the initial time point. An asterisk indicates a significant difference in the mRNA half-life ($t_{1/2}$) ($P < 0.05$ by two-tailed Student's t test) compared to the vector control depicted in panel A. Statistical analysis of the mRNA $t_{1/2}$ is summarized in Table S3 in the supplemental material.

homology to the yeast Pat1 sequence appears to contribute in particular to Lsm1 binding (Fig. 5D). This is in good agreement with the interactions in *S. cerevisiae*, in which Pat1 occurs in a stable complex with Lsm1-7 and Xrn1 (5, 6) and was found

to interact with Lsm1 via a middle domain that contains the H region (30). Edc3 and Dcp1 were shown by two-hybrid analysis to bind yeast Pat1 via its carboxy-terminal domain (30), which we find to be true for human Pat1b as well. In addition, and

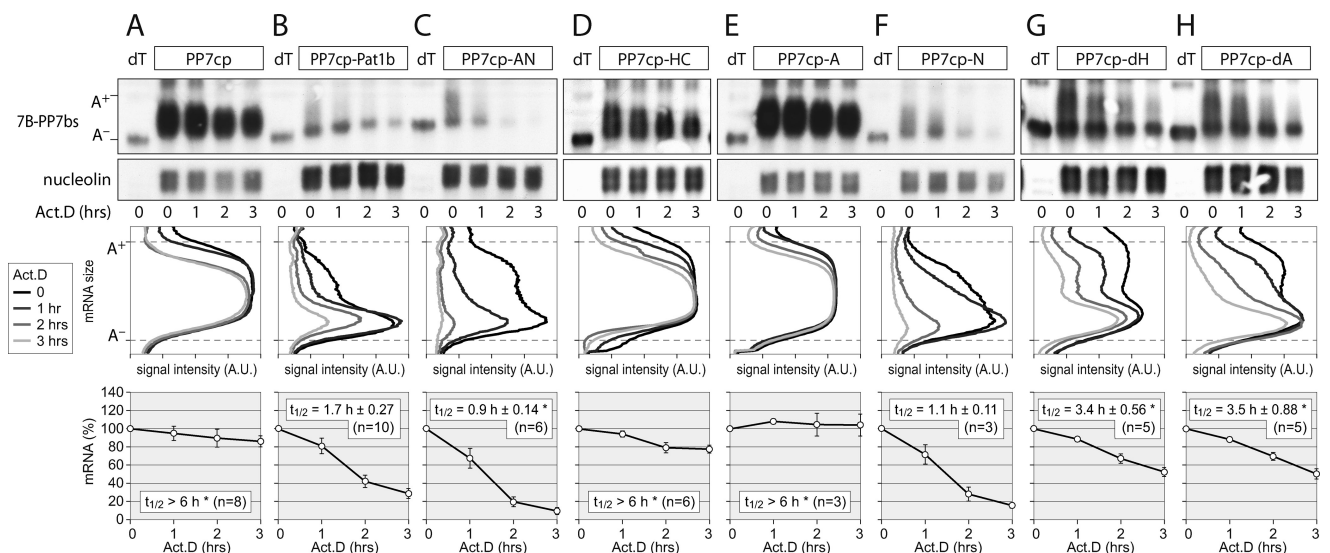


FIG. 9. Tethering of Pat1b fragments. HeLa cells were transiently transfected with the 7B-PP7bs reporter and HA-tagged PP7cp (A), PP7cp-Pat1b (B), PP7cp-AN (C), PP7cp-HC (D), PP7cp-A (E), PP7cp-N (F), PP7cp-dH (G), or PP7cp-dA (H). Degradation of the reporter mRNA was analyzed and quantified as described in the legend to Fig. 8. Average values \pm SE were plotted as a percentage of the initial time point. An asterisk indicates a significant difference in the mRNA $t_{1/2}$ ($P < 0.05$ by two-tailed Student's t test) compared to tethering of PP7cp-Pat1b depicted in panel B. Statistical analysis of mRNA $t_{1/2}$ is summarized in Table S4 in the supplemental material.

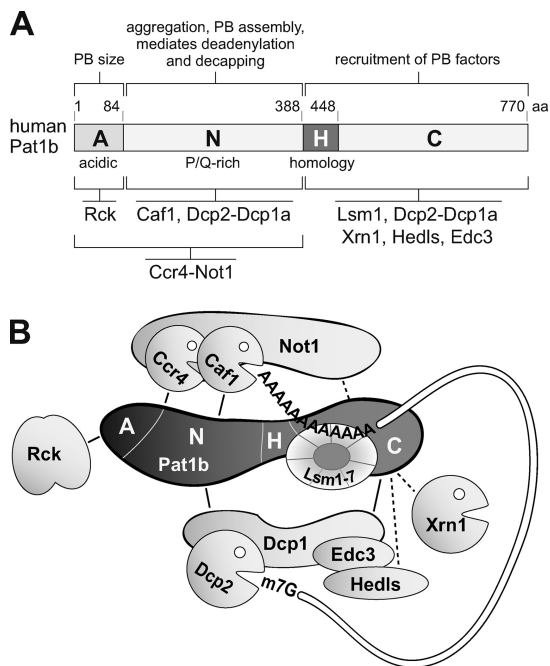


FIG. 10. Role of Pat1b in P-body assembly and mRNA degradation. (A) Schematic representation human Pat1b subdomains, together with interacting proteins and associated functions. All the interactions depicted are RNA independent yet may be direct or indirect. (B) Hypothetical model of the Pat1b-associated complex that connects deadenylation with mRNA decapping. The acidic region (A) associates with Rck, the AN fragment with the Ccr4-Not complex, and the N fragment with Caf1 and Dcp2-Dcp1a. The homology region (H) is required for Lsm1 binding, and the HC fragment further associates with Dcp2-Dcp1a. The HC fragment also shows weak association with Edc3, Hedls, and Xrn1.

different from the situation in yeast, human Pat1b also interacts very efficiently with Dcp2 and Dcp1a through the N domain (Fig. 6). Moreover, Dcp2 in yeast was found to interact with Pat1 and Lsm1 in an RNA-dependent manner by co-IP experiments (42). This is not the case for human Pat1b, in which the interaction with Dcp2 is RNA independent (see Fig. S8 in the supplemental material). Thus, human Pat1b differs substantially from its yeast counterpart: it makes very tight and RNA-independent contacts with both the Ccr4-Caf1-Not deadenylase and the Dcp2-Dcp1 decapping complexes and thereby enhances the interaction between Caf1a and Dcp2 (Fig. 6 and 7). Based on our findings, a speculative model of the human Pat1b complex is presented in Fig. 10B. While the manuscript was in revision, Haas et al. published that the homologous protein in *Drosophila*, HPat, also forms a tight link between the Ccr4-Not complex and the Dcp2 decapping enzyme (17).

It is interesting to note that the couplings of subsequent steps in mRNA decay appear to be different in human and yeast cells. While deletion of Xrn1 in yeast causes the accumulation of mRNAs lacking both a cap and a poly(A) tail (20, 26), knockdown of Xrn1 in human cells causes the accumulation of fully adenylated mRNAs (38). This indicates that coupling of deadenylation, decapping, and 5'-3' decay is more tight in human cells than in yeast. It is tempting to speculate

that the close association of human Pat1b with the deadenylase and decapping complexes may contribute to this tight coupling.

Analysis of Pat1b localization indicated that this protein plays an important role in P-body assembly. First, Pat1b localizes to P bodies (34) (Fig. 1) similarly to Pat1 in yeast (40), HPat in *Drosophila* (12), and PATR-1 in *C. elegans* (4). Second, knocking down Pat1b strongly reduces the number of P bodies in HeLa (34) and U2OS cells (Fig. 1; see also Fig. S5 in the supplemental material). Third, overexpression of Pat1b dramatically increases the number of P bodies in COS7 (Fig. 1) and U2OS cells (see Fig. S3 in the supplemental material). Many cells expressing YFP-Pat1b or HA-Pat1b had 50 or more P bodies with a “salt”-like appearance. We noticed that some of the small Pat1b foci did not contain other P-body proteins, whereas larger Pat1b foci consistently colocalized with all P-body proteins tested (Hedls, Lsm1, Lsm4, Xrn1, and Rck). This observation suggests that Pat1b could serve as a seed for P-body assembly. Pat1b may initially self-assemble into small foci and subsequently serve as a scaffold for additional P-body proteins as the aggregates grow in size. Other proteins, such as Dcp1a, can increase the size of P bodies when overexpressed (data not shown), yet the ability to serve as a “seed” and augment P-body numbers has not been reported for any other protein and thus appears to be a unique feature of Pat1b. Our finding that Pat1b co-IPs with itself (Fig. 2H) supports the idea of self-assembly. In addition, the ability of Pat1b-induced P bodies to resist disassembly in the presence of CHX (see Fig. S6 in the supplemental material) emphasizes that Pat1b plays a role in stabilizing P bodies. The fact that Pat1b interacts with other P-body proteins via at least three separate domains (Fig. 5 and 6) reflects its scaffolding function.

Our analysis of Pat1b subfragments suggests that the N region is critical for P-body assembly. By overexpression of YFP-AN or YFP-N, we observed a strong tendency of these fragments to form aggregates, many of which did not contain other P-body proteins (Fig. 2E and F and data not shown). Moreover, we observed that the AN and N fragments strongly reduced the number of P bodies in transfected cells. This may indicate that by forming autonomous aggregates, the N region when expressed alone can compete with the aggregation process within P bodies. This capacity is reminiscent of the C-terminal aggregation-prone domain of TIA-1, which when expressed on its own antagonizes stress granule formation (22). Similar to the C-terminal domain of TIA-1 that is strongly enriched in glutamine residues (21.6%), the N region of Pat1b contains a sequence of 120 aa (aa 261 to 380) with a high proportion of glutamine and asparagine (17%) as well as proline (17%) residues. This sequence is preceded by a stretch of 80 aa (aa 180 to 260) that is highly enriched in proline (28%). Glutamine/asparagine- and proline-rich sequences are characteristic of many aggregation-prone proteins, including yeast prion proteins as well as RNA-binding proteins that promote stress granule and P-body assembly (11, 16, 32, 36).

In addition to the N region, we found that the acidic domain (A) at the very amino terminus of Pat1b (aa 1 to 84) influences the size of P bodies. When mutant Pat1b lacking the A domain (dA) was overexpressed, Pat1b foci became smaller and more numerous, giving the protein a “pepper”-like distribution (Fig. 2D). These small foci still colocalized with P-body markers, such as Hedls. Thus, the A domain seems to control the size of

P bodies, maybe by promoting the fusion of small aggregates into larger P bodies. Since we found that the A domain interacts with Rck (Fig. 5C), it is possible that Rck may be an important driver of the aggregation process within P bodies. Indeed, Rck was shown to be essential for P-body formation in human cells (1).

In contrast to A and N, the H and C regions of Pat1b do not appear to play an active role in P-body assembly. The H, C, and HC fragments showed a mostly diffuse localization in the cell, with a rather weak accumulation in P bodies (Fig. 2G; see also Table S2 in the supplemental material). Localization of these fragments in P bodies presumably occurs through interactions with Lsm proteins, Xrn1, or decapping factors (Fig. 5 and 6). Since the overexpression of the H, C, or HC fragments did not affect the size or number of P bodies, it is likely that the HC region is recruited passively to P bodies. This may be different in yeast Pat1, in which the carboxy-terminal region (aa 422 to 797) was found to induce P bodies (30).

While Pat1b is clearly a central component of the RNA decay machinery, its paralog Pat1a does not share any of its functional characteristics: it does not localize to P bodies, does not augment P-body number or size, and has no influence on the expression level of a tethered reporter mRNA. In the cell lines we have tested so far, Pat1a mRNA was expressed at very low levels (data not shown). Rather, Pat1a seems to play an important role in the germ line since the *Xenopus* ortholog of Pat1a was recently shown to suppress translation during oocyte maturation (28).

In *S. cerevisiae*, Pat1 is a regulator of both mRNA decay and translation. Besides its role in decapping, yeast Pat1, together with the helicase Dhh1, is required for suppression of translation upon glucose starvation (9). This second function is probably linked to the finding that yeast Pat1 interacts with Pab1, eIF4E, and eIF4G in an RNA-dependent manner (30, 42). In our tethering experiments, human Pat1b did not have a strong effect on translation since luciferase activity and mRNA levels were reduced to similar degrees (Fig. 3C). We also measured global translation rates by [³⁵S]methionine-cysteine incorporation and polysome profile analysis but could not see changes after knocking down or overexpressing human Pat1b (data not shown). Finally, we did not observe an interaction of human Pat1b with either eIF4G (Fig. 4B) or eIF4E (data not shown). Thus, the role of human Pat1b appears to be restricted to mRNA degradation. One might speculate that the two functions of yeast Pat1 have segregated into two gene products in the course of vertebrate evolution: Pat1a as a regulator of translation and Pat1b as a scaffold of the mRNA decay machinery. During this process, human Pat1b seems to have acquired a much closer association with both the Ccr4-Caf1-Not deadenylase and the Dcp2-Dcp1 decapping complexes, thereby providing a tight physical link between deadenylation and decapping.

ACKNOWLEDGMENTS

We thank Jochen Kreth, Julia Luther, Oksana Seibert, and Gizem Olmezer for technical assistance, Sahil Sharma for cloning Caf1a expression vectors, Stefan Wiemann (German Cancer Research Center, Heidelberg, Germany) for providing the human Pat1b cDNA clone, Ann-Bin Shyu (University of Texas, Houston, TX) for the Caf1a antibody, Mark Timmers (University of Utrecht) for Flag-Not1, Jens Lykke-Andersen (University of California at San Diego) for myc-Ccr4,

Flag-Dcp1, and Flag-Dcp2, and Ulrike Engel (Nikon Imaging Center, University of Heidelberg) for generous support and advice on microscopy, as well as Witold Filipowicz (Friedrich Miescher Institute for Biomedical Research, Basel, Switzerland) and Nancy Kedersha (Brigham and Woman's Hospital, Boston, MA) for helpful discussions on the manuscript.

This work was supported by young investigator grant HZ-NG-210 from the Helmholtz Gemeinschaft and research grant STO 859/2-1 from the Deutsche Forschungsgemeinschaft.

REFERENCES

- Andrei, M. A., D. Ingelfinger, R. Heintzmann, T. Achsel, R. Rivera-Pomar, and R. Luhrmann. 2005. A role for eIF4E and eIF4E-transporter in targeting mRNPs to mammalian processing bodies. *RNA* **11**:717–727.
- Bashkirov, V. L., H. Scherthan, J. A. Solinger, J. M. Buerstedde, and W. D. Heyer. 1997. A mouse cytoplasmic exoribonuclease (mXRN1p) with preference for G4 tetraplex substrates. *J. Cell Biol.* **136**:761–773.
- Bhattacharyya, S. N., R. Habermacher, U. Martine, E. I. Closs, and W. Filipowicz. 2006. Relief of microRNA-mediated translational repression in human cells subjected to stress. *Cell* **125**:1111–1124.
- Boag, P. R., A. Atalay, S. Robida, V. Reinke, and T. K. Blackwell. 2008. Protection of specific maternal messenger RNAs by the P body protein CGH-1 (Dhh1/RCK) during *Caenorhabditis elegans* oogenesis. *J. Cell Biol.* **182**:543–557.
- Bonnerot, C., R. Boeck, and B. Lapeyre. 2000. The two proteins Pat1p (Mrt1p) and Spb8p interact in vivo, are required for mRNA decay, and are functionally linked to Pab1p. *Mol. Cell Biol.* **20**:5939–5946.
- Bouveret, E., G. Rigaut, A. Shevchenko, M. Wilm, and B. Seraphin. 2000. A Sm-like protein complex that participates in mRNA degradation. *EMBO J.* **19**:1661–1671.
- Chekulaeva, M., and W. Filipowicz. 2009. Mechanisms of miRNA-mediated post-transcriptional regulation in animal cells. *Curr. Opin. Cell Biol.* **21**:452–460.
- Chowdhury, A., J. Mukhopadhyay, and S. Tharun. 2007. The decapping activator Lsm1p-7p-Pat1p complex has the intrinsic ability to distinguish between oligoadenylated and polyadenylated RNAs. *RNA* **13**:998–1016.
- Coller, J., and R. Parker. 2005. General translational repression by activators of mRNA decapping. *Cell* **122**:875–886.
- Cougot, N., S. Babajko, and B. Seraphin. 2004. Cytoplasmic foci are sites of mRNA decay in human cells. *J. Cell Biol.* **165**:31–40.
- Decker, C. J., D. Teixeira, and R. Parker. 2007. Edc3p and a glutamine/asparagine-rich domain of Lsm4p function in processing body assembly in *Saccharomyces cerevisiae*. *J. Cell Biol.* **179**:437–449.
- Eulalio, A., I. Behm-Ansmant, D. Schweizer, and E. Izaurralde. 2007. P-body formation is a consequence, not the cause, of RNA-mediated gene silencing. *Mol. Cell Biol.* **27**:3970–3981.
- Fenger-Gron, M., C. Fillman, B. Norrild, and J. Lykke-Andersen. 2005. Multiple processing body factors and the ARE binding protein TTP activate mRNA decapping. *Mol. Cell* **20**:905–915.
- Franks, T. M., and J. Lykke-Andersen. 2007. TTP and BRF proteins nucleate processing body formation to silence mRNAs with AU-rich elements. *Genes Dev.* **21**:719–735.
- Garneau, N. L., J. Wilusz, and C. J. Wilusz. 2007. The highways and byways of mRNA decay. *Nat. Rev. Mol. Cell Biol.* **8**:113–126.
- Gilks, N., N. Kedersha, M. Ayodele, L. Shen, G. Stoecklin, L. M. Dember, and P. Anderson. 2004. Stress granule assembly is mediated by prion-like aggregation of TIA-1. *Mol. Biol. Cell* **15**:5383–5398.
- Haas, G., J. E. Braun, C. Igreja, F. Tritschler, T. Nishihara, and E. Izaurralde. 2010. HPat provides a link between deadenylation and decapping in metazoa. *J. Cell Biol.* **189**:289–302.
- Hatfield, L., C. A. Beelman, A. Stevens, and R. Parker. 1996. Mutations in *trans*-acting factors affecting mRNA decapping in *Saccharomyces cerevisiae*. *Mol. Cell Biol.* **16**:5830–5838.
- He, W., and R. Parker. 2001. The yeast cytoplasmic Lsm1/Pat1p complex protects mRNA 3' termini from partial degradation. *Genetics* **158**:1445–1455.
- Hsu, C. L., and A. Stevens. 1993. Yeast cells lacking 5'→3' exoribonuclease 1 contain mRNA species that are poly(A) deficient and partially lack the 5' cap structure. *Mol. Cell Biol.* **13**:4826–4835.
- Ingelfinger, D., D. J. Arndt-Jovin, R. Luhrmann, and T. Achsel. 2002. The human LSm1-7 proteins colocalize with the mRNA-degrading enzymes Dcp1/2 and Xrn1 in distinct cytoplasmic foci. *RNA* **8**:1489–1501.
- Kedersha, N. L., M. Gupta, W. Li, I. Miller, and P. Anderson. 1999. RNA-binding proteins TIA-1 and TIAR link the phosphorylation of eIF-2 alpha to the assembly of mammalian stress granules. *J. Cell Biol.* **147**:1431–1442.
- Lim, F., T. P. Downey, and D. S. Peabody. 2001. Translational repression and specific RNA binding by the coat protein of the Pseudomonas phage PP7. *J. Biol. Chem.* **276**:22507–22513.
- Liu, J., M. A. Valencia-Sanchez, G. J. Hannon, and R. Parker. 2005. MicroRNA-dependent localization of targeted mRNAs to mammalian P-bodies. *Nat. Cell Biol.* **7**:719–723.

25. Lykke-Andersen, J., and E. Wagner. 2005. Recruitment and activation of mRNA decay enzymes by two ARE-mediated decay activation domains in the proteins TTP and BRF-1. *Genes Dev.* **19**:351–361.
26. Muhlrads, D., C. J. Decker, and R. Parker. 1994. Deadenylation of the unstable mRNA encoded by the yeast MFA2 gene leads to decapping followed by 5'→3' digestion of the transcript. *Genes Dev.* **8**:855–866.
27. Muhlrads, D., and R. Parker. 2005. The yeast EDC1 mRNA undergoes deadenylation-independent decapping stimulated by Not2p, Not4p, and Not5p. *EMBO J.* **24**:1033–1045.
28. Nakamura, Y., K. J. Tanaka, M. Miyauchi, L. Huang, M. Tsujimoto, and K. Matsumoto. 21 May 2010. Translational repression by the oocyte-specific protein P100 in *Xenopus*. *Dev. Biol.* [Epub ahead of print.] doi:10.1016/j.ydbio.2010.05.006.
29. Parker, R., and H. Song. 2004. The enzymes and control of eukaryotic mRNA turnover. *Nat. Struct. Mol. Biol.* **11**:121–127.
30. Pilkington, G. R., and R. Parker. 2008. Pat1 contains distinct functional domains that promote P-body assembly and activation of decapping. *Mol. Cell. Biol.* **28**:1298–1312.
31. Pillai, R. S., S. N. Bhattacharyya, C. G. Artus, T. Zoller, N. Cougot, E. Basyuk, E. Bertrand, and W. Filipowicz. 2005. Inhibition of translational initiation by Let-7 microRNA in human cells. *Science* **309**:1573–1576.
32. Reijns, M. A., R. D. Alexander, M. P. Spiller, and J. D. Beggs. 2008. A role for Q/N-rich aggregation-prone regions in P-body localization. *J. Cell Sci.* **121**:2463–2472.
33. Rothbauer, U., K. Zolghadr, S. Muyldermans, A. Schepers, M. C. Cardoso, and H. Leonhardt. 2008. A versatile nanotrap for biochemical and functional studies with fluorescent fusion proteins. *Mol. Cell. Proteomics* **7**:282–289.
34. Scheller, N., P. Resa-Infante, S. de la Luna, R. P. Galao, M. Albrecht, L. Kaestner, P. Lipp, T. Lengauer, A. Meyerhans, and J. Diez. 2007. Identification of PatL1, a human homolog to yeast P body component Pat1. *Biochim. Biophys. Acta* **1773**:1786–1792.
35. Sheth, U., and R. Parker. 2003. Decapping and decay of messenger RNA occur in cytoplasmic processing bodies. *Science* **300**:805–808.
36. Shorter, J., and S. Lindquist. 2005. Prions as adaptive conduits of memory and inheritance. *Nat. Rev. Genet.* **6**:435–450.
37. Stoecklin, G., and P. Anderson. 2006. Posttranscriptional mechanisms regulating the inflammatory response. *Adv. Immunol.* **89**:1–37.
38. Stoecklin, G., T. Mayo, and P. Anderson. 2006. ARE-mRNA degradation requires the 5'-3' decay pathway. *EMBO Rep.* **7**:72–77.
39. Stoecklin, G., P. Stoeckle, M. Lu, O. Muehleemann, and C. Moroni. 2001. Cellular mutants define a common mRNA degradation pathway targeting cytokine AU-rich elements. *RNA* **7**:1578–1588.
40. Teixeira, D., and R. Parker. 2007. Analysis of P-body assembly in *Saccharomyces cerevisiae*. *Mol. Biol. Cell* **18**:2274–2287.
41. Temme, C., S. Zaessinger, S. Meyer, M. Simonelig, and E. Wahle. 2004. A complex containing the CCR4 and CAF1 proteins is involved in mRNA deadenylation in *Drosophila*. *EMBO J.* **23**:2862–2871.
42. Tharun, S., and R. Parker. 2001. Targeting an mRNA for decapping: displacement of translation factors and association of the Lsm1p-7p complex on deadenylated yeast mRNAs. *Mol. Cell* **8**:1075–1083.
43. van Dijk, E., N. Cougot, S. Meyer, S. Babajko, E. Wahle, and B. Seraphin. 2002. Human Dcp2: a catalytically active mRNA decapping enzyme located in specific cytoplasmic structures. *EMBO J.* **21**:6915–6924.
44. Wang, Z., X. Jiao, A. Carr-Schmid, and M. Kiledjian. 2002. The hDcp2 protein is a mammalian mRNA decapping enzyme. *Proc. Natl. Acad. Sci. U. S. A.* **99**:12663–12668.
45. Winkler, G. S., K. W. Mulder, V. J. Bardwell, E. Kalkhoven, and H. T. Timmers. 2006. Human Ccr4-Not complex is a ligand-dependent repressor of nuclear receptor-mediated transcription. *EMBO J.* **25**:3089–3099.
46. Yamasaki, S., G. Stoecklin, N. Kedersha, M. Simarro, and P. Anderson. 2007. T-cell intracellular antigen-1 (TIA-1)-induced translational silencing promotes the decay of selected mRNAs. *J. Biol. Chem.* **282**:30070–30077.
47. Zheng, D., N. Ezzeddine, C. Y. Chen, W. Zhu, X. He, and A. B. Shyu. 2008. Deadenylation is prerequisite for P-body formation and mRNA decay in mammalian cells. *J. Cell Biol.* **182**:89–101.

SUPPLEMENTAL MATERIAL

Human Pat1b Connects Deadenylation with mRNA Decapping and Controls the Assembly of Processing-Bodies

Sevim Ozgur, Marina Chekulaeva and Georg Stoecklin

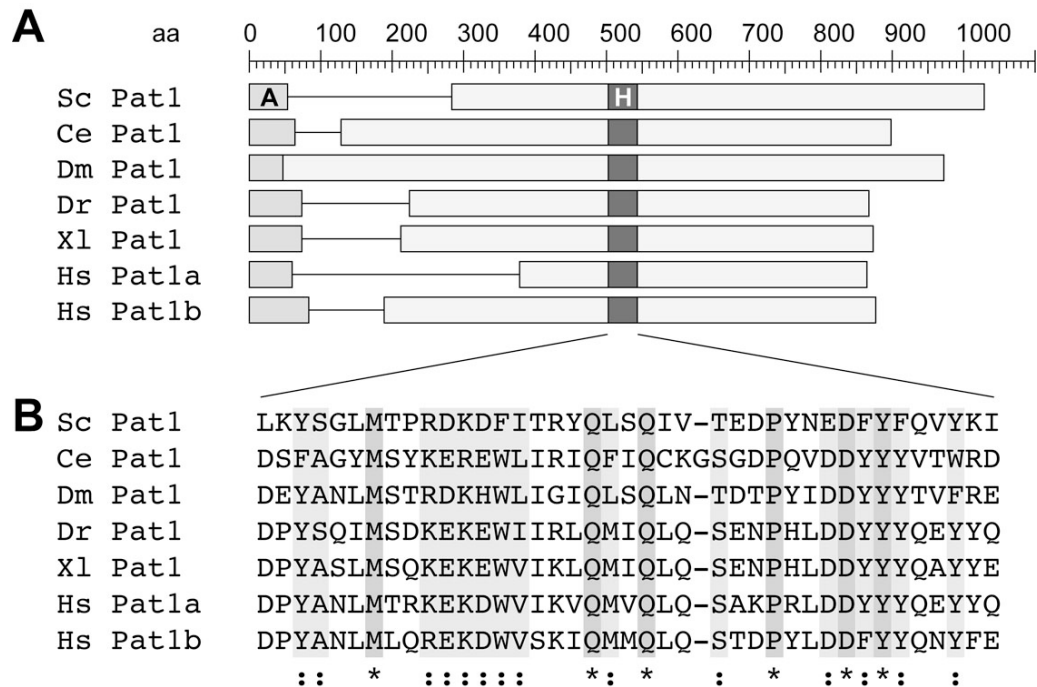


FIG. S1. Conservation among Pat1 Proteins. (A) Two domains are conserved at the level of the primary amino acid sequence between Pat1 proteins in fungi and metazoa: an acidic region "A" at the amino-terminus of the protein (medium grey) and a small region in the middle of the protein with highest sequence similarity termed the homology "H" domain (dark grey). Mammals have two Pat1b homologs that were designated Pat1a and Pat1b. Sc, *Saccharomyces cerevisiae*; Ce, *Caenorhabditis elegans*; Dm, *Drosophila melanogaster*; Dr, *Danio rerio*; Xl, *Xenopus laevis*; Hs, *Homo sapiens*. (B) Sequences of the homology domain were aligned using Clustal W. *, identical amino acids; :, similar amino acids.

```

hPat1a -----MNCLEGP GK-----TCGPLASEEELVSACQLEKEEENEG
hPat1b MFVAVNEQTCNGERDEMDLLGDHEEENLAERLSKMVIENELEDPAIMRAVQTRPVLQPPQGS
          :.:.:* * : * * . * : : . * : * * :
hPat1a -----EEEEEEDEEDLDPDLDPDLEE-----EENDLGDPAVLGAVHN-----
hPat1b PVAVNEQTCNGERDEMDLLGDHEEENLAERLSKMVIENELEDPAIMRAVQTRPVLQPPQGS
          : : * . ** ** * : * * ** : * ** : * : .
hPat1a -----
hPat1b LNSSIWDGSEVLRIRGPLLAQEMPTVSVLEYALPQRPPQGPEDDRDLSERALPRRSTSP
hPat1a -----
hPat1b IIGSPPVRAVPIGTPPKQMAVPSFTQQLCPKPVHVRPPMPRYPAPYGERMSPNQ LCSV
hPat1a -----TORALLS-----SPGVKAPGMLGMSLASH--
hPat1b PNSSLLGHFPFPPSVPPVLSPLQRAQLLGGAGLQPPGRMSPSQFARVPGFVGSPLAAMNPKL
          *** * * . . * . * : * . * :
hPat1a FLWQTLDYLSPIPFWPTFPSTSSPAQHFGPRLPSPDPTLFCSSLTSWPPRFSHLTQLHPR
hPat1b LQGRVGMQLPPAPGFRAFFSAPPSATPPPQQHPPGPGPHLQNLRSQAPMFRPDTTHLHPQ
          : . : * . * * : * * * . . . * : * . . : * . : * . . * : * : * :
hPat1a HQRILQQQQHSQTP-----SPPAKKPSQDPYANLMTRKEKDWIKVQMVQ
hPat1b HRLLHQRQQNRSQHRNLNGAGDRGSHRSSHQDHLRKDPYANLMLQREKDWVSKIOMMQ
          * : * : * : * : * : . * : : : * * * * * : * * * * * : * : * :
hPat1a LQSAKPRLDDYYQ EYYQKLEKKQADEELLGRRNRVESLKLVTPIPKAEAYESVVRIEG
hPat1b LQSTDPYLDDFYQ NYFEKLEKLSAAEEIQGDGPKKERTKLITPQVAKLEHAYKPVQFEG
          * * : . * * * : * * : * : * * * * * . * * : * : * * * * * : * * : * :
hPat1a SLGQVAVSTCFSPRAIDAVPHGTQEOD---IEAASSQRLRVLYRIEKMFQLLEIEEGW
hPat1b SLGKLTVSSVNNPRKMIDAVVTSRSEDETKEKQVRDKRRKTLVIEKTYSLLDVEDYE
          * * : : * * : . * : * * * . . * : * : . . * : . * * : * * : * : * :
hPat1a K-----YRPPPPCFSEQQSNQVEKLFQTLKTQEQQNLEEAADGFQVLSVRK GKALVARL
hPat1b RRYLLSLEEERPALMDDRKHKICSMYDNLRGKLPQGERPSDDHFVQIMCIRKGRMVARI
          : . * : : : : : : . : : * : * : * : * : * : * : * : * :
hPat1a LPFLPQDQAVTILLAITHHLPLLVRDVADQALQMLFKPLGKCISHLTLHELLQGLQGLT
hPat1b LPFLSTEQAADILMTTARNLPFLIKKDAQDEVLPCLLSPFSLLLYHLPVSVITSLLRQLM
          * * . : * * . * * : : * * * * * : * . * * * * . : * * . : . * : *
hPat1a LLP-----PGSSERPVTVVLQNFQGISLLYALLSHGEQLVSLHSSLEEPSNDHTAWTDMV
hPat1b NLPQSAATPALSNPHLTAVLQNKFGLSLLLILLSRGEDLQSSDPATES--TQNNQWTEVM
          * * * . * : : * . * * * : * * * * * * * * * * * . . : * . : : . * : * :
hPat1a VLIaweIAQMPTASLAELAFPSNLLPLFCHHVdKQLVQOLEARMEFAWIY-
hPat1b FMatRELLRIPQAALARPISIPTNLVSLFSRYVDRQKLNLETKLQLVQGIR
          . : : * : : * * * * * : * * * * * : * * * * * : * * * * * :
    
```

FIG. S2. Alignment of human Pat1a and Pat1b. The sequences of human Pat1b (PATL1, NP_689929) and human Pat1a (PATL2, NP_001138584) were aligned using Clustal W software. The amino-terminal acidic domain (A) is highlighted in blue, the central homology domain (H) is highlighted in yellow.

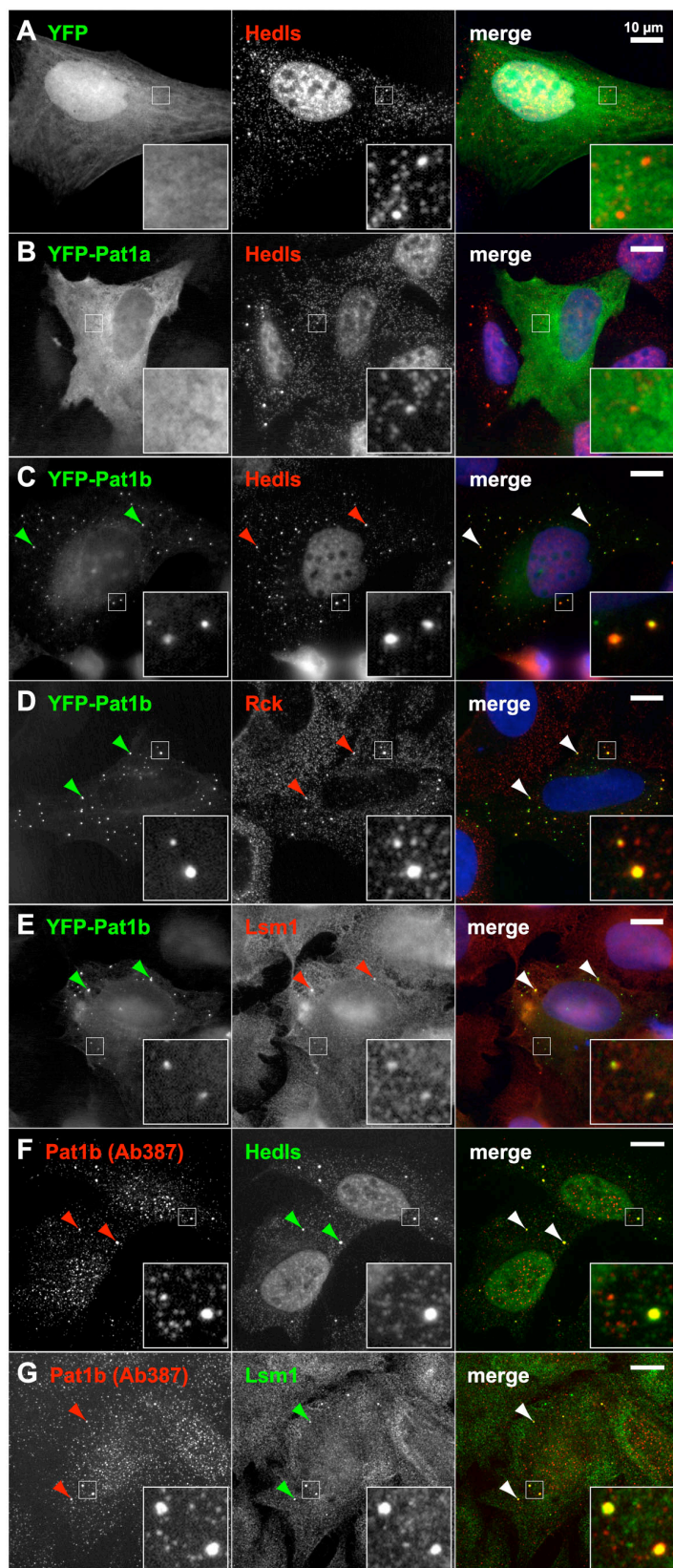


FIG. S3. Intracellular localization of human Pat1a and Pat1b in U2OS cells. (A-E) U2OS cells were transiently transfected with (A) YFP, (B) YFP-Pat1a or (C-E) YFP-Pat1b. Cells were then processed for immunofluorescence microscopy, and cytoplasmic P-bodies were counterstained in red using an antibody against (A-C) Hedls, (D) Rck or (E) Lsm1. Cells in panels A-E were also stained with Hoechst 33342 in blue to visualize nuclei. Images were acquired by spinning disc confocal microscopy, maximum projections of z-stacks are depicted. (F-G) Untransfected U2OS cells were stained in red for endogenous Pat1b with antibody 387, and in green for P-bodies using antibodies against (F) Hedls or (G) Lsm1. Arrows point towards P-bodies; bar, 10 μ m.

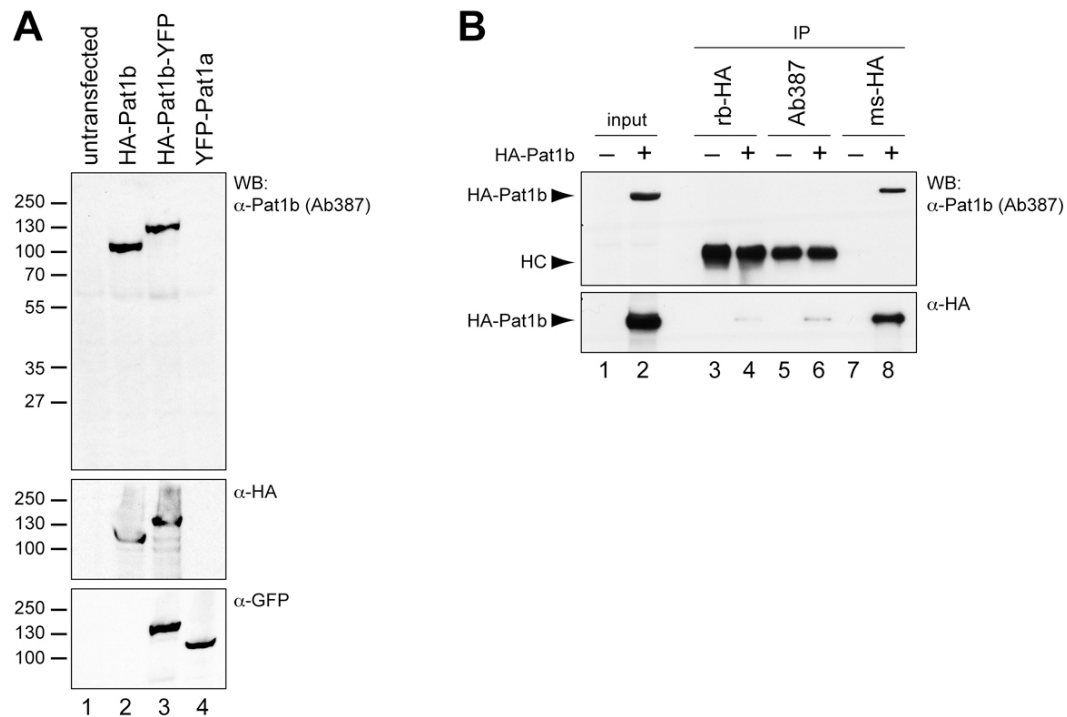
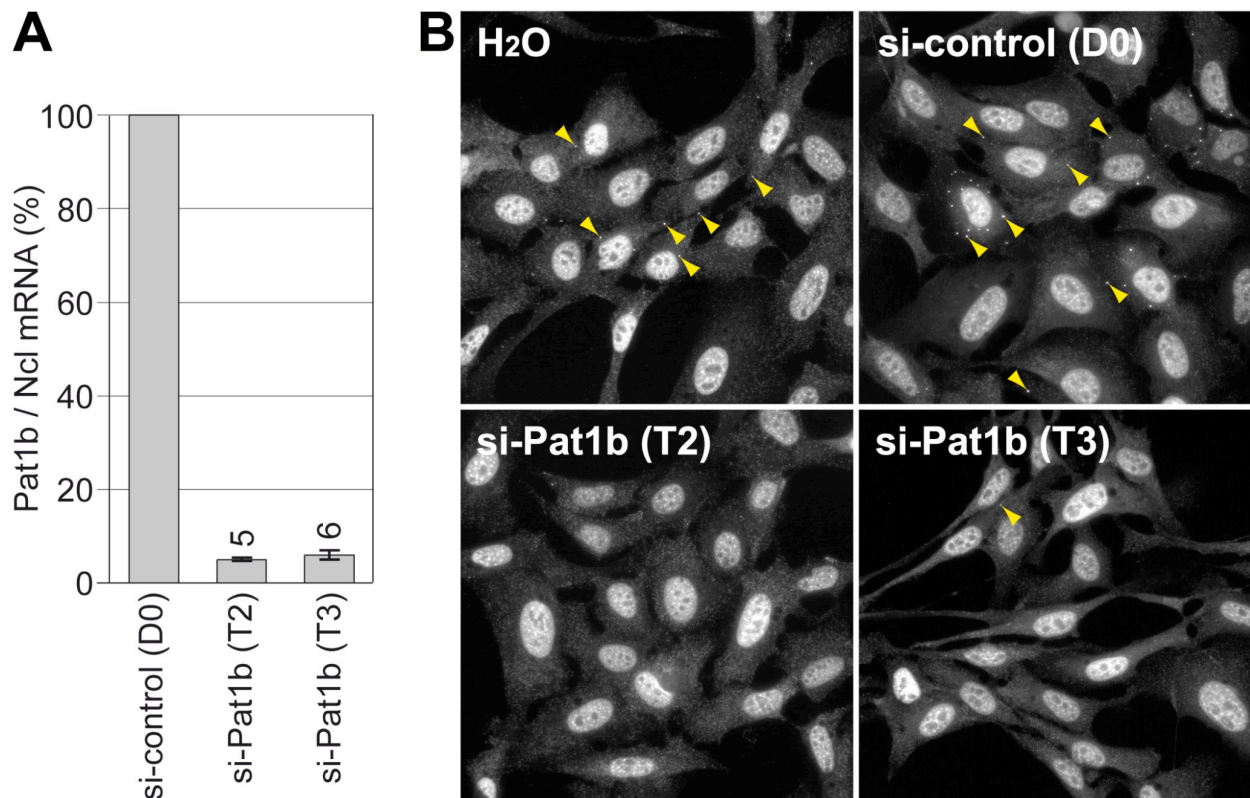


FIG. S4. Human Pat1b antibody. Cytoplasmic protein lysates were made from HEK293 cells that were either untransfected or transiently transfected with HA-Pat1b, HA-Pat1b-YFP or YFP-Pat1a. (A) Western blot analysis was carried out with Ab387, a polyclonal rabbit antibody raised against human Pat1b (upper panel). This antibody recognizes overexpressed Pat1b, but not endogenous Pat1b. The predicted size of human Pat1b is 87 kDa. Separate blots of the same lysates were probed with an HA antibody (HA.11, Covance, middle panel) and a GFP antibody (ab 293, Abcam, lower panel) that also recognizes YFP. (B) Cytoplasmic lysates of untransfected (-) or HA-Pat1b (+) transfected HEK293 cells were used for IP with rabbit α -HA, rabbit α -Pat1b (Ab387) or mouse α -HA antibody. Ab387 can weakly precipitate overexpressed HA-Pat1b, but not endogenous Pat1b.



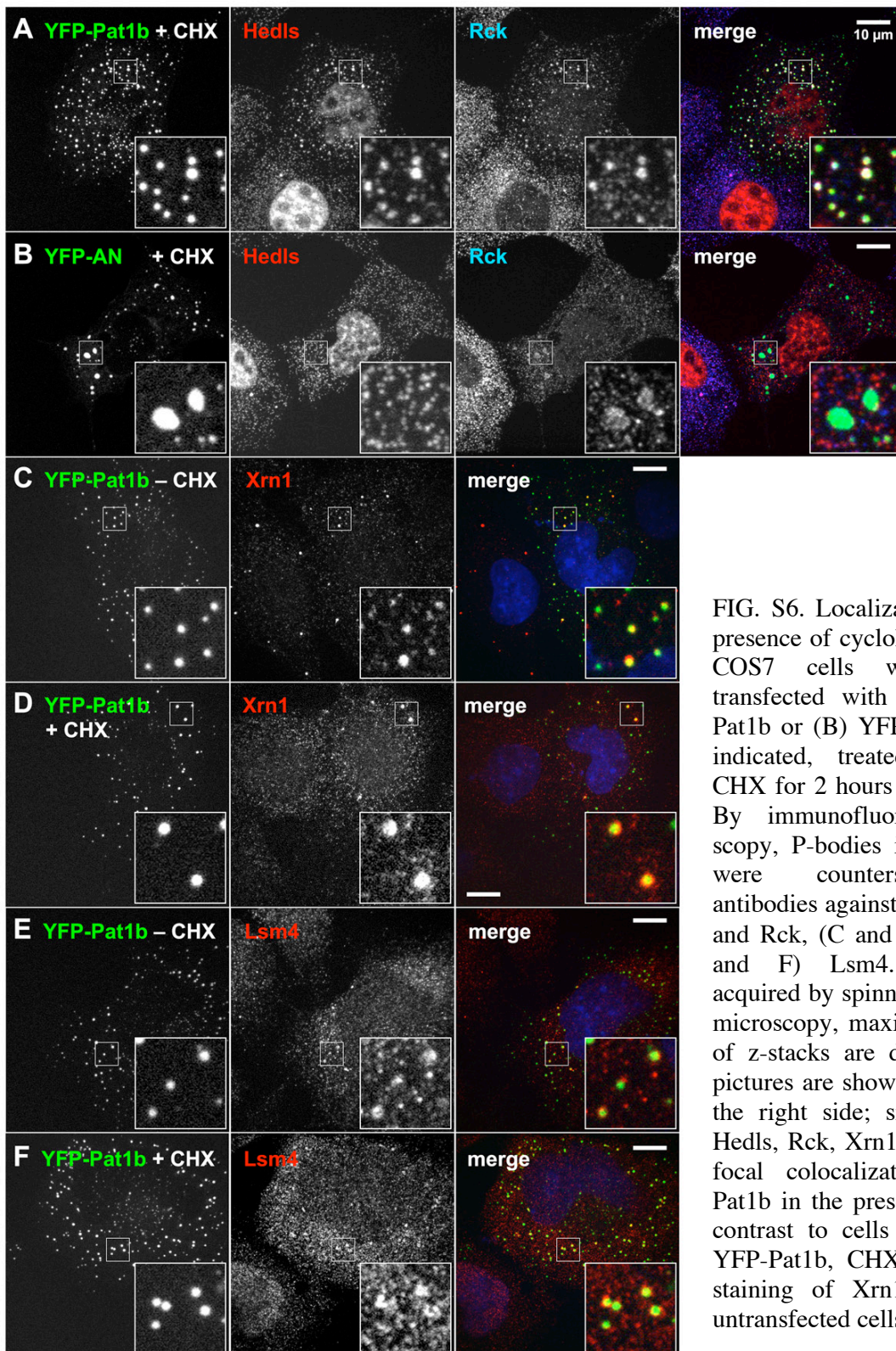


FIG. S6. Localization of Pat1b in presence of cycloheximide (CHX). COS7 cells were transiently transfected with (A, C-F) YFP-Pat1b or (B) YFP-AN and, where indicated, treated with $5\mu\text{g/ml}$ CHX for 2 hours prior to fixation. By immunofluorescence microscopy, P-bodies in the cytoplasm were counterstained using antibodies against (A and B) Hedls and Rck, (C and D) Xrn1 and (E and F) Lsm4. Images were acquired by spinning disc confocal microscopy, maximum projections of z-stacks are depicted. Merged pictures are shown in the panel on the right side; size bar, $10\mu\text{m}$. Hedls, Rck, Xrn1 and Lsm4 show focal colocalization with YFP-Pat1b in the presence of CHX. In contrast to cells transfected with YFP-Pat1b, CHX abolishes focal staining of Xrn1 and Lsm4 in untransfected cells.

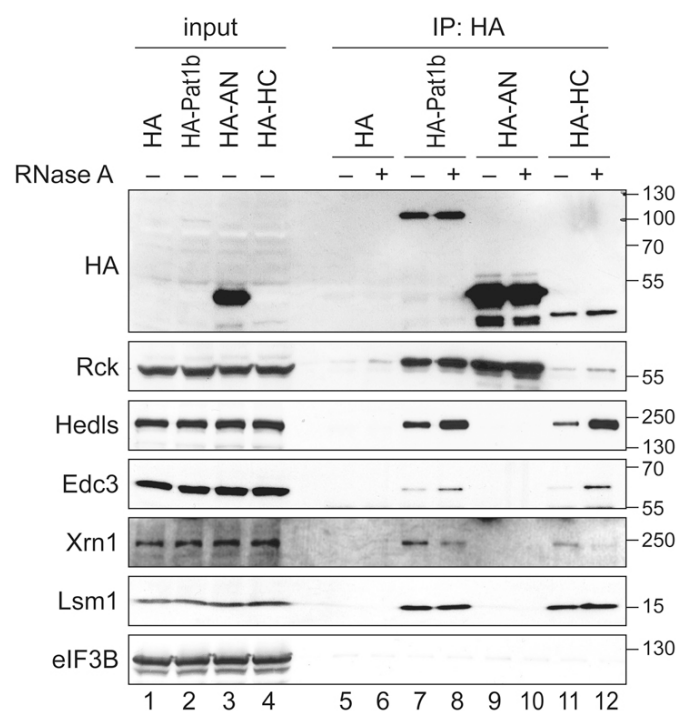


FIG. S7. Hedls, Edc3 and Xrn1 interact with the HC fragment of Pat1b. HEK293 cells were transiently transfected with vector alone, full length HA-Pat1b, HA-AN or HA-HC. After one day, cytoplasmic lysates (input) were prepared for IP with an anti-HA antibody. The HA-tagged proteins as well as endogenous Rck, Hedls, Edc3, Xrn1, Lsm1 and eIF3B were detected by Western blotting. Where indicated, RNase A was added to the lysates during IP. Rck interacts with the AN fragment of Pat1b, whereas Hedls, Edc3, Xrn1 and Lsm1 interact with the HC fragment. All interactions are RNA-independent.

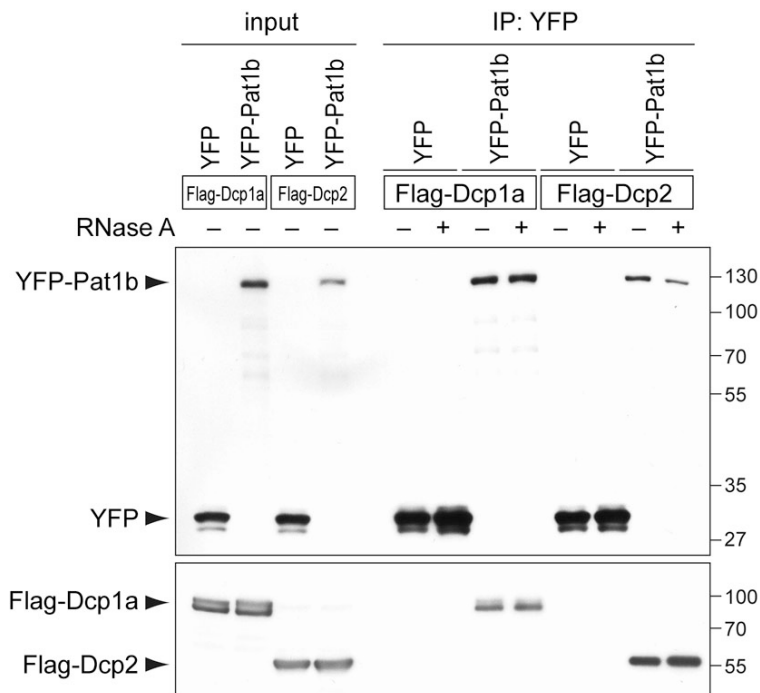


FIG. S8. Interaction of Dcp1a / Dcp2 with Pat1b is RNA-independent. HEK293 cells were transiently transfected with YFP or YFP-Pat1b together with either Flag-Dcp1a or Flag-Dcp2. GFP-binder was used for IP, and Western blots were carried out with anti-GFP and anti-Flag antibodies. Where indicated, RNase A was added to the lysates during IP.

TABLE S1. Primer Sequences

G18	5'-ACATTCGGCCGGGTCGACCACTG-3'
G19	5'-AATTGATATCCACCATGGCCAGCATGACCGGCGGCCAGCAGATGGGCGTGCATCTGTCCAG-3'
G78	5'-GGTGGTCCGAAAGCTATC-3'
G83	5'-TTACAAAGTCACTCAGGATG-3'
G85	5'-AGCTTACCACCATGTACCCATACGATGTTCCAGATTACGCTGGTACCGGATCCG-3'
G86	5'-AATTCGGATCCGGTACCAGCGTAATCTGGAACATCGTATGGGTACATGGTGGTA-3'
G243	5'-ATATAAGCTTCCACCATGGTGAG-3'
G244	5'-ATATGGTACCCTTGTACAGCTCG-3'
G1000	5'-GTGCATCTGTCCAGTG-3'
G1001	5'-GCCGATTTAGGTGACACTATAGAATACCCTGAAGTTCTC-3'
G1008	5'-GCCGATTTAGGTGACACTATAGAATACTATAGACACCAG-3'
G1009	5'-GCCGATTTAGGTGACACTATAGAATACTTAGCGTCTTCG-3'
G1122	5'-ATATGGATCCGCCACCATGCCAGCGGCAACTGTAG-3'
G1123	5'-TATACTCGAGTGACTGCTTGTGGCTTCC-3'
G1198	5'-TTAATCTAGATCAGTAAATCCAGGCAAACCTCC-3'
G1219	5'-GCCAAGATGAATTGCCTTGAAG-3'
G1221	5'-ACTGCTTGCAGCTTCTATATCC-3'
G1222	5'-GTCTGATGATTCAACTTCC-3'
G1225	5'-ATATGGTACCATGTTCCGCTACGAG-3'
G1226	5'-TATACTCGAGTTAGTGACTTCCTCTATCTCC-3'
G1227	5'-ATATGGTACCCGGAGCAGTCATCAAG-3'
G1228	5'-TATACTCGAGTTATTCTTCAGCAGCTGAC-3'
G1229	5'-ATATGGTACCATACAAGGTGATGGC-3'
G1230	5'-TATACTCGAGTTATCGTATCCCCTGAAC-3'
G1253	5'-ATATCTCGAGTTAACCTTGTACAGC-3'
G1256	5'-ATATAAGCTTCCACCATGGAAGACGCC-3'
G1257	5'-ATATGGTACCCACGGCGATCTTTC-3'
G1295	5'-CTCCAGTTTTTCAAACCTTTCGGAGATG-3'
G1296	5'-CATCTCCGAAAGTTTGAAAACTGGAG-3'
G1315	5'-CTTCTGAGGAGGAGCTGGTGTCTG-3'
G1332	5'-CTCGCCGAGCTATTGATGC-3'
G1340	5'-CAAGGAGGCAAGTGACATTC-3'
G1353	5'-ATATGGATCCGAATTCATGAATTGCCTTGAAGGGC-3'

TABLE S1. Primer Sequences (continued)

G1408	5'-ATATGGTACCAATCTGGCAGAAAGG-3'
G1425	5'-TATACTCGAGTTACTCCTCATGGTCACC-3'
G1501	5'-ATATGGTACCATGTCCAAAACCATC-3'
G1502	5'-ATATGGTACCACGGCCCAGCGGCAC-3'
G1730	5'-AGCGTTTAAACTTAAGCTTGG-3'
G1731	5'-CCTGAATTCTCCAATGGGTCTTGCAACCACACCTGGAAACGCGGTGGCCATAGCAAC-3'
G1883	5'-CAGGGGTACCTAGCAAAAATCAGG-3'
G1884	5'-CTTTGATATCAAAAACAGTTGCTGCAAAGACCTCTC-3'

TABLE S2. Intracellular Localization of Pat1b Fragments

	Diffuse	Aggregates or P-bodies	Effect on P-bodies
YFP	++++ nucl > cyto	–	no obvious effect
YFP-Pat1b	–	++++ small to medium size round foci containing P-body markers	"salt": strong increase in P-body numbers
YFP-dH	–	++++ small to medium size round foci containing P-body markers	"salt": strong increase in P-body numbers
YFP-dA	–	++++ very small size round foci containing P-body markers	"pepper": stronger increase in P-body numbers
YFP-AN	++ nucl < cyto	++ large round foci and irregular patches, only some containing P-body markers	suppression of P-bodies
YFP-N	+ nucl < cyto	+++ medium size round foci and irregular patches, only some containing P-body markers	suppression of P-bodies
YFP-A	++++ nucl > cyto	–	no obvious effect
YFP-HC	+++ nucl = cyto	+ medium size round foci containing P-body markers	no obvious effect

nucl, nuclear localization; cyto, cytoplasmic localization

TABLE S3. Statistical Analysis of PP7cp-Pat1b tethered 7B-PP7bs mRNA Decay Rates (Figure 8)

	Average mRNA $t_{1/2}$ (hrs)	SD	SE	n	P *
vector	1.25	0.070	0.041	3	
Caf1a-wt	0.96	0.154	0.089	3	0.044
Caf1a-AA	1.63	0.397	0.229	3	0.177
Dcp2-wt	2.40	1.546	0.892	3	0.266
Dcp2-AA	2.53	0.765	0.442	3	0.045
Caf1a-wt + Dcp2-AA	3.74	1.282	0.740	3	0.028
Caf1a-AA + Dcp2-wt	1.60	0.483	0.279	3	0.281
Caf1a-AA + Dcp2-AA	15.03 #	4.401	2.541	3	0.006

* P-value (two-tailed) was calculated in comparison to "vector"

mRNA $t_{1/2}$ is too long for reliable extrapolation from 3 hour time course experiments

TABLE S4. Statistical Analysis of 7B-PP7bs mRNA Decay Rates (Figure 9)

	Average mRNA $t_{1/2}$ (hrs)	SD	SE	n	P *
PP7cp	16.53 #	14.997	5.302	8	0.027
PP7cp-Pat1b	1.74	0.841	0.266	10	
PP7cp-AN	0.87	0.345	0.141	6	0.032
PP7cp-HC	9.16 #	5.353	2.185	6	0.001
PP7cp-A	37.66 #	48.526	28.017	3	0.023
PP7cp-N	1.08	0.193	0.112	3	0.218
PP7cp-dH	3.45	1.256	0.562	5	0.008
PP7cp-dA	3.48	1.972	0.882	5	0.030

* P-value (two-tailed) was calculated in comparison to "PP7cp-Pat1b"

mRNA $t_{1/2}$ is too long for reliable extrapolation from 3 hour time course experiments